Synthesis, Characterization and Biological Investigation of Self-delivering and Modified Short Interfering RNAs (siRNAs)

by

Lidya Salim

A thesis submitted to the
School of Graduate and Postdoctoral Studies in partial
fulfillment of the requirements for the degree of

Doctor of Philosophy in Applied Bioscience

Faculty of Science

University of Ontario Institute of Technology (Ontario Tech University)

Oshawa, Ontario, Canada

July 2021

© Lidya Salim, 2021

Thesis Examination Information

Submitted by: **Lidya Salim**

Doctor of Philosophy in Applied Bioscience

Thesis title: Synthesis, Characterization and Biological Investigation of Self-delivering and Modified Short Interfering RNAs (siRNAs)

An oral defense of this thesis took place on July 8, 2021, in front of the following examining committee:

Examining Committee:

Chair of Examining Committee	Prof. Janice Strap
Research Supervisor	Prof. Jean-Paul Desaulniers
Examining Committee Member	Prof. Yuri Bolshan
Examining Committee Member	Prof. Sean Forrester
University Examiner	Prof. Otto Sanchez
External Examiner	Prof. Christopher Wilds, Concordia University

The above committee determined that the thesis is acceptable in form and content and that a satisfactory knowledge of the field covered by the thesis was demonstrated by the candidate during an oral examination. A signed copy of the Certificate of Approval is available from the School of Graduate and Postdoctoral Studies.

Abstract

Aberrant gene expression is a hallmark of disease, so it is of great interest to develop targeted therapies that provide a means to regulate gene expression. The RNA interference pathway serves as a natural defense system against invasive genetic information and results in gene silencing by targeting and degrading mRNA. Synthetic short interfering RNAs (siRNAs) can use this endogenous machinery and have emerged as a novel class of gene-silencing therapeutics. Unfortunately, the development of RNAi therapeutics has been hindered by several challenges associated with the nature and structure of RNA. To harness their full potential, siRNAs must be chemically modified to improve their pharmacokinetic profiles. This dissertation reports the use of two bioconjugates, cholesterol and folic acid, to improve the cellular uptake and delivery of siRNAs and explores the incorporation of a novel sugar moiety within siRNAs to assess its effect on gene-silencing activity. Cholesterol has been extensively used as a delivery vector for nucleic acids. In this work, we show a novel way to functionalize siRNAs with cholesterol, via a triazole linkage, and demonstrate the efficacy of these self-delivering siRNA. Despite their promise, lipid-conjugated siRNAs tend to accumulate in areas like the liver and kidneys, so there is great interest in developing siRNA-conjugates to target other cells and tissues. Based on this, we explored the use of a folate ligand to selectively deliver siRNAs to cancer cells via the folate receptor. This receptor is highly overexpressed in numerous cancers and has become an important molecular marker in cancer research. Here, we show that centrally modified folate-siRNA conjugates display enhanced gene-silencing activity and can be selectively delivered to folate receptor-expressing cancer cells. Lastly, we explore the incorporation of a novel glucose moiety, triazole-linked to uracil at position one, in the sense or antisense strand of siRNAs. The resulting siRNA duplexes contained a single 3′-6′/2′-5′ phosphodiester linkage and achieved good gene-silencing activity. Together, this dissertation demonstrates the efficacy of several chemical modifications at improving some of the limitations associated with siRNAs, providing new avenues for the development of safe and effective RNAi therapeutics.

Keywords: nucleic acids; RNAi; siRNA; bioconjugates; drug delivery

Author′s Declaration

I hereby declare that this thesis consists of original work of which I have authored. This is a true copy of the thesis, including any required final revisions, as accepted by my examiners.

I authorize the University of Ontario Institute of Technology (Ontario Tech University) to lend this thesis to other institutions or individuals for the purpose of scholarly research. I further authorize University of Ontario Institute of Technology (Ontario Tech University) to reproduce this thesis by photocopying or by other means, in total or in part, at the request of other institutions or individuals for the purpose of scholarly research. I understand that my thesis will be made electronically available to the public.

Lidya Salim

Statement of Contributions

Published Manuscript I (Chapter 2): L. Salim, C. McKim, J.-P. Desaulniers, "Effective carrier-free gene-silencing activity of cholesterol-modified siRNAs", *RSC Advances*, 8 (2018), 22963-22966.

I developed and performed all the biological assays reported in this manuscript and was responsible for data analysis, figure preparation and manuscript writing. Chris McKim synthesized the siRNAs employed in this work. Prof. Jean-Paul Desaulniers was responsible for funding acquisition, project administration and revising the manuscript.

Published Manuscript II (Chapter 3): L. Salim, G. Islam, J.-P. Desaulniers, "Targeted delivery and enhanced gene-silencing activity of centrally modified folic acid–siRNA conjugates", *Nucleic Acids Research*, 48 (2020), 75-85.

I was responsible for all the chemical and oligonucleotide syntheses and purifications, the development and performance of most of the biological assays as well as data analysis (except for flow cytometry and RT-qPCR studies). I also prepared all the figures and wrote the manuscript. Dr. Golam Islam performed the flow cytometry and the RT-qPCR experiments and analyzed that data. Prof. Jean-Paul Desaulniers was responsible for funding acquisition, project administration and revising the manuscript.

Preparation Manuscript I (Chapter 4): L. Salim and J.-P. Desaulniers.

I co-conceptualized the project and performed all the chemical and oligonucleotide syntheses. Prof. Jean-Paul Desaulniers was responsible for conceptualization, funding acquisition and project administration.

Published Manuscript III (Chapter 5): L. Salim, E. Goss, J.-P. Desaulniers. "Synthesis and evaluation of modified siRNA molecules containing a novel glucose derivative", *RSC Advances*, 11 (2021), 9285-9289.

I performed the chemical and oligonucleotide syntheses and purifications, biological assays, and data analysis. I also created the figures and prepared the manuscript. Dr. Eva Goss provided some resources for this project and was responsible for funding acquisition and project administration. Prof. Jean-Paul Desaulniers was responsible for conceptualization, funding acquisition, project administration and revising the manuscript.

Published Review Manuscript I (Appendix E): L. Salim, J.-P. Desaulniers. "To conjugate or to package? A look at targeted siRNA delivery through folate receptors", *Nucleic Acid Therapeutics*, 31 (2021), 21-38.

I co-conceptualized the project, wrote the review manuscript, and prepared all figures. Prof. Jean-Paul Desaulniers was responsible for conceptualization and revising the manuscript.

Acknowledgements

First, I would like to thank my supervisor Prof. Jean-Paul Desaulniers for his outstanding support and mentorship over the past 6 years. Thank you for taking a chance with me, when I was an undergraduate student with no Chemistry background, and for providing me with endless tools and opportunities throughout this journey. Thank you for always being there, through ups and downs, to support and encourage me. I am taking many great memories and experiences with me.

I also want to thank my colleagues at the Desaulniers Lab. Matt, you have been a great friend and support system since we both started our respective journeys in 2015. Thank you for all the training and mentorship you have provided me with and for the much-needed coffee breaks – whether they were virtual or in the hallway. Ifrodet, thank you for always being willing to help me, in and out of the lab, and for bringing a fun and positive energy to our group. Charlene, I really enjoyed working with you not only through our shared industry partnership, but also through our Working for Inclusivity in Chemistry group. Andrew, I appreciate the different perspective and experience you brought to the lab, and I am glad we had the opportunity to work together. Autumn, you always have such a great and kind attitude and, although we worked on very different projects, I could always count on you to exchange thoughts and ideas. I also want to thank our outstanding postdoctoral fellow Dr. Golam Islam for all his assistance and mentorship in the lab. You have been a great addition to our team. Last, but not least, I want to thank all the undergraduate and exchange students that have been part of our group over the years.

Next, I would like to thank Prof. Sean Forrester, Prof. Yuri Bolshan and Prof. Julia Green-Johnson for their guidance and feedback. Thank you for sharing your expertise, laboratory

space and resources with me and for helping me improve upon my research projects. I also want to thank the members of the Forrester, Bolshan and Green-Johnson groups for always being willing to collaborate and exchange ideas. I am very grateful to Prof. Otto Sanchez and Prof. Chris Wilds, for being part of my committee, and Prof. Janice Strap for chairing it in addition to being a very supportive Graduate Program Director throughout my studies.

I also extend my gratitude to everyone I have had the opportunity to work with at Ontario Tech, the Faculty of Science, and the Applied Bioscience program. This has been my second home for almost 9 years, and my journey would not have been the same without the amazing individuals we have at this institution. I want to thank Annette Tavares, Mary Olaveson and George Stamatiou for the huge impact they have had on my academic journey. Thank you as well to my good friends Sarah, Samira, and Sierra. I am very lucky to have been able to go through this journey with you.

Finally, I would like to thank my loved ones. Words are not enough to express my gratitude, so just know that I truly would not be here without you.

Table of Contents

List of Tables

Chapter 2

Chapter 3

Chapter 4

Chapter 5

List of Figures and Schemes

Figures

Chapter 1

Chapter 2

Chapter 3

Chapter 4

Chapter 5

Schemes

Chapter 3

Chapter 4

Chapter 5

List of Abbreviations and Symbols

2′-F	2′-deoxy-2′-fluoro
2′-OH	2′-hydroxyl
2′-OMe	2′-O-methyl
ACN	Acetonitrile
Ago2	Argonaute 2
ANA	Altritol nucleic acid
ASGPR	Asialoglycoprotein receptor
CD	Circular dichroism
$CDCl_3$	Deuterated chloroform
CeNA	Cyclohexenyl nucleic acid
CH_2Cl_2	Dichloromethane
CPG	Controlled pore glass
CuAAC	Copper(I)-catalyzed azide-alkyne cycloaddition
$CuSO_4$	Copper sulfate
DCC	Dicyclohexylcarbodiimide
DCM	Dichloromethane
DMEM	Dulbecco′s modified eagle medium
DMF	Dimethylformamide
DMSO	Dimethylsulfoxide
DMSO-d6	Deuterated dimethylsulfoxide
DMT	Dimethoxytrityl
DMT-Cl	Dimethoxytrityl chloride
DNA	Deoxyribonucleic acid
EDTA	Ethylenediaminetetraacetic acid
EMAM	Ethanolic methylamine-aqueous methylamine
ESI MS	Electrospray ionization mass spectrometry
Et_3N	Triethylamine

EtOAc	Ethyl acetate
EtOH	Ethanol
FBS	Fetal bovine serum
FDA	Food and Drug Administration
FR	Folate receptor
GalNAc	*n*-acetylgalactosamine
HDL	High-density lipoprotein
HF	Hydrofluoric acid
HNA	Hexitol nucleic acid
HPLC	High-performance liquid chromatography
HRMS	High-resolution mass spectrometry
IFN	Interferon
KCl	Potassium chloride
LAR II	Luciferase Assay Reagent II
LDL	Low-density lipoprotein
LNA	Locked nucleic acid
MALDI-TOF	Matrix-assisted laser desorption/ionization time-of-flight
MeOH	Methanol
$MgCl_2$	Magnesium chloride
mRNA	Messenger RNA
miRNA	MicroRNA
Na_2HPO_4	Disodium phosphate
Na_2SO_4	Sodium sulfate
$NaHCO_3$	Sodium bicarbonate
NH_4OH	Ammonium hydroxide
NMR	Nuclear magnetic resonance
PAGE	Polyacrylamide gel electrophoresis
PAZ	Piwi-Argonaute-Zwille
PBS	Phosphate-buffered saline

PCFT	Proton-coupled folate transporter
PIWI	P-element-induced wimpy testes
PKR	Protein kinase R
PRR	Pattern-recognition receptor
PS	Phosphorothioate
qRT-PCR	Quantitative real-time polymerase chain reaction
RFC	Reduced folate carrier
RIGI	Retinoic acid-inducible gene I
RISC	RNA-induced silencing complex
RNA	Ribonucleic acid
RNAi	RNA interference
RPMI	Roswell Park Memorial Institute
SDOM	Standard deviation of mean
siRNA	Short interfering ribonucleic acid
TBTA	Tris((1-benzyl-4-triazolyl)methyl)amine
TEAA	Triethylammonium acetate
TEG	Triethylene glycol
THF	Tetrahydrofuran
TLR	Toll-like receptor
T_m	Melting temperature
TRBP	Trans-activation response-RNA binding protein
Tris-HCl	Tris(hydroxymethyl)aminomethane hydrochloride
UNA	Unlocked nucleic acid
UTR	Untranslated region

Chapter 1. Introduction

1.1 RNA Interference (RNAi)

RNA interference is an endogenous pathway that utilizes small non-coding RNA molecules to target mRNA and inhibit translation [1]. This mechanism was discovered by Andrew Fire and Craig Mello in 1998 while studying the effect of single-stranded and double-stranded *unc-22* RNA in the nematode *Caenorhabditis elegans* [2]. The *unc-22* gene encodes the myofilament protein twitchin and its downregulation results in a severe twitching phenotype. At the time, it was known that antisense RNA could repress the expression of a target mRNA [3] and that the expression of *unc-22* could be reduced by introduction of sense RNA, which in turned produced antisense RNA in the cell [4]. Fire and Mello established that double-stranded RNA, but not single-stranded RNA, induced the twitching phenotype in *C. elegans* (Figure 1.1).

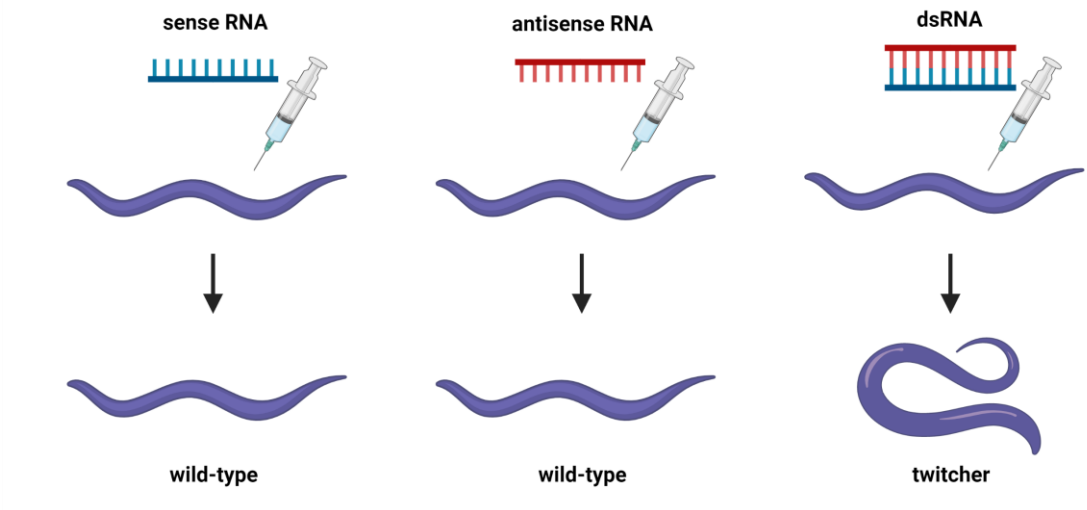

Figure 1.1. Phenotypic effect of injecting single and double-stranded *unc-22* RNA into *C. elegans*. Reduction in *unc-22* activity produces a twitching phenotype, which was observed with double-stranded, but not single-stranded, RNA. Adapted from [5]. Created with BioRender.com.

In a follow-up study, Fire provided evidence to support that dsRNAs achieve gene silencing at the post-transcriptional level [6]. Shortly after, it was shown that 21-nucleotide duplexes can suppress the expression of exogenous and endogenous genes in mammalian and plant cells [7,8]. The discovery of RNAi, and its gene-silencing applications, have been revolutionary and earned Fire and Mello the 2006 Nobel Prize in Physiology or Medicine.

1.1.1 RNAi Mechanism

The endogenous triggers of RNAi include short interfering RNAs (siRNAs) and microRNAs (miRNAs) (Figure 1.2). Long, dsRNA is processed by a Dicer family RNase III enzyme into ~21-23 nucleotide siRNAs, with 3′ overhangs, which are then incorporated into the RNA-induced silencing complex (RISC) [9,10]. It should be noted that the RISC relies on the action of the RISC-loading complex (RLC), a trimeric protein complex composed of Dicer, transactivation response element RNA-binding protein (TRBP) and Argonaute-2 (Ago2), which mediates siRNA loading [11,12]. In the latent complex, Ago2 unwinds and cleaves the duplex between base pairs 9 and 10 relative to the sense strand 5′ end [13]. The active complex retains the antisense strand, which is used as a guide sequence to locate the target mRNA using Watson-Crick complementarity. This mechanism is slightly different with miRNAs. A pri-miRNA is cleaved by Drosha to form a pre-miRNA which is transported to the cytoplasm by Exportin 5 [14] and processed into ~19-25 nucleotide miRNAs, with 3′ overhangs [15]. These miRNAs are loaded into the RISC which unwinds the duplex, retaining the antisense strand. Unlike siRNAs, however, miRNA molecules are only partially complementary to the target mRNA and mediate gene silencing via translational repression and mRNA cleavage [16,17].

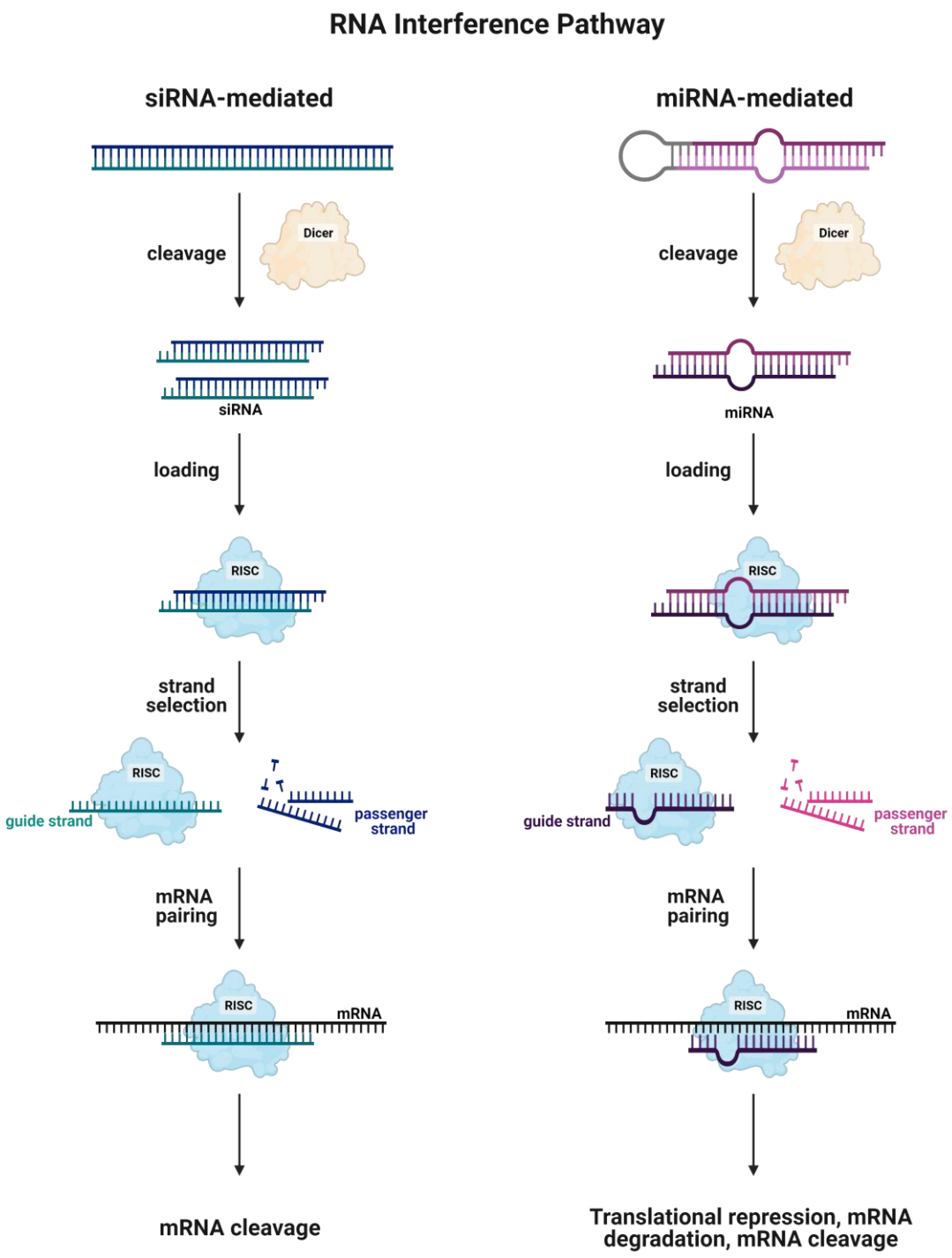

Figure 1.2. Mechanism of RNA interference in mammalian cells mediated by siRNAs (left) and miRNAs (right). Created with BioRender.com.

1.1.2 Argonaute 2 (Ago2)

Human Argonaute proteins can be divided into two subfamilies: AGO and PIWI. AGO includes AGO1, AGO2, AGO3 and AGO4, whereas PIWI includes HIWI1, HIWI2, HIWI3 and HIWI4. AGO proteins are broadly expressed in most tissues whereas PIWI proteins are exclusively expressed in germ-line cells [18]. In the human AGO family, only Ago2 has catalytic activity and plays an essential role within the RNAi pathway [19]. Ago2 is composed of four domains (N, PAZ, MID and PIWI) which adopt a bi-lobe conformation consisting of N-PAZ and MID-PIWI. The N-terminal and PAZ domains are connected by linker L1 while the PAZ and MID domains are connected by linker L2 (Figure 1.3). The groove between the two lobes accommodates the guide strand of the siRNA and the complementary mRNA target [20].

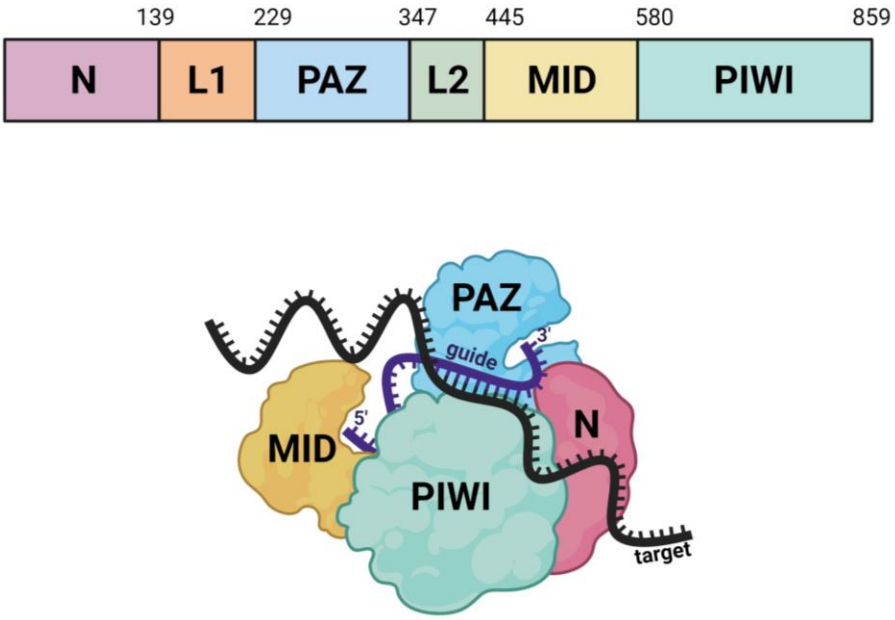

Figure 1.3. Schematic of the human Ago2 primary sequence (top) and model for the siRNA guide strand tethering by Ago2. Adapted from [21]. Created with BioRender.com.

Each Ago2 domain has a distinct role. The N domain is required for RNA loading and assists in unwinding the duplex [22]. The PAZ domain anchors the 3′ dinucleotide overhang. The MID domain provides a binding pocket, between the MID-PIWI interface, for the 5′ monophosphate group. Lastly, the PIWI domain plays a key role in RNA cleavage due to its slicer activity, similar to RNase H [23]. It also harbors a conserved DDH/DDD catalytic core that cleaves the passenger strand of the siRNA duplex [24].

1.1.3 siRNA cleavage by Ago2

The loading of an siRNA duplex into the RISC and subsequent selection of the guide strand are crucial steps for RNAi activity. Under normal conditions, Ago2 mediates the dissociation of the passenger and guide strands by cleaving the phosphodiester bond between nucleotides 9 and 10 from the passenger strand 5′ end [13]. This facilitates the removal of the passenger strand and leaves the guide strand bound to Ago2 (Figure 1.4). Although this is the dominant mechanism for siRNA loading and strand selection, passenger strand cleavage is not required for proper RNAi function. In fact, when mismatches or chemical modifications prevent Ago2 cleavage from occurring, a slower bypass mechanism removes the passenger strand without disrupting RNAi activity [13] (Figure 1.4). Notably, the incorporation of destabilizing chemical modifications within the central region of siRNAs has been shown to promote this bypass mechanism and, in many cases, boost gene-silencing activity [25,26].

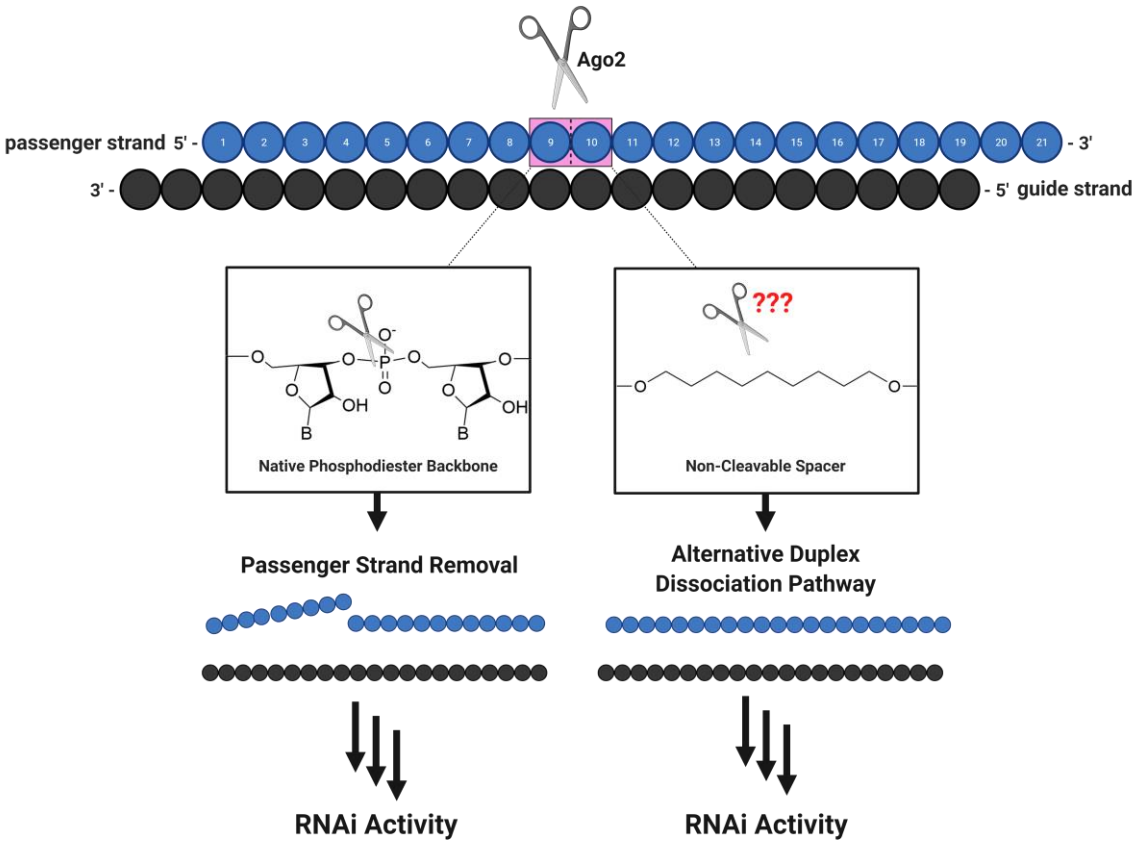

Figure 1.4. Removal of the passenger strand by Ago2 (left) and by the alternative dissociation pathway (right). Created with BioRender.com.

1.2 Limitations of RNAi molecules

Synthetic RNAi molecules can exploit the endogenous RNAi pathway to achieve sequence-specific gene silencing. Because of this, they offer potential applications as both experimental tools and therapeutics. Nevertheless, there are many limitations associated with the inherent nature of RNA which poses challenges like low stability, immunogenicity, off-target effects, and poor cellular uptake.

1.2.1 Low Stability of RNAi molecules

Ribonucleases make up one of the first biological barriers faced by RNAi molecules. Although RNA duplexes are more resistant to enzymatic degradation than single-stranded RNAs, they are still rapidly degraded in human plasma and have a half-life of only a few minutes [27,28]. RNAse A-like enzymes, which are prominently found in blood serum, degrade RNAi molecules by cleaving their phosphodiester backbones [29]. Reports show that local clustering of A/Us, particularly by the 3′ overhangs, strongly enhanced the susceptibility of RNAi molecules toward serum degradation [29]. Therefore, it is of crucial importance to consider both the siRNA design and sequence.

1.2.2 Immunogenicity of RNAi molecules

Another hurdle for RNAi molecules is their potential to activate an innate immune response. Pattern-recognition receptors (PRRs) activate downstream signaling pathways that induce the production of mediators like type I interferon (IFN) and pro-inflammatory cytokines [30]. Although several pathways recognize RNA molecules, the immune response can occur via a Toll-like receptor (TLR)-mediated or a non-Toll-like receptor (non-TLR)-mediated route. The family of TLRs is able to recognize structurally conserved regions associated with foreign pathogens. Out of the TLRs, only TLR3, TLR7 and TLR8 recognize RNA. TLR3 is expressed on the cell surface of blood endothelial cells and recognizes dsRNA [31]. TLR7 and TLR8, on the other hand, are phylogenetically related and are usually expressed in endosomal compartments. These receptors recognize GU-rich short ssRNAs [32,33]. Stimulation of TLR3, TLR7 or TLR8 by a ligand will then trigger the activation of downstream signaling molecules.

Non-TLR-mediated immune responses are triggered when RNA binds to sensor molecules such as protein kinase R (PKR) or retinoic acid-inducible gene I (RIG-I). PKR is an IFN-inducible serine-threonine kinase activated by N-terminal binding to long dsRNA [34,35]. On the other hand, RIG-I is a cytoplasmic RNA helicase that binds to both ssRNA and dsRNA molecules containing uncapped 5′-triphosphates [36,37]. RIG-I activates the mitochondrial antiviral signaling protein (MAVS), which in turn recruits multiple signaling molecules like TRAFs, TBK1 and IRF3/7. This eventually leads the transcriptional upregulation of type I interferons and other proinflammatory cytokines. It should be noted that unlike TLR-mediated immune recognition, RIG-I and PKR recognize RNA in a sequence-independent manner.

1.2.3 Off-target effects of RNAi molecules

Off-target activity of RNAi molecules occurs when there is knockdown of unintended genes, rather than the target gene, and can lead to undesired phenotypes. Because miRNAs only require a 6-base match between their seed sequence (positions 2 to 7 from the 5′ end of the guide strand) and the mRNA 3′ untranslated region (3′ UTR), they can modulate the activity of numerous target genes [38]. On the other hand, siRNAs require a full 19-base match between the guide strand and the mRNA but can still trigger miRNA-like off-target effects if there is partial sequence complementarity of the siRNA to the 3′ UTR [39]. Other mechanisms leading to off-target activity include the induction of an immune response and the saturation of the RNAi machine [40,41].

1.2.4 Cellular uptake and biodistribution of RNAi molecules

Delivery of RNAi molecules to target cells and tissues remains one of the biggest challenges in the development of RNAi therapeutics. Due to their large size, hydrophilic nature and

polyanionic backbone, RNAi molecules are unable to cross the hydrophobic cell membrane and often depend on delivery vehicles or conjugates for transfection [42]. Regardless of the delivery strategy employed, RNAi molecules are generally internalized by endocytosis and must be translocated into the cytoplasm from the late endosome. Unfortunately, many oligonucleotides tend to remain trapped in endosomal compartments, highlighting the importance of optimizing oligonucleotide design not only for cellular uptake but also for endosomal escape [43,44]. Lastly, RNAi molecules display poor biodistribution, accumulating in the liver and kidney, after systemic administration, and resulting in rapid renal clearance [45].

1.3 Chemical Modifications

Chemical modifications provide a means to overcome the limitations associated with the inherent nature of RNAi molecules and have opened doors for the development of safe and effective RNAi therapeutics. Oligonucleotides can be modified at three main sites: the sugar, the nitrogenous base, and the phosphodiester linkage between nucleotides (Figure 1.5). Although numerous chemical modification strategies have been developed and documented, there is no universal modification that simultaneously addresses all the aforementioned challenges. Because of this, it is often necessary to strategically combine several modifications to achieve an optimal oligonucleotide design. However, the specific choice of chemical modifications employed will depend on the oligonucleotide sequence, the chosen delivery platform and intended application [46,47].

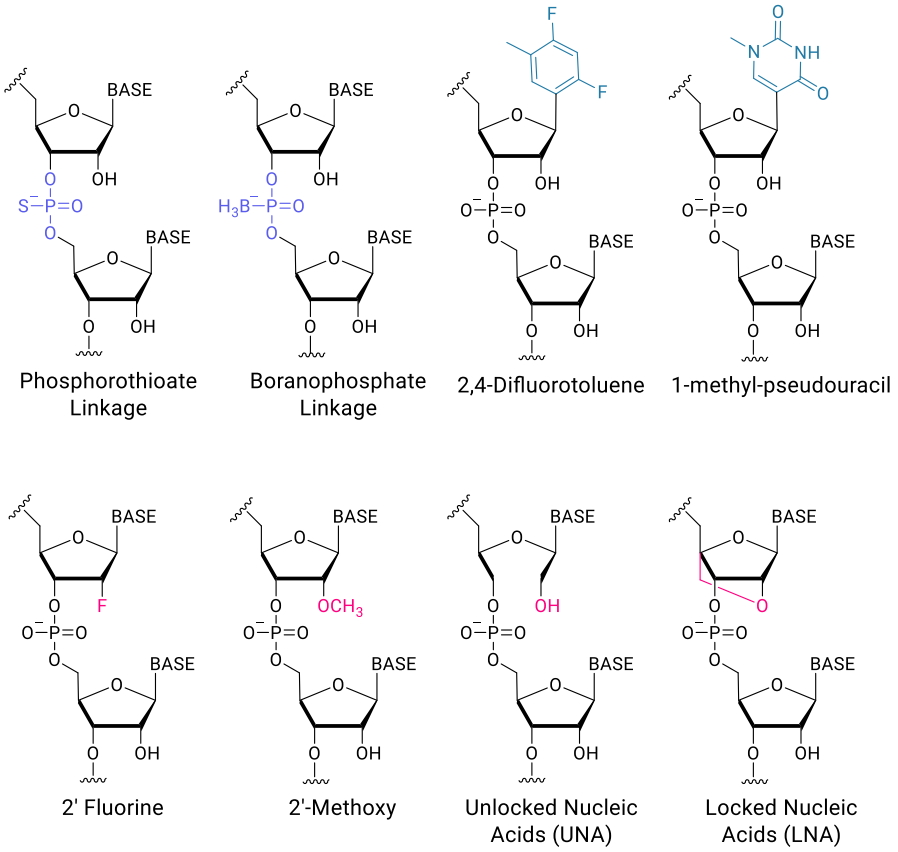

Figure 1.5. Common chemical modifications of the ribose sugar, nitrogenous base, and phosphodiester linkage of RNA.

1.3.1 Backbone Modifications

The native backbone has low stability toward nucleases and is commonly modified by replacing a non-bridging oxygen with sulfur (phosphorothioate) or boron (boranophosphate) groups. The sulfur atom found within the phosphorothioate linkage confers excellent resistance towards nucleases and increases the oligonucleotide′s hydrophobicity and affinity for serum transport proteins [48]. PS linkages are usually incorporated at key positions within the oligonucleotide sequence, as fully modifying the backbone with PS linkages leads to reduced gene-silencing activity [49,50]. Like PS, boranophosphate linkages are incorporated into oligonucleotides to confer resistance to nuclease degradation while maintaining RNAi activity. It has been shown that RNAi

molecules are very tolerant to boranophosphate modifications, as long as they are not incorporated within the central portion of the antisense strand [51].

1.3.2 Nucleobase Modifications

Several nucleobase analogs, with diverse properties, have been reported to date. For example, the incorporation of 2,4-difluorotoluene, an isostere of thymine, within the sense strand of siRNAs has been shown to destabilize nucleic acid duplexes and confer pronounced gene-silencing enhancement [52]. Similarly, pseudouracil modifications have been shown to increase gene silencing while also preventing the immunostimulatory effects often associated with siRNAs [53,54]. Other modifications that show protection against TLR-mediated immune activation include N^6-methyl adenosine and 2-thiouridine [53].

1.3.3 Sugar Modifications

Changes in the 2′-OH of the ribose sugar are well tolerated, as this group is not involved in the catalytic activity of the RISC [55]. Two common modifications are 2′-OMe and 2′-F which preserve the A-form helical structure of the duplex. These modifications also enhance nuclease stability and provide some protection against immune activation [56]. Locked nucleic acids (LNAs) feature a methylene bridge joining the C4′ of the ribose sugar to the 2′-OH that locks the ribose sugar in the 3′-*endo* conformation [57]. A single LNA modification can increase the thermodynamic stability of the duplex by 5-10 °C [50]. When placed at the 3′ ends, LNA modifications also confer resistance against 3′-exonucleases [58]. On the other hand, unlocked nucleic acids (UNAs) lack the covalent bond between C2′ and C3′ of the ribose sugar, which destabilizes the duplex and can facilitate antisense strand loading into the RISC [59,60].

A more recent approach involves the replacement of the ribose with a six-carbon sugar. Altritol nucleic acids (ANA) have a six-membered sugar bearing a 2′-nucleobase and a 3′-OH group [61]. ANA-modified siRNAs adopt the appropriate A-form helical structure recognized by the RISC and display potent activity compared to unmodified siRNAs, particularly when the ANA modification is placed at either 3′ end [62]. Cyclohexenyl nucleic acids (CeNA) and hexitol nucleic acids (HNA) have also shown increased potency well as nuclease stability [62,63], displaying a lot of promise for the development of siRNAs bearing non-native sugar modifications.

1.4 Delivery Vehicles and Bioconjugates

There are two main approaches to mediate the cellular uptake of RNAi molecules: the encapsulation of the oligonucleotide within a delivery vehicle and the conjugation of the oligonucleotide to a targeting ligand. Common delivery vehicles include cationic polymers, liposomes and nanoparticles [64,65]. Unfortunately, many of these require IV administration, display high toxicity *in vivo*, and can only target select tissues [66,67]. In addition, only a 1-2% of the total administered siRNA end up being release into the cytosol, with most of the siRNAs being removed from the cell via exocytosis [68,69]. Altogether, these factors have limited the clinical applications of encapsulated siRNAs.

Another popular delivery strategy involves the conjugation of oligonucleotide to small biomolecules, including lipids, vitamins, and peptides. Some of these bioconjugates are able to mediate cellular uptake through natural transport mechanisms and many are able to improve the pharmacokinetic profiles of RNAi molecules [70]. One of the most well-studied bioconjugates for systemic siRNA delivery is cholesterol, which has been widely used for the functionalization of delivery vehicles and for direct oligonucleotide conjugation. Other

bioconjugates target cell-surface receptors and enable selective delivery to target cells and tissues. The most successful targeting ligand to date is GalNAc, which binds hepatic asialoglycoprotein receptors (ASGPRs) with high affinity [71]. The ASGPR has a recycling time of only 10-15 minutes and can rapidly internalize GalNAc conjugates by receptor-mediated endocytosis [72,73]. A similar strategy involves the use of folate to target folate receptor α (FRα)-expressing cells and tissues. The FRα has become an important biomarker in cancer research, as it is highly overexpressed on the surface of numerous cancers despite being expressed at very low levels in non-malignant tissues. Because of this, there are many clinical applications for FRα targeting in oncology.

1.4.1 Cholesterol

Cholesterol is a hydrophobic biomolecule and an important structural component of cellular membranes. It was one of the first lipophilic conjugate employed for systemic siRNA delivery and it has been shown to increase the bioavailability and half-life of siRNA in serum [74]. Cholesterol conjugates can be internalized by endocytosis, since cholesterol can intercalate into the cellular membrane, or by interactions with lipoprotein receptors like HDL and LDL [75]. Although cholesterol conjugates primarily accumulate in the liver, there are several reports of extrahepatic delivery to tissues like the kidneys, muscles and placenta [76] (Figure 1.6). Cholesterol has also been used to functionalize lipid nanoparticles, including the FDA-approved RNAi-based therapeutic Patisiran [77].

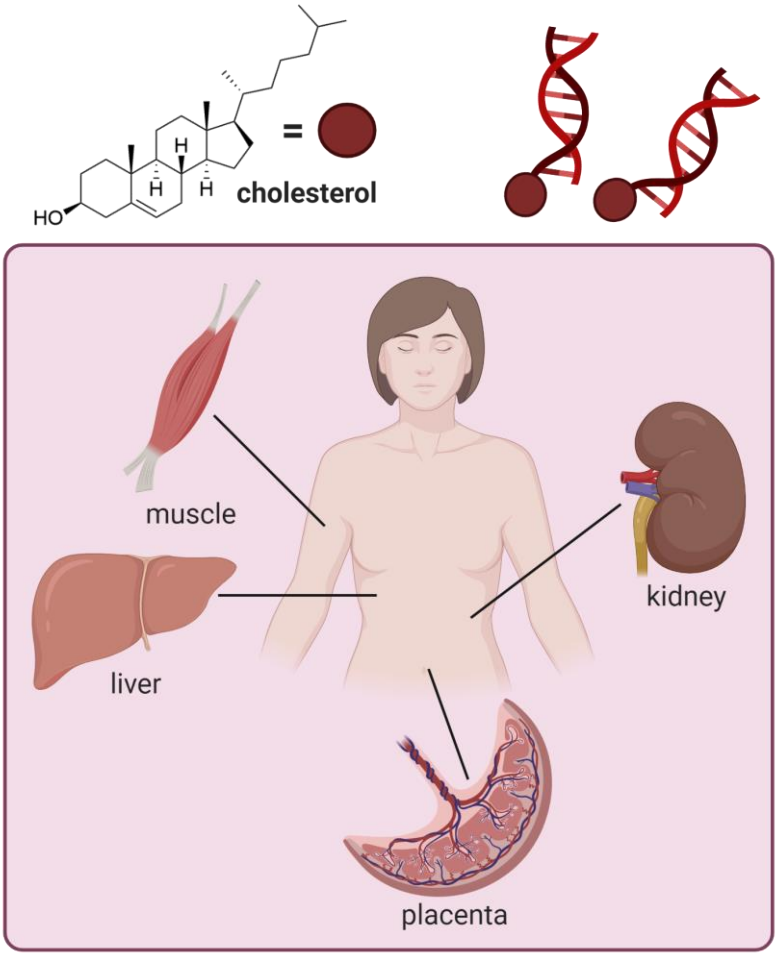

Figure 1.6. Biodistribution of cholesterol-conjugated siRNAs. Created with BioRender.com.

1.4.2 Folate

Folate (vitamin B_9) is an essential nutrient involved in mammalian one-carbon metabolism. It serves as a co-factor in the biosynthesis of purines, thymidine, glycine, serine and methionine [78,79]. The structure of folic acid is illustrated in Figure 1.7. At physiological pH, this molecule is anionic and cannot diffuse across the cellular membrane. Nevertheless, there are several transport mechanisms for folate, and folate derivatives, in mammals (Figure 1.8). The major transport system for folates is the reduced folate carrier (RFC), which is expressed ubiquitously and is responsible for the cellular uptake of folate from the

systemic circulation [80]. The RFC has a high affinity for reduced folates but a low affinity for oxidized folic acid, and it relies on a bidirectional anion-exchange mechanism [81]. On the other hand, the proton-coupled folate transporter (PCFT) functions optimally at low pH (5.0-5.5) and transports folates using a transmembrane proton gradient [82]. The PCFT is mainly expressed in the apical membrane of the duodenum and the proximal jejunum as well as in the placenta, the apical membrane of the kidney and the sinusoidal membrane of the liver [83].

Folate receptors are cell-surface receptors that bind folates with high affinity. There are four known FR isoforms in humans: FRα, FRβ, FRγ and FRδ encoded by *FOLR1*, *FOLR2*, *FOLR3* and *FOLR4*, respectively. The γ isoform is a soluble protein found only in hematopoietic cells whereas the α, β and δ isoforms are all glycosylphosphatidylinositol (GPI)-anchored receptors [84-86]. Although FRα and FRβ share ~70% homology, they have distinct tissue distribution profiles [87]. FRα is the most widely expressed and studied isoform in humans. Because this isoform has minimal physiological roles after embryogenesis, its expression is restricted to tissues involved in folate resorption or embryonic development, including placenta, kidney, and choroid plexus tissues [88-91]. FRβ is expressed on activated myeloid cells involved in inflammatory and autoimmune diseases [92,93] and FR-δ has been found on ova and regulatory T-cells [94].

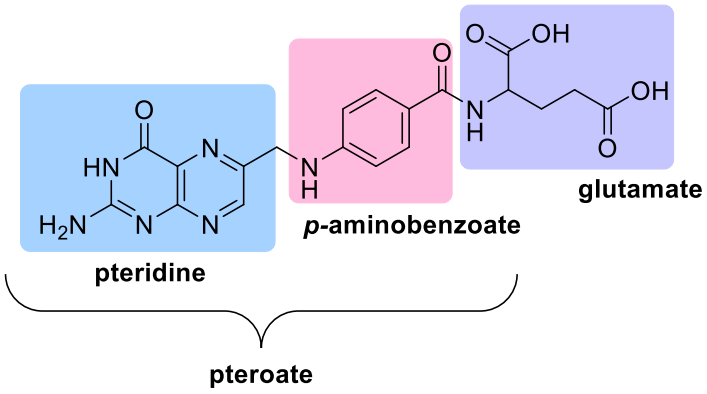

Figure 1.7. Chemical structure of folic acid, highlighting the glutamate moiety and the pteroate moiety (composed of pteridine and *p*-aminobenzoate).

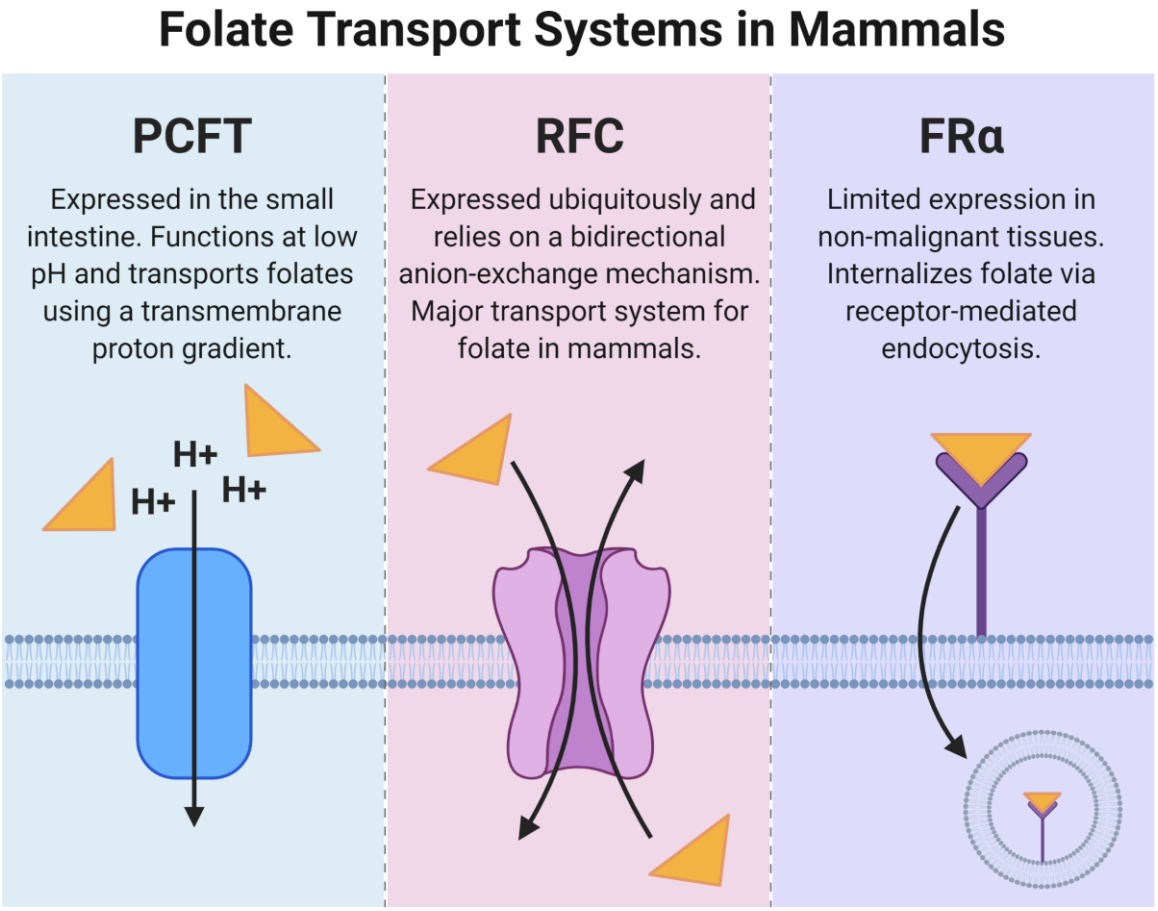

Figure 1.8. Folate transport systems in mammals. PCFT: proton-coupled folate transporter; RFC: reduced folate carrier; FRα: folate receptor α. Created with BioRender.com.

Leamon and Low first described the use of folate conjugation to deliver macromolecules via FRα in 1991 [95]. This has led to the development of numerous clinical applications for FRα targeting, ranging from imaging agents to drug conjugates [96]. Given the success of FRα targeting and the need for extra-hepatic RNAi delivery systems, folate is being investigated as a delivery vector for oligonucleotides.

1.5 RNAi Therapeutics

In August 2018, almost two decades after the discovery of RNAi, Alnylam′s ONPATTRO® (Patisiran) became the first RNAi-based drug to receive US FDA approval. Patisiran targets transthyretin (TTR) and is used for the treatment of hereditary transthyretin amyloidosis (hATTR), a rare genetic condition [77]. Since then, two more RNAi-based drugs, also developed by Alnylam, have received US FDA approval. GIVLAARI® (Givosiran) was approved in November 2019 for the treatment of acute hepatic porphyria [97] and OXLUMO™ (Lumasiran) was approved in November 2020 for the treatment of primary hyperoxaluria type 1 (PH1). Although all these drugs target the liver, they rely on different delivery platforms. Patisiran is administered intravenously and uses a multi-component lipid nanoparticle (LNP) formulation [77]. It has been proposed that apolipoprotein E (ApoE) mediates LNP uptake in the liver (Figure 1.9) [98,99]. In this mechanism, ApoE associates with the LNP and facilitates endocytosis via ApoE-binding cell surface receptors, such as the low-density lipoprotein receptor (LDLR). As the endosome is acidified, the ionizable lipids of the LNP become protonated and interact with the negatively charged endosomal lipids, thus destabilizing the endosomal membrane and causing the disintegration of the LNP [98,99]. On the other hand, Givosiran and Lumasiran are administered subcutaneously and are formulated as modified siRNAs conjugated to a tri-GalNAc ligand [100,101].

GalNAc-siRNA conjugates are internalized via receptor-mediated endocytosis (Figure 1.9). As the endosome is acidified, siRNAs are released into the cytoplasm and the ASGPR is recycled onto the cell surface [101].

Despite recent progress in this field, there is still a significant need to develop safe and effective delivery platforms for extrahepatic targeting. In addition, it is crucial to explore the effect of novel chemical modifications in order to assess their impact on the pharmacokinetic profiles of RNAi molecules.

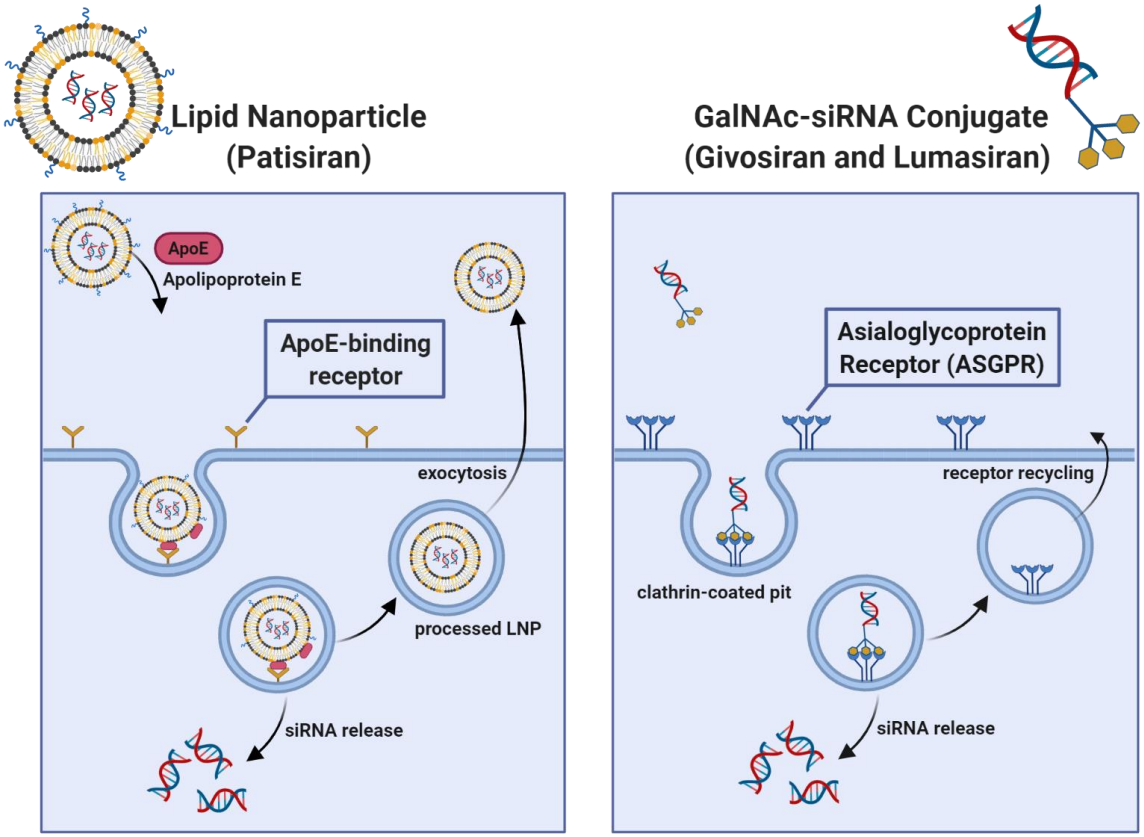

Figure 1.9. Proposed internalization mechanisms of LNP (Patisiran) and GalNAc-siRNA conjugates (Givosiran and Lumasiran). Adapted from [102]. Created with BioRender.com.

1.6 Research Goals and Objectives

RNAi molecules have become potent experimental tools to study gene function due to their ability to silence genes in a sequence-specific manner. More recently, their application has evolved to the development of a novel class of gene-silencing therapeutics that, in many cases, allows for the treatment of rare conditions that otherwise had few therapeutic options available. Unfortunately, there are many limitations associated with the nature and structure of RNAs which have limited their therapeutic applications. These drawbacks can be mitigated with the use of chemical modifications which can improve the pharmacokinetic profiles of RNAi molecules. Despite recent advances in the field, the development of safe and effective delivery systems for siRNAs remains a challenge.

The primary focus of this study involves the investigation of two bioconjugates to mediate siRNA uptake into cells. Cholesterol is an important component of cellular membranes and has been widely employed as a delivery vector for siRNAs. Recently, our lab group reported the synthesis of siRNAs bearing a triazole-linked cholesterol modification at different positions within the sense strand. We hypothesized that these siRNAs can be delivered to cells without the use of transfection reagents while retaining RNAi activity. The first objective was to evaluate the activity of cholesterol-modified siRNAs after carrier-free transfection. Next, we explored a second bioconjugate, folic acid, which binds to cell-surface folate receptors. These receptors are overexpressed on the surface of numerous cancers despite being expressed at low levels in most non-malignant tissues, making folate an ideal ligand for targeted delivery to folate receptor-expressing cancer cells. Nonetheless, we identified the need to boost the gene-silencing activity of folate-siRNA conjugates. The second objective was then to synthesize siRNAs bearing a novel triazole-linked folic acid

modification within the central region of the sense strand and evaluate their ability to mediate selective uptake in cancer cells and overall potency. Folic acid has shown a lot of promise as a vector for targeted cancer therapeutics but the lack of reliable synthetic approaches to prepare folate phosphoramidites has limited their incorporation into oligonucleotides. Based on this, the third objective involved the development of a straightforward and cost-effective strategy to prepare a folate phosphoramidite that was compatible with standard solid-phase oligonucleotide synthesis. Although poor cellular uptake and biodistribution represent the major drawbacks of siRNAs, it is not the only limitation to consider. Unfortunately, there is no single modification that addresses all these challenges, so there is great interest in the development of novel modifications that could be useful for clinical applications. For the final stage of this study, we expanded the scope of our research to investigate the incorporation of a single glucose derivative, triazole-linked to uracil at position 1, within siRNAs. The final objective was then to synthesize a novel glucose phosphoramidite and investigate the gene-silencing efficacy of the resulting duplexes which contained a single 3′-6′/2′-5′ phosphodiester linkage.

1.7 References

1. Hannon GJ. (2002) RNA Interference. Nature 418:244-251.

2. Fire A, S Xu, MK Montgomery, SA Kostas, SE Driver and CC Mello. (1998) Potent and specific genetic interference by double-stranded RNA in Caenorhabditis elegans. Nature 391:806-811.

3. Izant JG and H Weintraub. (1984) Inhibition of thymidine kinase gene expression by anti-sense RNA: a molecular approach to genetic analysis. Cell 36:1007-1015.

4. Fire A, D Albertson, SW Harrison and DG Moerman. (1991) Production of antisense RNA leads to effective and specific inhibition of gene expression in C. elegans muscle. Development 113:503.

5. Advanced Information on The Nobel Prize in Physiology or Medicine 2006. Nobel Assembly at Karolinska Institutet.

6. Montgomery MK, S Xu and A Fire. (1998) RNA as a target of double-stranded RNA-mediated genetic interference in Caenorhabditis elegans. Proc Natl Acad Sci U S A 95:15502-15507.

7. Tuschl T, PD Zamore, R Lehmann, DP Bartel and PA Sharp. (1999) Targeted mRNA degradation by double-stranded RNA in vitro. Genes Dev 13:3191-3197.

8. Elbashir SM, J Harborth, W Lendeckel, A Yalcin, K Weber and T Tuschl. (2001) Duplexes of 21-nucleotide RNAs Mediate RNA Interference in Cultured Mammalian Cells. Nature 411:494-498.

9. Wilson RC and JA Doudna. (2013) Molecular mechanisms of RNA interference. Annu Rev Biophys 42:217-239.

10. Ameres SL and RS Javier Martinez. (2007) Molecular Basis for Target RNA Recognition and Cleavage by Human RISC. Cell 130:101-112.

11. Gredell JA, MJ Dittmer, M Wu, C Chan and SP Walton. (2010) Recognition of siRNA asymmetry by TAR RNA binding protein (TRBP). Biochemistry 49:3148-3155.

12. De N and IJ Macrae. (2011) Purification and assembly of human Argonaute, Dicer, and TRBP complexes. Methods Mol Biol 725:107-119.

13. Matranga C, Y Tomari, C Shin, DP Bartel and PD Zamore. (2005) Passenger-strand Cleavage Facilitates Assembly of siRNA Into Ago2-containing RNAi Enzyme Complexes. Cell 123:607-620.

14. Yi R, Y Qin, IG Macara and BR Cullen. (2003) Exportin-5 mediates the nuclear export of pre-microRNAs and short hairpin RNAs. Genes Dev. 17:3011-3016.

15. Fabian MR and N Sonenberg. (2012) The mechanics of miRNA-mediated gene silencing: a look under the hood of miRISC. Nature Structural and Molecular Biology 19:586–593.

16. Ha M and VN Kim. (2014) Regulation of microRNA biogenesis. Nature Reviews Molecular Cell Biology 15:509-524.

17. van den Berg A, J Mols and J Han. (2008) RISC-target interaction: cleavage and translational suppression. Biochim Biophys Acta 1779:668-677.

18. Meister G. (2013) Argonaute proteins: functional insights and emerging roles. Nature Reviews Genetics 14:447+.

19. Höck J and G Meister. (2008) The Argonaute protein family. Genome Biol 9:210.

20. Kuhn CD and L Joshua-Tor. (2013) Eukaryotic Argonautes come into focus. Trends Biochem Sci 38:263-271.

21. Gavrilov K and WM Saltzman. (2012) Therapeutic siRNA: principles, challenges, and strategies. Yale J Biol Med 85:187-200.

22. Kwak PB and Y Tomari. (2012) The N domain of Argonaute drives duplex unwinding during RISC assembly. Nat Struct Mol Biol 19:145-151.

23. Wang Y, S Juranek, H Li, G Sheng, GS Wardle, T Tuschl and DJ Patel. (2009) Nucleation, propagation and cleavage of target RNAs in Ago silencing complexes. Nature 461:754-761.

24. Zhang X, D Niu, A Carbonell, A Wang, A Lee, V Tun, Z Wang, JC Carrington, C-eA Chang and H Jin. (2014) ARGONAUTE PIWI domain and microRNA duplex structure regulate small RNA sorting in Arabidopsis. Nature Communications 5:5468.

25. Petrova NS, MI Meschaninova, AG Venyaminova, MA Zenkova, VV Vlassov and EL Chernolovskaya. (2011) Silencing activity of 2′ -O-methyl modified anti-MDR1 siRNAs with mismatches in the central part of the duplexes. FEBS Letters 585:2352-2356.

26. Efthymiou TC, B Peel, V Huynh and J-P Desaulniers. (2012) Evaluation of siRNAs that contain internal variable-length spacer linkages. Bioorganic & Medicinal Chemistry Letters 22:5590-5594.

27. Layzer JM, AP McCaffrey, AK Tanner, Z Huang, MA Kay and BA Sullenger. (2004) In vivo activity of nuclease-resistant siRNAs. RNA 10:766-771.

28. Turner JJ, SW Jones, SA Moschos, MA Lindsay and MJ Gait. (2007) MALDI-TOF mass spectral analysis of siRNA degradation in serum confirms an RNAse A-like activity. Molecular BioSystems 3:43-50.

29. Haupenthal J, C Baehr, S Kiermayer, S Zeuzem and A Piiper. (2006) Inhibition of RNAse A family enzymes prevents degradation and loss of silencing activity of siRNAs in serum. Biochem. Pharmacol. 71:702-710.

30. Whitehead KA, JE Dahlman, RS Langer and DG Anderson. (2011) Silencing or stimulation? siRNA delivery and the immune system. Annu Rev Chem Biomol Eng 2:77-96.

31. Cho WG, RJ Albuquerque, ME Kleinman, V Tarallo, A Greco, M Nozaki, MG Green, JZ Baffi, BK Ambati, M De Falco *et al.* (2009) Small interfering RNA-induced TLR3 activation inhibits blood and lymphatic vessel growth. Proc Natl Acad Sci U S A 106:7137-7142.

32. Diebold SS, T Kaisho, H Hemmi, S Akira and C Reis e Sousa. (2004) Innate Antiviral Responses by Means of TLR7-Mediated Recognition of Single-Stranded RNA. Science 303:1529.

33. Heil F, H Hemmi, H Hochrein, F Ampenberger, C Kirschning, S Akira, G Lipford, H Wagner and S Bauer. (2004) Species-Specific Recognition of Single-Stranded RNA via Toll-like Receptor 7 and 8. Science 303:1526.

34. Meurs E, K Chong, J Galabru, NS Thomas, IM Kerr, BR Williams and AG Hovanessian. (1990) Molecular cloning and characterization of the human double-stranded RNA-activated protein kinase induced by interferon. Cell 62:379-390.

35. Clemens MJ and A Elia. (1997) The double-stranded RNA-dependent protein kinase PKR: structure and function. J Interferon Cytokine Res 17:503-524.

36. Yoneyama M, M Kikuchi, T Natsukawa, N Shinobu, T Imaizumi, M Miyagishi, K Taira, S Akira and T Fujita. (2004) The RNA helicase RIG-I has an essential function in double-stranded RNA-induced innate antiviral responses. Nature Immunology 5:730+.

37. Hornung V, J Ellegast, S Kim, K Brzózka, A Jung, H Kato, H Poeck, S Akira, K-K Conzelmann, M Schlee *et al.* (2006) 5'-Triphosphate RNA Is the Ligand for RIG-I. Science 314:994.

38. Jackson AL and PS Linsley. (2010) Recognizing and avoiding siRNA off-target effects for target identification and therapeutic application. Nature Reviews Drug Discovery 9:57+.

39. Lin X, X Ruan, MG Anderson, JA McDowell, PE Kroeger, SW Fesik and Y Shen. (2005) siRNA-mediated off-target gene silencing triggered by a 7 nt complementation. Nucleic acids research 33:4527-4535.

40. Sledz CA, M Holko, MJ de Veer, RH Silverman and BRG Williams. (2003) Activation of the interferon system by short-interfering RNAs. Nature Cell Biology 5:834-839.

41. Persengiev SP, X Zhu and MR Green. (2004) Nonspecific, concentration-dependent stimulation and repression of mammalian gene expression by small interfering RNAs (siRNAs). RNA 10:12-18.

42. Johannes L and M Lucchino. (2018) Current Challenges in Delivery and Cytosolic Translocation of Therapeutic RNAs. Nucleic Acid Therapeutics 28:178-193.

43. Vocelle D, C Chan and SP Walton. (2019) Endocytosis Controls siRNA Efficiency: Implications for siRNA Delivery Vehicle Design and Cell-Specific Targeting. Nucleic Acid Ther. 30:22-32.

44. Hu Y-B, EB Dammer, R-J Ren and G Wang. (2015) The endosomal-lysosomal system: from acidification and cargo sorting to neurodegeneration. Translational Neurodegeneration 4:18.

45. Whitehead KA, R Langer and DG Anderson. (2009) Knocking down barriers: advances in siRNA delivery. Nature Reviews Drug Discovery 8:129-138.

46. Behlke MA. (2008) Chemical modification of siRNAs for in vivo use. Oligonucleotides 18:305-319.

47. Deleavey GF, JK Watts and MJ Damha. (2009) Chemical Modification of siRNA. Current Protocols in Nucleic Acid Chemistry 39:16.13.11-16.13.22.

48. Eckstein F. (2014) Phosphorothioates, essential components of therapeutic oligonucleotides. Nucleic Acid Ther 24:374-387.

49. Prakash TP, CR Allerson, P Dande, TA Vickers, N Sioufi, R Jarres, BF Baker, EE Swayze, RH Griffey and B Bhat. (2005) Positional Effect of Chemical Modifications on Short Interference RNA Activity in Mammalian Cells. Journal of Medicinal Chemistry 48:4247-4253.

50. Braasch DA, S Jensen, Y Liu, K Kaur, K Arar, MA White and DR Corey. (2003) RNA Interference in Mammalian Cells by Chemically-Modified RNA. Biochemistry 42:7967-7975.

51. Hall AH, J Wan, EE Shaughnessy, B Ramsay Shaw and KA Alexander. (2004) RNA interference using boranophosphate siRNAs: structure-activity relationships. Nucleic Acids Res 32:5991-6000.

52. Addepalli H, Meena, CG Peng, G Wang, Y Fan, K Charisse, KN Jayaprakash, KG Rajeev, RK Pandey, G Lavine *et al.* (2010) Modulation of thermal stability can enhance the potency of siRNA. Nucleic acids research 38:7320-7331.

53. Meng Z and M Lu. (2017) RNA Interference-Induced Innate Immunity, Off-Target Effect, or Immune Adjuvant? Frontiers in Immunology 8.

54. Bramsen J and J Kjems. (2012) Development of Therapeutic-Grade Small Interfering RNAs by Chemical Engineering. Frontiers in Genetics, 3:1-22.

55. Chiu Y-L and TM Rana. (2003) siRNA function in RNAi: a chemical modification analysis. RNA 9:1034-1048.

56. Kenski DM, G Butora, AT Willingham, AJ Cooper, W Fu, N Qi, F Soriano, IW Davies and WM Flanagan. (2012) siRNA-optimized Modifications for Enhanced In Vivo Activity. Molecular Therapy - Nucleic Acids 1.

57. Deleavey GF and MJ Damha. (2012) Designing Chemically Modified Oligonucleotides for Targeted Gene Silencing. Chemistry & Biology 19:937-954.

58. Elmén J, H Thonberg, K Ljungberg, M Frieden, M Westergaard, Y Xu, B Wahren, Z Liang, H Ørum, T Koch *et al.* (2005) Locked nucleic acid (LNA) mediated improvements in siRNA stability and functionality. Nucleic Acids Res 33:439-447.

59. Langkjær N, A Pasternak and J Wengel. (2009) UNA (unlocked nucleic acid): A flexible RNA mimic that allows engineering of nucleic acid duplex stability. Bioorganic & Medicinal Chemistry 17:5420-5425.

60. Campbell MA and J Wengel. (2011) Locked vs. unlocked nucleic acids (LNA vs. UNA): contrasting structures work towards common therapeutic goals. Chem Soc Rev 40:5680-5689.

61. Kumar P, R Degaonkar, DC Guenther, M Abramov, G Schepers, M Capobianco, Y Jiang, J Harp, C Kaittanis, MM Janas *et al.* (2020) Chimeric siRNAs with chemically modified pentofuranose and hexopyranose nucleotides: altritol-nucleotide (ANA) containing GalNAc-siRNA conjugates: in vitro and in vivo RNAi activity and resistance to 5′-exonuclease. Nucleic Acids Research 48:4028-4040.

62. Fisher M, M Abramov, A Van Aerschot, J Rozenski, V Dixit, RL Juliano and P Herdewijn. (2009) Biological effects of hexitol and altritol-modified siRNAs targeting B-Raf. Eur J Pharmacol 606:38-44.

63. Herdewijn P. (2000) Heterocyclic modifications of oligonucleotides and antisense technology. Antisense Nucleic Acid Drug Dev 10:297-310.

64. Lee J-M, T-J Yoon and Y-S Cho. (2013) Recent Developments in Nanoparticle-Based siRNA Delivery for Cancer Therapy. BioMed Research International 2013:782041.

65. Song H, SL Hart and Z Du. (2021) Assembly strategy of liposome and polymer systems for siRNA delivery. Int. J. Pharm. 592:120033.

66. Vlashi E, LE Kelderhouse, JE Sturgis and PS Low. (2013) Effect of Folate-Targeted Nanoparticle Size on Their Rates of Penetration into Solid Tumors. ACS Nano 7:8573-8582.

67. Xue HY, S Liu and HL Wong. (2014) Nanotoxicity: a key obstacle to clinical translation of siRNA-based nanomedicine. Nanomedicine (Lond) 9:295-312.

68. Sahay G, W Querbes, C Alabi, A Eltoukhy, S Sarkar, C Zurenko, E Karagiannis, K Love, D Chen, R Zoncu *et al.* (2013) Efficiency of siRNA delivery by lipid nanoparticles is limited by endocytic recycling. Nat. Biotechnol. 31:653-658.

69. Gilleron J, W Querbes, A Zeigerer, A Borodovsky, G Marsico, U Schubert, K Manygoats, S Seifert, C Andree, M Stöter *et al.* (2013) Image-based analysis of lipid nanoparticle–mediated siRNA delivery, intracellular trafficking and endosomal escape. Nat. Biotechnol. 31:638-646.

70. Osborn MF and A Khvorova. (2018) Cholesteryl-conjugated oligonucleotides: synthesis, properties, and activity as inhibitors of replication of human immunodeficiency. Nucleic Acid Ther. 28:128-136.

71. Willoughby JLS, A Chan, A Sehgal, JS Butler, JK Nair, T Racie, S Shulga-Morskaya, T Nguyen, K Qian, K Yucius *et al.* (2018) Evaluation of GalNAc-siRNA Conjugate Activity in Pre-clinical Animal Models with Reduced Asialoglycoprotein Receptor Expression. Mol Ther 26:105-114.

72. Schwartz AL, SE Fridovich and HF Lodish. (1982) Kinetics of internalization and recycling of the asialoglycoprotein receptor in a hepatoma cell line. Journal of Biological Chemistry 257:4230-4237.

73. Spiess M. (1990) The asialoglycoprotein receptor: a model for endocytic transport receptors. Biochemistry 29:10009-10018.

74. Soutschek J, A Akinc, B Bramlage, K Charisse, R Constien, M Donoghue, S Elbashir, A Geick, P Hadwiger, J Harborth *et al.* (2004) Therapeutic silencing of an endogenous gene by systemic administration of modified siRNAs. Nature 432:173-178.

75. Gaibelet G, S Allart, F Tercé, V Azalbert, J Bertrand-Michel, S Hamdi, X Collet and S Orlowski. (2015) Specific cellular incorporation of a pyrene-labelled cholesterol: lipoprotein-mediated delivery toward ordered intracellular membranes. PLoS One 10:e0121563.

76. Biscans A, A Coles, R Haraszti, D Echeverria, M Hassler, M Osborn and A Khvorova. (2018) Diverse lipid conjugates for functional extra-hepatic siRNA delivery in vivo. Nucleic Acids Res. 47:1082-1096.

77. Adams D, A Gonzalez-Duarte, WD O'Riordan, CC Yang, M Ueda, AV Kristen, I Tournev, HH Schmidt, T Coelho, JL Berk *et al.* (2018) Patisiran, an RNAi Therapeutic, for Hereditary Transthyretin Amyloidosis. N Engl J Med 379:11-21.

78. Choi S-W and JB Mason. (2000) Folate and Carcinogenesis: An Integrated Scheme. The Journal of Nutrition 130:129-132.

79. Ducker GS and JD Rabinowitz. (2017) One-Carbon Metabolism in Health and Disease. Cell Metab. 25:27-42.

80. Zhao R, N Diop-Bove, M Visentin and ID Goldman. (2011) Mechanisms of membrane transport of folates into cells and across epithelia. Annu. Rev. Nutr. 31:177-201.

81. Zhao R, R Seither, K Brigle, I Sharina, P Wang and I Goldman. (1997) Impact of Overexpression of the Reduced Folate Carrier (RFC1), an Anion Exchanger, on Concentrative Transport in Murine L1210 Leukemia Cells. The Journal of biological chemistry 272:21207-21212.

82. Desmoulin SK, Z Hou, A Gangjee and LH Matherly. (2012) The human proton-coupled folate transporter: Biology and therapeutic applications to cancer. Cancer biology & therapy 13:1355-1373.

83. Zhao R and ID Goldman. (2013) Folate and thiamine transporters mediated by facilitative carriers (SLC19A1-3 and SLC46A1) and folate receptors. Mol. Aspects Med. 34:373-385.

84. Ledermann JA, S Canevari and T Thigpen. (2015) Targeting the folate receptor: diagnostic and therapeutic approaches to personalize cancer treatments. Annals of Oncology 26:2034-2043.

85. Sabharanjak S and S Mayor. (2004) Folate receptor endocytosis and trafficking. Adv. Drug Del. Rev. 56:1099-1109.

86. Mironava T, M Simon, MH Rafailovich and B Rigas. (2013) Platinum folate nanoparticles toxicity: cancer vs. normal cells. Toxicol. In Vitro 27:882-889.

87. Lynn RC, M Poussin, A Kalota, Y Feng, PS Low, DS Dimitrov and DJP Jr. (2015) Targeting of folate receptor β on acute myeloid leukemia blasts with chimeric antigen receptor–expressing T cells. Blood 125:3466-3476.

88. O'Shannessy DJ, EB Somers, L-c Wang, H Wang and R Hsu. (2015) Expression of folate receptors alpha and beta in normal and cancerous gynecologic tissues: correlation of expression of the beta isoform with macrophage markers. Journal of Ovarian Research 8.

89. Weitman SD, RH Lark, LR Coney, DW Fort, V Frasca, VRZ Jr and BA Kamen. (1992) Distribution of the Folate Receptor GP38 in Normal and Malignant Cell Lines and Tissues. Cancer Res. 52:3396-3401.

90. Parker N, MJ Turk, E Westrick, JD Lewis, P Low and CP Leamon. (2005) Folate receptor expression in carcinomas and normal tissues determined by a quantitative radioligand binding assay. Anal. Biochem. 338:284-293.

91. Chen C, J Ke, XE Zhou, W Yi, JS Brunzelle, J Li, E-L Yong, HE Xu and K Melcher. (2013) Structural Basis for Molecular Recognition of Folic Acid by Folate Receptors. Nature 500:486-489.

92. Fernández M, F Javaid and V Chudasama. (2018) Advances in targeting the folate receptor in the treatment/imaging of cancers. Chemical Science 9:790-810.

93. Shen J, Y Hu, KS Putt, S Singhal, H Han, DW Visscher, LM Murphy and PS Low. (2018) Assessment of folate receptor alpha and beta expression in selection of lung and pancreatic cancer patients for receptor targeted therapies. Oncotarget 9:4485-4495.

94. Tian Y, G Wu, J-C Xing, J Tang, Y Zhang, Z-M Huang, Z-C Jia, R Zhao, Z-Q Tian, S-F Wang *et al.* (2009) A novel splice variant of folate receptor 4 predominantly expressed in regulatory T cells. BMC Immunol. 13.

95. Leamon CP and PS Low. (1991) Delivery of macromolecules into living cells: a method that exploits folate receptor endocytosis. Proc. Natl. Acad. Sci. U. S. A. 88:5572-5576.

96. Salim L and JP Desaulniers. (2021) To Conjugate or to Package? A Look at Targeted siRNA Delivery Through Folate Receptors. Nucleic Acid Ther 31:21-38.

97. Scott LJ. (2020) Givosiran: First Approval. Drugs 80:335-339.

98. Zhang X, V Goel and GJ Robbie. (2019) Pharmacokinetics of Patisiran, the First Approved RNA Interference Therapy in Patients With Hereditary Transthyretin‐Mediated Amyloidosis. The Journal of Clinical Pharmacology 60:573-585.

99. Cullis PR and MJ Hope. (2017) Lipid Nanoparticle Systems for Enabling Gene Therapies. Mol Ther 25:1467-1475.

100. Ashwell G and AG Morell. (1974) The Role of Surface Carbohydrates in the Hepatic Recognition and Transport of Circulating Glycoproteins. Advances in Enzymology and Related Areas of Molecular Biology 41:99-128.

101. Springer AD and SF Dowdy. (2018) GalNAc-siRNA Conjugates: Leading the Way for Delivery of RNAi Therapeutics. Nucleic Acid Ther. 23:109-118.

102. Salim L and J-P Desaulniers. (2020) To Conjugate or to Package? A Look at Targeted siRNA Delivery Through Folate Receptors. Nucleic Acid Ther. 31:21-38.

Chapter 2. Manuscript I

Effective Carrier-free Gene-silencing Activity of Cholesterol-modified siRNAs

Lidya Salim, Chris McKim and Jean-Paul Desaulniers

Published in:

RSC Advances **2018**, *8*, 22963–22966

DOI: 10.1039/c8ra03908a

2.1 Abstract

The use of short interfering RNAs (siRNAs) as therapeutics holds great promise, but chemical modifications must first be employed to improve their pharmacokinetic properties. This study evaluates the in vitro cellular uptake and knock-down efficacy of cholesterol-modified triazole-linked siRNAs targeting firefly luciferase in the absence of a transfection carrier. These siRNAs displayed low cytotoxicity and excellent dose-dependent knockdown in HeLa cells in the 500 to 3000 nM concentration range, with a 70–80% reduction in firefly luciferase activity. Our results indicate that this modification is compatible with the RNA interference pathway and is less cytotoxic and more effective than a commercially available triethylene glycol (TEG) cholesterol modification.

2.2 Introduction

RNA interference (RNAi) is an endogenous pathway that utilizes double-stranded RNA to suppress translation, resulting in sequence-specific gene silencing [1]. The initial step involves cleavage of long double-stranded RNA into smaller 21–23 nucleotide fragments, termed short interfering RNAs (siRNAs), which are incorporated into the RNA-induced silencing complex (RISC) [2]. RISC unwinds and dissociates the duplex, retaining the antisense strand which is used as a guiding sequence to recognize and degrade complementary mRNA [2,3]. Since many diseases are characterized by aberrant gene expression, the use of siRNAs as therapeutics holds great promise [4,5]. Unfortunately, there are some limitations associated with the structure of siRNAs, including low stability, poor cellular uptake and off-target effects, which must be addressed in order to harness the full potential of RNAi therapeutics [6,7]. Although several chemical modifications have

been employed to improve the pharmacological properties of siRNAs, there is still no universal modification able to simultaneously improve all of these limitations [8,9].

Due to their large size and anionic backbone, siRNAs have difficulties crossing cellular membranes. Therefore, several delivery systems and carriers have been investigated, including viral vectors, cationic polymers and liposomes [10-13]. Another strategy involves direct conjugation of siRNAs to small molecules such as GalNAc or hydrophobic molecules to enhance cellular uptake [14]. Cholesterol is a hydrophobic biomolecule and a key component of cellular membranes, as it helps maintain their integrity [15]. Various cholesterol-conjugated drugs and anticancer agents have been studied and have demonstrated enhanced pharmacokinetic profiles, bioavailability and delivery [16,17]. Cholesterol modifications have also been successful at increasing siRNA lipophilicity and improving cellular uptake without the need of transfection carriers [18-20].

Recently, our group reported a straightforward synthesis of a cholesterol phosphoramidite, bound covalently to a spacer via a triazole linkage [21]. This cholesterol-bearing spacer was then incorporated within the central region of the siRNA sense strand through solid-phase RNA synthesis [21]. Our biological studies in HeLa cells showed that these siRNAs were able to downregulate exogenous firefly luciferase mRNA in a dose-dependent manner using the transfection carrier Lipofectamine 2000™. In this study, we further investigate the biological activity and gene-silencing efficacy of these siRNAs in the absence of a transfection carrier. Figure 2.1 compares the structure of native RNA with our cholesterol-modified triazole-linked spacer (X) and a commercially available 3′-end triethylene glycol cholesterol (Chol-TEG) modification.

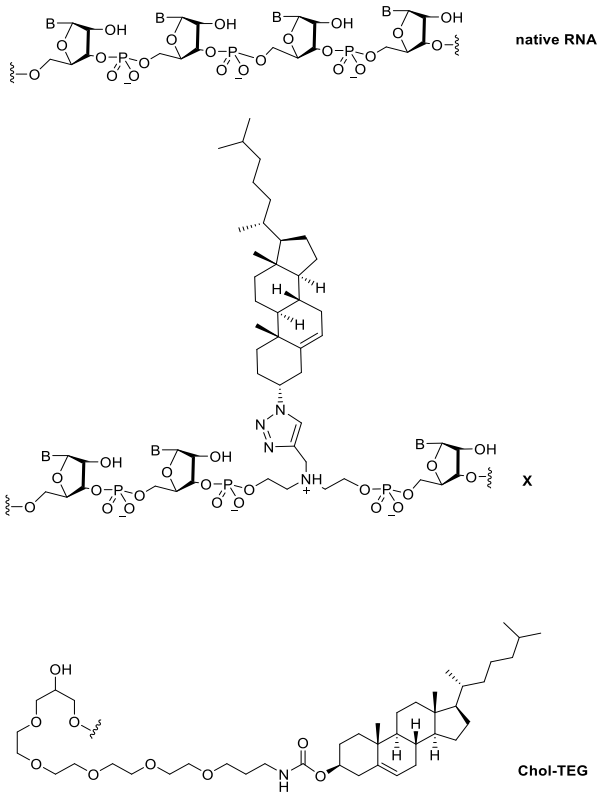

Figure 2.1 Structural differences between native RNA, cholesterol-modified triazole-linked spacer (**X**) and the commercially available 3′-end cholesterol triethylene glycol (**Chol-TEG**) modification.

2.3 Materials and Methods

2.3.1 General Methods

Unless otherwise stated, all starting reagents were obtained from commercial sources without additional purification. Cholesterol oligonucleotides (X1, X2 and X5) were synthesized as described [21]. Oligonucleotide antisense strands and CHOL-TEG RNA sequences were purchased from and characterized by Integrated DNA Technologies (IDT). Equimolar amounts of sense and antisense RNAs were incubated at 95 °C for 2 min in a binding buffer (75.0 mM KCl, 50.0 mM Tris-HCl, 3.00 mM $MgCl_2$, pH 8.30). This solution was cooled slowly to room temperature, allowing the siRNAs to anneal.

2.3.2 Procedure for Characterizing Oligonucleotides through ESI Q-TOF

All single-stranded RNAs (ssX1, ssX2, and ssX5) were gradient eluted through a Zorbax Extend C18 HPLC column with a MeOH/H_2O (5:95) solution containing 200 mM hexafluoroisopropyl alcohol and 8.1 mM triethylamine, and finally with 70% MeOH. The eluted RNAs were subjected to ESI-MS (ES-), producing raw spectra of multiply charged anions and through resolved isotope deconvolution, the molecular weights of the resultant neutral oligonucleotides were confirmed. The final neutral mass of the RNAs were confirmed using this method.

2.3.3 Procedure for HPLC Characterization

HPLC was performed using a C18 4.6 mm x 150 mm reverse phase column on a Waters 1525 Binary HPLC Pump with a Waters 2489 UV/Visible Detector, eluting from 5% to 95% ACN in 0.1 M TEAA buffer (pH: 7). Spectra were processed using the Empower 3 software.

2.3.4 Procedure for Sub-culturing HeLa cells

Biological assays were performed using the human epithelial cervix carcinoma cell line HeLa. Cells were maintained in DMEM supplemented with 10% FBS and 1% penicillin-streptomycin (Sigma) and incubated at 37 °C with 5% CO_2. Once they reached 80-90% confluency, cells were passaged and diluted to a concentration of $1x10^6$ cells/mL. To continue the cell line, 1 mL of this was added to a new cell culture flask containing 24 mL DMEM (10% FBS, 1% penicillin-streptomycin).

2.3.5 Procedure for *in vitro* Dual-Reporter Luciferase Assay in the presence of a Transfection Reagent

Prior to transfection, HeLa cells were seeded on 12-well plates (Falcon®) containing 1 mL DMEM (10% FBS, 1% penicillin-streptomycin) at a density of 100,000 cells per well. Cells were incubated at 37 ºC with 5% CO_2 for 24 hours until they reached 90% confluence. Then, varying concentrations of anti-luciferase siRNAs (8, 80 and 800 pM) were co-transfected with both pGL3 and pRLSV40 luciferase-expressing plasmids using Lipofectamine 2000™ (Invitrogen) in 1X Gibco′s Opti-Mem Reduced Serum according to the manufacturer′s protocol. Cells were incubated for an additional 24 hours at 37 ºC in 5% CO_2. The medium was discarded, cells were washed twice with 1X PBS and lysed with 1X passive lysis buffer (Promega) over a 20-minute period at room temperature. Cell lysates were loaded onto white and opaque 96-well plates (Costar) in triplicate. Using the Dual-Luciferase® Reporter Kit (Promega), Lar II and Stop & Glo® substrates were added to the cell lysates and enzymatic activity of firefly and *Renilla* luciferase vectors were measured independently using a Synergy HT (Bio-Tek) plate luminometer. The ratio of firefly/*Renilla* luminescence expressed as a percentage relates the reduction in firefly expression to siRNA efficacy when compared to untreated controls. Each data point represents the average of at least two independent assays, each with three technical replicates, with the indicated error (SDOM). The IC_{50} values were determined with Prism using the variable slope model when the log(inhibitor) was plotted against normalized expression.

2.3.6 Procedure for *in vitro* Dual-Reporter Luciferase Assay in the Absence of a Transfection Reagent

Prior to transfection, HeLa cells were seeded on 24-well plates (Falcon®) containing 350 μL DMEM (10% FBS, 1% penicillin-streptomycin) at a density of 50,000 cells per well. Cells were incubated at 37 ºC with 5% CO_2 for 24 hours until they reached 90% confluence. Then, cells were co-transfected with both pGL3 and pRLSV40 luciferase-expressing plasmids using Lipofectamine 2000™ (Invitrogen) in 1X Gibco′s Opti-Mem Reduced Serum according to the manufacturer′s protocol. Cells were incubated for 4 hours at 37 ºC in 5% CO_2 after which the growth medium was discarded and each well was washed twice with 1 mL of 1X PBS to ensure that no transfection reagent remained in solution. 50 μL DMEM (10% FBS, 1% penicillin-streptomycin) was then added to each well. Anti-luciferase siRNA treatments were prepared by adding 1 μL of the respective siRNA to 20 μL 1X Gibco′s Opti-Mem Reduced Serum. Each treatment was added to the respective well, at concentrations of 1, 5, 10, 25, 50, 250, 500, 1000, 2000 and 3000 nM. Cells were incubated for an additional 16 hours at 37 ºC in 5% CO_2 before cell lysing. Luciferase activity was assessed as described above. Each value is the average of at least 3 different experiments with the indicated error (SDOM). The IC_{50} values were determined with Prism using the variable slope model when the log(inhibitor) was plotted against normalized expression.

2.3.7 Procedure for XTT cell viability assay

Cellular viability after siRNA treatment was determined using the XTT Cell Proliferation Assay Kit (ATCC®). Prior to transfection, HeLa cells were seeded on 96-well plates (Falcon®) containing 150 μL DMEM (10% FBS, 1% penicillin-streptomycin) at a density

of 2,500 cells per well. Cells were incubated at 37 °C in 5% CO_2 for 24 hours, after which they were co-transfected with pGL3 and pRLSV40 luciferase-expressing plasmids and incubated for an additional 4 hours, as previously described. After this incubation period, the growth medium was discarded, and each well was washed twice with 250 μL 1X PBS. Cells were then treated in triplicate with varying concentrations (1, 5, 10, 25, 50, 250, 500, 1000, 2000 and 3000 nM) of each siRNA and then incubated for an additional 24 hours at 37 °C with 5% CO_2 before treatment with 50 μL of XTT reagent, activated with 2% N-methyl dibenzopyrazine methyl sulfate. Cells were incubated for 2 hours at 37 °C with 5% CO_2. Absorbance was measured at 475 nm and 660 nm using a Synergy HT (BioTek) microplate reader. Specific absorbance was calculated: A_{475nm} (experimental) – A_{475nm} (Blank) – A_{660nm} (experimental). Results were normalized to an untreated control.

2.4 Results

2.4.1 Thermal Stability of Oligonucleotides

All siRNAs target firefly luciferase. **X1** and **X2** contain the triazole-linked cholesterol modification within the central region of the sense strand (positions 9 and 10 from the 5′-end, respectively). **X5** contains the triazole-linked cholesterol modification at the 3′-end of the sense strand. **Chol-TEG** contains the commercially available 3′-end triethylene glycol cholesterol derivative. The thermal stability of each duplex is reported in Table 2.1.

Table 2.1 Sequences and T_m data of anti-luciferase cholesterol siRNAs

RNA	Duplex	T_m	ΔT_m
wt	5′-CUUACGCUGAGUACUUCGAtt-3′ 3′-ttGAAUGCGACUCAUGAAGCU-5′	72.7	-
X1	5′-CUUACGCU**X**AGUACUUCGAtt-3′ 3′-ttGAAUGCGACUCAUGAAGCU-5′	61.6	-11.1
X2	5′-CUUACGCUG**X**GUACUUCGAtt-3′ 3′-ttGAAUGCGACUCAUGAAGCU-5′	62.5	-10.2
X5	5′-CUUACGCUGAGUACUUCGA**X**t-3′ 3′-ttGAAUGCGACUCAUGAAGCU-5′	69.8	-2.9
Chol-TEG	5′-CUUACGCUGAGUACUUCGAtt**Ch**-3′ 3′-ttGAAUGCGACUCAUGAAGCU-5′	65.3	-6.7

X corresponds to the triazole-linked cholesterol modification. **Ch** corresponds to the commercial cholesterol-TEG modification. The top strand corresponds to the sense strand; the bottom strand corresponds to the antisense strand.

2.4.2 Silencing Activity of siRNAs after Transfection with Lipofectamine 2000™

To first ensure that the siRNAs used in this study were effective in silencing firefly luciferase, a gene-silencing assay was conducted using Lipofectamine 2000™ as a transfection carrier (Figure 2.2). These siRNAs show effective gene-silencing activity in a dose-dependent manner at low concentrations (8 to 800 pM).

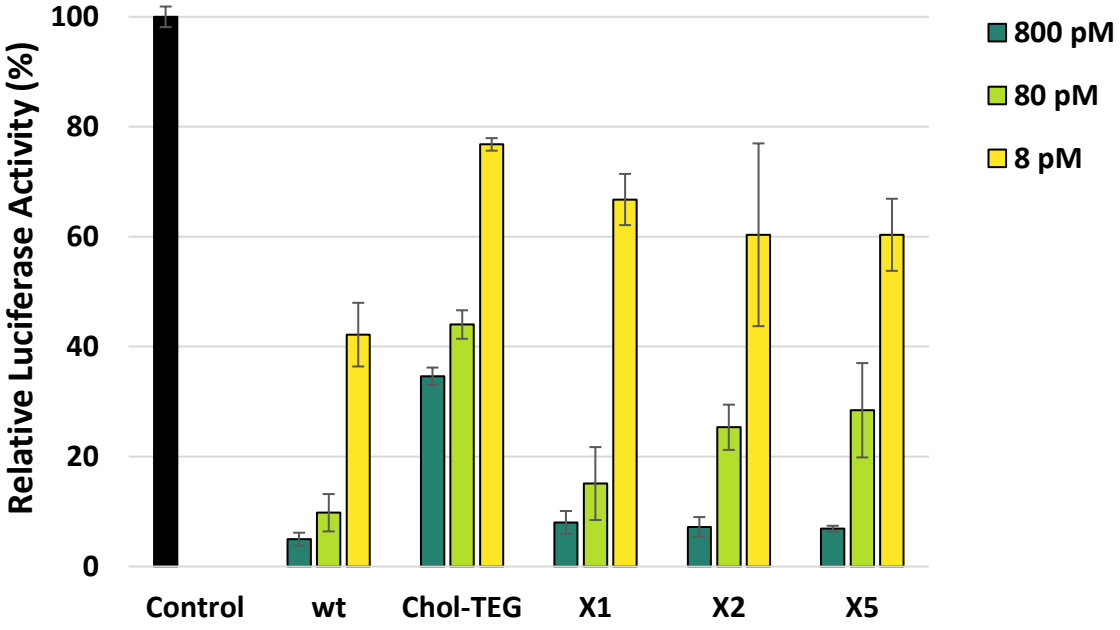

Figure 2.2 Silencing activity of wt and cholesterol siRNAs after transfection with Lipofectamine 2000™. All siRNAs were tested in HeLa cells at 8, 80 and 800 pM concentrations. Firefly luciferase expression was normalized to *Renilla* luciferase.

2.4.3 Silencing Activity of siRNAs after Carrier-Free Transfection

In the absence of a transfection carrier, as observed in Figure 2.3, the cholesterol-modified triazole-linked siRNAs (**X1**, **X2**, and **X5**) exhibited potent gene silencing, with 70–80% reduction in firefly luciferase activity in the 500 to 3000 nM concentration range. The calculated IC_{50} values are summarized in Table 2.2.

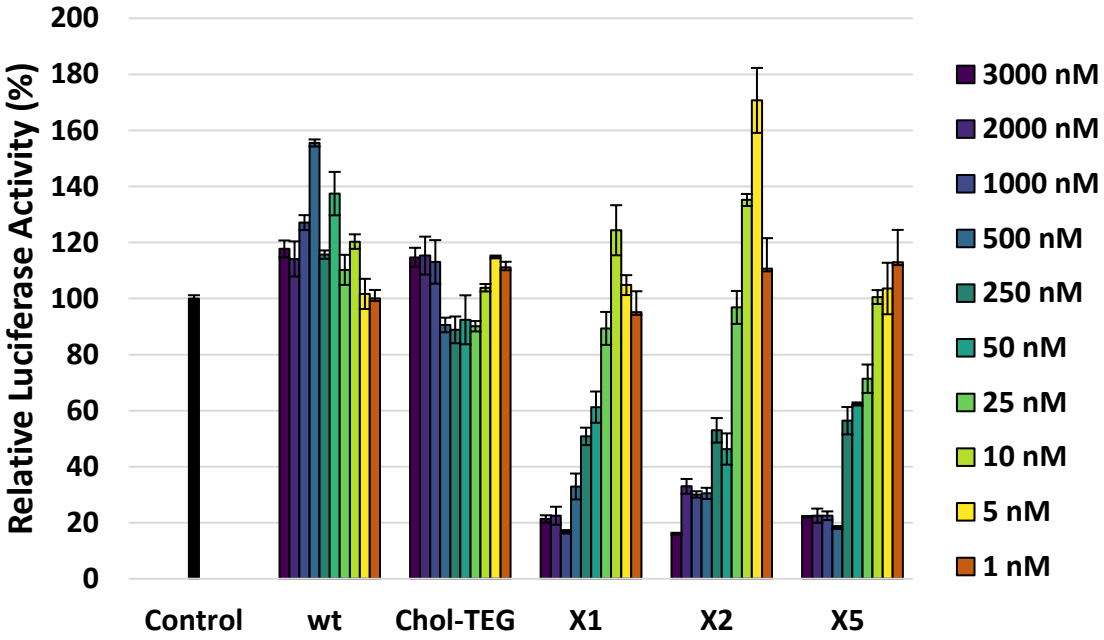

Figure 2.3. Silencing activity of wt and cholesterol siRNAs after carrier-free transfection. All siRNAs were tested in HeLa cells at concentrations ranging from 1 to 3000 nM. Firefly luciferase expression was normalized to *Renilla* luciferase.

Table 2.2 IC_{50} data of cholesterol siRNAs after carrier-free transfection

RNA	Sense Strand Sequence	IC_{50}
wt	5′-CUUACGCUGAGUACUUCGAtt-3′	inactive
X1	5′-CUUACGCU**X**AGUACUUCGAtt-3′	243.6
X2	5′-CUUACGCUG**X**GUACUUCGAtt-3′	307.1
X5	5′-CUUACGCUGAGUACUUCGA**X**t-3′	189.2
Chol-TEG	5′-CUUACGCUGAGUACUUCGAtt**Ch**-3′	inactive

X corresponds to the single triazole-linked cholesterol modification. **Ch** corresponds to the commercial TEG modification. IC_{50} values were calculated after siRNA transfection in a carrier-free environment.

2.4.4 Cell Viability after siRNA Treatment

The XTT reagent is reduced by mitochondrial succinic dehydrogenase in metabolically active cells to a highly pigmented formazan derivative. The absorbance of this product can

be quantified and used to assess cellular viability. As seen in Figure 2.4, siRNAs bearing the **X** spacer (siRNAs **X1**, **X2** and **X5**) cause minimal toxicity even at high concentrations. HeLa cells treated with 3000 nM **wt** siRNA show a 20–30% decrease in viability compared to cells treated with our cholesterol-modified siRNAs. In addition, high concentrations (1000–3000 nM) of **Chol-TEG** siRNA imparted high cytotoxicity, causing a 60–80% reduction in cell viability.

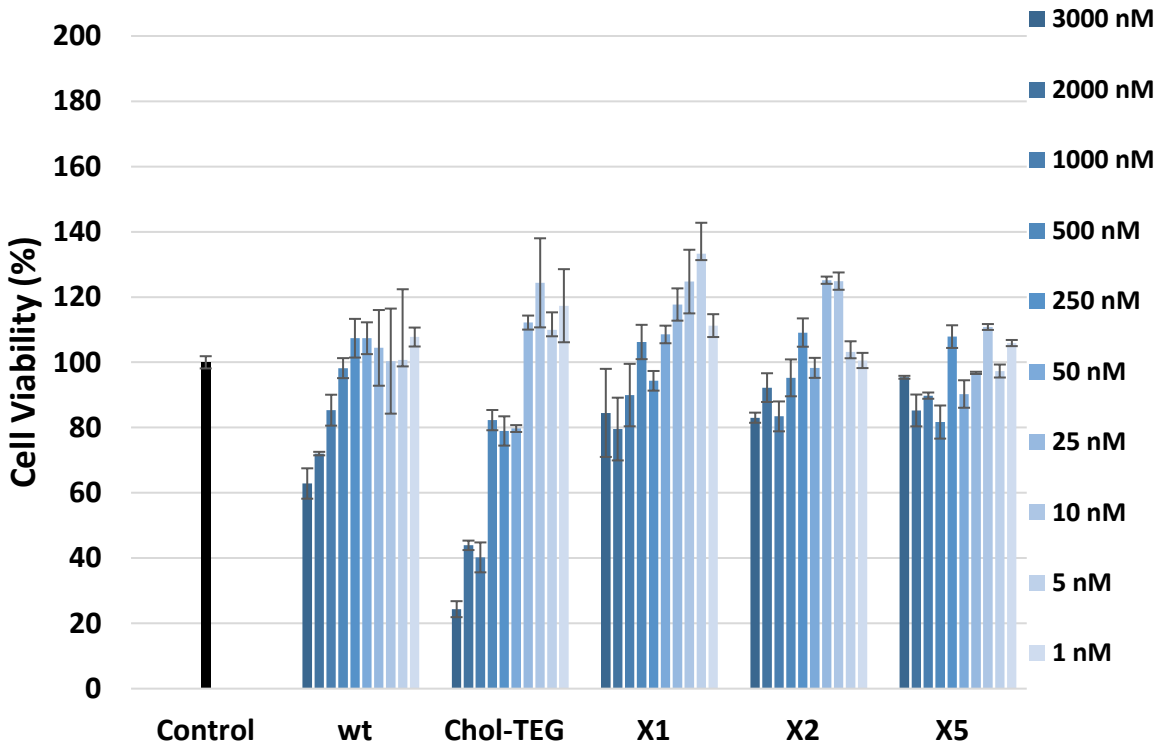

Figure 2.4. HeLa viability after wt and cholesterol siRNA treatment using the XTT Cell Proliferation Assay.

2.5 Discussion and Conclusions

In this study, we investigated the *in vitro* cellular uptake and potency of triazole-linked cholesterol siRNAs without the use of transfection reagents. It was previously reported that placing a chemical modification within the central region of the sense strand may impact

thermal destabilization [22-24], however, this does not seem to alter gene-silencing efficacy. The IC_{50} values for these thermally destabilized centrally modified siRNAs **X1** and **X2** were 243.6 nM and 307.1 nM respectively. The 3′-modified siRNA **X5** also exhibited effective gene silencing, with an IC_{50} of 189.2 nM. Previous studies have reported that the 3′-end of the sense strand is able to accommodate bulky groups [25].

The wild-type siRNA (**wt**), which lacks a cholesterol modification, did not display any gene-silencing activity in our carrier-free study. This was expected as unmodified siRNAs are known to have difficulties in crossing the cellular membrane unassisted. The use of 3′-end cholesterol modifications has been reported in the literature with varying degrees of success [18,26,27]. As such, we decided to investigate the gene-silencing efficacy of a commercially available 3′-end triethylene glycol (TEG) cholesterol modification (**Chol-TEG**) using our carrier-free transfection protocol as a comparison to our cholesterol-modified triazole-linked siRNAs (**X1**, **X2**, and **X5**). Interestingly, the **Chol-TEG** siRNAs displayed poor gene-silencing abilities in the entire range between 1 to 3000 nM.

It is not entirely clear why the cholesterol-modified triazole-linked siRNAs (**X1**, **X2** and **X5**) exhibit potent gene silencing compared to the siRNA **Chol-TEG**. One possibility is that the conformationally constrained triazole functionality in some way is benefiting the siRNA. Furthermore, the nitrogen atom used to functionalize the molecule with the triazole-cholesterol group is positive under physiological pH, which may also assist in cellular uptake. In contrast, the **Chol-TEG** group contains a neutral, polar, and flexible polyethylene linker, which may poorly impact the overall cellular uptake profile of the siRNA. In addition, **Chol-TEG** siRNA imparted high cytotoxicity, perhaps explaining why these siRNAs did not display successful gene-silencing activity. It is unclear why

siRNAs **X1**, **X2** and **X5** are the least toxic compared to **wt** and **Chol-TEG**. However, some studies have identified that molecules functionalized with triazoles are non-toxic [28,29]. Thus, it is possible that the triazole functionality reduces the cytotoxicity of siRNAs.

In conclusion, cholesterol-modified triazole-linked siRNAs show excellent dose-dependent gene silencing of exogenous firefly luciferase mRNA in the absence of a transfection carrier. These results indicate that our modification is compatible with the RNA interference pathway when placed at both the central region and 3′-end of the sense strand of siRNAs. This could provide a novel approach to improve cellular uptake, and perhaps assist with other downstream applications such as packaging of liposomes and lipid-nanoparticles.

2.6 Acknowledgements

We acknowledge the National Sciences and Engineering Research Council for funding.

2.7 Supplementary Data

Refer to Appendix A for the original manuscript and corresponding supplementary data.

2.8 References

1. Fire A, S Xu, MK Montgomery, SA Kostas, SE Driver and CC Mello. (1998) Potent and specific genetic interference by double-stranded RNA in Caenorhabditis elegans. Nature 391:806-811.

2. Hannon GJ. (2002) RNA Interference. Nature 418:244-251.

3. Wilson RC and JA Doudna. (2013) Molecular mechanisms of RNA interference. Annu Rev Biophys 42:217-239.

4. Elbashir SM, J Harborth, W Lendeckel, A Yalcin, K Weber and T Tuschl. (2001) Duplexes of 21-nucleotide RNAs Mediate RNA Interference in Cultured Mammalian Cells. Nature 411:494-498.

5. Selvam C, D Mutisya, S Prakash, K Ranganna and R Thilagavathi. (2017) Therapeutic potential of chemically modified siRNA: Recent trends. Chem. Biol. Drug Des. 90:665-678.

6. Aagaard L and JJ Rossi. (2007) RNAi therapeutics: principles, prospects and challenges. Adv Drug Deliv Rev 59:75-86.

7. Haussecker D. (2014) Current issues of RNAi therapeutics delivery and development. Journal of Controlled Release 195:49-54.

8. Shukla S, CS Sumaria and PI Pradeepkumar. (2010) Exploring chemical modifications for siRNA therapeutics: a structural and functional outlook. ChemMedChem 5:328-349.

9. Behlke MA. (2008) Chemical modification of siRNAs for in vivo use. Oligonucleotides 18:305-319.

10. Oh YK and TG Park. (2009) siRNA delivery systems for cancer treatment. Adv Drug Deliv Rev 61:850-862.

11. Oliveira S, G Storm and RM Schiffelers. (2006) Targeted delivery of siRNA. J. Biomed. Biotechnol. 2006:63675-63675.

12. Tatiparti K, S Sau, SK Kashaw and AK Iyer. (2017) siRNA Delivery Strategies: A Comprehensive Review of Recent Developments. Nanomaterials (Basel) 7:77.

13. de Jonge J, M Holtrop, J Wilschut and A Huckriede. (2006) Reconstituted influenza virus envelopes as an efficient carrier system for cellular delivery of small-interfering RNAs. Gene Ther. 13:400-411.

14. Janas MM, MK Schlegel, CE Harbison, VO Yilmaz, Y Jiang, R Parmar, I Zlatev, A Castoreno, H Xu, S Shulga-Morskaya *et al.* (2018) Selection of GalNAc-conjugated siRNAs with limited off-target-driven rat hepatotoxicity. Nat Commun 9:723.

15. Goluszko P and B Nowicki. (2005) Membrane cholesterol: a crucial molecule affecting interactions of microbial pathogens with mammalian cells. Infect Immun 73:7791-7796.

16. Chernikov IV, DV Gladkikh, MI Meschaninova, AG Ven'yaminova, MA Zenkova, VV Vlassov and EL Chernolovskaya. (2017) Cholesterol-Containing Nuclease-Resistant siRNA Accumulates in Tumors in a Carrier-free Mode and Silences MDR1 Gene. Mol Ther Nucleic Acids 6:209-220.

17. Irby D, C Du and F Li. (2017) Lipid-Drug Conjugate for Enhancing Drug Delivery. Mol. Pharm. 14:1325-1338.

18. Willibald J, J Harder, K Sparrer, KK Conzelmann and T Carell. (2012) Click-modified anandamide siRNA enables delivery and gene silencing in neuronal and immune cells. J. Am. Chem. Soc. 134:12330-12333.

19. Lorenz C, P Hadwiger, M John, HP Vornlocher and C Unverzagt. (2004) Steroid and lipid conjugates of siRNAs to enhance cellular uptake and gene silencing in liver cells. Bioorg Med Chem Lett 14:4975-4977.

20. De Paula D, MV Bentley and RI Mahato. (2007) Hydrophobization and bioconjugation for enhanced siRNA delivery and targeting. RNA 13:431-456.

21. Desaulniers J-P, G Hagen, J Anderson, C McKim and B Roberts. (2017) Effective gene-silencing of siRNAs that contain functionalized spacer linkages within the central region. RSC Advances 7:3450-3454.

22. Efthymiou TC, B Peel, V Huynh and JP Desaulniers. (2012) Evaluation of siRNAs that contain internal variable-length spacer linkages. Bioorg Med Chem Lett 22:5590-5594.

23. Peel BJ, G Hagen, K Krishnamurthy and JP Desaulniers. (2015) Conjugation and Evaluation of Small Hydrophobic Molecules to Triazole-Linked siRNAs. ACS Med. Chem. Lett. 6:117-122.

24. Addepalli H, Meena, CG Peng, G Wang, Y Fan, K Charisse, KN Jayaprakash, KG Rajeev, RK Pandey, G Lavine *et al.* (2010) Modulation of thermal stability can enhance the potency of siRNA. Nucleic Acids Res. 38:7320-7331.

25. Valenzuela RA, K Onizuka, AA Ball-Jones, T Hu, SR Suter and PA Beal. (2016) Guide Strand 3'-End Modifications Regulate siRNA Specificity. Chembiochem 17:2340-2345.

26. Soutschek J, A Akinc, B Bramlage, K Charisse, R Constien, M Donoghue, S Elbashir, A Geick, P Hadwiger, J Harborth *et al.* (2004) Therapeutic silencing of an endogenous gene by systemic administration of modified siRNAs. Nature 432:173-178.

27. Ambardekar VV, HY Han, ML Varney, SV Vinogradov, RK Singh and JA Vetro. (2011) The modification of siRNA with 3' cholesterol to increase nuclease protection and suppression of native mRNA by select siRNA polyplexes. Biomaterials 32:1404-1411.

28. Hou J, X Liu, J Shen, G Zhao and PG Wang. (2012) The impact of click chemistry in medicinal chemistry. Expert Opin Drug Discov 7:489-501.

29. Thirumurugan P, D Matosiuk and K Jozwiak. (2013) Click chemistry for drug development and diverse chemical-biology applications. Chem Rev 113:4905-4979.

Connecting Statement I

In Chapter 2, we report the use of a triazole-linked cholesterol moiety to improve the cellular uptake of siRNAs in the absence of a transfection carrier. Despite the success of cholesterol as a delivery vector for siRNAs, the use of this bioconjugate is limited by its biodistribution. Although extrahepatic delivery has been achieved with select formulations, most cholesterol conjugates accumulate in the liver. Based on this, we identified the need to investigate an alternate ligand for targeted siRNA delivery. In the following study, we focus on the chemical synthesis of a novel folate conjugate for incorporation into siRNAs and report a novel approach to boost the gene-silencing activity of these biomolecules. These self-delivering siRNAs were selectively taken up by folate receptor-expressing cancer cells and achieved potent activity against exogenous and endogenous gene targets.

Chapter 3. Manuscript II

Targeted Delivery and Enhanced Gene-silencing Activity of Centrally Modified Folic Acid–siRNA Conjugates

Lidya Salim, Golam Islam, Jean-Paul Desaulniers

Published in:

Nucleic Acids Research **2020**, *48*, 75-85

DOI: 10.1093/nar/gkz1115

3.1 Abstract

One of the major hurdles in RNAi research has been the development of safe and effective delivery systems for siRNAs. Although various chemical modifications have been proposed to improve their pharmacokinetic behaviour, their delivery to target cells and tissues presents many challenges. In this work, we implemented a receptor-targeting strategy to selectively deliver siRNAs to cancer cells using folic acid as a ligand. Folic acid is capable of binding to cell-surface folate receptors with high affinity. These receptors have become important molecular targets for cancer research as they are overexpressed in numerous cancers despite being expressed at low levels in normal tissues. Employing a post-column copper-catalyzed alkyne–azide cycloaddition (CuAAC), we report the synthesis of siRNAs bearing folic acid modifications at different positions within the sense strand. In the absence of a transfection carrier, these siRNAs were selectively taken up by cancer cells expressing folate receptors. We show that centrally modified folic acid–siRNAs display enhanced gene-silencing activity against an exogenous gene target (~80% knockdown after 0.75 μM treatment) and low cytotoxicity. In addition, these siRNAs achieved potent dose-dependent knockdown of endogenous Bcl-2, an important anti-apoptotic gene.

3.2 Introduction

RNAi is an endogenous pathway that utilizes double-stranded RNA to suppress the expression of a target mRNA, resulting in sequence-specific gene silencing [1,2]. In the effector step of RNAi, siRNAs of 21–23 nucleotides are incorporated into a protein complex, the RNA-induced silencing complex (RISC) [3]. This is followed by a duplex dissociation step, promoted by the catalytic activity of the endonuclease Ago2 which cleaves between base pairs 9 and 10 from the sense strand 5′ end [4,5]. RISC retains the

antisense strand which is used as a guide sequence to locate and degrade the target mRNA [6,7]. Synthetic siRNAs are able to induce gene silencing through the RNAi pathway [8], becoming powerful tools to study gene function [9,10]. RNAi-based therapies also hold great promise as siRNAs can be used to down-regulate the expression of deleterious proteins involved in disease onset and progression [11-13]. However, this system comes with several limitations given by the inherent nature of siRNAs such as low stability, poor cellular uptake, potential for immune activation and off-target effects [14-16]. Chemical modifications are able to mitigate some of these challenges and improve the pharmacokinetic properties of siRNAs [17,18] but despite advancements in the field [19], there is still no universal modification able to address all of the challenges associated with siRNAs.

The delivery of siRNAs to target cells or tissues has been one of the major challenges in RNAi research. Naked siRNAs are unable to diffuse across cellular membranes due to their large size and polyanionic backbone [20]. Current delivery strategies include the encapsulation of siRNAs within nanoparticles or liposomes and the conjugation of siRNAs to hydrophobic molecules [21]. Because siRNAs lack selectivity for specific cell types, receptor-targeting ligands can be used to deliver siRNAs to target cells and tissues [22]. One example is the vitamin folic acid, which has been extensively used as a drug delivery system to target FRs in tumour cells [23,24]. FRs are cell-surface glycoproteins able to bind folic acid with high affinity. These receptors are expressed at low levels in most tissues, as their expression is limited to cells important for folate resorption and embryonic development, yet they are highly overexpressed on the surface of numerous cancers [25]. This includes ~90% of ovarian carcinomas as well as breast, endometrial, brain and kidney cancers [26,27]. Once bound to the FR, folic acid enters the cell through receptor-mediated

endocytosis. Notably, folic acid conjugates retain the ability to bind to and be internalized by this receptor, making the FR an attractive molecular target for cancer research [28]. This receptor-targeting strategy has been used to deliver siRNAs by functionalizing liposomes and nanoparticles with folic acid [29-33] although selective delivery can also be achieved by direct conjugation of folic acid to siRNAs.

Previous studies have successfully incorporated folic acid modifications at either the 3′ or 5′ end of siRNA and achieved selective, carrier-free delivery to target cells [34,35]. In these studies, moderate gene-silencing activity against exogenous gene targets (40–60% knockdown after 1 μM treatment) was reported. These results show promise in the use of folic acid as a delivery system for siRNAs. However, there is a need to improve the gene-silencing potency of folic acid–siRNA constructs. Recently, our lab group reported a method to destabilize the central region of siRNAs, which spans the Ago2 cleavage site. We showed that chemical modifications within this region can lead to potent gene-silencing [36,37]. To the best of our knowledge, folic acid has not been incorporated into the central region of siRNAs. Based on this, we report the copper-catalyzed azide-alkyne cycloaddition (CuAAC) synthesis of siRNAs bearing folic acid modifications at different positions within the sense strand, with a particular emphasis on the central region. In the absence of a transfection carrier, these siRNAs were selectively taken up by FR-expressing cell lines. We show that internal modified folic acid–siRNAs display enhanced gene-silencing activity, with minimal toxicity, against exogenous firefly luciferase mRNA (~80% knockdown after 0.75 μM treatment). In addition, these siRNAs achieved potent dose-dependent knockdown of the oncogene Bcl-2 (~72% knockdown after 1 μM treatment).

3.3 Materials and Methods

3.3.1 General Methods

Unless otherwise indicated, all starting reagents and solvents were obtained from commercial sources and used without further purification. Anhydrous CH_2Cl_2 and Et_3N were purchased from Sigma-Aldrich and kept dry using a PureSolv 400 Solvent Purification System. Standard flash chromatography was performed using Silicycle Siliaflash 60 (230-400 mesh) while automated flash chromatography was performed on a Biotage® Isolera flash chromatography system using a 100 g Biotage® SNAP KP-Sil cartridge. ^{1}H, ^{13}C and ^{31}P NMRs were recorded in $CDCl_3$ or DMSO-d6 using a Bruker Ascend (600 MHz) NMR spectrometer. NMR spectra were processed with ACD/NMR Processor. High-performance liquid chromatography (HPLC) was performed on a Waters 1525 binary HPLC pump with a Waters 2489 UV/Vis detector, using a C18 4.6 mm x 150 mm reverse-phase column and eluting from 5 to 100% acetonitrile in a TEAA buffer (pH 7.00) over 30 minutes. ESI-HRMS were recorded on an Agilent Q-TOF and analysed through positive electrospray ionization using a mobile phase of ACN/MeOH (95:5) with 0.1% formic acid.

3.3.2 Synthesis of Propargyl Phosphoramidite

3.3.2.1 Synthesis of Compound 1

To a solution of diethanolamine (10 g, 95.1 mmol) in 150 mL of anhydrous CH_2Cl_2, cooled in an ice bath, was added anhydrous potassium carbonate (65.7 g, 0.476 mol) under an argon atmosphere. Propargyl bromide (80 wt% in toluene, 8.5 mL, 95.1 mmol) was added dropwise over a 5-minute period and the solution was left to stir vigorously for 60 h at room temperature. The crude product was filtered to remove the potassium carbonate and the collected filtrate was concentrated in vacuo to produce a dark amber oil, which was purified

by flash chromatography (elution with 2 to 10% MeOH/CH_2Cl_2). The final product was isolated as a clear amber oil (9.53 g, 70%). ^{1}H NMR (400 MHz, $CDCl_3$) δ 2.19 (t, 1H), 2.68 (t, 4H), 3.40 (s, 2H), 3.60 (t, 4H). ^{13}C NMR (101 MHz, $CDCl_3$) δ 42.05, 55.21, 59.05, 73.15, 78.31. (Scheme 3.1)

3.3.2.2 Synthesis of Compound 2

To a solution of 1 (2 g, 14 mmol) in 25 mL anhydrous CH_2Cl_2 was added freshly distilled triethylamine (1.7 mL, 12.6 mmol) under an argon atmosphere. This was followed by the drop-wise addition of 4,4′-dimethoxytriphenylmethyl chloride (3.79 g, 11.2 mmol) in 5 mL anhydrous CH_2Cl_2. The reaction mixture was stirred overnight at room temperature after which the crude product was extracted three times with a saturated $NaHCO_3$ solution. The combined organic layers were dried over Na_2SO_4 and concentrated in vacuo to produce a cloudy yellow oil which was purified by flash chromatography (elution with 2 to 10% MeOH/ CH_2Cl_2). The final product was isolated as a clear yellow oil (2.8 g, 45%). ^{1}H NMR (400 MHz, $CDCl_3$) δ 2.23 (t, 1H), 2.75 (t, 2H), 2.83 (t, 2H), 3.23 (t, 2H), 3.44(d, 2H), 3.60 (t, 2H), 3.80 (s, 6H), 6.87 (dt, 4H), 7.29 (m, 1H), 7.31 (td, 2H), 7.38 (dt, 4H), 7.47 (d, 2H); ^{13}C NMR (101 MHz, $CDCl_3$) δ 42.76, 52.58, 55.19, 55.65, 58.57, 61.94, 72.83, 78.82, 86.21, 113.07, 126.71, 127.77, 128.13, 129.96, 136.28, 144.95, 158.41.

3.3.2.3 Synthesis of Compound 3

To a flame-dried round-bottomed flask containing a solution of 2 (180 mg, 0.404 mmol) in 5 mL anhydrous CH_2Cl_2 was added freshly distilled triethylamine (0.28 mL, 2.02 mmol) under an argon atmosphere. This was followed by the dropwise addition of 2-cyanoethyl-N,N-diisopropylchlorophosphoramidite (0.27 mL, 1.21 mmol). The reaction mixture was stirred for 3 h and then concentrated in vacuo to produce a cloudy oil which was purified

by flash chromatography (elution 20–60% EtOAc/hexanes, maintaining 5% triethylamine). The product was isolated as a clear oil (0.22 g, 84%). ^{1}H NMR (400 MHz, $CDCl_3$) δ 1.17 (dd, 12H), 2.19 (t, 1H), 2.55 (m, 2H), 2.82 (dt, 4H), 3.15 (t, 2H), 3.45 (d, 2H), 3.57 (m, 2H), 3.66 (m, 2H), 3.76 (m, 2H), 3.78 (s, 6H), 6.83 (dt, 4H), 7.20 (tt, 1H), 7.27 (t, 2H), 7.32 (dt, 4H), 7.44 (d, 2H). ^{13}C NMR (101 MHz, $CDCl_3$) δ 20.33, 21.02, 24.63, 42.98, 43.10, 46.30, 54.20, 55.15, 58.41, 62.03, 62.65, 72.79, 79.27, 86.05, 113.04, 117.71, 126.58, 127.75, 128.18, 130.02, 136.46, 145.22, 158.36. ^{31}P (162 MHz, $CDCl_3$) δ 147.28.

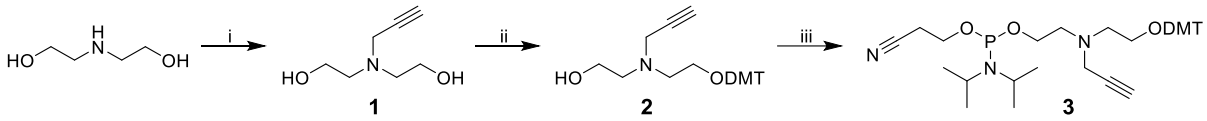

Scheme 3.1. Synthesis of propargyl phosphoramidite. Reagents and conditions: (i) propargyl bromide, K_2CO_3, CH_2Cl_2, 60 h, 69%; (ii) DMT-Cl, Et_3N, CH_2Cl_2, rt, overnight, 45%; (iii) 2-cyanoethyl N,N-diisopropylchlorophosphoramidite, Et_3N, CH_2Cl_2, rt, 3 h, 84%.

3.3.3 Oligonucleotide synthesis, deprotection and purification

Wild-type and propargyl oligonucleotides were synthesized using an Applied Biosystems 394 DNA/RNA synthesizer using a 1.0 μM dT controlled-pore glass (CPG) support and a 1.0 μM cycle with a 999-second coupling time. Immediately prior to synthesis, phosphoramidites were resuspended in anhydrous acetonitrile to a final concentration of 0.1 M. Oligonucleotide sense strands were chemically phosphorylated at the 5′ end using 2-[2-(4,4-dimethoxytrityloxy)ethylsulfonyl]ethyl-(2-cyanoethyl)-(N,N-diisopropyl)-phosphoramidite. Cleavage of oligonucleotides from the solid support was achieved by flushing the CPG columns with 1 mL EMAM solution (1:1 methylamine 33 wt% in ethanol and methylamine 40% wt. in H_2O) for 1 h at room temperature, followed by overnight incubation in EMAM to deprotect the bases. Oligonucleotides were concentrated in a miVac Quattro concentrator and desilylated in DMSO (100 μL) and 3HF-Et_3N (125 μL) for 3 h at

65°C. Crude oligonucleotides were precipitated in ethanol and desalted using Millipore Amicon Ultra 3000 MW cellulose centrifugal filters. Strands were purified using reverse-phase HPLC eluting from 5% to 95% ACN in 0.1 M TEAA buffer (pH 7.0).

3.3.4 Synthesis and purification of folic acid–conjugated siRNAs

3.3.4.1 Synthesis of Compound 4

Folic acid (0.5 g, 1.13 mmol) was dissolved in anhydrous DMSO (30 mL) under an argon atmosphere. N-Hydroxysuccinimide (0.26 g, 2.27 mmol) and N,N′-dicyclohexylcarbodiimide (0.26 g, 1.25 mmol) were simultaneously added and the reaction mixture was left to stir overnight in the dark. The dicyclohexylurea by-product was removed by filtration and the filtrate was collected in a round-bottomed flask to which a solution 2-azidoethanamine (0.12 g, 1.37 mmol) in 10 mL anhydrous DMSO was added. The reaction mixture was left to stir in the dark for an additional 24 h. After removing most of the DMSO in vacuo, the crude product was precipitated in cold diethyl ether and the collected yellow crystals were washed with THF and CH_2Cl_2. The product was further purified by automated flash chromatography, eluting with a slow gradient (0–100%) of solution A (2:1:1 NH_4OH/MeOH/ACN) to solution B (ACN). The product was isolated as bright yellow crystals (0.48 g, 84%). ^{1}H NMR (400 MHz, DMSO-d6) δ 1.84–2.00 (m, 2H), 2.05–2.20 (m, 2H), 3.19 (t, 2H), 3.32 (t, 2H), 4.30 (m, 1H), 4.45 (d, 2H), 6.61 (d, 2H), 6.90 (m, 1H), 7.66 (d, 2H), 8.04 (m, 1H), 8.59 (s, 1H), 11.86 (br, 1H). ESI-HRMS (ES+) *m/z* calculated for $C_{21}H_{23}N_{11}O_5$: 510.1956, found 510.1953 $[M+H]^+$ (Scheme 3.2).

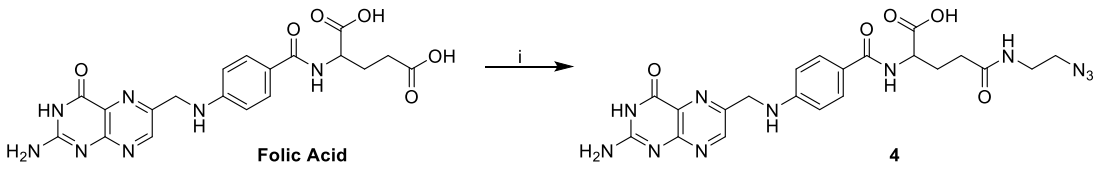

Scheme 3.2. Synthesis of azido-folate. Reagents and conditions: (i) N-Hydroxysuccinimide, N,N′-Dicyclohexylcarbodiimide, DMSO, rt, overnight, 2-azidoethanamine, 24 h., 83%.

3.3.4.2 Copper-catalyzed azide-alkyne cycloaddition (CuAAC) procedure

To a solution of propargyl-modified RNA (100 μM, 5 μL) in DMSO/H_2O/t-BuOH (1:2:1) was added 4 (2.5 mM, 5 μL) under an argon atmosphere. This was followed by the addition of a pre-chelated mixture of $CuSO_4$ (2.5 mM) and TBTA (12.5 mM, 5 μL). A fresh solution of sodium ascorbate (2.5 mM, 10 μL) was added, and the reaction mixture was stirred at 40 °C in the dark for 3.5 h. At this point, sodium acetate (0.3 M solution in H_2O, 50 μL) was added and the mixture was stirred for an additional 20 min at room temperature. Crude RNA was precipitated in cold EtOH, centrifuged at 13 400 rpm for 15 min and washed twice with cold EtOH. Strands were purified using reverse-phase HPLC eluting from 5% to 95% ACN in 0.1 M TEAA buffer (pH 7.0) (Scheme 3.3).

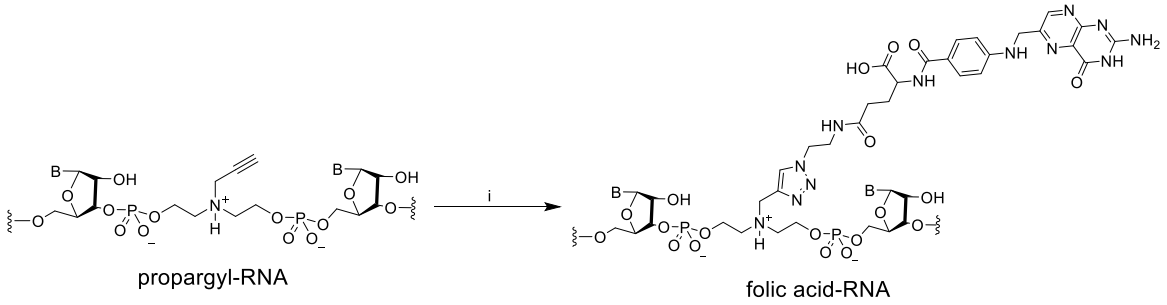

Scheme 3.3. CuAAC procedure to synthesize folate RNAs. Reagents and conditions: (i) **4**, $CuSO_4.5H_2O$, TBTA, sodium ascorbate, DMSO/H_2O/t-BuOH (1:2:1), 40 °C, 4 h., 69-80%

3.3.5 Thermal denaturation and CD studies

Thermal denaturation and CD studies were performed using a Jasco J-815 Circular Dichroism (CD) Spectropolarimeter equipped with a temperature controller. For duplex

formation, equimolar amounts of complementary sequences were combined, dried down and resuspended in 300 μL pH 7 sodium phosphate buffer (90.0 mM NaCl, 10.0 mM Na_2HPO_4, 1.00 mM EDTA). Samples were heated at 90 °C for 2 min and then allowed to slowly cool to room temperature. To determine melting temperature (T_m), UV absorbance was measured at 260 nm and temperature was increased from 10 to 95 °C at a rate of 0.5 °C per minute. T_m data was analysed using Meltwin v3.5 software and represents the average of three independent runs. Circular dichroism spectra were recorded at 25°C, scanning from 200 to 350 nm with a screening rate of 20.0 nm/min and a 0.20 nm data pitch. All scans were performed in triplicate and averaged using Jasco′s Spectra Manager v2 software.

3.3.6 Cell culture

HeLa and HT-29 cells were maintained in Dulbecco′s modified Eagle′s medium (DMEM) and Roswell Park Memorial Institute (RPMI) 1640 Medium respectively, both supplemented with 10% fetal bovine serum (FBS) and 1% penicillin–streptomycin (Sigma). Cells were maintained at 37 °C in a humidified atmosphere with 5% CO_2 and passaged at 80% confluency.

3.3.7 Flow cytometry

PE anti-FOLR1 (Folate Binding Protein) Antibody and PE Mouse IgG2a, κ Isotype Control (FC) Antibody were purchased from Biolegend. Cells were dislodged from the culture flask using trypsin and transferred into tubes. Cells were then centrifuged at 300 g for 10 min (4°C). After aspirating the supernatant, cells were resuspended in 150 μL cell staining buffer (2.5 mL FBS, 47.5 mL PBS). Cells were stained with trypan blue and counted using a Haemocytometer. For each study, cells were resuspended in staining buffer to achieve a final concentration of 1×10^6 cells/100 μL. Antibodies were added to each cell suspension

and cells were incubated in the dark for 30 min (on ice). Samples were centrifuged at 300 g for 5 min (4°C) after which the supernatant was aspirated, and cells were washed with 1 mL staining buffer. The last two steps, centrifugation and washing, were repeated once more. Samples were then centrifuged one last time. After removing the supernatant, cells were resuspended in 500 μL ice-cold PBS and incubated at room temperature for 5 min. Flow cytometry studies were performed immediately on a BD Accuri C6 Plus flow cytometer following the manufacturer′s protocol.

3.3.8 siRNA transfections with Lipofectamine for luciferase assay

3.3.8.1 Lipofectamine transfection in HeLa cells

HeLa cells were seeded into 24-well plates, containing 400 μL DMEM (10% FBS), at a density of 5.0×10^4 cells per well. Plates were incubated for 24 hours at 37 °C in a humidified atmosphere with 5% CO_2. For each transfection sample, a mixture of 1 μL of Lipofectamine 2000™ (Invitrogen) and 49 μL of Gibco′s 1X Opti-Mem Reduced Serum Medium was prepared and incubated at room temperature for 5 minutes. Each siRNA was diluted in 1X Gibco′s Opti-MEM Reduced Serum Medium (Invitrogen) on ice and mixed with 200 ng pGL3 and 50 ng pRLSV40 plasmids to a total volume of 50 μL. The diluted siRNA/plasmid mixture was combined with the diluted Lipofectamine 2000™ mixture and incubated at room temperature. After 20 minutes, the complexes were transferred to the respective wells and the plates were gently rocked back and forth for a few minutes. Plates were incubated for an additional 24 hours at 37 °C in a humidified atmosphere with 5% CO_2.

3.3.8.2 Lipofectamine transfection in HT-29 cells

HT-29 cells were seeded into 24-well plates, containing 350 μL RPMI 1640 (10% FBS), at a density of 1.5×10^5 cells per well (for a total volume of 500 μL). Plates were incubated for

24 hours at 37 °C in a humidified atmosphere with 5% CO_2 after which the medium was removed from each well and replaced with 400 μL fresh medium. Each siRNA was diluted in 1X Gibco′s Opti-MEM Reduced Serum Medium (Invitrogen) and mixed with 600 ng pGL3 and 150 ng pRLSV40 plasmids to a total volume of 100 μL. To each tube containing the siRNA/plasmid mixture, 4 μL Lipofectamine® LTX (ThermoFisher) was added. After a 30-minute incubation at room temperature, complexes were transferred to the respective wells and the plates were gently rocked back and forth for a few minutes. Plates were incubated for an additional 24 hours at 37 °C in a humidified atmosphere with 5% CO_2.

3.3.9 Carrier-free siRNA transfections for luciferase assay

3.3.9.1 Carrier-free transfection in HeLa cells

The day before transfection, HeLa cells were seeded into 96-well plates, containing 50 μL folate-free RPMI 1640, at a density of 1.0×10^4 cells per well and incubated for 24 h. Two plasmids, pGL3 (firefly luciferase, 200 ng) and pRLSV40 (*Renilla* luciferase, 50 ng), were co-transfected using 1 μL Lipofectamine 2000™ (Invitrogen) following the manufacturer′s protocol. Plates were incubated for 4 hours at 37 °C in a humidified atmosphere with 5% CO_2 after which the medium was removed from each well. Cells were washed twice with 1X phosphate-buffered saline (PBS) after which 50 μL folate-free RPMI 1640 medium (without antibiotics) was added to each well. Each siRNA was diluted in 50 μL 1X Gibco′s Opti-MEM Reduced Serum Medium (Invitrogen) on ice and the diluted samples were immediately transferred to the respective wells of the 96-well plate. Plates were gently rocked back and forth for a few minutes and then incubated for an additional 16 h prior to cell lysis.

3.3.9.2 Carrier-free transfection in HT-29 cells

The day before transfection, HT-29 cells were seeded into 96-well plates, containing 50 μL folate-free RPMI 1640, at a density of 5.0×10^4 cells per well and incubated for 24 h. For plasmid transfection, pGL3 (firefly luciferase, 600 ng) and pRLSV40 (*Renilla* luciferase, 150 ng) were combined and diluted in 1X Gibco′s Opti-MEM Reduced Serum Medium (Invitrogen) to a final volume of 50 μL. This was followed by the addition of 4 μL Lipofectamine® LTX (Thermo Fisher). After a 30-minute incubation period at room temperature, complexes were transferred to each well and plates were incubated for 6 h at 37 °C in a humidified atmosphere with 5% CO_2 after which the medium was removed from each well. Cells were washed twice with 1X phosphate-buffered saline (PBS) after which 50 μL folate-free RPMI 1640 medium (without antibiotics) was added to each well. Each siRNA was diluted in 50 μL 1X Gibco′s Opti-MEM Reduced Serum Medium (Invitrogen) on ice and the diluted samples were immediately transferred to the respective wells of the 96-well plate. Plates were gently rocked back and forth for a few minutes and then incubated for an additional 20 h prior to cell lysis.

3.3.10 Dual-luciferase® reporter assay

Cells were lysed with 1X passive lysis buffer for 20 min at room temperature. Cell lysates were transferred to microcentrifuge tubes and were immediately used to assess the gene-silencing activity of siRNAs using a Dual-Luciferase® Reporter Assay (Promega). Luciferase Assay Reagent II (LAR II) and Stop & Glo® Reagent were prepared following the manufacturer′s protocol. Cell lysates (10 μL) were transferred to Costar 96-well plates in triplicate. LAR II reagent (50 μL) was added to each well and the first luminescence measurement was taken on a Synergy HT (Bio-Tek) plate luminometer. Stop & Glo®

Reagent (50 μL) was then added to each well and the second luminescence measurement was taken. Results are expressed as the ratio of firefly/*Renilla* luminescence taken as a percentage of an untreated control. Each value is the average of at least three biological replicates and error bars indicate standard deviation.

3.3.11 Statistical analysis

Prism 8.0 (GraphPad Software, San Diego, CA, USA) was used to generate dose-response curves after carrier-free siRNA transfection in HeLa cells. The half-maximal inhibitory concentration (IC_{50}) of each siRNA was determined using Prism′s variable slope (four-parameter) model. Anti-luciferase siRNAs were tested at seven concentrations in carrier-free conditions. Anti-Bcl-2 siRNAs were tested at three concentrations in carrier-free conditions. Standard errors (S.E.) were determined for a minimum of two biological replicates.

3.3.12 anti-Bcl-2 siRNA transfection in HeLa cells

3.3.12.1 Lipofectamine transfection of anti-Bcl-2 siRNA

HeLa cells were seeded into 24-well plates, containing 400 μL DMEM (10% FBS), at a density of 4.0×10^4 cells per well. Plates were incubated for 24 hours at 37 °C in a humidified atmosphere with 5% CO_2. For each transfection sample, a mixture of 1 μL of Lipofectamine 2000™ (Invitrogen) and 49 μL of Gibco′s 1X Opti-Mem Reduced Serum Medium was prepared and incubated at room temperature for 5 minutes. Each siRNA was diluted in 1X Gibco′s Opti-MEM Reduced Serum Medium (Invitrogen) on ice. Diluted siRNAs were combined with the diluted Lipofectamine 2000™ mixture and incubated at room temperature for 20 minutes. Complexes were then transferred to the respective wells and

the plates were gently rocked back and forth for a few minutes. Plates were incubated for an additional 24 hours at 37 °C in a humidified atmosphere with 5% CO_2.

3.3.12.2 Carrier-free transfection of anti-Bcl-2 siRNA

HeLa cells were seeded into 96-well plates, containing 50 µL folate-free RPMI 1640 (10% FBS), at a density of 2.0×10^4 cells per well. Plates were incubated for 24 hours at 37 °C in a humidified atmosphere with 5% CO_2. Each siRNA was diluted in 50 µL 1X Gibco′s Opti-MEM Reduced Serum Medium (Invitrogen) on ice and the diluted samples were immediately transferred to the respective wells of the 96- well plate. Plates were incubated for an additional 24 hours at 37 °C in a humidified atmosphere with 5% CO_2.

3.3.13 Biological activity of anti-Bcl-2 siRNAs

3.3.13.1 RNA extraction and cDNA synthesis

HeLa cells were transfected with anti-Bcl-2 siRNAs as described above. RNA extraction, cDNA production and RT-qPCR. Prior to the RNA extraction, each well of the 24-well plate washed twice with 1X PBS. Total RNA was extracted from the Hela cells using the manufacturer′s instructions of the Total RNA Purification Plus Kit (Cat#: 48400. Norgen BioTek Corp, Thorold, ON, Canada). In addition, an on-column DNA digestion was performed using RNase Free DNase I Kit (Cat#:25710. Norgen BioTek Corp, Thorold, ON, Canada). Two microliter of each extracted RNA sample was used to measure the concentration and RNA integrity (A260/280) on the BioDrop Duo Plus (UK), and the presence of the RNA was confirmed by gel electrophoresis on a 1% (w vol^{-1}) agarose.

The RT reaction was performed using the IScript cDNA synthesis kit (Cat #: 1708891. Bio-Rad, Hercules, California) in a total reaction volume of 20µL. The reaction mixture

contained 400 ng of total RNA, M-MLV reverse transcriptase, oligo (DT) and random primers. Two negative controls were performed with all reactions. The first control contained the RNA template and all DNAse/RT reagents, except for the final addition of the RT enzyme. A second control contained no template (water only) to ensure that all reagents were free from possible contaminants. RT reactions were placed in 200 µL PCR tubes and incubated within a BIORAD T100 Thermal Cycler for 5 min at 25 °C followed by 20 min at 46 °C, 1 min at 95 °C and then held at 4°C. Once cDNA was produced, the products could be amplified (RT-qPCR).

3.3.13.2 RT-qPCR

Real-time PCR was performed in a total reaction volume of 20 µL including 10 ul SsoFast EvaGreen Supermix (Bio-Rad, Hercules, CA, USA) containing Sso 7-d Fusion Polymerase, 0.5 µM forward primer and reverse primer and 2 µL cDNA template. In the final reaction, cDNA was diluted 40X to produce the best results. Pre-designed primers BCL-2F 5′-CTG GTG GGA GCT TGC ATC AC-3′ and BCL-2R 5′-ACA GCC TGC AGC TTT GTT TC-3′ were purchased to target the Bcl-2 gene and yielding a 150-bp amplicon and 18S-F 5′-CGG CTA CCA CAT CCA AGG AAG-3′ and 18S-R 5′-CGC TCC CAA GAT CCA ACT ACT-3′ (Integrated DNA Technologies Inc, San Diego, California) were used to target the 18s gene in HeLa cells and yielding a 247-bp amplicon. Reactions were incubated in the Bio-Rad CFX 96 Real-Time Detection System using the following cycle conditions: 50 °C for 10 min, 95 °C for 10 min, followed by 40 cycles at 95 °C for 15 s and 60 °C for 1 min. Reaction specificity was assessed by melting curve analysis immediately after the qPCR experiment. The efficiency of each primer set for RT-qPCR was determined to be between 95 and 100% using the standard curve method. NRT controls were performed during

standard curve analysis to confirm that amplification of the PCR product was cDNA and not genomic DNA. NTC controls were also performed to ensure that amplification of the PCR product was not a result of primer–dimers. Results were analyzed using the Bio-Rad CFX manager 3.1 software where the Bcl-2 expression data was normalized against 18s gene as the reference and expression profiles were generated using the comparative Delta-CT method of analysis. The final data was represented by averages and standard deviations compiled from two biological replicates for each treatment for which three technical replicates were included for the qPCR experiments.

3.3.14 Cell viability assay

HeLa and HT-29 cells were seeded into 96-well plates at a density 5.0×10^3 cells per well and incubated for 24 h. Cells were transfected following the described carrier-free protocol and were incubated for an additional 24 h. Cell viability was assessed using the XTT Cell Proliferation Assay Kit (ATCC™) following the manufacturer′s protocol. Absorbance readings were taken using a Synergy HT (Bio-Tek) plate luminometer.

3.4 Results

3.4.1 Preparation of propargyl and folic acid-modified oligonucleotides

Propargyl phosphoramidite **3** was synthesized as described above. Propargyl and wild-type oligonucleotides were synthesized following standard solid-phase phosphoramidite chemistry. Propargyl-modified oligonucleotides were conjugated with azido-folate derivative **4** as described above. Oligonucleotides were purified using reverse-phase HPLC and characterized by mass spectrometry.

3.4.2 Thermal stability and CD studies

Synthesized sense strands were annealed to their complementary antisense sequences as described above. CD studies were performed to confirm that siRNAs adopted an A-form helical conformation (Figure 3.1) Melting temperatures (T_m) were measured for anti-firefly luciferase and anti-Bcl-2 siRNAs (Table 3.1). Modifications placed at the 3′ end of the sense strand were well-tolerated and did not cause significant destabilizing effects. In these siRNAs, the propargyl and folic acid modifications replaced the 3′ dTdT overhang, leading to a 3.5 and 4.7 °C decrease in melting temperature for aL-P4 and aL-F4, respectively. This is likely due to the loss of stacking interactions which have been reported with 3′ dTdT overhangs [38]. We observed a similar destabilizing effect when the modifications were placed at position 5 from the sense strand 3′ end ($\Delta T_m = -6.0$ and -5.5 °C for propargyl and folic acid–siRNAs, respectively). On the other hand, internally-modified anti-luciferase siRNAs exhibited significant thermal destabilization. The greatest decrease in T_m was observed when the propargyl spacer replaced a single nucleotide at position 9 from the sense strand 5′ end (aL-P1, $\Delta T_m = -22.2$ °C). Placing the folic acid modification at this position produced a similar effect (aL-F1, $\Delta T_m = -17.2$ °C). This thermal destabilization is consistent with previous studies examining the effect of central region modifications on siRNA stability [39]. Next, we tested whether our propargyl and folic acid modifications would be better accommodated within the helix if they replaced two nucleotides instead of one (positions 9 and 10 from the sense strand 5′ end). However, there was no significant increase in melting temperature ($\Delta T_m = -20.5$ and -19.9 for aL-P2 and aL-F2 siRNAs respectively). Similar destabilizing effects were observed with internal modified anti-Bcl-2 siRNAs (aB-P and aB-F) and scramble siRNAs (aL-scr-P, aL-scr-F, aB-scr-P and aB-scr-F).

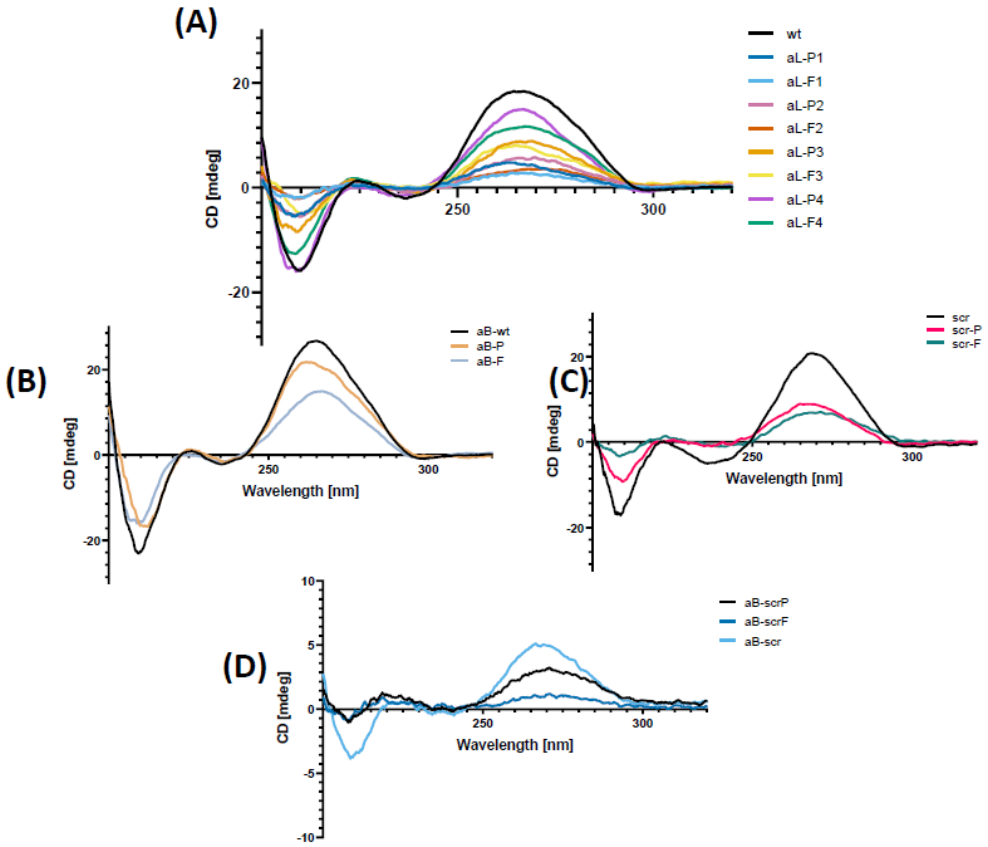

Figure 3.1. CD spectra of (A) anti-firefly luciferase siRNAs, (B) anti-luciferase scramble controls, (C) antiBcl-2 siRNAs and (D) anti-Bcl-2 scramble controls

Table 3.1. siRNA sequences, melting temperatures and IC_{50} values

anti-luciferase siRNA	Duplex	T_m (°C)	ΔT_m (°C)	IC_{50} ± S.E. (nM)
aL-wt	5′ CUUACGCUGAGUACUUCGAtt 3′ 3′ ttGAAUGCGACUCAUGAAGCU 5′	76.1	-	inactive
aL-P1	5′ CUUACGCU**P**AGUACUUCGAtt 3′ 3′ ttGAAUGCGACUCAUGAAGCU 5′	53.9	-22.2	inactive
aL-F1	5′ CUUACGCU**F**AGUACUUCGAtt 3′ 3′ ttGAAUGCGACUCAUGAAGCU 5′	58.9	-17.2	171.0 ± 48.8
aL-P2	5′ CUUACGCU**P**GUACUUCGAtt 3′ 3′ ttGAAUGCGACUCAUGAAGCU 5′	55.6	-20.5	inactive
aL-F2	5′ CUUACGCU**F**GUACUUCGAtt 3′ 3′ ttGAAUGCGACUCAUGAAGCU 5′	56.2	-19.9	128.95 ± 9.7
aL-P3	5′ CUUACGCUGAGUACU**P**GAtt 3′ 3′ ttGAAUGCGACUCAUGAAGCU 5′	70.1	-6.0	inactive
aL-F3	5′ CUUACGCUGAGUACU**F**GAtt 3′ 3′ ttGAAUGCGACUCAUGAAGCU 5′	70.6	-5.5	283.9 ± 62.9
aL-P4	5′ CUUACGCUGAGUACUUCGA**P** 3′ 3′ ttGAAUGCGACUCAUGAAGCU 5′	72.6	-3.5	inactive
aL-F4	5′ CUUACGCUGAGUACUUCGA**F** 3′ 3′ ttGAAUGCGACUCAUGAAGCU 5′	71.4	-4.7	1044 ± 23.0
aL-scr	5′ GGUAUCCCUCGUGAAUCAUtt 3′ 3′ ttCCAUAGGGAGCACUUAGUA 5′	74.5	-	inactive
aL-scr-P	5′ GGUAUCCC**P**GUGAAUCAUtt 3′ 3′ ttCCAUAGGGAGCACUUAGUA 5′	59.1	-15.4	inactive
aL-scr-F	5′ GGUAUCCC**F**GUGAAUCAUtt 3′ 3′ ttCCAUAGGGAGCACUUAGUA 5′	54.6	-19.9	inactive
anti-Bcl-2 siRNA	**Duplex**	**T_m (°C)**	**ΔT_m (°C)**	**IC_{50} (nM)**
aB-wt	5′ GCCUUCUUUGAGUUCGGUGtt 3′ 3′ ttCGGAAGAAACUCAAGCCAC 5′	72.8	-	inactive
aB-P	5′ GCCUUCUUU**P**AGUUCGGUGtt 3′ 3′ ttCGGAAGAAACUCAAGCCAC 5′	56.6	-16.2	inactive
aB-F	5′ GCCUUCUUU**F**AGUUCGGUGtt 3′ 3′ ttCGGAAGAAACUCAAGCCAC 5′	47.6	-25.2	419.3
aB-scr	5′ GGUGUACGUCGUCUGUUCUtt 3′ 3′ ttCCACAUGCAGCAGACAAGA 5′	73.1	-	inactive
aB-scr-P	5′ GGUGUACG**P**GUCUGUUCUtt 3′ 3′ ttCCACAUGCAGCAGACAAGA 5′	67.1	-6.0	inactive
aB-scr-F	5′ GGUGUACG**F**GUCUGUUCUtt 3′ 3′ ttCCACAUGCAGCAGACAAGA 5′	55.0	-18.1	inactive

The top strand corresponds to the sense strand; the bottom strand corresponds to the antisense strand. **P** corresponds to the propargyl spacer. **F** represents the folic acid spacer. The Argonaute2 cleavage site is underlined.

*IC_{50} values were calculated after siRNA transfection in a carrier-free environment. Inhibitory dose-response curves can be found in Figure 3.6.

3.4.3 Relative expression of folate receptor α in HeLa and HT-29 cells

The relative expression of cell-surface folate receptor α (FRα) was assessed in HeLa and HT-29 cells using flow cytometry. The procedure was performed as described above and results are summarized in Figure 3.2. HeLa cells displayed a 3-fold increase in FRα expression compared to HT-29 cells.

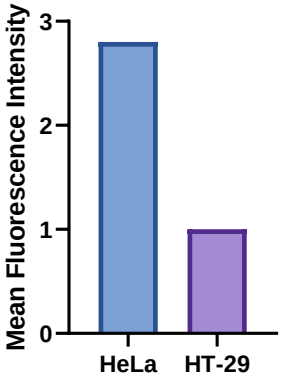

Figure 3.2. Relative expression of folate receptor α (FRα) levels in HeLa and HT-29 cells determined by flow cytometry.

3.4.4 Carrier-free gene silencing of exogenous firefly luciferase mRNA

Prior to carrier-free studies, we confirmed the biological activity of all siRNAs in HeLa and HT-29 cells after transfection with Lipofectamine reagent (Lipofectamine 2000™ in HeLa and Lipofectamine® LTX in HT-29). In both cell lines, anti-luciferase siRNAs achieved excellent dose-dependent knockdown of firefly luciferase after 8, 80 and 800 pM treatments (Figure 3.3). Consistently, siRNAs bearing internal modifications (propargyl or folic acid) showed much higher gene-silencing potency than the 3′-end modified siRNAs. As expected, scramble controls displayed no gene-silencing activity.

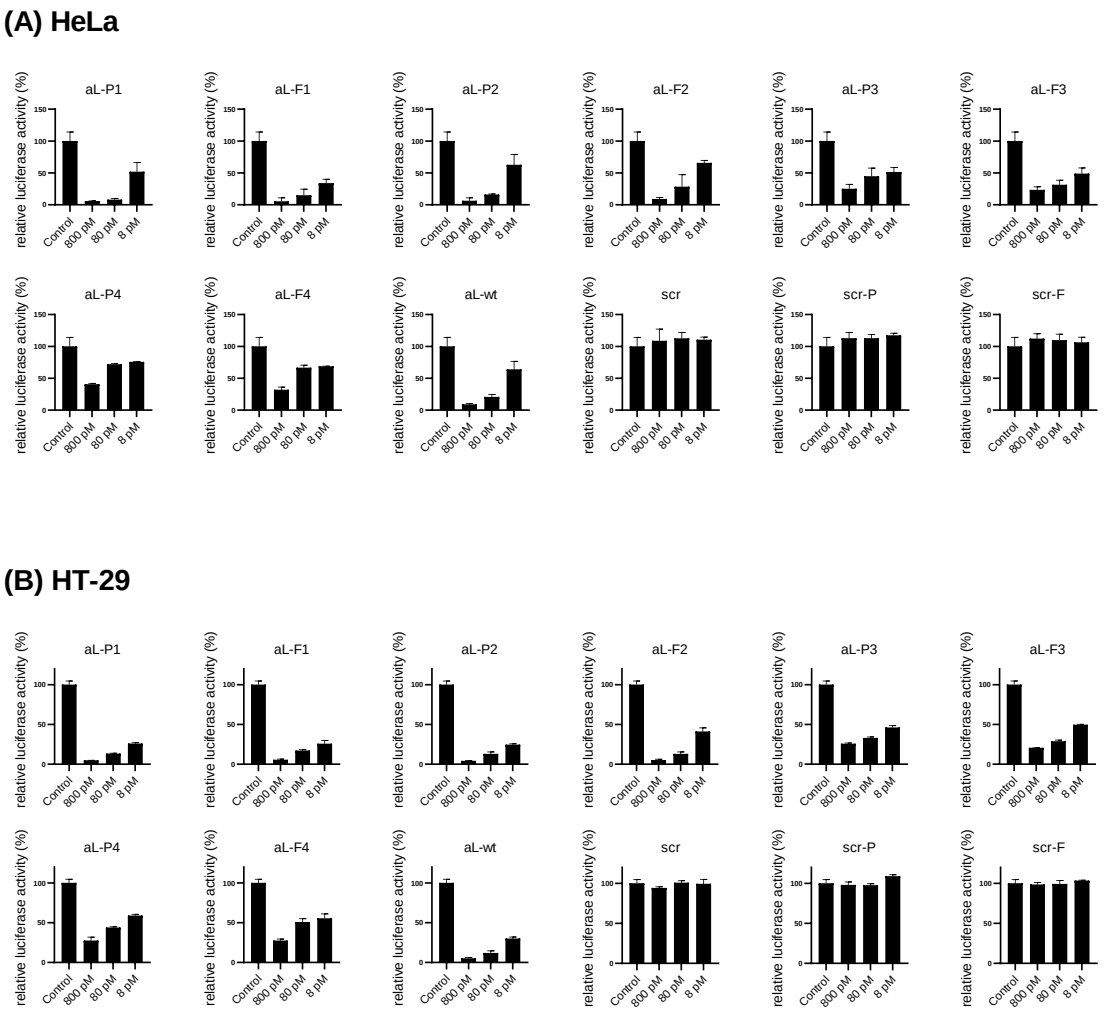

Figure 3.3. Relative expression of firefly luciferase in HeLa (A) and HT-29 cells (B) 24 h after anti-luciferase siRNA transfections at 8, 80 and 800 pM using Lipofectamine. Firefly luciferase expression was assessed with a dual-luciferase reporter assay and was normalized to *Renilla* luciferase. Error bars indicate SD of at least two independent biological replicates.

To assess the cellular uptake and delivery of siRNAs, HeLa and HT-29 cells were transfected following the respective carrier-free protocols described earlier with siRNA concentrations ranging from 1 to 3000 nM. In HeLa cells, gene-silencing activity was only observed in anti-luciferase siRNAs bearing folic acid modifications and not in the wild-type (aL-wt) or propargyl siRNAs (aL-P1 to aL-P4) (Figure 3.4). As expected, scramble controls showed no gene-silencing activity, even with the folic acid modification present. The two

siRNAs bearing centrally placed folic acid modifications displayed the highest gene-silencing potency with IC50 values of 171.0±48.8 and 128.95±9.7 nM for aL-F1 and aL-F2 respectively. Notably, at the lowest concentration tested, 1 nM, the centrally modified folic acid siRNAs still showed ~20% gene-silencing activity. When the folic acid modification was placed at position 5 from sense strand 3′ end (aL-F3), the gene-silencing potency was decreased by more than half (IC50: 283.9±62.9 nM) whereas placing the folic acid modification at the 3′ greatly reduced siRNA activity (IC50: 1044±23.0 nM). Figure 3.5 illustrates the dose-response curves for folic acid-conjugated anti-luciferase siRNAs.

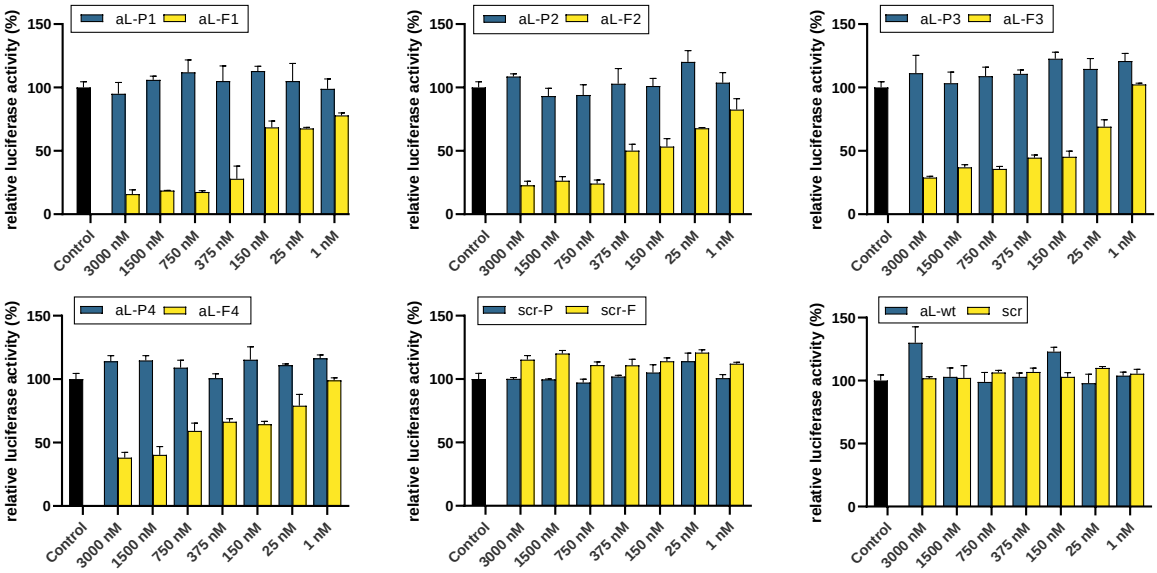

Figure 3.4. Relative expression of firefly luciferase in HeLa cells 16 h after anti-luciferase siRNA transfections at 1, 25, 150, 375, 750, 1500 and 3000 nM without the use of a transfection reagent. Firefly luciferase expression was assessed with a dual-luciferase reporter assay and was normalized to *Renilla* luciferase. Error bars indicate SD of at least two independent biological replicates.

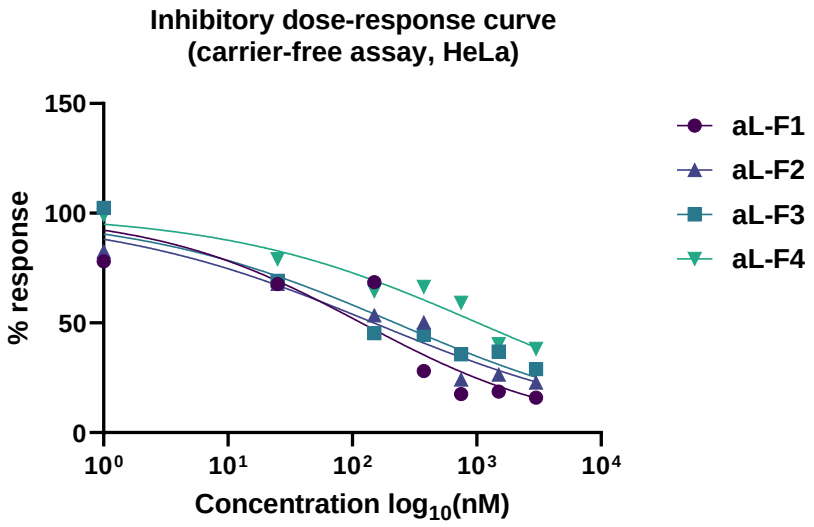

Figure 3.5. Inhibitory dose-response curve for folic acid-conjugated siRNAs targeting exogenous firefly luciferase in HeLa cells following a carrier-free transfection protocol.

To validate that the folic-acid siRNAs are being internalized via FR, we subjected the same type of experiment to HeLa cells that were maintained in DMEM supplemented with folic acid. As seen in Figure 3.6, there is a significant decrease in the gene-silencing activity of centrally modified folic acid–siRNAs (aL-F1 and aL-F2) when free folic acid is present in the media. When the carrier-free siRNA transfection was performed in HT-29 cells, we observed no silencing activity for any of the tested siRNAs (Figure 3.7).

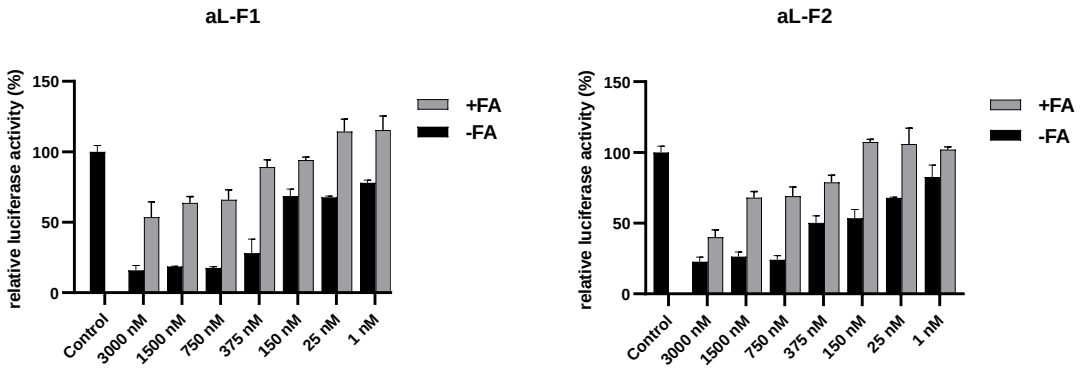

Figure 3.6. Relative expression of firefly luciferase in HeLa cells 16 h after carrier-free transfection of centrally-modified folic acid–siRNAs (aL-F1 and aL-F2). Cells were maintained in either folate-free RPMI 1640 (–FA) or folate-containing DMEM (+FA). Firefly luciferase expression was assessed with a dual-luciferase reporter assay and was normalized to *Renilla* luciferase. Error bars indicate SD of at least two independent biological replicates.

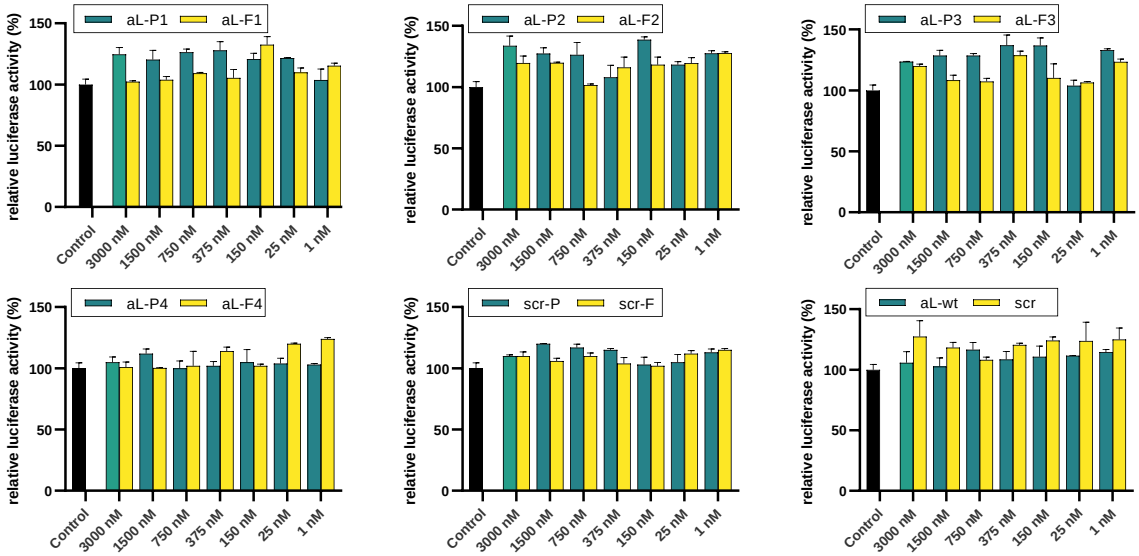

Figure 3.7. Relative expression of firefly luciferase in HT-29 cells 16 h after anti-luciferase siRNA transfections at 1, 25, 150, 375, 750, 1500 and 3000 nM without the use of a transfection reagent. Firefly luciferase expression was assessed with a dual-luciferase reporter assay and was normalized to *Renilla* luciferase. Error bars indicate SD of at least two independent biological replicates.

3.4.4 Viability of HeLa and HT-29 cells after siRNA treatment

The XTT Cell Proliferation Assay was employed to assess HeLa and HT-29 cell viability after treatment with increasing siRNA concentrations (1, 25, 75, 150, 375, 750, 1500 and 3000 nM). At the highest concentration tested (3000 nM), cells treated with propargyl and folic acid–siRNAs displayed 80–90% viability, whereas cells treated with wild-type anti-firefly luciferase siRNA displayed reduced viability in HeLa cells (67%) (Figure 3.8). At lower concentrations, cell viability remained high even after siRNA treatment.

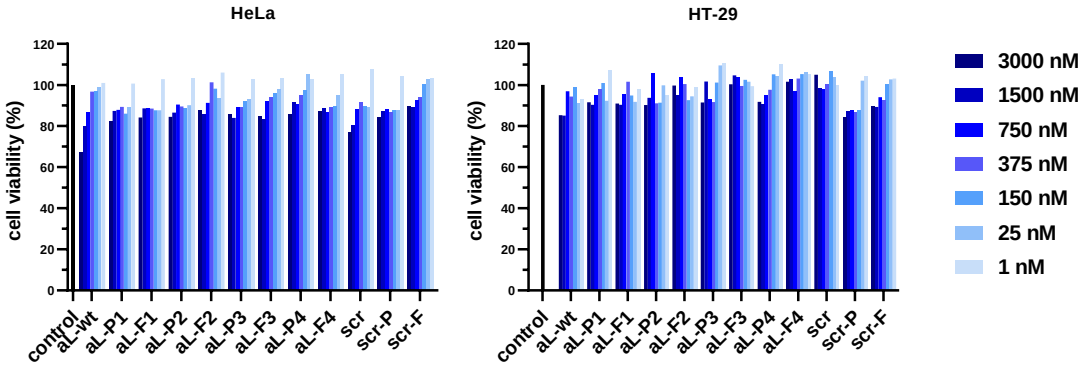

Figure 3.8. Relative viability of HeLa and HT-29 cells after treatment with anti-luciferase siRNAs (1, 25,75, 150, 375, 750, 1500 and 3000 nM).

3.4.5 Viability of HeLa and HT-29 cells after siRNA treatment

The gene-silencing activity of internally-modified anti-Bcl-2 siRNAs was first tested in HeLa cells after transfection with Lipofectamine 2000^{TM}. Both the propargyl and folic acid-modified siRNAs (aB-P and aB-F, respectively) displayed ~70% knockdown after 20 nM treatment, comparable to wild-type siRNA (aB-wt), whereas scramble controls displayed no activity (Figure 3.9). In a carrier-free environment, the internally-modified folic acid–siRNA, aB-F, displayed potent gene-silencing activity of endogenous Bcl-2. At the highest concentration tested, 1 μM, 70% knockdown was achieved (Figure 3.10).

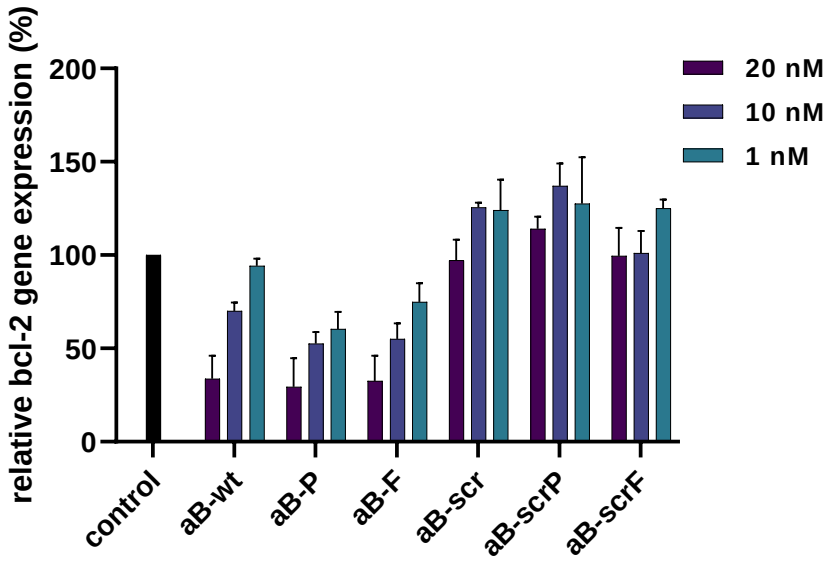

Figure 3.9. Normalized Bcl-2 gene expression in HeLa cells 24 hours after transfection with internally modified propargyl-siRNA (aB-P), folic acid-siRNA (aB-F), wild-type siRNA (aB-wt) or scramble controls (aB-scr-P and aB-scr-F). siRNAs were tested at 1, 10, and 20 nM concentrations and were transfected using Lipofectamine 2000™. Data was normalized using the 18s gene as a reference gene. Error bars indicate SD of two independent biological replicates.

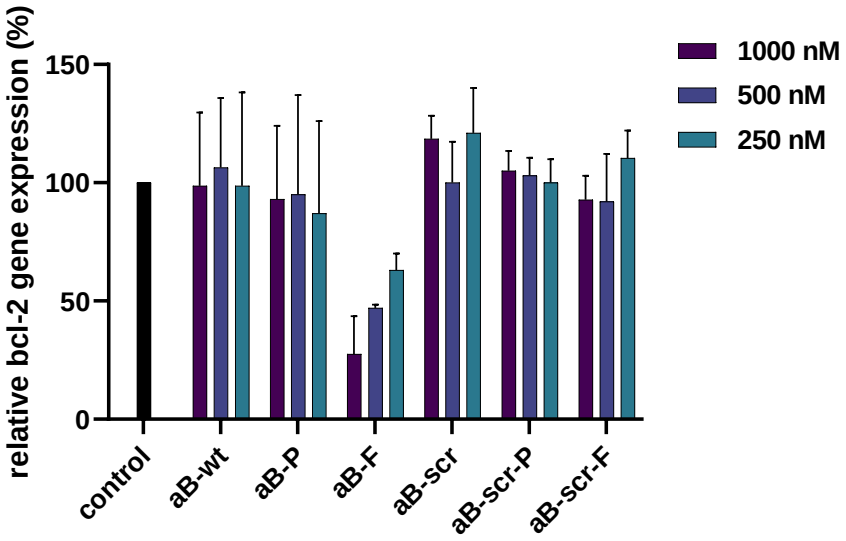

Figure 3.10. Normalized Bcl-2 gene expression in HeLa cells 24 h after carrier-free transfection with internally modified anti-Bcl-2 and scramble siRNAs at 250, 500, 1000 nM concentrations. Data was normalized using the 18S gene as a reference gene. Error bars indicate SD of two independent biological replicates.

3.5 Discussion

Direct conjugation of folic acid to siRNAs has shown great success as a selective, self-delivering system to target cancer cells. Nevertheless, only 40–60% gene silencing has been achieved even after 1 μM siRNA treatment [34]. Therefore, given the promise of using folic acid as a delivery vehicle for siRNAs, there is room for improving its efficacy. Here we have investigated the gene-silencing activity of siRNAs bearing a triazole-linked folic acid modification at different positions within the sense strand, as previous work has only focused on the 3′ and 5′ ends. We have shown that placing the folic acid modification within the central region, spanning the Ago2 cleavage site of the sense strand, increased the gene-silencing activity of anti-luciferase and anti-Bcl-2 siRNAs.

We first assessed the biophysical properties of our synthesized siRNAs. Using CD spectroscopy, we confirmed that our siRNA duplexes adopted an A-form alpha helix conformation (Figure 3.1). RISC recognizes the A-form major groove of the siRNA helix, so the ability of modified siRNAs to adopt an A-form helical structure is desirable for proper RNAi activity [40]. We then assessed the thermal stability of each siRNA duplex, as the thermodynamic properties of siRNA have been shown to play a role in their silencing activity [41]. Modifications placed at or close to the 3′ end did not cause significant thermal destabilization. This was expected, as this area has been shown to be fairly tolerant to chemical modifications [14]. On the other hand, modifications spanning the central region of the sense strand caused significant thermal destabilization. Some studies suggest that destabilization in this region can lead to increase silencing activity [39,42] and previous work from our group has reported success using internally-modified siRNAs bearing a variety of chemically-modified spacer linkages [36,43]. A crucial step for RNAi function is

the dissociation of the sense strand, facilitated by Ago2 cleavage at the central region. It has been proposed that low thermal stability in this region could improve RNAi activity by facilitating passenger strand release [44]. To investigate the gene-silencing potency of centrally-modified folic acid–siRNAs, we first targeted the exogenous gene firefly luciferase in two cell lines, HeLa and HT-29. HeLa cells are derived from human cervical cancer and HT-29 cells are derived from human colon cancer. We assessed the relative expression of FRs in HeLa and HT-29 cells using flow cytometry and found that HeLa cells displayed a 3-fold increase in FR expression compared to HT-29 (Figure 3.2). Although this is not a quantitative measure, a 3-fold increase in receptor expression can be biologically significant. Multiple examples are provided in Leamon′s study [26], which quantitatively measured the expression of FR in various human cancer and normal tissues. High FR-positive tissues and cells, such as HeLa, express at least 6 pmol FR/mg protein whereas tissues or cells expressing no more than 2.5 pmol FR/mg protein are considered to have low FR expression, suggesting that a small difference in expression can lead to significantly different biological activity. Several literature reports indicate that HeLa cells express high levels of FR [45] whereas HT-29 cells express low levels of FR [46]. Based on this, HeLa was chosen as the FR-positive cell line and HT-29 as the FR-negative cell line.

In HeLa cells, we show that internally-modified propargyl and folic acid–siRNAs displayed more potent gene-silencing activity than their 3′-modified counterparts after transfection with Lipofectamine 2000™ (Figure 3.3 - A). Even in the absence of a transfection reagent, internally-modified folic acid–siRNAs aL-F1 and aL-F2 still displayed enhanced gene-silencing potency and much lower IC_{50} values than aL-F3 (modified at position 5 from sense strand 3′ end) and aL-F4 (modified at the 3′ end). We only observed 40–65% knockdown after 0.75 μM treatment of aL-F3 and aL-F4. However, treatment with the centrally

modified folic acid siRNAs aL-F1 and aL-F2 at the same 0.75 μM concentration led to 80% knockdown (Figure 3.4), a significant improvement from literature reports. Although Low′s study reported selective in vivo delivery of 5′-modified folic acid–siRNAs to tumours in mice bearing KB tumour xenografts, these siRNAs were trapped in intracellular endosomes after internalization and did not display efficient gene-silencing activity [35]. Carell′s study, on the other hand, achieved moderate gene-silencing activity with a 3′-modified folic-acid siRNA [34]. This study targeted exogenous luciferase mRNA in HeLa cells and reported ∼50% gene-silencing activity after 1 μM siRNA treatment. One potential reason for this saturation could be due to off-target effects, namely, the strand selection process. If the 3′ folic acid-modified passenger strand is selected as the guide strand for the RISC complex, it is possible that reduced overall gene silencing may occur. The central region of the antisense strand has been shown to be less tolerant to chemical modifications [47]. Therefore, by using the central region in the passenger strand for a folic acid modification, it is possible that enhanced efficacy could be attributed to loss of passenger strand uptake by the RISC complex.

To validate that the folic-acid siRNAs are being internalized via FRs, we performed a folic acid competition study. Following the same carrier-free protocol described earlier, we transfected the two centrally-modified folic acid–siRNAs (aL-F1 and aL-F2) into HeLa cells that were maintained in DMEM supplemented with folic acid (9 μM). FRs are found on the cell surface and are able to internalize folic acid and folic acid-conjugates via receptor-mediated endocytosis. When excess folic acid was present in the media, there was a significant decrease in siRNA gene-silencing activity compared to previously described studies in folate-free media (Figure 3.6). After confirming the self-delivering properties of our anti-luciferase folic acid–siRNAs in HeLa cells, we investigated their selectivity for FR-

expressing cell lines by testing them in FR-negative HT-29 cells. We first performed the transfection using Lipofectamine® LTX to ensure that the siRNAs were biologically active once inside the cell. We observed a similar pattern of gene-silencing activity as we did in HeLa cells, with internally modified siRNAs displaying much higher potency than 3′-modified siRNAs (Figure 3.3 - B). In the absence of a transfection carrier, however, none of the tested siRNAs displayed activity, confirming their selectivity for FR-expressing cells (Figure 3.7). In both cell lines, siRNA treatment caused low to no cytotoxic effects (Figure 3.8), even at the highest concentrations tested (3000 nM). Given the selectivity and potent gene-silencing activity of our internally-modified folic acid–siRNAs against the exogenous target firefly luciferase, we designed siRNAs targeting the endogenous gene Bcl-2. This oncogene is overexpressed in 50–70% of all human cancers and is a desirable target for siRNA therapeutics [48-50]. The triazole-linked folic acid modification was incorporated at position 10 from the sense strand 5′ end of our anti-Bcl-2 siRNA (aB-F) and gene-silencing activity was assessed using real-time polymerase chain reaction (RT-PCR) in HeLa cells, which endogenously express bcl-2. This internally-modified folic acid–siRNA displayed potent gene-silencing activity even in the absence of a transfection reagent (Figure 3.10). Notably, we observed ∼72% knockdown of endogenous Bcl-2 after 1 μM siRNA treatment.

In summary, we report a straightforward and efficient post-column CuAAC synthetic strategy to prepare self-delivering folic acid–siRNAs that selectively target FR-expressing cells. Furthermore, we have developed an approach to enhance the gene-silencing potency of folic acid–siRNA constructs by modifying the central region of the siRNA sense strand and achieved improvement in siRNA activity compared to literature reports. Overall, our data show that siRNAs with internal folic acid modifications are able to effectively downregulate the expression of both exogenous and endogenous gene targets with minimal

toxicity. Given that folate receptors are vastly overexpressed in a variety of cancers, our synthetic approach could be employed to achieve selective delivery of siRNAs to cancer cells without the use of transfection reagents or sophisticated carriers while maintaining potent RNAi activity. Next steps could involve examining our folic acid–siRNA conjugates in higher-level organisms that have folic receptor alpha positive tumors. Therefore, our work can open new avenues for the design and development of novel RNAi-based cancer therapeutics.

3.6 Supplementary Data

Refer to Appendix B for the original manuscript and corresponding supplementary data.

3.7 References

1. Hannon GJ. (2002) RNA Interference. Nature 418:244-251.

2. Sharp PA and PD Zamore. (2000) Molecular biology. RNA interference. Science 287:2431-2433.

3. Kobayashi H and Y Tomari. (2016) RISC assembly: Coordination between small RNAs and Argonaute proteins. Biochim Biophys Acta 1859:71-81.

4. Wang Y, S Juranek, H Li, G Sheng, GS Wardle, T Tuschl and DJ Patel. (2009) Nucleation, propagation and cleavage of target RNAs in Ago silencing complexes. Nature 461:754-761.

5. Leuschner PJ, SL Ameres, S Kueng and J Martinez. (2006) Cleavage of the siRNA passenger strand during RISC assembly in human cells. EMBO Rep 7:314-320.

6. Pratt AJ and IJ MacRae. (2009) The RNA-induced silencing complex: a versatile gene-silencing machine. J. Biol. Chem. 284:17897-17901.

7. Tang G. (2005) siRNA and miRNA: an insight into RISCs. Trends Biochem Sci 30:106-114.

8. Elbashir SM, J Harborth, W Lendeckel, A Yalcin, K Weber and T Tuschl. (2001) Duplexes of 21-nucleotide RNAs Mediate RNA Interference in Cultured Mammalian Cells. Nature 411:494-498.

9. Curtis CD and AM Nardulli. (2014) Using RNA Interference to Study Protein Function. Methods Mol. Biol. 505:187-204.

10. Dana H, GM Chalbatani, H Mahmoodzadeh, R Karimloo, O Rezaiean, A Moradzadeh, N Mehmandoost, F Moazzen, A Mazraeh, V Marmari *et al.* (2017) Molecular Mechanisms and Biological Functions of siRNA. Int. J. Biomed. Sci. 13:48-57.

11. Aagaard L and JJ Rossi. (2007) RNAi therapeutics: principles, prospects and challenges. Adv Drug Deliv Rev 59:75-86.

12. Ryther RC, AS Flynt, JA Phillips, 3rd and JG Patton. (2005) siRNA therapeutics: big potential from small RNAs. Gene Ther. 12:5-11.

13. Wittrup A and J Lieberman. (2015) Knocking down disease: a progress report on siRNA therapeutics. Nat. Rev. Genet. 16:543-552.

14. Bramsen J and J Kjems. (2012) Development of Therapeutic-Grade Small Interfering RNAs by Chemical Engineering. Frontiers in Genetics, 3:1-22.

15. Haussecker D. (2014) Current issues of RNAi therapeutics delivery and development. Journal of Controlled Release 195:49-54.

16. Haupenthal J, C Baehr, S Kiermayer, S Zeuzem and A Piiper. (2006) Inhibition of RNAse A family enzymes prevents degradation and loss of silencing activity of siRNAs in serum. Biochem. Pharmacol. 71:702-710.

17. Shukla S, CS Sumaria and PI Pradeepkumar. (2010) Exploring chemical modifications for siRNA therapeutics: a structural and functional outlook. ChemMedChem 5:328-349.

18. Braasch DA, S Jensen, Y Liu, K Kaur, K Arar, MA White and DR Corey. (2003) RNA interference in mammalian cells by chemically-modified RNA. Biochemistry 42:7967-7975.

19. Adams D, A Gonzalez-Duarte, WD O'Riordan, CC Yang, M Ueda, AV Kristen, I Tournev, HH Schmidt, T Coelho, JL Berk *et al.* (2018) Patisiran, an RNAi Therapeutic, for Hereditary Transthyretin Amyloidosis. N Engl J Med 379:11-21.

20. Wang J, Z Lu, MG Wientjes and JL Au. (2010) Delivery of siRNA therapeutics: barriers and carriers. Aaps j 12:492-503.

21. Meade BR and SF Dowdy. (2009) The road to therapeutic RNA interference (RNAi): Tackling the 800 pound siRNA delivery gorilla. Discov. Med. 8:253-256.

22. Nair JK, JL Willoughby, A Chan, K Charisse, MR Alam, Q Wang, M Hoekstra, P Kandasamy, AV Kel'in, S Milstein *et al.* (2014) Multivalent N-acetylgalactosamine-conjugated siRNA localizes in hepatocytes and elicits robust RNAi-mediated gene silencing. J. Am. Chem. Soc. 136:16958-16961.

23. Liang X, J Fan, Y Zhao, M Cheng, X Wang, R Jin and T Sun. (2017) A targeted drug delivery system based on folic acid-functionalized upconversion luminescent nanoparticles. J. Biomater. Appl. 31:1247-1256.

24. Moghimipour E, M Rezaei, Z Ramezani, M Kouchak, M Amini, KA Angali, FA Dorkoosh and S Handali. (2018) Folic acid-modified liposomal drug delivery strategy for tumor targeting of 5-fluorouracil. Eur. J. Pharm. Sci. 114:166-174.

25. Chen C, J Ke, XE Zhou, W Yi, JS Brunzelle, J Li, E-L Yong, HE Xu and K Melcher. (2013) Structural Basis for Molecular Recognition of Folic Acid by Folate Receptors. Nature 500:486-489.

26. Parker N, MJ Turk, E Westrick, JD Lewis, P Low and CP Leamon. (2005) Folate receptor expression in carcinomas and normal tissues determined by a quantitative radioligand binding assay. Anal. Biochem. 338:284-293.

27. Toffoli G, C Cernigoi, A Russo, A Gallo, M Bagnoli and M Boiocchi. (1997) Overexpression of folate binding protein in ovarian cancers. Int. J. Cancer 74:193-198.

28. Zwicke GL, G Ali Mansoori and CJ Jeffery. (2012) Utilizing the folate receptor for active targeting of cancer nanotherapeutics. Nano Reviews 3:18496.

29. Babu A, R Muralidharan, N Amreddy, M Mehta, A Munshi and R Ramesh. (2016) Nanoparticles for siRNA-Based Gene Silencing in Tumor Therapy. IEEE Trans Nanobioscience 15:849-863.

30. Li JM, YY Wang, W Zhang, H Su, LN Ji and ZW Mao. (2013) Low-weight polyethylenimine cross-linked 2-hydroxypopyl-β-cyclodextrin and folic acid as an efficient and nontoxic siRNA carrier for gene silencing and tumor inhibition by VEGF siRNA. Int J Nanomedicine 8:2101-2117.

31. Leng Q, MC Woodle and AJ Mixson. (2017) Targeted Delivery of siRNA Therapeutics to Malignant Tumors. Journal of Drug Delivery 2017:6971297.

32. Yoshizawa T, Y Hattori, M Hakoshima, K Koga and Y Maitani. (2008) Folate-linked lipid-based nanoparticles for synthetic siRNA delivery in KB tumor xenografts. Eur. J. Pharm. Biopharm. 70:718-725.

33. Zheng B, S Yang, M Wang, X Yang, L Teng, J Xie, L Teng and RJ Lee. (2015) Non-covalent Nanocomplexes of Folic Acid and Reducible Polyethylenimine for Survivin siRNA Delivery. Anticancer Res. 35:5433-5441.

34. Willibald J, J Harder, K Sparrer, KK Conzelmann and T Carell. (2012) Click-modified anandamide siRNA enables delivery and gene silencing in neuronal and immune cells. J. Am. Chem. Soc. 134:12330-12333.

35. Thomas M, SA Kularatne, L Qi, P Kleindl, CP Leamon, MJ Hansen and PS Low. (2009) Ligand-Targeted Delivery of Small Interfering RNAs to Malignant Cells and Tissues. Annals of the New York Academy of Sciences 1175:32-39.

36. Desaulniers J-P, G Hagen, J Anderson, C McKim and B Roberts. (2017) Effective gene-silencing of siRNAs that contain functionalized spacer linkages within the central region. RSC Advances 7:3450-3454.

37. Salim L, C McKim and J-P Desaulniers. (2018) Effective carrier-free gene-silencing activity of cholesterol-modified siRNAs. RSC Advances 8:22963-22966.

38. O'Toole AS, S Miller and MJ Serra. (2005) Stability of 3' double nucleotide overhangs that model the 3' ends of siRNA. RNA 11:512-516.

39. Addepalli H, Meena, CG Peng, G Wang, Y Fan, K Charisse, KN Jayaprakash, KG Rajeev, RK Pandey, G Lavine *et al.* (2010) Modulation of thermal stability can enhance the potency of siRNA. Nucleic Acids Res. 38:7320-7331.

40. Hernández AR, LW Peterson and ET Kool. (2012) Steric Restrictions of RISC in RNA Interference Identified with Size-Expanded RNA Nucleobases. ACS Chemical Biology 7:1454-1461.

41. Kurreck J. (2006) siRNA Efficiency: Structure or Sequence—That Is the Question. Journal of Biomedicine and Biotechnology 2006:083757.

42. Petrova NS, MI Meschaninova, AG Venyaminova, MA Zenkova, VV Vlassov and EL Chernolovskaya. (2011) Silencing activity of 2'-O-methyl modified anti-MDR1 siRNAs with mismatches in the central part of the duplexes. FEBS Lett 585:2352-2356.

43. Efthymiou TC, B Peel, V Huynh and JP Desaulniers. (2012) Evaluation of siRNAs that contain internal variable-length spacer linkages. Bioorg Med Chem Lett 22:5590-5594.

44. Khvorova A, A Reynolds and SD Jayasena. (2003) Functional siRNAs and miRNAs exhibit strand bias. Cell 115:209-216.

45. Siwowska K, RM Schmid, S Cohrs, R Schibli and C Müller. (2017) Folate Receptor-Positive Gynecological Cancer Cells: In Vitro and In Vivo Characterization. Pharmaceuticals 10:72.

46. Yin JJ, S Sharma, SP Shumyak, ZX Wang, ZW Zhou, Y Zhang, P Guo, CZ Li, JR Kanwar, T Yang *et al.* (2013) Synthesis and biological evaluation of novel folic acid receptor-targeted, β-cyclodextrin-based drug complexes for cancer treatment. PLoS One 8:e62289.

47. Chernikov IV, VV Vlassov and EL Chernolovskaya. (2019) Current Development of siRNA Bioconjugates: From Research to the Clinic. Front Pharmacol 10:444.

48. Akar U, A Chaves-Reyez, M Barria, A Tari, A Sanguino, Y Kondo, S Kondo, B Arun, G Lopez-Berestein and B Ozpolat. (2008) Silencing of Bcl-2 expression by small interfering RNA induces autophagic cell death in MCF-7 breast cancer cells. Autophagy 4:669-679.

49. Feng LF, M Zhong, XY Lei, BY Zhu, SS Tang and DF Liao. (2006) Bcl-2 siRNA induced apoptosis and increased sensitivity to 5-fluorouracil and HCPT in HepG2 cells. J Drug Target 14:21-26.

50. Tekedereli I, SN Alpay, U Akar, E Yuca, C Ayugo-Rodriguez, HD Han, AK Sood, G Lopez-Berestein and B Ozpolat. (2013) Therapeutic Silencing of Bcl-2 by Systemically Administered siRNA Nanotherapeutics Inhibits Tumor Growth by Autophagy and Apoptosis and Enhances the Efficacy of Chemotherapy in Orthotopic Xenograft Models of ER (-) and ER (+) Breast Cancer. Mol Ther Nucleic Acids 2:e121.

Connecting Statement II

In Chapter 3, we report the synthesis of self-delivering folate-conjugated siRNAs using a straightforward post-column Cu(I)-catalyzed azide/alkyne cycloaddition approach. These siRNAs selectively targeted folate receptor-expressing cancer cells. By incorporating the folate modification within the central region of the sense strand, we were able to enhance the gene-silencing activity of these siRNAs compared to 3′-modified siRNAs. Although folate conjugation is a promising approach for the development of safe delivery systems for cancer therapeutics, its use in RNAi research has been limited by sophisticated, and often expensive, chemistry. Folate phosphoramidites are not commercially available and there is a lack of reliable protocols for their synthesis. In Chapter 4, we report a simple and cost-effective strategy to synthesize a novel folate phosphoramidite for incorporation into oligonucleotides via solid-phase synthesis.

Chapter 4. Synthesis of Novel Folate Phosphoramidites

4.1 Introduction

With the success of the receptor-targeting ligand GalNAc and the need for selective extra-hepatic RNAi delivery systems, folate has gained a lot of attention as a targeting ligand due to its relevance in oncology. The FRα is expressed at very low levels in non-malignant tissues but is highly expressed on numerous cancers, including 90% of ovarian carcinomas as well as breast, endometrial, lung, brain, and kidney cancers [1,2]. Folate conjugates are recognized and internalized by FRα, making folate a promising ligand for tumor targeting clinical applications. Recently, there has been some success with select folate-conjugated siRNAs. However, the field has been limited by the sophisticated, and often expensive, synthetic approaches as well as by the lack of reliable protocols to prepare folate phosphoramidites.

Notably, folate phosphoramidites are not commercially available although Berry & Associates offered a 5′-folate-TEG cyanoethyl phosphoramidite (BA 0349), at a cost of $843 USD for 100 µmol, about a decade ago (Figure 4.1). This product has since been discontinued and there are no reports using this molecule. Because of this, most of the current synthetic approaches, including the one we employed for our triazole-linked folate siRNAs (Chapter 3), require the use of Cu(I) in the final synthetic step. Although effective, this approach poses challenges with scalability and potential cytotoxicity. Based on this, we identified a need to streamline the synthesis of folate-siRNAs. In this work, we report a simple and cost-effective strategy to prepare a novel folate phosphoramidite that is compatible with standard solid-phase oligonucleotide synthesis protocols. We show that

these folate siRNAs are taken up by folate receptor-expressing cancer cells, in the absence of a transfection, and can mediate potent gene-silencing activity.

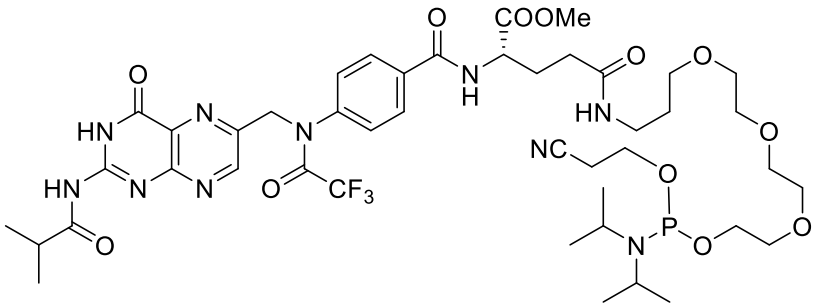

Figure 4.1. Structure of 5′-folate-TEG cyanoethyl phosphoramidite (BA 0349) previously offered by Berry & Associates.

4.2 Materials and Methods

4.2.1 General Methods

All starting reagents and solvents were obtained from commercial sources and used without additional purification, unless otherwise stated. Compounds **A** and **B** were synthesized as previously described [3]. Standard flash chromatography was performed using Silicycle Siliaflash 60 (230-400 mesh). ^{1}H, ^{13}C and ^{31}P NMRs were recorded in DMSO-d6, $CDCl_3$ or CD_3OD using a Bruker Avance III NMR spectrometer. The corresponding spectra can be found in Appendix C.

4.2.2 Synthesis of folate phosphoramidite

4.2.2.1 Synthesis of Compound C

Compound **A** (0.7 g, 1.57 mmol) was first dissolved in anhydrous ACN and triethylamine (0.5 eq, 0.785 mmol, 0.11 mL) under an Argon atmosphere. Compound **B** (1.5 eq., 2.36 mmol, 0.2 g) was then added and the mixture was stirred for 5 minutes at room temperature. CuI (0.3 eq., 0.471 mmol, 0.090 g) and sodium ascorbate (0.5 eq., 0.785 mmol, 0.16 g) were

subsequently added, and the reaction was stirred vigorously for 3 hours at room temperature. After the reaction reached completion, the mixture was dried under vacuum. The resulting residue was purified using silica gel column chromatography (5 to 40% MeOH/CH_2Cl_2 with 2% triethylamine) to afford compound **C** as a crystalline foam (0.63 g, 76%). ^{1}H NMR (400 MHz, CD_3OD) δ ppm 2.66 (t, 2 H) 2.78 (t, 2 H) 3.11 (s, 2 H), 3.23 (t, 2 H), 3.61 (t, 2 H), 3.78 (s, 6 H), 3.84 (s, 2 H), 4.44 (t, 2 H), 6.79 - 6.89 (m, 4 H), 7.16 – 7.44 (m, 9 H), 7.85 (s, 1 H). ^{13}C NMR (101 MHz, CD_3OD) δ ppm 158.64, 145.24, 136.17, 129.86, 127.92, 127.39, 126.38, 124.02, 112.69, 86.24, 61.83, 59.33, 56.00, 54.37, 53.71, 49.31. ESI HRMS (ES+) *m/z* calculated for $C_{30}H_{37}N_5O_4$: 531.2846, found: 531.2100 $[M+H]^+$

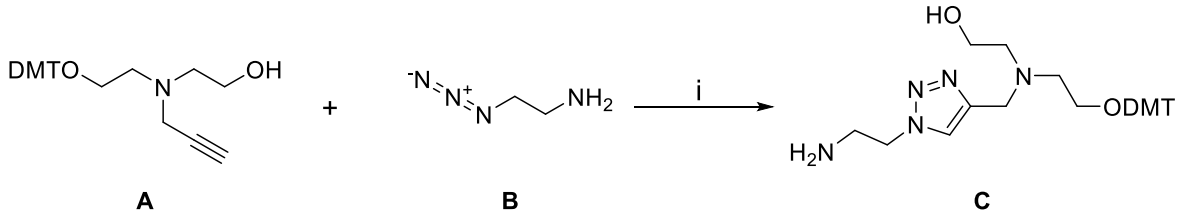

Scheme 4.1 Synthesis of triazole-linker **C**. Reagents and conditions: (i) CuI, sodium ascorbate, Et_3N/ACN, rt, 3 h, 76%.

4.2.2.2 Synthesis of Compound 1

Folic acid (2 g, 4.5 mmol) was suspended in anhydrous THF (20 mL) and stirred at 0 °C in the dark, under an argon atmosphere. Trifluoroacetic anhydride (8 eq., 36 mmol, 5 mL) was added over a 30 min period, and the reaction mixture was then allowed to equilibrate to room temperature. As the reaction proceeded, the mixture turned into a dark brown homogenous phase. After 12 hours, the solvent was evaporated under vacuum and the product was precipitated in ether (~100 mL). The dark brown crystals were collected by filtration and washed with ether (30 mL x 3). ^{1}H NMR (400 MHz, DMSO-d6) δ ppm 1.99 - 2.07 (m, 1 H), 2.41-2.60 (overlap, 3H), 4.73 (dd, 1 H), 5.76 (s, 2 H), 7.64 (s, 4 H), 8.68 (s,

1 H). ^{19}F NMR (377 MHz, DMSO-d6) δ ppm -74.30, -66.09. ESI HRMS (ES+) *m/z* calculated for $C_{23}H_{15}F_6N_7O_7$: 615.0937, found: 615.0987 $[M+H]^+$

4.2.2.3 Synthesis of Compound 2

Compound **C** (0.5 g, 0.94 mmol) was dissolved in anhydrous DMF (20 mL) under argon. Compound **1** (0.87 g, 1.41 mmol) was added and the reaction was allowed to stir in the dark under an argon atmosphere for 36 hours. DMF was removed using a miVac Quattro concentrator. The resulting residue was purified using silica gel chromatography, eluting from 5 to 60% MeOH/CH_2Cl_2 with 5% triethylamine to yield compound **2** as brown crystals (0.70 g, 74%). ^{19}F NMR (377 MHz, DMSO-d6) δ ppm -73.46, -66.09. ESI HRMS (ES+) *m/z* calculated for $C_{48}H_{45}F_6N_{11}O_8$: 1017.3357, found: 1016.4338 $[M+H]^+$

4.2.2.4 Synthesis of Compound 3

To a flame-dried round-bottomed flask was added a solution of compound **2** (0.2 g, 0.196 mmol) in anhydrous 1:1 DCM and THF (10 mL) and triethylamine (0.16 mL, 1.18 mmol), under an argon atmosphere. This was followed by the dropwise addition of 2-cyanoethyl-*N*,*N*-diisopropylchlorophosphoramidite (0.13 mL, 0.59 mmol). The reaction was stirred at room temperature, and in the dark, for 3 hours. After removing the solvent in vacuo, the crude product was taken up in dichloromethane, washed with water and dried with anhydrous sodium sulphate. The organic layer was then concentrated in vacuo. The extracted product was dissolved in 1 mL dichloromethane and crashed out by adding 50 mL of *n*-hexanes. The resulting crystals were collected by filtration and dried in vacuo to yield compound **3**, which was immediately used for solid-phase oligonucleotide synthesis (0.19 g, 79%). ^{19}F NMR (377 MHz, $CDCl_3$) δ ppm -75.48, -67.01. ^{31}P NMR (162 MHz, $CDCl_3$)

δ ppm 149.43, 149.37. ESI HRMS (ES+) *m/z* calculated for $C_{48}H_{45}F_6N_{11}O_8$: 1217.4435, found: 1134.1402 $[M+H]^+$ (hydrolyzed product).

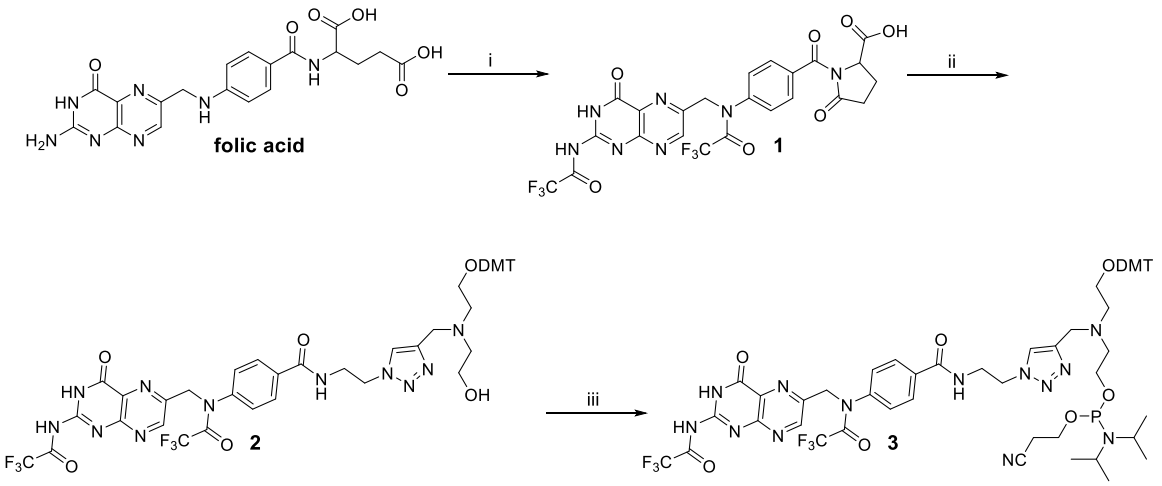

Scheme 4.2 Synthesis of folate phosphoramidite **3**. Reagents and conditions: (i) TFAA, THF, 0 °C, 30 min, 0 °C → rt, 12 h (91%), (ii) **C**, DMF, rt, 36 h (74%), (iii) 2-cyanoethyl-*N*,*N*-diisopropylchlorophosphoramidite, THF/DCM (1:1), Et_3N, rt, 3 h.

4.2.3 Oligonucleotide synthesis

Oligonucleotides were prepared following standard solid-phase oligonucleotide synthetic procedures, using a 1.0 μM controlled-pore glass (CPG) support on an Applied Biosystems 394 DNA/RNA synthesizer. Immediately before use, phosphoramidites were resuspended to a final concentration of 0.1 M. Commercial phosphoramidites were resuspended in anhydrous acetonitrile whereas phosphoramidite **3** was resuspended in a 1:1 mixture of anhydrous THF and DCM. To cleave the oligonucleotides from the solid support, each CPG column was flushed with 1 mL EMAM solution (1:1 methylamine 33 wt% in ethanol/methylamine 40 wt% in water) for 1 hour at room temperature and then incubated overnight in EMAM to deprotect the bases. Oligonucleotides were concentrated in a miVac Quattro Concentrator before being resuspended in DMSO (100 μL). To remove the remaining protecting groups, each oligonucleotide was treated with 3HF-Et_3N (125 μL) and

incubated for 3 hours at 65°C. After drying the DMSO in a miVac Quattro Concentrator, oligonucleotides were precipitated in ethanol and desalted using Millipore Amicon Ultra 3000 MW cellulose centrifugal filters. Strands were purified using reverse-phase HPLC eluting from 5% to 95% ACN in 0.1 M TEAA buffer (pH 7.0).

4.2.4 Biophysical characterization

CD and thermal denaturation studies were performed on a Jasco J-815 Circular Dichroism (CD) Spectropolarimeter equipped with a temperature controller. Duplexes were formed by combining equimolar amounts of complementary sense and antisense strands in 300 μL pH 7 sodium phosphate buffer (90.0 mM NaCl, 10.0 mM Na_2HPO_4, 1.00 mM EDTA), heating them to at 90 °C for 2 min and allowing them to equilibrate to room temperature. Circular dichroism spectra were recorded at 25°C, scanning from 200 to 350 nm with a screening rate of 100 nm/min and a 0.20 nm data pitch. The melting temperature (T_m) of each duplex was determined by measuring the change in absorbance at 260 nm against a temperature gradient from 15 to 90 °C at a rate of 1 °C per minute. Data were analysed using Meltwin v3.5 software.

4.2.5 Cell culture and transfections

HeLa and HT-29 cells were maintained in Dulbecco′s modified Eagle′s medium (DMEM) and Roswell Park Memorial Institute (RPMI) 1640 Medium, respectively, at 37 °C in a humidified atmosphere with 5% CO2. Media were supplemented with 10% fetal bovine serum (FBS) and 1% penicillin–streptomycin (Sigma). HeLa and HT-29 cells were transfected as previously described for both the standard and carrier-free assays [3].

4.2.6 Dual-luciferase® reporter assay

Cells were lysed with 1X passive lysis buffer for 30 min at room temperature. Cell lysates were transferred to microcentrifuge tubes and were immediately used to assess the gene-silencing activity of siRNAs using the Dual-Luciferase® Reporter Assay (Promega) following the manufacturer′s protocol. Cell lysates (10 μL) were transferred to Costar 96-well plates in triplicate. Luminescence measurements were taken on a Synergy HT (Bio-Tek) plate luminometer. Results are expressed as the ratio of firefly/*Renilla* luminescence taken as a percentage of an untreated control.

4.2.7 MTT cell viability assay

HeLa cells were seeded into 96-well plates at a density of 5.0×10^3 cells per well. Prior to transfection, cells were incubated for 24 hours at 37 °C in a humidified atmosphere with 5% CO_2. Cells were transfected following the same carrier-free protocol used for the dual-luciferase® reporter assay. After a 16-hour incubation period, cell viability was assessed using the CyQUANT™ MTT Cell Viability Assay Kit (ThermoFisher) following the manufacturer's quick protocol. Absorbance readings were taken using a Synergy HT (Bio-Tek) plate luminometer.

4.3 Results

4.3.1 Preparation and characterization of folate oligonucleotides

Folate phosphoramidite **3** was prepared and purified as described above. The few previous reports of folate phosphoramidites, such as the one commercialized by Berry and Associates, do not employ silica gel chromatography as a purification method [4]. These phosphoramidite derivatives have poor solubility profiles and can be very labile, so an

alternative approach involves precipitating them out of solution, using an appropriate solvent, and then immediately using them for solid-phase oligonucleotide synthesis. Once the oligonucleotides were cleaved from the solid support and deprotected, they were purified using reverse-phase HPLC and characterized by mass spectrometry (Table 4.1).

Table 3.1. Oligonucleotide sequences and mass spectrometry data

Code	*Sequence*	*Mass (predicted)*	*Mass (found)*
Fol1	5' CUU ACG CUG AGU ACU UCG A**F** 3'	6580.9985	6580.4427
Fol2	5' CUU ACG CUG AGU ACU **F**CG ATT 3'	6886.3612	6886.4511
Fol3	5' CUU ACG CUG **F**GU ACU UCG ATT 3'	6859.0428	6858.7023
Fol4	5' CUU ACG CU**F** AGU ACU UCG ATT 3'	6844.0431	6844.3508

All strands code for firefly luciferase and correspond to the sense strand. **F** indicates the position of the folate modification.

Synthesized oligonucleotides were annealed to their complementary antisense sequences prior to CD and thermal denaturation studies. As see in Figure 4.2, all siRNAs adopted the desired A-form helical conformation which is recognized by the RISC [5]. Consistent with previous findings, we observed higher thermal destabilization when the folate modification was placed within the central region of the sense strand, compared to the 3′ end. The T_m values of unmodified (wt) and folate siRNA are summarized in Table 4.2. In siRNA Fol1, the folate modification replaces the 3′ dTdT overhang and imparts a small destabilizing effect ($\Delta T_m = -6$), likely due to the loss of stacking interactions in this region [6]. We observed a similar effect when replacing the nucleotide at position 6 from the sense strand 3′ end ($\Delta T_m = -6$). Notably, this novel modification was more destabilizing than the one we reported previously [3], particularly when placed at position 9 (Fol4) or 10 (Fol3) from the sense strand 5′ end ($\Delta T_m = -25$ and -24 °C, respectively). This trend is consistent not only with our previous findings, but also with literature reports examining the effect of central modifications on the thermal stability of the siRNA duplex [7].

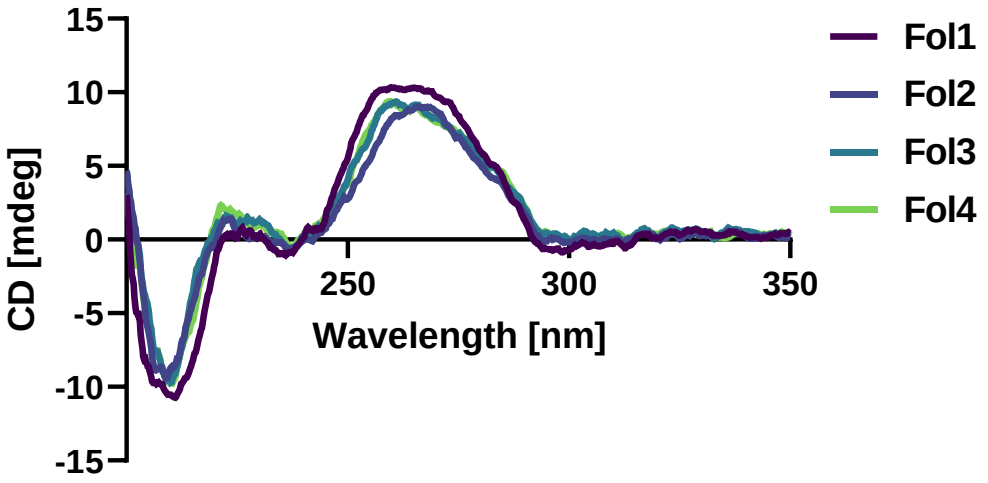

Figure 4.2. Circular dichroism spectra of anti-luciferase folate siRNAs.

Table 4.2. Sequences and T_m data of anti-luciferase wt and folate-siRNAs.

Code	*Sequence*	T_m (°C)	ΔT_m (°C)	IC_{50} ± *SE* (*nM*)
wt	5′ CUU ACG CUG AGU ACU UCG ATT 3′ 3′ TTG AAU GCG ACU CAU GAA GCU 5′	76	-	NA
Fol1	5′ CUU ACG CUG AGU ACU UCG A**F** 3′ 3′ TTG AAU GCG ACU CAU GAA GCU 5′	70	-6	98.5 ± 48.4
Fol2	5′ CUU ACG CUG AGU ACU **F**CG ATT 3′ 3′ TTG AAU GCG ACU CAU GAA GCU 5′	67	-9	23.2 ± 6.4
Fol3	5′ CUU ACG CUG **F**GU ACU UCG ATT 3′ 3′ TTG AAU GCG ACU CAU GAA GCU 5′	52	-24	26.2 ± 8.2
Fol4	5′ CUU ACG CU**F** AGU ACU UCG ATT 3′ 3′ TTG AAU GCG ACU CAU GAA GCU 5′	51	-25	46.3 ± 28.5

The top strand corresponds to the sense strand; the bottom strand corresponds to the antisense strand. ***F*** indicates the location of the folate modification. IC_{50} values were calculated after carrier-free siRNA transfections in HeLa cells.

4.3.2 Gene-silencing activity in HeLa cells

We first assessed the biological activity of the folate siRNAs in HeLa cells after transfection with Lipofectamine 2000™. As seen in Figure 4.3, all siRNAs displayed excellent dose-dependent activity. At the highest concentration tested (800 pM), all siRNAs achieved potent knockdown of exogenous firefly luciferase mRNA. We then investigated the ability

of the folate modification to mediate siRNA uptake into these folate receptor-expressing cells. To achieve this, we transfected siRNAs into HeLa cells at concentrations ranging from 0.5 to 3000 nM, without the use of a transfection reagent. As expected, the unmodified (wt) siRNA was unable to cross the cellular membrane and thus did not result in gene silencing. On the other hand, all folate siRNAs achieved potent gene-silencing activity in the absence of a transfection carrier (Figure 4.4). With our previous folate modification, discussed in Chapter 3, we observed enhanced potency when placing it within the central region, as opposed to the 3′ end, of the siRNA. The novel folate modification presented herein did not impart a position-dependent effect on siRNA potency although it was placed in the same regions that we previously investigated. Overall, siRNAs Fol1-Fol4 displayed potent and comparable activity, with IC_{50} values ranging from 23.2 to 98.5 nM.

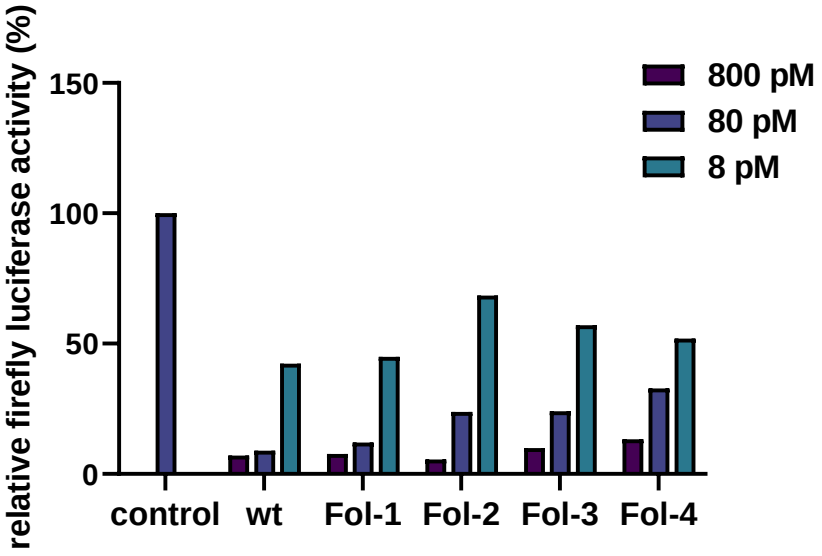

Figure 4.3. Relative expression of firefly luciferase in HeLa cells 24 hours after siRNA transfection using Lipofectamine 2000™. Firefly luciferase expression was normalized to *Renilla* luciferase.

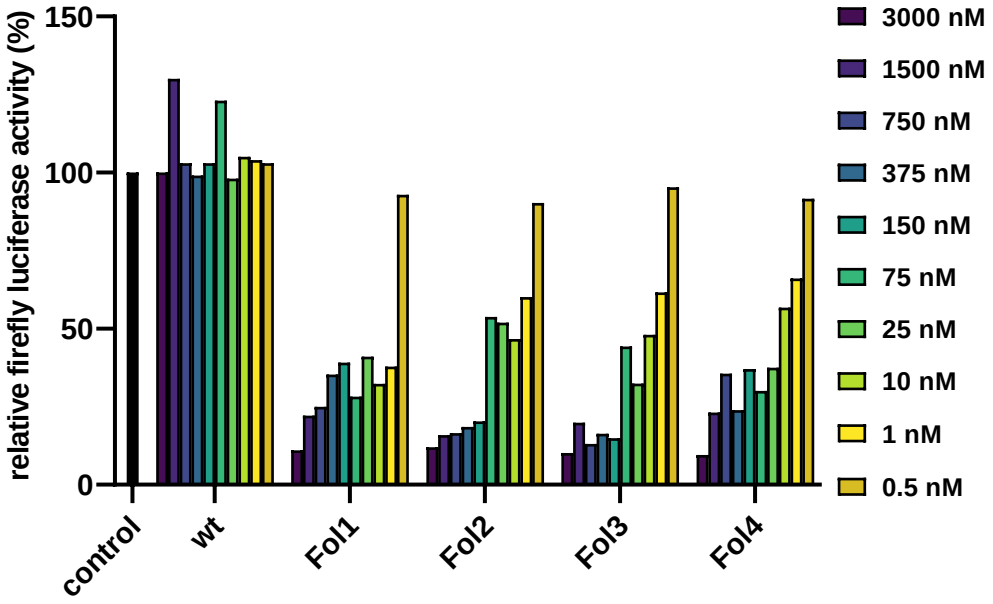

Figure 4.4. Relative expression of firefly luciferase in HeLa cells 16 hours after carrier-free siRNA transfection. Firefly luciferase expression was normalized to *Renilla* luciferase.

4.3.4 Gene-silencing activity in HT-29 cells

To assess the selectivity of our folate siRNAs for FR-expressing cells, we repeated the dual-luciferase® reporter assays in the FR-negative cell line HT-29. We first transfected siRNAs into HT-29 cells at concentrations ranging from 8 to 800 pM, using Lipofectamine® LTX. As seen in Figure 4.5, when siRNAs are internalized by the transfection carrier, all siRNAs show dose-dependent knockdown. The gene-silencing trend displayed by the siRNAs in HT-29 cells was comparable to that observed in HeLa cells. Next, we assessed the ability of the folate modification to mediate uptake in the absence of a transfection carrier. None of the siRNAs displayed gene-silencing activity in HT-29 cells when tested without a transfection reagent (Figure 4.6). This was expected since the internalization of these molecules is mediated by cell-surface folate receptors.

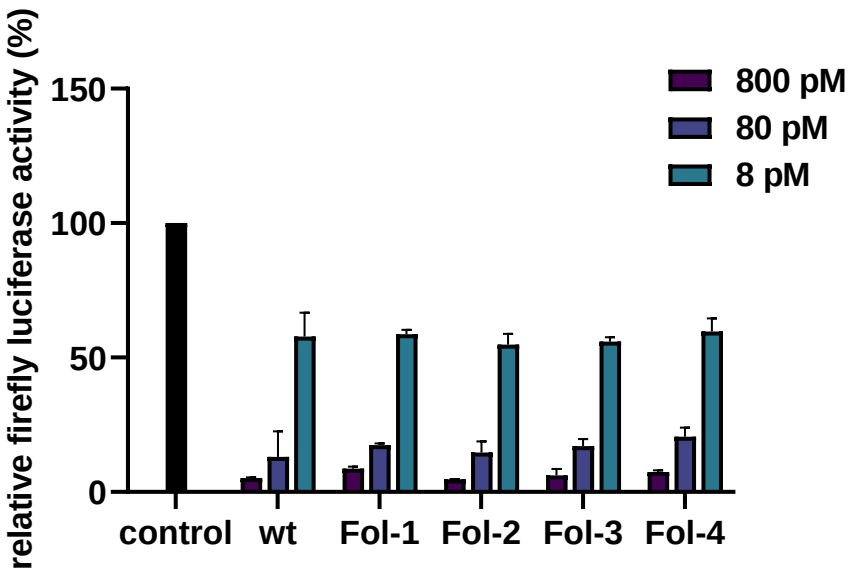

Figure 4.5. Relative expression of firefly luciferase in HT-29 cells 24 hours after siRNA transfection using Lipofectamine® LTX. Firefly luciferase expression was normalized to *Renilla* luciferase. Error bars indicate SD of at least two independent biological replicates.

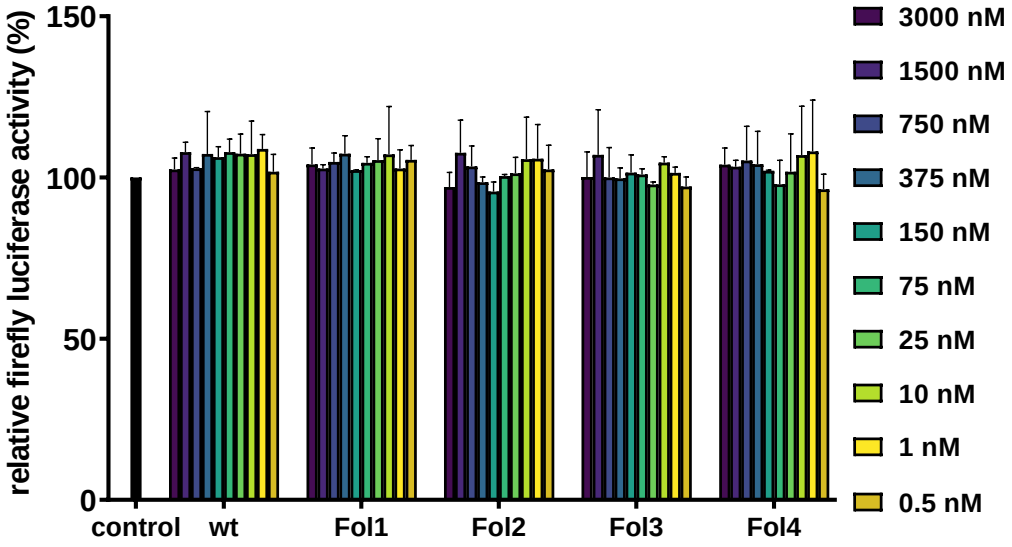

Figure 4.6. Relative expression of firefly luciferase in HT-29 cells 16 hours after carrier-free siRNA transfection. Firefly luciferase expression was normalized to *Renilla* luciferase. Error bars indicate SD of at least two independent biological replicates.

4.3.4 HeLa cell viability after siRNA treatment

We assessed HeLa cell viability after carrier-free treatment with unmodified (wt) and folate siRNAs at five concentrations (5, 25, 100, 750 and 3000 nM) using a colorimetric MTT assay, as described earlier. As seen in Figure 4.7, treatment with high concentrations of wild-type siRNA (750 and 3000 nM) led to ~24% decrease in HeLa cell viability. This is consistent with our previous findings [3]. On the other hand, our novel folate-modified siRNAs did not impart any cytotoxic effects, resulting in over 90% cell viability across all concentrations tested. Our previous folate siRNA formulation led to 80-90% cell viability after siRNA treatment, indicating that low cytotoxic effects were present with some of the concentrations tested [3].

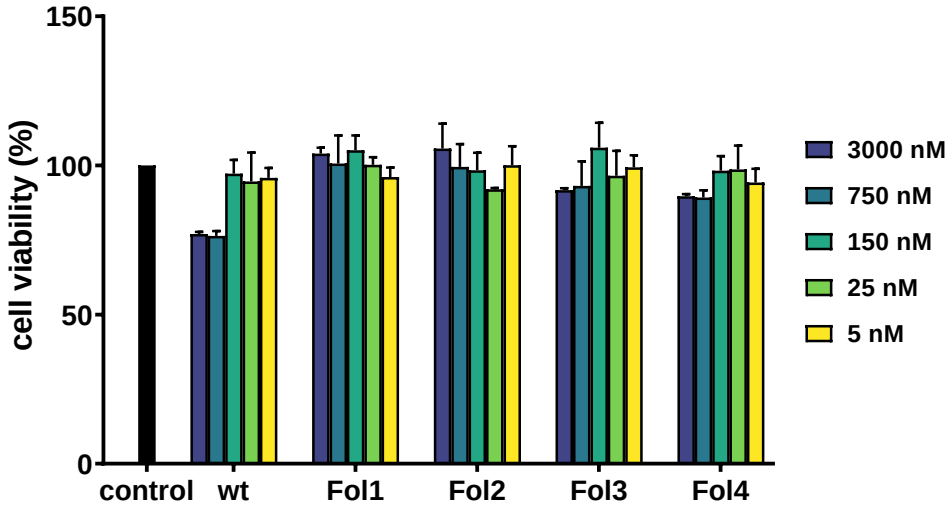

Figure 4.7. HeLa cell viability after carrier-free transfection with wild-type (wt) and folate-modified siRNAs. Error bars indicate SD of two independent biological replicates.

4.4 Conclusion

Overall, we report a straightforward and cost-effective approach to prepare a folate phosphoramidite that is compatible with solid-phase oligonucleotide synthesis. Incorporation of this folate modification at different positions within the siRNA sense strand resulted in a new generation of self-delivering folate siRNAs, selective for FR-expressing cells. All siRNAs displayed potent gene-silencing activity, regardless of where the modification was placed within the sequence. This work is very significant as folate phosphoramidites are not commercially available and there are not many reliable protocols to synthesize them. This has limited the application of folate-based gene-silencing therapies, as most current approaches rely on post-column Cu(I)-catalyzed azide/alkyne cycloaddition which can pose challenges when it comes to cytotoxicity and scalability. Our current synthetic approach will allow us to streamline the synthesis of folate-conjugated oligonucleotides and provide a means to better investigate these molecules for therapeutic applications.

4.5 References

1. Parker N, MJ Turk, E Westrick, JD Lewis, P Low and CP Leamon. (2005) Folate receptor expression in carcinomas and normal tissues determined by a quantitative radioligand binding assay. Anal. Biochem. 338:284-293.

2. Chen C, J Ke, XE Zhou, W Yi, JS Brunzelle, J Li, E-L Yong, HE Xu and K Melcher. (2013) Structural Basis for Molecular Recognition of Folic Acid by Folate Receptors. Nature 500:486-489.

3. Salim L, G Islam and J-P Desaulniers. (2020) Targeted delivery and enhanced gene-silencing activity of centrally modified folic acid–siRNA conjugates. Nucleic Acids Research 48:75-85.

4. Barta NS and JC Hodges. (2011); C07F 9/24 (2006.01).

5. Hernández AR, LW Peterson and ET Kool. (2012) Steric Restrictions of RISC in RNA Interference Identified with Size-Expanded RNA Nucleobases. ACS Chemical Biology 7:1454-1461.

6. O'Toole AS, S Miller and MJ Serra. (2005) Stability of 3' double nucleotide overhangs that model the 3' ends of siRNA. RNA 11:512-516.

7. Addepalli H, Meena, CG Peng, G Wang, Y Fan, K Charisse, KN Jayaprakash, KG Rajeev, RK Pandey, G Lavine *et al.* (2010) Modulation of thermal stability can enhance the potency of siRNA. Nucleic acids research 38:7320-7331.

Connecting Statement III

The work outlined in Chapter 2-4 focuses on the development of effective delivery platforms for siRNAs using two promising bioconjugates. However, poor cellular uptake is not the only shortcoming of RNAi molecules. The inherent structure of RNA poses additional challenges like off-targets and immune activation, so it is of great interest to investigate novel chemical modifications that could improve the pharmacokinetic profiles of RNAi molecules. A novel chemical modification approach involves replacing the ribose sugar of RNA with a six-carbon moiety. In the following chapter, we discuss the synthesis of a novel glucose phosphoramidite derivative which is triazole-linked to uracil at position one. This molecule was introduced at various positions within the sense or antisense strand, resulting in duplexes containing a single 3′-6′/2′-5′ phosphodiester linkage.

Chapter 5. Manuscript III

Synthesis and evaluation of modified siRNA molecules containing a novel glucose derivative

Lidya Salim, Eva Goss and Jean-Paul Desaulniers

Published in:

RSC Advances **2021**, *11*, 9285-9289

DOI: 10.1039/d1ra00922b

5.1 Abstract

Chemical modifications are critical for the development of safe and effective siRNAs for downstream applications. In this study, we report the synthesis of a novel glucose phosphoramidite, a triazole-linked to uracil at position one, for incorporation into oligonucleotides. Biological testing revealed that the glucose derivative at key positions within the sense or antisense strand can lead to potent gene-silencing activity, thus highlighting its tolerance in both sense and antisense positions. Furthermore, the A-form helical formation was maintained with this modification. Overall, placing the modification at the 3′ end and at key internal positions led to effective RNAi gene-silencing activity modification.

5.2 Introduction

RNA interference (RNAi) is a natural mechanism that mediates sequence-specific gene silencing by targeting messenger RNA and supressing translation [1]. This pathway involves the assembly of an RNA-induced silencing complex (RISC) which incorporates double-stranded RNA sequences called short interfering RNAs (siRNAs) [2]. Each siRNA duplex is ~21 nucleotides in length and is made up of a guide (antisense) strand and a passenger (sense) strand. After the siRNA duplex is unwound by RISC, the passenger strand is removed by the endonuclease Argonaute2 (Ago2), while the guide strand is retained and used as a guide sequence to locate and cleave the mRNA target [3]. Synthetic siRNAs are compatible with the endogenous RNAi pathway and are able to reduce the expression of target proteins, serving not only as experimental tools but also as gene-silencing therapeutics. Despite recent advances in the field, such as the U.S. FDA approval of three RNAi-based therapies [4,5], the development of safe and effective siRNA therapeutics has

been limited by the inherent structure of RNA which poses challenges like low stability, poor cellular uptake, and off-target effects [6,7].

Chemical modifications can be used to optimize the pharmacokinetic properties of siRNAs for in vivo applications. Several modifications have been developed to date, including backbone, nucleobase, and sugar modifications, which can be incorporated individually or in combination [8-10]. Nevertheless, there is still no universal modification that mitigates all the aforementioned challenges, so there is great interest in designing and investigating novel modifications that could be incorporated in for future siRNA design.

Modifications of the ribose sugar have been extensively studied to improve stability and siRNA potency. The presence of the 2′ hydroxyl group makes RNA more susceptible to hydrolysis and is often modified, as it is not required for RNAi activity [11]. Common 2′ modifications include 2′-fluoro and 2′-methoxy, which increase siRNA stability [12]. Other modifications include bicyclic derivatives like locked nucleic acids (LNA), which lock the ribose sugar in the C3′-*endo* conformation[13], and acyclic derivatives like unlocked nucleic acids (UNA), which lack the C2′-C3′-bond of the ribose sugar [14].

A more recent approach involves replacing the ribose sugar with six-carbon moieties. Altritol nucleic acids have displayed stronger activity than unmodified siRNAs, particularly when placed at the 3′ end of the sense or antisense strand [15]. Cyclohexenyl and hexitol nucleic acids have also shown increased activity as well as nuclease stability [16,17]. Herein, we explore the synthesis of a novel glucose phosphoramidite derivative, which is a triazole-linked to a uracil nucleobase at position one. This modification was introduced at either terminal or internal positions of the sense or antisense strand, resulting in siRNA duplexes containing a single 3′-6′/2′-5′ phosphodiester linkage.

5.3 Experimental

5.3.1 Chemicals and general methods

β-D-glucopyranosyl azide was obtained from Synthose, Inc. Canada. Other starting reagents and solvents were obtained from other commercial sources such as Sigma Aldrich and used without further purification, unless otherwise stated. Standard flash chromatography was performed using Silicycle Siliaflash 60 (230-400 mesh). ^{1}H, ^{13}C and ^{31}P NMRs were recorded in $CDCl_3$ or CD_3OD using a Bruker Avance III NMR spectrometer.

5.3.2 Compound 1

To a solution of β-D-glucopyranosyl azide (0.5 g, 2.44 mmol) in anhydrous pyridine (7 mL) at 0 °C was added 1,3-dichloro-1,1,3,3-tetraisopropyldisiloxane (1.1 eq., 2.68 mmol, 0.86 mL). The mixture was allowed to equilibrate to room temperature and was stirred under argon for 6 hours. The reaction was quenched with methanol and concentrated in vacuo. The crude product was taken up in ethyl acetate and washed with water and sodium bicarbonate. The organic layer was dried over sodium sulphate, concentrated in vacuo and purified using flash chromatography (3:7 ethyl acetate/n-hexanes) to yield compound **1** as a white solid (0.677 g, 62%). ^{1}H NMR (400 MHz, $CDCl_3$). δ 4.59 (d, 1H), 4.10 (dd, 1H), 4.00 (dd, 1H), 3.82 (t, 1H), 3.6 (t, 1H), 3.33-3.28 (m, 2H), 1.11-1.02 (m, 28H). ^{13}C NMR (101 MHz, $CDCl_3$). δ 90.8, 78.7, 76.5, 73.4, 68.8, 60.6, 17.4, 17.3, 17.2, 17.1, 13.6, 13.2, 12.5.

5.3.3 Compound 2

To a solution of compound **1** (0.45 g, 1 mmol) in DMF (5.5 mL) was added *p*-Toluenesulfonic acid monohydrate (0.2 eq., 0.2 mmol, 0.038 g). The mixture was stirred at room temperature under argon. After 6.5 hours, the reaction mixture was diluted with ethyl acetate and washed with water and sodium bicarbonate. The organic layer was dried over sodium sulphate, concentrated in vacuo and purified using flash chromatography (3:7 ethyl acetate/n-hexanes) to yield compound **2** as a white solid (0.248 g, 55%). ^{1}H NMR (400 MHz, $CDCl_3$). δ 4.62 (d, 1H), 3.95 (dd, 1H), 3.78 (dd, 1H), 3.73-3.66 (m, 2H), 3.48-3.44 (m, 1H), 3.39 (t, 1H), 2.62 (d, 1H), 1.12-1.02 (m, 28H). ^{13}C NMR (101 MHz, $CDCl_3$). δ 89.6, 79.8, 78.4, 73.8, 72.1, 61.9, 17.2, 12.9, 12.8, 12.1.

5.3.4 Compound 3

To a solution of compound **2** (0.6 gg, 1.34 mmol) in anhydrous pyridine (3 mL) was added anhydrous trimethylamine (0.56 mL, 4 mmol) under argon. While stirring the reaction at 0 °C, 4,4′-dimethoxytrityl chloride (1.5 eq., 2 mmol, 0.681 g) was added in 5 equal portions over a 5-hour period. The reaction mixture was allowed to equilibrate to room temperature and was stirred for an additional 7 hours. The solvent was removed in vacuo and the crude product was taken up in dichloromethane and washed with sodium bicarbonate. The organic layer was dried over sodium sulphate, concentrated in vacuo and purified using flash chromatography (3:7 ethyl acetate/n-hexane) to yield compound **3** as a yellow oil (0.75 g, 75%). ^{1}H NMR (400 MHz, $CDCl_3$). δ 7.22-7.08 (m, 9H), 6.75-6.73 (m, 4H), 4.5 (d, 1H), 3.85 (ddd, 1H), 3.7 (s, 6H), 3.7-3.64 (m, 1H), 3.61-3.58 (m, 1H), 3.38-3.34 (m, 1H), 3.31-3.27 (td, 1H), 2.6 (d, 1H), 1.03-0.93 (m, 28H). ^{13}C NMR (101 MHz, $CDCl_3$). δ 158.6, 147.3,

139.5, 129.1, 127.8, 127.1, 113.6, 113.2, 112.6, 89.6, 79.8, 73.9, 72.1, 61.9, 60.4, 17.2, 12.8, 12.1

5.3.5 Compound 4

To a mixture of compound **3** (0.25 g, 0.33 mmol) and propargyl uracil (0.055 g, 0.37 mmol) in anhydrous acetonitrile (5 mL) was added Copper(I) iodide (0.007 g, 0.036 mmol) under argon. The solution was stirred at room temperature for 6 hours. The solvent was removed in vacuo and the crude product was purified using flash chromatography (gradient: 0% to 5% methanol/dichloromethane) to yield compound **4** as an off-yellow foam (0.23 g, 77%). ^{1}H NMR (400 MHz, CD_3OD). δ 9.10 (s, 1H), 7.52 (d, 1H), 7.46 (d, 1H), 7.36-7.31 (m, 5H), 7.25-7.19 (m, 4H), 7.10 (d, 1H), 6.87-6.84 (m, 4H), 5.73-5.64 (m, 1H), 5.0 (s, 1H), 4.10 (t, 1H), 3.97-3.87 (m, 2H), 3.72-3.63 (m, 2H), 3.57 (d, 1H), 2.8 (brs, 1H), 1.33-1.03 (m, 28H). ^{13}C NMR (101 MHz, $CDCl_3$). δ 158.6, 158.4, 147.3, 144.9, 139.5, 130.1, 129.1, 127.9, 127.8, 127.1, 113.6, 113.2, 102.8, 87.26, 86.44, 81.4, 79.9, 72.9, 71.9, 61.6, 51.9, 29.7, 17.3, 12.8, 12.1. ESI-HRMS (ES+) m/z calculated for $C_{46}H_{61}N_5O_{10}Si_2$: 900.19, found 900.40 [$M+H^+$].

5.3.6 Compound 5

To a flame-dried round-bottomed flask was added a solution of compound **4** (0.25 g, 0.29 mmol) in anhydrous dichloromethane (4 mL), followed by the addition of anhydrous triethylamine (0.14 mL, 1.4 mmol) under an argon atmosphere. 2-cyanoethyl-*N*,*N*-diisopropylchlorophosphoramidite (0.19 mL, 0.833 mmol) was then added drop-wise and the reaction was stirred at room temperature for 1.5 hours. Due to stability concerns, the crude product was purified using a short flash chromatography column (gradient: 20% to 70% ethyl acetate/*n*-hexane, maintaining 5% triethylamine) to yield compound **5** as a yellow

oil (0.26 g, 84%), which was immediately used for solid-phase oligonucleotide synthesis. ^{31}P NMR (162 MHz, $CDCl_3$). δ ppm 147.83, 147.79.

5.3.7 Oligonucleotide synthesis

Oligonucleotides were synthesized on an Applied Biosystems 394 DNA/RNA synthesizer using 1.0 μM controlled-pore glass (CPG) support columns and a 1.0 μM cycle with a 999-second coupling time. Phosphoramidites were resuspended in anhydrous acetonitrile, immediately before use, to a final concentration of 0.1 M. Oligonucleotide cleavage from the solid support columns was achieved by flushing the CPG columns with 1 mL EMAM solution (1:1 methylamine 33 wt% in ethanol/ methylamine 40 wt% in water) for 1 hour at room temperature, followed by overnight incubation in EMAM to deprotect the bases. Oligonucleotides were concentrated in a miVac Quattro Concentrator and later resuspended in DMSO (100 μL). The silyl protecting groups were removed by incubating the oligonucleotides with 3HF-Et_3N (125 μL) for 3 hours at 65°C. Crude oligonucleotides were precipitated in ethanol and desalted using Millipore Amicon Ultra 3000 MW cellulose centrifugal filters. Strands were purified using reverse-phase HPLC eluting from 5% to 95% ACN in 0.1 M TEAA buffer (pH 7.0).

5.3.8 Thermal denaturation and circular dichroism (CD) studies

For duplex formation, equimolar amounts of the respective sense and antisense strands were combined, dried down and resuspended in 400 μL sodium phosphate buffer (90 mM NaCl, 10 mM Na_2HPO_4, 1 mM EDTA; pH 7.0). Samples were heated for 2 minutes at 90 °C and allowed to slowly equilibrate to room temperature. Thermal denaturation and CD studies were performed using a Jasco J-815 CD Spectropolarimeter equipped with a temperature controller. To determine the melting temperature (T_m) of each duplex, the change in

absorbance at 260 nm was measured against a temperature gradient from 15 to 95°C, at 0.5°C/min. Data were analysed using Meltwin v3.5 software. CD spectra were recorded at 25°C, scanning from 200 to 40 nm with a screening rate of 20.0 nm/min and a 0.20 nm data pitch. Scans were performed in triplicate and averaged using Jasco′s Spectra Manager v2 software.

5.3.9 Biological assays

5.3.9.1 Cell culture and transfection

HeLa cells were maintained in Dulbecco′s Modified Eagle′s Medium (DMEM) supplemented with 10% fetal bovine serum (FBS) and 1% penicillin-streptomycin (Sigma). Cells were maintained at 37 °C in a humidified atmosphere with 5% CO_2 and were passaged at 80% confluency. HeLa cells were seeded into 24-well plates, containing 400 μL DMEM (10% FBS), at a density of 5.0×10^4 cells per well. Cells were incubated for 24 hours at 37 °C in a humidified atmosphere with 5% CO_2 after which the culture medium was removed. For each transfection sample, a mixture of 1 μL Lipofectamine 2000™ (Invitrogen) and 49 μL 1X Gibco′s Opti-MEM Reduced Serum Medium (Invitrogen) was incubated at room temperature for 5 min. Each siRNA was diluted in 1X Gibco′s Opti-MEM Reduced Serum Medium on ice and mixed with 200 ng pGL3 and 50 ng pRLSV40 plasmids to achieve a final volume of 50 μL. The siRNA-plasmid mix was added to the Lipofectamine 2000™-Opti-MEM mix and incubated for 40 minutes at room temperature. These samples were then transferred to the respective wells of the 24-well plate and incubated for 24 hours at 37 °C prior to cell lysis.

5.3.9.2 Dual-Luciferase® Reporter Assay

Cells were lysed with 1X passive lysis buffer for 30 min at room temperature. Cell lysates (10 μL) were transferred to opaque Costar 96-well plates in triplicate for the Dual-Luciferase® Reporter Assay (Promega). Luciferase Assay Reagent II (LAR II) and Stop & Glo® Reagent were prepared following the manufacturer′s protocol. LAR II (50 μL) was added to each well and luminescence was immediately measured using a Synergy HT (Bio-Tek) plate luminometer. Stop & Glo® (50 μL) was then added to each well and a second luminescence measurement was taken. Results are expressed as the ratio of firefly/*Renilla* luminescence taken as a percentage of an untreated control.

5.4 Results and Discussion

5.4.1 Preparation of oligonucleotides

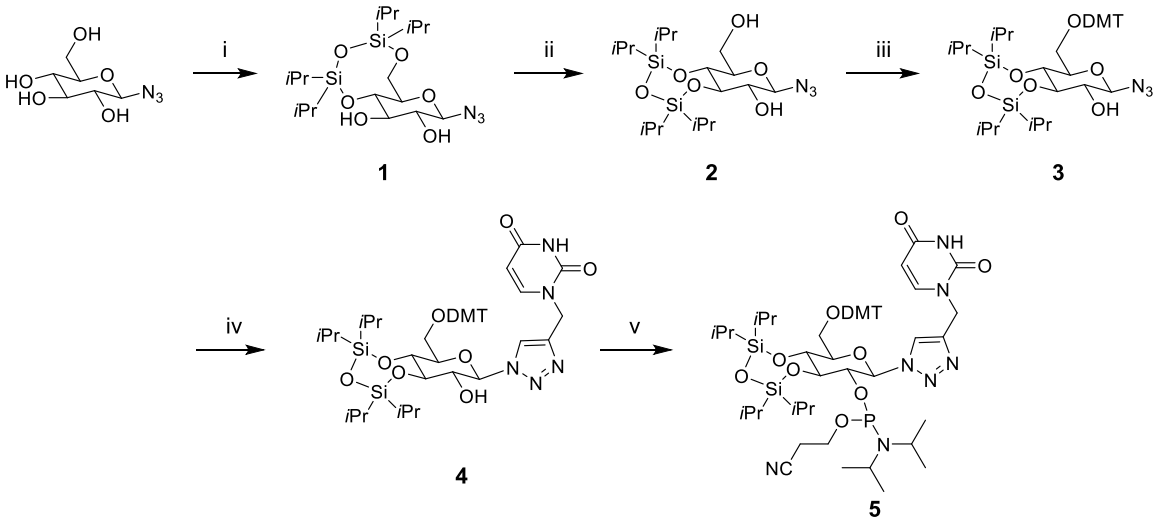

Scheme 5.1. Synthesis of glucose nucleosides with a triazole-linked uracil, and its phosphoramidite derivative. Reagents and conditions: (i) $TIPDSCl_2$, pyridine, 0 °C → rt, 6 h (62%); (ii) p-TsOH·H2O, DMF, RT, 6.5 h (55%); (iii) DMT-Cl, Et_3N/pyridine, 0 °C, 5 h, 0 °C → rt, 7 h (75%); (iv) N1-propargyl uracil, CuI, ACN, rt, 6 h (77%); (v) 2-cyanoethyl-N,N-diisopropylchlorophosphoramidite, Et_3N/DCM, rt, 1.5 h (84%).

To synthesize the glucose phosphoramidite **5**, we first treated β-D-glucopyranosyl azide with $TIPDSCl_2$. This was followed by the acid-catalyzed migration of the 4,6-TIPDS protecting group to yield the 3,4-protected derivative **2**, as previously reported in the literature [18]. This compound was protected with a 4,4′-dimethoxytrityl (DMT) group and then reacted with N1-propargyl uracil via copper(I)-catalyzed azide-alkyne cycloaddition (CuAAC). The resulting compound **4** was phosphitylated with 2-cyanoethyl-*N*,*N*-diisopropylchlorophosphoramidite to yield the phosphoramidite derivative **5** (Scheme 5.1), which was used for solid-phase oligonucleotide synthesis as described above. The modification was incorporated at key positions within the sense or antisense strand, replacing either the 3′ dTdT overhang or an internal uridine nucleotide. Oligonucleotides strands were purified using reverse-phase HPLC (Figure 5.1) and characterized by mass spectrometry (Table 5.1).

Table 5.1. Sequences and mass spectrometry data of modified oligonucleotide strands

Code	***Sequence***	***Mass (predicted)***	***Mass (found)***
S1	5′ CUU ACG CUG AGU ACU UCG A**X** 3′ (S)	6796.88	6796.52
S2	5′ CUU ACG CUG AGU ACU **X**CG ATT 3′ (S)	6794.90	6795.56
S3	5′ CUU ACG CUG AG**X** ACU UCG ATT 3′ (S)	6794.90	6794.62
AS1	3′ **X**G AAU GCG ACU CAU GAA GCU 5′ (AS)	6882.94	6882.87
AS2	3′ TTG AA**X** GCG ACU CAU GAA GCU 5′ (AS)	6880.96	6880.80
AS3	3′ TTG AAU GCG AC**X** CAU GAA GCU 5′ (AS)	6880.96	6880.61

(S) corresponds to the sense strand; (AS) corresponds to the antisense strand. **X** corresponds to the position of the glucose nucleoside with a triazole-linked uracil.

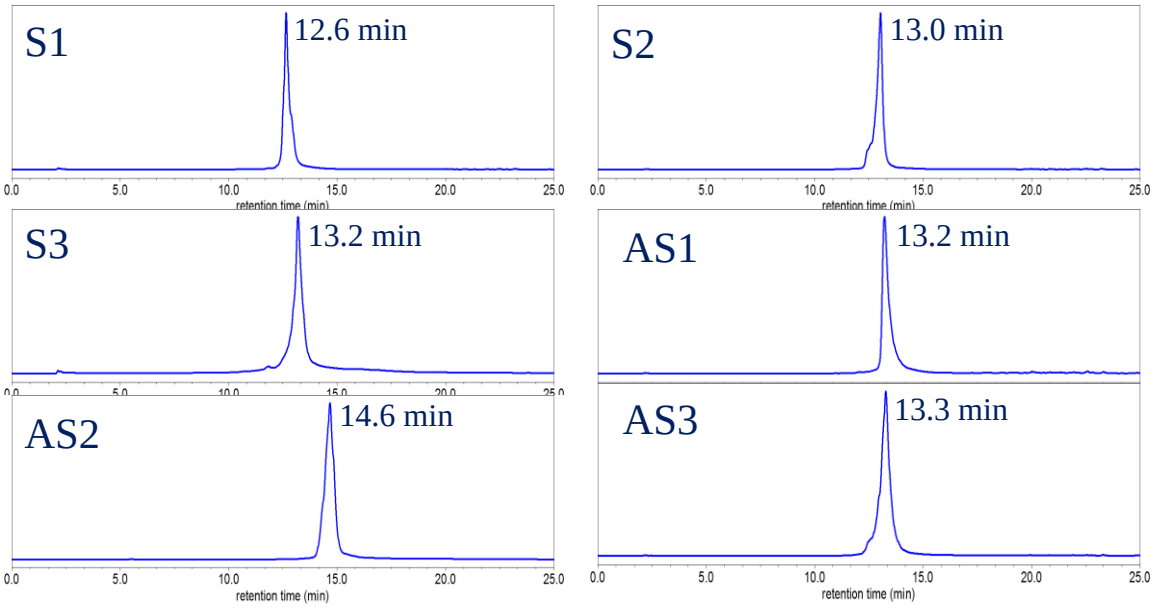

Figure 5.1. Analytical HPLC traces of modified oligonucleotides incorporating a novel glucose modification. Corresponding sequences can be found in Table 5.1. HPLC was performed on a Waters 1525 binary HPLC pump with a Waters 2489 UV/Vis detector, using a C18 4.6 x 150 mm reverse-phase column, eluting from 5 to 95% ACN in 0.1 M TEAA buffer (pH 7.0).

5.4.2 CD studies

Modified sense and antisense strands were annealed to their complementary wild-type sequences. The resulting duplexes were characterized using circular dichroism spectroscopy as described above to confirm that siRNAs adopted an A-form helical conformation. Recognition of the A-form major groove by RISC is required for proper RNAi activity, so this is an important criterion in siRNA design [19]. An A-form helical structure is characterized by a broad positive band at 260 nm in addition to a negative band at ~210 nm [20]. As seen in Figure 5.2, our modification did not distort the A-form helical structure of the siRNA duplex, regardless of its placement in the sequence.

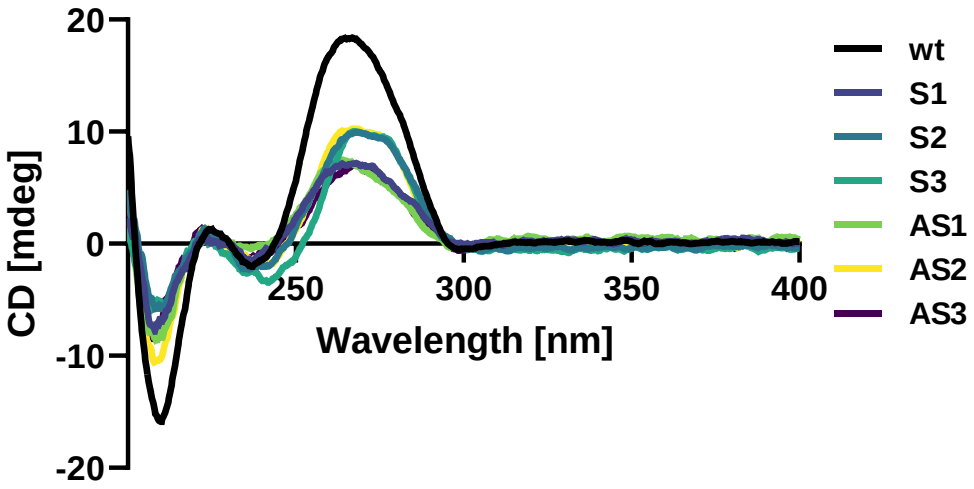

Figure 5.2. Circular dichroism spectra of anti-luciferase siRNAs incorporating a novel glucose modification.

5.4.3 Thermal denaturation

Since the thermodynamic properties of siRNAs have been shown to impact siRNA potency, we assessed the thermal stability of each duplex. The resulting melting temperatures (T_m) are indicated in Table 5.2. Placing our modification at the 3′ end of the sense or antisense strand, replacing the dTdT overhang, had a small impact on thermal stability with ΔT_m values of -5°C. This could be due to the loss of stacking interactions which have been reported with 3′ dTdT overhangs [21]. Internal modifications resulted in strong thermal destabilization.

Placing the modification at positions 12 or 16 from the sense strand 5′ end resulted in ΔT_m values of -22 °C and -26 °C, respectively. Similar effects were observed when placing the modification at positions 10 and 16 from the antisense strand 5′ end, with ΔT_m values of -22.5 °C and -17 °C, respectively. These results were expected as the internal region of siRNA is far less tolerant to bulky chemical modifications than the 3′ end [22].

Table 5.2. Sequences, melting temperatures and IC_{50} values of anti-firefly luciferase siRNAs

Code	*Duplex*	T_m (°C)	ΔT_m (°C)	[I]IC_{50} (pM)
wt	5′ CUU ACG CUG AGU ACU UCG ATT 3′ 3′ TTG AAU GCG ACU CAU GAA GCU 5′	76.1	-	1.90
S1	5′ CUU ACG CUG AGU ACU UCG AX 3′ 3′ TTG AAU GCG ACU CAU GAA GCU 5′	71.1	-5.0	218
S2	5′ CUU ACG CUG AGU ACU XCG ATT 3′ 3′ TTG AAU GCG ACU CAU GAA GCU 5′	50.1	-26.0	219
S3	5′ CUU ACG CUG AGX ACU UCG ATT 3′ 3′ TTG AAU GCG ACU CAU GAA GCU 5′	54.1	-22.0	524
AS1	5′ CUU ACG CUG AGU ACU UCG ATT 3′ 3′ XG AAU GCG ACU CAU GAA GCU 5′	71.1	-5.0	226
AS2	5′ CUU ACG CUG AGU ACU UCG ATT 3′ 3′ TTG AAX GCG ACU CAU GAA GCU 5′	59.1	-17.0	219
AS3	5′ CUU ACG CUG AGU ACU UCG ATT 3′ 3′ TTG AAU GCG ACX CAU GAA GCU 5′	53.6	-22.5	483

The top strand corresponds to the sense strand. The bottom strand corresponds to the antisense strand. X corresponds to the triazole-linked uracil modification. [I]Inhibitory dose-response curves can be found in Figure 5.3.

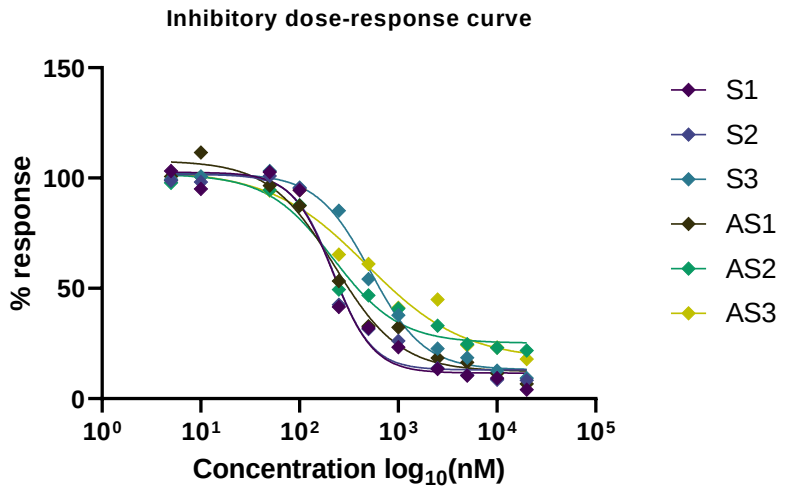

Figure 5.3. Inhibitory dose-response curves for glucose-modified anti-luciferase siRNAs, tested in HeLa at concentrations from 5 to 20,000 pM.

5.4.4 Gene-silencing activity

To assess the gene-silencing activity of siRNAs, HeLa cells were co-transfected with plasmids coding for firefly and *Renilla* luciferases as well as siRNAs, using Lipofectamine

2000™ (Invitrogen). We then used the Dual-Luciferase® Reporter Assay to evaluate the relative expression of target firefly luciferase after siRNA treatments ranging from 5 to 20,000 pM. As seen in Figure 5.4, all tested siRNAs showed dose-dependent knockdown of firefly luciferase after 24 hours. IC_{50} values are summarized in Table 5.2.

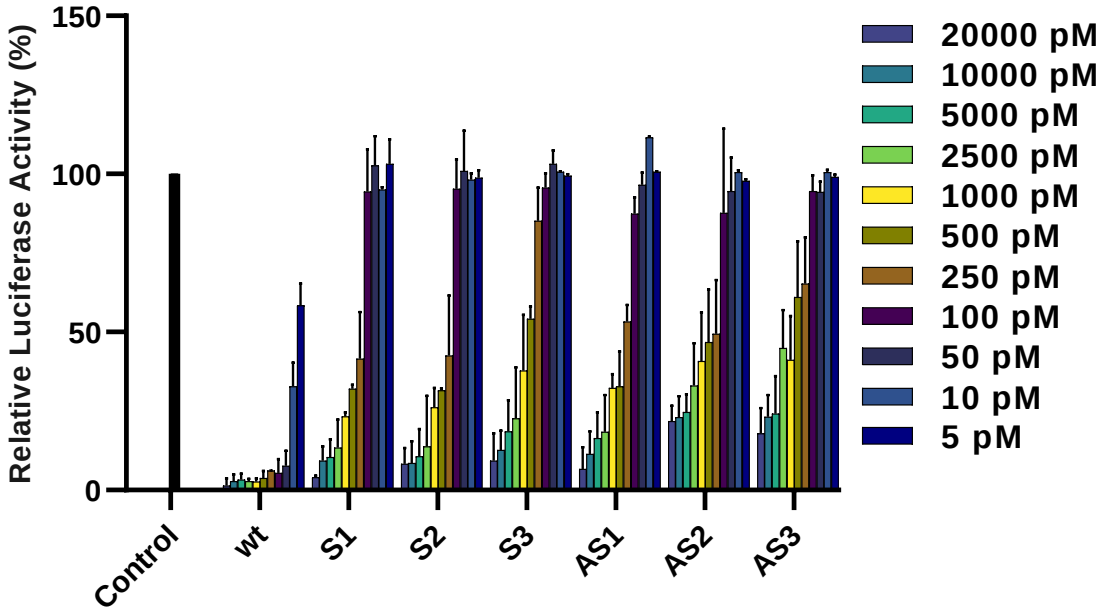

Figure 5.4. Relative expression of normalized firefly luciferase in HeLa cells 24 hours after treatment with siRNAs incorporating a novel glucose modification. Error bars indicate standard deviation of at least two independent biological replicates.

Duplexes bearing terminal modifications, placed at the 3′ end of the sense or antisense strand, showed high gene-silencing activity with IC_{50} values of 218 pM and 226 pM, respectively. This is consistent with literature reports showing that six-carbon sugar derivatives are well-tolerated and can lead to strong gene-silencing activity when placed at the 3′ end of the siRNA sense or antisense strand. Although internal modifications were tolerated in both the sense and the antisense strand, their effect on siRNA activity was position dependent. Placing our modification at position 16 from the sense or antisense strand 5′ end led to efficient gene-silencing activity (IC_{50} of 219 pM), comparable to our

terminal-modified siRNAs. On the other hand, placing our modification at position 10 from the antisense strand 5′ end led to a decrease in gene-silencing activity (IC_{50} of 483 pM). It has been reported that the seed region, which directs the initial target recognition by RISC, is more sensitive to chemical modifications, particularly if they disrupt the thermal stability of the duplex [22]. The lowest activity, however, was observed with siRNA S3, bearing the modification at position 12 from the sense strand 5′ end (IC_{50} of 524 pM). Some reports suggest that this position can be less tolerant to chemical modifications, including altritol nucleic acids [23]. Given the proximity to the Ago2 cleavage site, it has been proposed that some chemical modifications at this position can interfere with the enzymatic activity of Ago2 thus compromising siRNA potency [24]. Based on these data, this modification may be better suited for incorporation at the 3′ end of the sense or antisense strand as well as at some internal in order to maximize gene-silencing activity.

5.5 Conclusions

In summary, we report the synthesis of a novel glucose phosphoramidite with a triazole-linked uracil moiety at position 1 for incorporation into oligonucleotides using standard solid-phase synthetic conditions. This modification was placed at terminal and internal positions of the siRNA sense or antisense strand to investigate its biophysical and biological effects. Overall, this modification was well-tolerated within the sense and the antisense strand and did not distort the A-form helical conformation of the siRNAs, making it suitable for RNAi applications. Notably, our modified siRNAs show position-dependent gene-silencing activity. Replacing the dT overhang at the 3′ end or modifying position 16 from the 5′ end of either stand resulted in high siRNA activity. This position-dependent effect could be further investigated to optimize siRNA potency. Although there are some general

guidelines for siRNA design, these criteria are not universally applicable, highlighting the importance of assessing the effect of each chemical modification individually. To the best of our knowledge, this is the first report of an siRNA bearing a single 3′-6′/2′-5′ phosphodiester linkage.

5.6 Supplementary Data

Refer to Appendix D for the original manuscript and corresponding supplementary data.

5.7 References

1. Agrawal N, PVN Dasaradhi, A Mohmmed, P Malhotra, RK Bhatnagar and SK Mukherjee. (2003) RNA Interference: Biology, Mechanism, and Applications. Microbiology and Molecular Biology Reviews 67:657.

2. Hannon GJ. (2002) RNA Interference. Nature 418:244-251.

3. Elbashir SM, J Harborth, W Lendeckel, A Yalcin, K Weber and T Tuschl. (2001) Duplexes of 21-nucleotide RNAs Mediate RNA Interference in Cultured Mammalian Cells. Nature 411:494-498.

4. Adams D, A Gonzalez-Duarte, WD O'Riordan, CC Yang, M Ueda, AV Kristen, I Tournev, HH Schmidt, T Coelho, JL Berk *et al.* (2018) Patisiran, an RNAi Therapeutic, for Hereditary Transthyretin Amyloidosis. N Engl J Med 379:11-21.

5. Scott LJ. (2020) Givosiran: First Approval. Drugs 80:335-339.

6. Aagaard L and JJ Rossi. (2007) RNAi therapeutics: principles, prospects and challenges. Adv Drug Deliv Rev 59:75-86.

7. Haussecker D. (2014) Current issues of RNAi therapeutics delivery and development. Journal of Controlled Release 195:49-54.

8. Selvam C, D Mutisya, S Prakash, K Ranganna and R Thilagavathi. (2017) Therapeutic potential of chemically modified siRNA: Recent trends. Chem. Biol. Drug Des. 90:665-678.

9. Watts JK, GF Deleavey and MJ Damha. (2008) Chemically modified siRNA: tools and applications. Drug Discovery Today 13:842-855.

10. Braasch DA, S Jensen, Y Liu, K Kaur, K Arar, MA White and DR Corey. (2003) RNA interference in mammalian cells by chemically-modified RNA. Biochemistry 42:7967-7975.

11. Chiu Y-L and TM Rana. (2003) siRNA function in RNAi: a chemical modification analysis. RNA 9:1034-1048.

12. Kenski DM, G Butora, AT Willingham, AJ Cooper, W Fu, N Qi, F Soriano, IW Davies and WM Flanagan. (2012) siRNA-optimized Modifications for Enhanced In Vivo Activity. Molecular Therapy - Nucleic Acids 1.

13. Elmén J, H Thonberg, K Ljungberg, M Frieden, M Westergaard, Y Xu, B Wahren, Z Liang, H Ørum, T Koch *et al.* (2005) Locked nucleic acid (LNA) mediated improvements in siRNA stability and functionality. Nucleic Acids Res 33:439-447.

14. Nielsen P, LH Dreiøe and J Wengel. (1995) Synthesis and evaluation of oligodeoxynucleotides containing acyclic nucleosides: Introduction of three novel analogues and a summary. Bioorganic & Medicinal Chemistry 3:19-28.

15. Fisher M, M Abramov, A Van Aerschot, D Xu, RL Juliano and P Herdewijn. (2007) Inhibition of MDR1 expression with altritol-modified siRNAs. Nucleic Acids Res 35:1064-1074.

16. Nauwelaerts K, M Fisher, M Froeyen, E Lescrinier, A Van Aerschot, D Xu, R DeLong, H Kang, RL Juliano and P Herdewijn. (2007) Structural Characterization and

Biological Evaluation of Small Interfering RNAs Containing Cyclohexenyl Nucleosides. Journal of the American Chemical Society 129:9340-9348.

17. Fisher M, M Abramov, A Van Aerschot, J Rozenski, V Dixit, RL Juliano and P Herdewijn. (2009) Biological effects of hexitol and altritol-modified siRNAs targeting B-Raf. Eur J Pharmacol 606:38-44.

18. Farrell M, J Zhou and PV Murphy. (2013) Regiospecific Anomerisation of Acylated Glycosyl Azides and Benzoylated Disaccharides by Using TiCl4. Chemistry – A European Journal 19:14836-14851.

19. Hernández AR, LW Peterson and ET Kool. (2012) Steric Restrictions of RISC in RNA Interference Identified with Size-Expanded RNA Nucleobases. ACS Chemical Biology 7:1454-1461.

20. Kypr J, I Kejnovská, D Renciuk and M Vorlícková. (2009) Circular dichroism and conformational polymorphism of DNA. Nucleic acids research 37:1713-1725.

21. O'Toole AS, S Miller and MJ Serra. (2005) Stability of 3' double nucleotide overhangs that model the 3' ends of siRNA. RNA 11:512-516.

22. Bramsen J and J Kjems. (2012) Development of Therapeutic-Grade Small Interfering RNAs by Chemical Engineering. Frontiers in Genetics, 3:1-22.

23. Kumar P, R Degaonkar, DC Guenther, M Abramov, G Schepers, M Capobianco, Y Jiang, J Harp, C Kaittanis, MM Janas *et al.* (2020) Chimeric siRNAs with chemically modified pentofuranose and hexopyranose nucleotides: altritol-nucleotide (ANA) containing GalNAc–siRNA conjugates: in vitro and in vivo RNAi activity and resistance to 5′-exonuclease. Nucleic Acids Research 48:4028-4040.

24. Zheng J, L Zhang, J Zhang, X Wang, K Ye, Z Xi, Q Du and Z Liang. (2013) Single modification at position 14 of siRNA strand abolishes its gene-silencing activity by decreasing both RISC loading and target degradation. The FASEB Journal 27:4017-4026.

25. Desaulniers J-P, G Hagen, J Anderson, C McKim and B Roberts. (2017) Effective gene-silencing of siRNAs that contain functionalized spacer linkages within the central region. RSC Advances 7:3450-3454.

26. Salim L, C McKim and J-P Desaulniers. (2018) Effective carrier-free gene-silencing activity of cholesterol-modified siRNAs. RSC Advances 8:22963-22966.

27. Klein D, S Goldberg, CS Theile, R Dambra, K Haskell, E Kuhar, T Lin, R Parmar, M Manoharan, M Richter *et al.* (2021) Centyrin ligands for extrahepatic delivery of siRNA. Mol. Ther.

28. Willibald J, J Harder, K Sparrer, KK Conzelmann and T Carell. (2012) Click-modified anandamide siRNA enables delivery and gene silencing in neuronal and immune cells. J. Am. Chem. Soc. 134:12330-12333.

29. Thomas M, SA Kularatne, L Qi, P Kleindl, CP Leamon, MJ Hansen and PS Low. (2009) Ligand-Targeted Delivery of Small Interfering RNAs to Malignant Cells and Tissues. Annals of the New York Academy of Sciences 1175:32-39.

30. Addepalli H, Meena, CG Peng, G Wang, Y Fan, K Charisse, KN Jayaprakash, KG Rajeev, RK Pandey, G Lavine *et al.* (2010) Modulation of thermal stability can enhance the potency of siRNA. Nucleic Acids Res. 38:7320-7331.

31. Petrova NS, MI Meschaninova, AG Venyaminova, MA Zenkova, VV Vlassov and EL Chernolovskaya. (2011) Silencing activity of 2'-O-methyl modified anti-MDR1 siRNAs with mismatches in the central part of the duplexes. FEBS Lett 585:2352-2356.

32. Chen C, J Ke, XE Zhou, W Yi, JS Brunzelle, J Li, E-L Yong, HE Xu and K Melcher. (2013) Structural Basis for Molecular Recognition of Folic Acid by Folate Receptors. Nature 500:486-489.

33. Boss SD, T Betzel, C Müller, CR Fischer, S Haller, J Reber, V Groehn, R Schibli and SM Ametamey. (2016) Comparative Studies of Three Pairs of α- and γ-Conjugated Folic Acid Derivatives Labeled with Fluorine-18. Bioconjugate Chemistry 27:74-86.

Chapter 6. General Discussion

RNAi molecules have emerged as a novel class of gene-silencing therapeutics, opening doors for the treatment of conditions that otherwise had limited therapeutic options available. Despite recent advances in the field, with the US FDA approval of three RNAi-based drugs, there are still numerous barriers to overcome before we can harness the full potential of RNAi therapeutics. The work presented in this thesis explores two different bioconjugate systems to address the major hurdle in RNAi research: delivery.

The first bioconjugate that we investigate is cholesterol, an important structural component of cellular membranes and a common carrier for RNAi molecules. Our lab group had previously described the synthesis of a novel cholesterol phosphoramidite [25]. The cholesterol moiety is covalently bound to a spacer via a triazole linkage and is incorporated at different positions within the siRNA sense strand. Herein, we expand on this work by assessing the efficacy of these novel triazole-linked cholesterol siRNAs at mediating cellular uptake in the absence of a transfection reagent. We also compared its efficacy to that of a commercially available cholesterol-TEG siRNA. We found that our triazole-linked cholesterol siRNAs not only displayed potent gene-silencing activity but also low cytotoxicity. On the other hand, the cholesterol-TEG siRNAs imparted high cytotoxicity while displaying low gene silencing. Taken together, our results show that our cholesterol modification is compatible with the RNAi pathway and could also be used for future downstream applications, including the functionalization of delivery vehicles, because the straightforward synthetic design [26]. One limitation to the use of hydrophilic bioconjugates and many other delivery systems, however, is that they tend to accumulate in the liver. Because of this, it is not surprising that all current US FDA-approved RNAi formulations

target the liver. Unfortunately, attempts to deliver siRNAs to extrahepatic targets have not been as successful [27].

Based on this, we aimed to design an effective delivery system for siRNAs that could selectively target cancer cells. A very promising ligand for this purpose is folate, or vitamin B9, an essential nutrient required for various metabolic functions. Folate binds cell-surface folate receptors with high affinity and is internalized via receptor-mediated endocytosis. Out of the four folate receptor isoforms, FRα is the most clinically significant as it is highly overexpressed in numerous cancers despite being expressed at low levels in most non-malignant tissues. Previous studies have successfully incorporated folate modifications at either the 3′ or 5′ end of siRNA, demonstrating selective delivery to FRα-expressing cancer cells in the absence of a transfection reagent. Nevertheless, only moderate gene-silencing activity (40-60%) against exogenous targets was achieved. Herein, we report a method to increase the gene-silencing activity of folate siRNAs [28,29]. Employing a post-column copper-catalyzed alkyne-azide cycloaddition (CuAAC), we prepared a library of siRNAs bearing a novel triazole-linked folate modification. These siRNAs were tested in FRα-positive HeLa cells and FRα-negative HT-29 cells to assess the specificity of delivery. As expected, folate siRNAs were only internalized by HeLa, and not HT-29, cells. Notably, we found that modifying the central region of the siRNA sense strand imparted significant thermal destabilization, yet these siRNAs were able to achieve potent gene-silencing activity against exogenous firefly luciferase and endogenous *Bcl-2* targets. Some studies suggest that destabilization of the central region can lead to increased gene silencing [30,31]. Consistent with literature reports, our 3′-modified folate siRNAs showed only moderate activity. Overall, we report a straightforward CuAAC strategy to prepare self-delivering folate-modified siRNAs. Our data shows that modifying the central region of the

sense strand can lead to enhanced gene silencing against both exogenous and endogenous targets with minimal toxicity. Given the proven clinical applications for FRα targeting, the use of folate as a delivery vector for siRNAs holds great promise and could open new avenues for the design of novel RNA-based cancer therapeutics.

For the most part, the development of folate-based delivery systems has been limited by the inherent nature of folate itself, which displays low solubility in organic solvents and can be difficult to purify using conventional chromatography approaches. Furthermore, many of the synthetic approaches to prepare folate derivates rely on sophisticated, and often expensive, chemistry. The biggest limitation, however, is the lack of reliable protocols to synthesis folate phosphoramidites for solid-phase oligonucleotide synthesis. Folate phosphoramidites are not currently commercially available. About a decade ago, Berry & Associates offered a 5′-folate-TEG cyanoethyl phosphoramidite (BA 0349) at a cost of $843 USD for 100 μmol. However, this product has been discontinued and there are no reports using this molecule. Most of the current synthetic approaches, including the one we employed for our triazole-linked folate siRNAs, rely on a post-column CuAAC and, therefore, require the use of copper in the final synthetic step. If the synthesis of folate-conjugates can be streamlined by developing an effective folate phosphoramidite for solid-phase synthesis, these molecules have the potential of contributing to the next generation of RNAi-based cancer therapeutics.

The pteroate moiety of folate is buried inside the binding pocket of the FRα whereas the glutamate moiety sticks out of the receptor pocket and is solvent exposed. Therefore, conjugation or modification at the glutamate end does not adversely affect FRα binding [32]. Nevertheless, direct conjugation of folate at this position leads to a mixture α- and γ-

isomers due to the presence of two carboxylic acid groups [33]. In order to avoid this, and to improve the overall solubility of folate, we propose the synthesis of a triazole-linked folate derivative phosphoramidite that replaces the glutamate moiety with a short linker. This straightforward and cost-effective strategy is compatible with solid-phase oligonucleotide synthesis and many of the folate derivatives can be purified using conventional silica gel chromatography. These siRNAs are currently being characterized and their biological activity will be compared to that of our first-generation folate siRNAs described earlier.

Although the bulk of this work has focused on the development of effective delivery platforms for siRNAs, we should note that poor cellular uptake is not the only shortcoming of RNAi molecules. Various chemical modifications must be employed, in combination with the bioconjugate of choice, to improve the pharmacokinetic profile of siRNAs. The choice of chemical modifications, and its efficacy, will depend on factors like the siRNA sequence, chosen delivery vector and intended applications. Because of this, it is of crucial important to develop and evaluate the efficacy of novel modifications that could be of clinical significance. As discussed earlier, a novel chemical modification approach involves replacing the ribose sugar of RNA with a six-carbon moiety. Herein, we report the synthesis of a novel glucose phosphoramidite derivative which is triazole-linked to uracil at position one. We introduced this modification at various positions within the sense or antisense strand to assess whether gene-silencing activity was position-dependent Our resulting duplexes contained a single 3′-6′/2′-5′ phosphodiester linkage which, to the best of our knowledge, has not been reported previously. Our data suggests that this novel modification is well-tolerated within the sense and antisense strand and does not distort the A-form helical conformation recognized by the RISC. We observed the highest siRNA activity when

modifying the 3′-end of either strand or modifying position 16 from the 5′-end of either strand. This highlights the importance of assessing the effect of each chemical modification individually, as criteria for siRNA design are not universally applicable.

Together, the research work summarized in this dissertation demonstrates the efficacy of several chemical modifications at improving some of the limitations associated with the nature of RNAi molecules. Ultimately, these modifications could provide new avenues for the functionalization of currently existing delivery vehicles, the development of novel extrahepatic delivery strategies, and the improvement of the pharmacokinetic profile of therapeutic siRNAs.

Appendix A. Manuscript I and Supplementary Data

RSC Advances

PAPER

View Article Online
View Journal | View Issue

Open Access Article. Published on 22 June 2018. Downloaded on 2/7/2021 11:22:43 PM.
This article is licensed under a Creative Commons Attribution 3.0 Unported Licence.

Check for updates

Cite this: *RSC Adv.*, 2018, **8**, 22963

Effective carrier-free gene-silencing activity of cholesterol-modified siRNAs†

Lidya Salim, Chris McKim and Jean-Paul Desaulniers *

Received 7th May 2018
Accepted 18th June 2018

DOI: 10.1039/c8ra03908a

rsc.li/rsc-advances

The use of short interfering RNAs (siRNAs) as therapeutics holds great promise, but chemical modifications must first be employed to improve their pharmacokinetic properties. This study evaluates the *in vitro* cellular uptake and knock-down efficacy of cholesterol-modified triazole-linked siRNAs targeting firefly luciferase in the absence of a transfection carrier. These siRNAs displayed low cytotoxicity and excellent dose-dependent knockdown in HeLa cells in the 500 to 3000 nM concentration range, with a 70–80% reduction in firefly luciferase activity. Our results indicate that this modification is compatible with the RNA interference pathway, and is less cytotoxic and more effective than a commercially-available triethylene glycol (TEG) cholesterol modification.

RNA interference (RNAi) is an endogenous pathway that utilizes double-stranded RNA to suppress translation, resulting in sequence-specific gene silencing.[1] The initial step involves cleavage of long double-stranded RNA into smaller 21–23 nucleotide fragments, termed short interfering RNAs (siRNAs), which are incorporated into the RNA-induced silencing complex (RISC).[2] RISC unwinds and dissociates the duplex, retaining the antisense strand which is used as a guiding sequence to recognize and degrade complementary mRNA.[2,3] Since many diseases are characterized by aberrant gene expression, the use of siRNAs as therapeutics holds great promise.[4,5] Unfortunately, there are some limitations associated with the structure of siRNAs, including low stability, poor cellular uptake and off-target effects, which must be addressed in order to harness the full potential of RNAi therapeutics.[6,7] Although several chemical modifications have been employed to improve the pharmacological properties of siRNAs, there is still no universal modification able to simultaneously improve all of these limitations.[8,9]

Due to their large size and anionic backbone, siRNAs have difficulties crossing cellular membranes. Therefore, several delivery systems and carriers have been investigated, including viral vectors, cationic polymers and liposomes.[10–13] Another strategy involves direct conjugation of siRNAs to small molecules such as GalNac or hydrophobic molecules to enhance cellular uptake.[14] Cholesterol is a hydrophobic biomolecule and a key component of cellular membranes, as it helps maintain their integrity.[15] Various cholesterol-conjugated drugs and anticancer agents have been studied and have demonstrated enhanced pharmacokinetic profiles, bioavailability and delivery.[16,17] Cholesterol modifications have also been successful at increasing siRNA lipophilicity and improving cellular uptake without the need of transfection carriers.[18–20]

Recently, we reported a straightforward synthesis of a cholesterol phosphoramidite, bound covalently to a spacer *via* a triazole linkage.[21] This cholesterol-bearing spacer was then incorporated within the central region of the siRNA sense strand through solid-phase RNA synthesis.[21] Our biological studies in HeLa cells showed that these siRNAs were able to downregulate exogenous firefly luciferase mRNA in a dose-

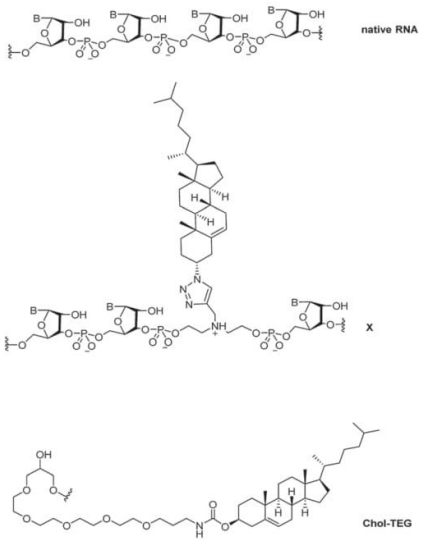

Fig. 1 Structural differences between native RNA, cholesterol-modified triazole-linked spacer (**X**) and the commercially-available 3′-end cholesterol triethylene glycol (**Chol-TEG**) modification.

University of Ontario Institute of Technology, Faculty of Science, 2000 Simcoe Street North, Oshawa, ON L1H 7K4, Canada. E-mail: Jean-Paul.Desaulniers@uoit.ca

† Electronic supplementary information (ESI) available. See DOI: 10.1039/c8ra03908a

Open Access Article. Published on 22 June 2018. Downloaded on 2/7/2021 11:22:43 PM.
This article is licensed under a Creative Commons Attribution 3.0 Unported Licence.

Table 1 Sequences of anti-luciferase siRNA and T_m data[a]

RNA	siRNA duplex	T_m	ΔT_m
wt	5′-CUUACGCUGAGUACUUCGAtt-3′ 3′-ttGAAUGCGACUCAUGAAGCU-5′	72.7	—
X1	5′-CUUACGCU***X***AGUACUUCGAtt-3′ 3′-ttGAAUGCGACUCAUGAAGCU-5′	61.6	−11.1
X2	5′-CUUACGCUG***X***GUACUUCGAtt-3′ 3′-ttGAAUGCGACUCAUGAAGCU-5′	62.5	−10.2
X5	5′-CUUACGCUGAGUACUUCGA***X***t-3′ 3′-ttGAAUGCGACUCAUGAAGCU-5′	69.8	−2.9
Chol-TEG	5′-CUUACGCUGAGUACUUCGAtt***Ch***-3′ 3′-ttGAAUGCGACUCAUGAAGCU-5′	65.3	−6.7

[a] ***X*** corresponds to the single triazole-linked cholesterol modification. ***Ch*** corresponds to the commercial triethylene glycol modification. The top strand corresponds to the sense strand; the bottom strand corresponds to the antisense strand. In all duplexes, the 5′-end of the bottom antisense strand contains a phosphate group.

dependent manner using the transfection carrier Lipofectamine® 2000. In this study, we further investigate the biological activity and gene-silencing efficacy of these siRNAs in the absence of a transfection carrier. Fig. 1 compares the structure of native RNA with our cholesterol-modified triazole-linked spacer (**X**) and a commercially-available 3′-end triethylene glycol cholesterol (**Chol-TEG**) modification.

To examine the silencing potential of these siRNAs, HeLa cells were co-transfected with plasmids coding for firefly luciferase (target) and *Renilla* luciferase (internal control) respectively. After a 4 hour incubation period, culture media was discarded and cells were washed twice with phosphate-buffer saline to remove any traces of Lipofectamine® 2000. Fresh media was added to each well, followed by addition of the respective siRNA treatment with concentrations ranging from 1 to 3000 nM. After an additional 16 hour incubation period, cells were lysed and the gene-silencing efficacy of siRNAs was assessed using the dual-luciferase reporter gene assay. All siRNAs target firefly luciferase and their sequences are highlighted in Table 1. siRNAs **X1** and **X2** contain the triazole-linked cholesterol modification within the central region of the sense strand (positions 9 and 10 from the 5′-end, respectively). siRNA **X5** contains the triazole-linked cholesterol modification at the 3′-end of the sense strand. **Chol-TEG** contains the commercially-available 3′-end triethylene glycol cholesterol derivative.

To first ensure that the siRNAs used in this study were effective in silencing firefly luciferase, a gene-silencing assay was conducted using Lipofectamine® 2000 as a transfection carrier. These siRNAs show effective gene-silencing activity in a dose-dependent manner at low concentrations (8 to 800 pM) (Fig. S1 in ESI†). In a carrier-free protocol, as observed in Fig. 2, the cholesterol-modified triazole-linked siRNAs (**X1**, **X2**, and **X5**) exhibit potent gene silencing, with 70–80% reduction in firefly luciferase activity in the 500 to 3000 nM concentration range. As previously reported, placing a chemical modification within the central region of the sense strand may impact thermal destabilization,[22–24] however, this does not seem to alter gene-silencing efficacy. In fact, the IC_{50}s for these thermally-destabilized centrally-modified siRNAs **X1** and **X2** were 243.6 nM and 307.1 nM respectively. The 3′-modified siRNA **X5** also exhibited effective gene silencing, with an IC_{50} of 189.2 nM. Previous studies have reported that the 3′-end of the sense strand is able to accommodate bulky groups.[25]

The wild-type siRNA (**wt**), which lacks a cholesterol modification, did not display any gene-silencing activity in our carrier-free study. This was expected as unmodified siRNAs are known to have difficulties in crossing the cellular membrane unassisted. The use of 3′-end cholesterol modifications has been reported in the literature with varying degrees of success.[18,26,27] As such, we decided to investigate the gene-silencing efficacy of a commercially-available 3′-end triethylene glycol (TEG) cholesterol modification (**Chol-TEG**) using our carrier-free transfection protocol as a comparison to our cholesterol-modified triazole-linked siRNAs (**X1**, **X2**, and **X5**). Interestingly, the **Chol-TEG** siRNAs displayed poor gene-silencing abilities in the entire range between 1 to 3000 nM.

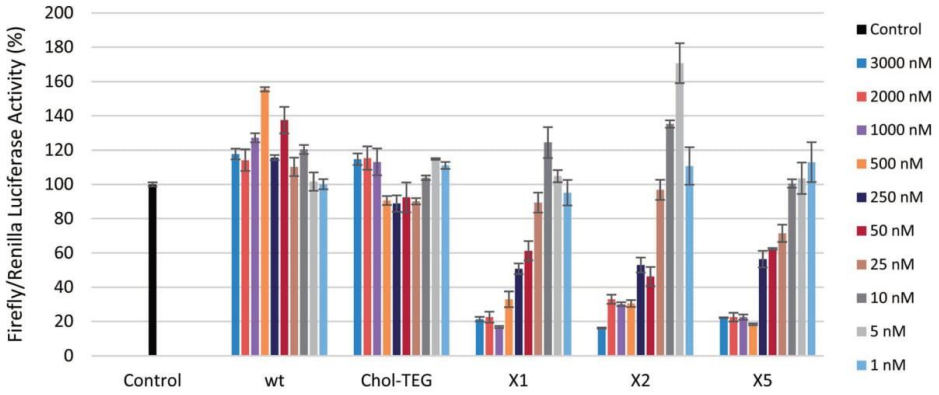

Fig. 2 Reduction in firefly luciferase expression in HeLa cells as a function of siRNA activity ranging from 1 to 3000 nM in the absence of a transfection carrier. Firefly luciferase expression was normalized to *Renilla* luciferase.

Open Access Article. Published on 22 June 2018. Downloaded on 2/7/2021 11:22:43 PM.
This article is licensed under a Creative Commons Attribution 3.0 Unported Licence.

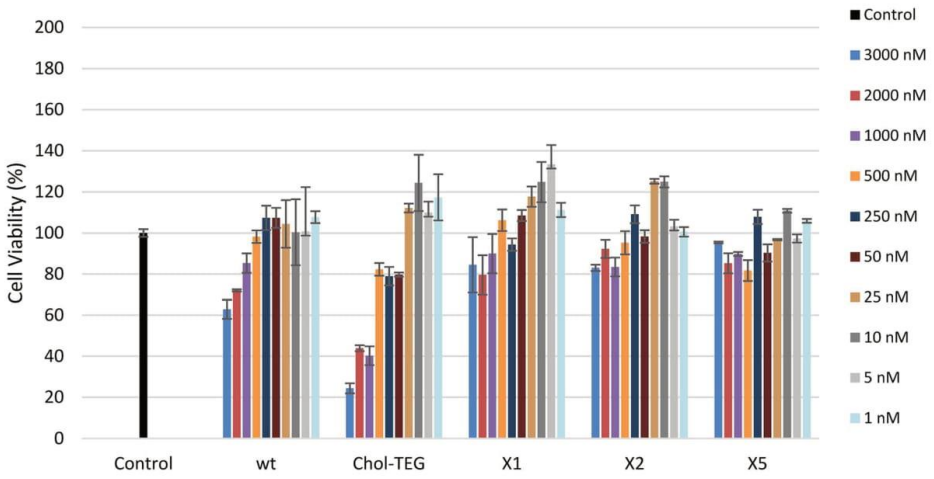

Fig. 3 HeLa cell viability after treatment with various siRNA concentrations (1–3000 nM) using the XTT Cell Proliferation Assay.

It is not entirely clear why the cholesterol-modified triazole-linked siRNAs (**X1**, **X2** and **X5**) exhibit potent gene silencing compared to the siRNA **Chol-TEG**. One possibility is that the conformationally constrained triazole functionality in some way is benefiting the siRNA. Furthermore, the nitrogen atom used to functionalize the molecule with the triazole-cholesterol group is positive under physiological pH, which may also assist in cellular uptake. In contrast, the **Chol-TEG** group contains a neutral, polar and flexible polyethylene linker, which may poorly impact the overall cellular uptake profile of the siRNA.

In order to determine the toxicological effect of siRNA treatments, an XTT cell proliferation assay was performed. The XTT reagent is reduced by mitochondrial succinic dehydrogenase in metabolically-active cells to a highly-pigmented formazan derivative. The absorbance of this product can be quantified and used to assess cellular viability. As seen in Fig. 3, siRNAs bearing the **X** spacer (siRNAs **X1**, **X2** and **X5**) cause minimal toxicity even at high concentrations. HeLa cells treated with 3000 nM **wt** siRNA show a 20–30% decrease in viability compared to cells treated with our cholesterol-modified siRNAs. In addition, high concentrations (1000–3000 nM) of **Chol-TEG** siRNA imparted high cytotoxicity, causing a 60–80% reduction in cell viability, perhaps explaining why these siRNAs did not display successful gene-silencing activity. It is unclear why siRNAs **X1**, **X2** and **X5** are the least toxic compared to **wt** and **Chol-TEG**. However, some studies have identified that molecules functionalized with triazoles are non-toxic.[28,29] Thus, it is possible that the triazole functionality reduces the cytotoxicity of siRNAs.

Conclusions

In conclusion, cholesterol-modified triazole-linked siRNAs show excellent dose-dependent gene silencing of exogenous firefly luciferase mRNA in the absence of a transfection carrier. These results indicate that our modification is compatible with the RNA interference pathway when placed at both the central region and 3′-end of the sense strand of siRNAs. This could provide a novel approach to improve cellular uptake, and perhaps assist with other downstream applications such as packaging of liposomes and lipid-nanoparticles.

Conflicts of interest

There are no conflicts to declare.

Acknowledgements

We acknowledge the Natural Sciences and Engineering Research Council (NSERC) for funding.

Notes and references

1 A. Fire, S. Q. Xu, M. K. Montgomery, S. A. Kostas, S. E. Driver and C. C. Mello, *Nature*, 1998, **391**, 806–811.
2 G. J. Hannon, *Nature*, 2002, **418**, 244–251.
3 R. C. Wilson and J. A. Doudna, *Annu. Rev. Biophys.*, 2013, **42**, 217–239.
4 S. M. Elbashir, J. Harborth, W. Lendeckel, A. Yalcin, K. Weber and T. Tuschl, *Nature*, 2001, **411**, 494–498.
5 C. Selvam, D. Mutisya, S. Prakash, K. Ranganna and R. Thilagavathi, *Chem. Biol. Drug Des.*, 2017, **90**, 665–678.
6 L. Aagaard and J. J. Rossi, *Adv. Drug Delivery Rev.*, 2007, **59**, 75–86.
7 D. Haussecker, *J. Controlled Release*, 2014, **195**, 49–54.
8 S. Shukla, C. S. Sumaria and P. I. Pradeepkumar, *ChemMedChem*, 2010, **5**, 328–349.
9 M. A. Behlke, *Oligonucleotides*, 2008, **18**, 305–320.
10 Y.-K. Oh and T. G. Park, *Adv. Drug Delivery Rev.*, 2009, **61**, 850–862.
11 S. Oliveira, G. Storm and R. M. Schiffelers, *J. Biomed. Biotechnol.*, 2006, **2006**, 63675.

Open Access Article. Published on 22 June 2018. Downloaded on 2/7/2021 11:22:43 PM.
This article is licensed under a Creative Commons Attribution 3.0 Unported Licence.

12 K. Tatiparti, S. Sau, K. S. Kashaw and K. A. Iyer, *Nanomaterials*, 2017, **7**, 77.
13 J. de Jonge, M. Holtrop, J. Wilschut and A. Huckriede, *Gene Ther.*, 2005, **13**, 400–411.
14 M. M. Janas, M. K. Schlegel, C. E. Harbison, V. O. Yilmaz, Y. Jiang, R. Parmar, I. Zlatev, A. Castoreno, H. Xu, S. Shulga-Morskaya, K. G. Rajeev, M. Manoharan, N. D. Keirstead, M. A. Maier and V. Jadhav, *Nat. Commun.*, 2018, **9**, 723.
15 P. Goluszko and B. Nowicki, *Infect. Immun.*, 2005, **73**, 7791–7796.
16 I. V. Chernikov, D. V. Gladkikh, M. I. Meschaninova, A. G. Ven'yaminova, M. A. Zenkova, V. V. Vlassov and E. L. Chernolovskaya, *Mol. Ther.–Nucleic Acids*, 2017, **6**, 209–220.
17 D. Irby, C. Du and F. Li, *Mol. Pharm.*, 2017, **14**, 1325–1338.
18 J. Willibald, J. Harder, K. Sparrer, K.-K. Conzelmann and T. Carell, *J. Am. Chem. Soc.*, 2012, **134**, 12330–12333.
19 C. Lorenz, P. Hadwiger, M. John, H.-P. Vornlocher and C. Unverzagt, *Bioorg. Med. Chem. Lett.*, 2004, **14**, 4975–4977.
20 D. De Paula, M. V. Bentley and R. I. Mahato, *RNA*, 2007, **13**, 431–456.
21 J.-P. Desaulniers, G. Hagen, J. Anderson, C. McKim and B. Roberts, *RSC Adv.*, 2017, **7**, 3450–3454.
22 T. C. Efthymiou, B. Peel, V. Huynh and J.-P. Desaulniers, *Bioorg. Med. Chem. Lett.*, 2012, **22**, 5590–5594.
23 B. J. Peel, G. Hagen, K. Krishnamurthy and J.-P. Desaulniers, *ACS Med. Chem. Lett.*, 2015, **6**, 117–122.
24 H. Addepalli, Meena, C. G. Peng, G. Wang, Y. Fan, K. Charisse, K. N. Jayaprakash, K. G. Rajeev, R. K. Pandey, G. Lavine, L. Zhang, K. Jahn-Hofmann, P. Hadwiger, M. Manoharan and M. A. Maier, *Nucleic Acids Res.*, 2010, **38**, 7320–7331.
25 R. Valenzuela, K. Onizuka, A. A. Ball-Jones, T. Hu, S. Suter and P. A. Beal, *ChemBioChem*, 2016, **17**, 2340–2345.
26 J. Soutschek, A. Akinc, B. Bramlage, K. Charisse, R. Constien, M. Donoghue, S. Elbashir, A. Geick, P. Hadwiger, J. Harborth, M. John, V. Kesavan, G. Lavine, R. K. Pandey, T. Racie, K. G. Rajeev, I. Rohl, I. Toudjarska, G. Wang, S. Wuschko, D. Bumcrot, V. Koteliansky, S. Limmer, M. Manoharan and H. P. Vornlocher, *Nature*, 2004, **432**, 173–178.
27 V. V. Ambardekar, H.-Y. Han, M. L. Varney, S. V. Vinogradov, R. K. Singh and J. A. Vetro, *Biomaterials*, 2011, **32**, 1404–1411.
28 J. Hou, X. Liu, J. Shen, G. Zhao and P. G. Wang, *Expert Opin. Drug Discovery*, 2012, **7**, 489–501.
29 P. Thirumurugan, D. Matosiuk and K. Jozwiak, *Chem. Rev.*, 2013, **113**, 4905–4979.

This journal is © The Royal Society of Chemistry 2018

Electronic Supplementary Material (ESI) for RSC Advances.
This journal is © The Royal Society of Chemistry 2018

Supporting Information

Effective Carrier-Free Gene-Silencing Activity of Cholesterol-Modified siRNAs

Lidya Salim, Chris McKim and Jean-Paul Desaulniers

Faculty of Science, University of Ontario Institute of Technology, 2000 Simcoe Street North, Oshawa, Ontario L1H 7K4 Canada

Jean-Paul.Desaulniers@uoit.ca

Table of Contents

Experimental Nucleic Acid and Biological Procedures

Figures and Tables

Experimental Nucleic Acid and Biological Procedures

General

Unless otherwise stated, all starting reagents were obtained from commercial sources without additional purification. Antisense strand RNA and CHOL-TEG RNA sequences were purchased from and characterized by IDTDNA. Equimolar amounts of sense and antisense RNAs were incubated at 95°C for 2 min in a binding buffer (75.0 mM KCl, 50.0 mM Tris-HCl, 3.00 mM MgCl2, pH 8.30). This solution was cooled slowly to room temperature, allowing the siRNAs to anneal.

Procedure for Characterizing Oligonucleotides through ESI Q-TOF

All single-stranded RNAs (ssX1, ssX2, and ssX5) were gradient eluted through a Zorbax Extend C18 HPLC column with a MeOH/H2O (5 : 95) solution containing 200 mM hexafluoroisopropyl alcohol and 8.1 mM triethylamine, and finally with 70% MeOH. The eluted RNAs were subjected to ESI-MS (ES-), producing raw spectra of multiply-charged anions and through resolved isotope deconvolution, the molecular weights of the resultant neutral oligonucleotides were confirmed. The final neutral mass of the RNAs were confirmed using this method.

Procedure for HPLC Characterization

High-performance liquid chromatography (HPLC) using a C18 4.6 mm x 150 mm reverse phase column on a Waters 1525 Binary HPLC Pump with a Waters 2489 UV/Visible Detector, eluting from 5% to 95% acetonitrile in 0.1 M triethylammonium acetate (TEAA) buffer (pH: 7). Spectra were processed using the Empower 3 software.

Sub-Culturing of HeLa Cells (Passaging)

Biological assays were performed using human epithelial cervix carcinoma cells (HeLa cells). Cells were maintained in Dulbecco's Modified Eagle's Medium (DMEM), supplemented with 10% fetal bovine serum (FBS) and 1% penicillin-streptomycin (Sigma), and incubated at 37°C with 5% CO_2. Once they reached 80-90% confluency, cells were passaged and diluted to a concentration of $1x10^6$ cells/mL. To continue the cell line, 1 mL of this was added to a new cell culture flask containing 24 mL DMEM (10% FBS, 1% penicillin-streptomycin).

Procedure for *in vitro* Dual-Reporter Luciferase Assay in the Presence of a Transfection Reagent

Prior to transfection, HeLa cells were seeded on 12-well plates (Falcon®) containing 1 mL DMEM (10% FBS, 1% penicillin-streptomycin) at a density of 100,000 cells per well. Cells were incubated at 37 ^{0}C with 5% CO_2 for 24 hours until they reached 90% confluence. Then, varying concentrations of anti-luciferase siRNAs (8, 80 and 800 pM) were co-transfected with both pGL3 and pRLSV40 luciferase-expressing plasmids using Lipofectamine 2000® (Invitrogen) in 1X Gibco's Opti-Mem Reduced Serum according to the manufacturer's protocol. Cells were incubated for an additional 24 hours at 37 ^{0}C in 5% CO_2. The medium was discarded, cells were

washed twice with 1X phosphate buffered saline (PBS) and lysed with 1X passive lysis buffer (Promega) over a 20-minute period at room temperature. Cell lysates were loaded onto white and opaque 96-well plates (Costar) in triplicate. Using the Dual-Luciferase® Reporter Kit (Promega), Lar II and Stop & Glo® substrates were added to the cell lysates and enzymatic activity of firefly and *Renilla* luciferase vectors were measured independently using a Synergy HT (Bio-Tek) plate luminometer. The ratio of firefly/*Renilla* luminescence expressed as a percentage relates the reduction in firefly expression to siRNA efficacy when compared to untreated controls. Each data point represents the average of at least two independent assays, each with three technical replicates, with the indicated error (SDOM). The IC50 values were determined with Prism using the variable slope model when the log(inhibitor) was plotted against normalized expression.

Procedure for *in vitro* Dual-Reporter Luciferase Assay in the Absence of a Transfection Reagent

Prior to transfection, HeLa cells were seeded on 24-well plates (Falcon®) containing 350 µL DMEM (10% FBS, 1% penicillin-streptomycin) at a density of 50,000 cells per well. Cells were incubated at 37 ^{0}C with 5% CO_2 for 24 hours until they reached 90% confluence. Then, cells were co-transfected with both pGL3 and pRLSV40 luciferase-expressing plasmids using Lipofectamine 2000® (Invitrogen) in 1X Gibco's Opti-Mem Reduced Serum according to the manufacturer's protocol. Cells were incubated for 4 hours at 37 ^{0}C in 5% CO_2 after which the growth medium was discarded and each well was washed twice with 1 mL of 1X PBS to ensure that no transfection reagent remained in solution. 50 µL DMEM (10% FBS, 1% penicillin-streptomycin) was then added to each well. Anti-luciferase siRNA treatments were prepared by adding 1 µL of the respective siRNA to 20 µL 1X Gibco's Opti-Mem Reduced Serum. Each treatment was added to the respective well, at concentrations of 1, 5, 10, 25, 50, 250, 500, 1000, 2000 and 3000 nM. Cells were incubated for an additional 16 hours at 37 ^{0}C in 5% CO_2 before cell lysing. Luciferase activity was assessed as described above. Each value is the average of at least 3 different experiments with the indicated error (SDOM). The IC50 values were determined with Prism using the variable slope model when the log(inhibitor) was plotted against normalized expression.

Procedure for XTT Cellular Proliferation Assay

Cellular viability after siRNA treatment was determined using the XTT Cell Proliferation Assay Kit (ATCC®). Prior to transfection, HeLa cells were seeded on 96-well plates (Falcon®) containing 150 µL DMEM (10% FBS, 1% penicillin-streptomycin) at a density of 2,500 cells per well. Cells were incubated at 37 °C in 5% CO_2 for 24 hours, after which they were co-transfected with pGL3 and pRLSV40 luciferase-expressing plasmids and incubated for an additional 4 hours, as previously described. After this incubation period, the growth medium was discarded and each well was washed twice with 250 µL 1X PBS. Cells were then treated in triplicate with varying concentrations (1, 5, 10, 25, 50, 250, 500, 1000, 2000 and 3000 nM) of each siRNA and then incubated for an additional 24 hours at 37 °C with 5% CO_2 before treatment with 50 µL of XTT, activated with 2% *N*-methyl dibenzopyrazine methyl sulfate. Cells were incubated for 2 hours at 37 °C with 5% CO_2. Absorbance was measured at 475 nm and 660 nm using a Synergy HT (Bio-Tek) microplate reader. Specific absorbance was calculated: A_{475nm} (experimental) – A_{475nm} (Blank) – A_{660nm} (experimental). Results were normalized to an untreated control.

Figures and Tables

Table S1: Predicted and recorded masses for chemically-modified RNAs

Sample Number	Sense RNAs	Predicted Neutral Mass	Observed Neutral Mass
ssX1	5'- CUUACGCU***X***AGUACUUCGAtt -3'	6958.6	6959.2
ssX2	5'- CUUACGCUG***X***GUACUUCGAtt -3'	6955.2	6953.2
ssX5	5'- CUUACGCUGAGUACUUCGA***X***t -3'	6998.6	6998.8

ESI Q-TOF were recorded in a negative electrospray mode after HPLC elution using two mobile phases; MeOH/H_2O 5:95 (v/v) with 200 mM hexafluoroisopropyl alcohol and 8.1 mM triethylamine, and 70% MeOH. ***X*** corresponds to the single triazole-linked cholesterol modification. The top strand corresponds to the sense strand; the bottom strand corresponds to the antisense strand. In all duplexes, the 5′-end of the bottom antisense strand contains a phosphate group.

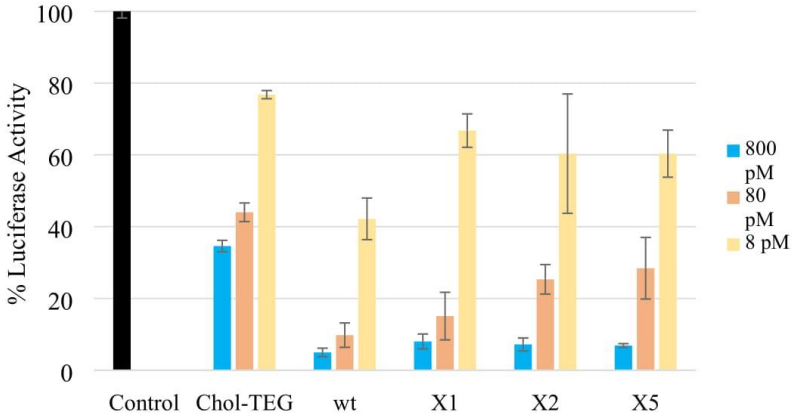

Figure S1. Reduction in firefly luciferase activity as a function of siRNA activity. The commercially-available 3'-end triethylene glycol cholesterol siRNA (**Chol-TEG**), **wt** siRNA and triazole-linked cholesterol siRNAs (**X1**, **X2** and **X5**) were tested in HeLa cells at 8, 80 and 800 pM in the presence of a transfection reagent, with firefly luciferase expression normalized to *Renilla* luciferase.

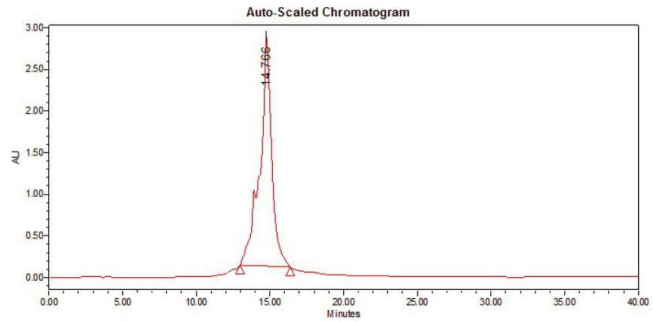

Figure S2. HPLC chromatogram of X1 siRNA, eluting from 5% to 100% acetonitrile in 0.1 M TEAA buffer over 40 min.

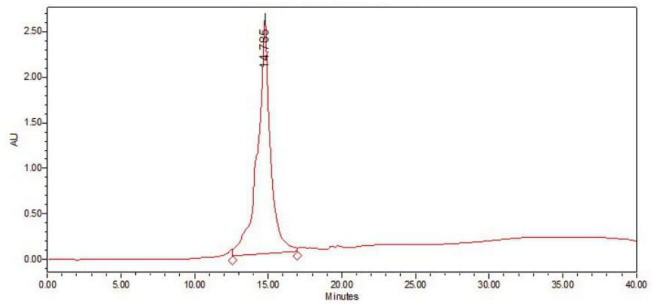

Figure S3. HPLC chromatogram of X2 siRNA, eluting from 5% to 100% acetonitrile in 0.1 M TEAA buffer over 40 min.

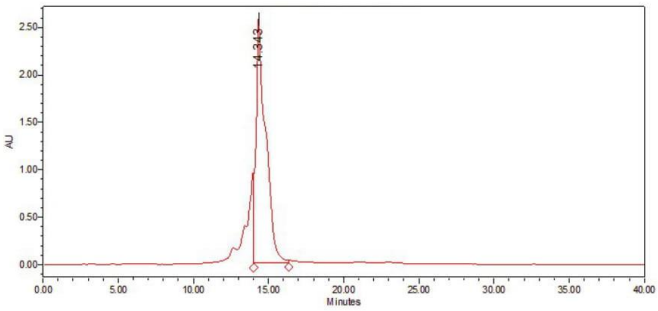

Figure S4. HPLC chromatogram of X5 siRNA, eluting from 5% to 100% acetonitrile in 0.1 M TEAA buffer over 40 min.

Appendix B. Manuscript II and Supplementary Data

Published online 28 November 2019

Nucleic Acids Research, 2020, Vol. 48, No. 1 ***75–85***
doi: 10.1093/nar/gkz1115

Targeted delivery and enhanced gene-silencing activity of centrally modified folic acid–siRNA conjugates

Lidya Salim, Golam Islam and Jean-Paul Desaulniers*

Faculty of Science, University of Ontario Institute of Technology, Oshawa, Ontario L1G 0C5, Canada

Received September 17, 2019; Revised October 28, 2019; Editorial Decision November 10, 2019; Accepted November 11, 2019

ABSTRACT

One of the major hurdles in RNAi research has been the development of safe and effective delivery systems for siRNAs. Although various chemical modifications have been proposed to improve their pharmacokinetic behaviour, their delivery to target cells and tissues presents many challenges. In this work, we implemented a receptor-targeting strategy to selectively deliver siRNAs to cancer cells using folic acid as a ligand. Folic acid is capable of binding to cell-surface folate receptors with high affinity. These receptors have become important molecular targets for cancer research as they are overexpressed in numerous cancers despite being expressed at low levels in normal tissues. Employing a post-column copper-catalyzed alkyne–azide cycloaddition (CuAAC), we report the synthesis of siRNAs bearing folic acid modifications at different positions within the sense strand. In the absence of a transfection carrier, these siRNAs were selectively taken up by cancer cells expressing folate receptors. We show that centrally modified folic acid–siRNAs display enhanced gene-silencing activity against an exogenous gene target (∼80% knockdown after 0.75 μM treatment) and low cytotoxicity. In addition, these siRNAs achieved potent dose-dependent knockdown of endogenous Bcl-2, an important anti-apoptotic gene.

INTRODUCTION

RNA interference (RNAi) is an endogenous pathway that utilizes double-stranded RNA to suppress the expression of a target mRNA, resulting in sequence-specific gene silencing (1,2). In the effector step of RNAi, short interfering RNAs (siRNAs) of 21–23 nucleotides are incorporated into a protein complex, the RNA-induced silencing complex (RISC) (3). This is followed by a duplex dissociation step, promoted by the catalytic activity of the endonuclease Argonaute2 (Ago2) which cleaves between base pairs 9 and 10 from the sense strand 5′ end (4,5). RISC retains the antisense strand which is used as a guide sequence to locate and degrade the target mRNA (6,7). Synthetic siRNAs are able to induce gene silencing through the RNAi pathway (8), becoming powerful tools to study gene function (9,10). RNAi-based therapies also hold great promise as siRNAs can be used to down-regulate the expression of deleterious proteins involved in disease onset and progression (11–13). However, this system comes with several limitations given by the inherent nature of siRNAs such as low stability, poor cellular uptake, potential for immune activation and off-target effects (14–16). Chemical modifications are able to mitigate some of these challenges and improve the pharmacokinetic properties of siRNAs (17,18) but despite advancements in the field (19), there is still no universal modification able to address all of the challenges associated with siRNAs.

The delivery of siRNAs to target cells or tissues has been one of the major challenges in RNAi research. Naked siRNAs are unable to diffuse across cellular membranes due to their large size and polyanionic backbone (20). Current delivery strategies include the encapsulation of siRNAs within nanoparticles or liposomes and the conjugation of siRNAs to hydrophobic molecules (21). Because siRNAs lack selectivity for specific cell types, receptor-targeting ligands can be used to deliver siRNAs to target cells and tissues (22). One example is the vitamin folic acid, which has been extensively used as a drug delivery system to target folate receptors (FRs) in tumour cells (23,24). FRs are cell-surface glycoproteins able to bind folic acid with high affinity. These receptors are expressed at low levels in most tissues, as their expression is limited to cells important for folate resorption and embryonic development, yet they are highly overexpressed on the surface of numerous cancers (25). This includes ∼90% of ovarian carcinomas as well as breast, endometrial, brain and kidney cancers (26,27). Once bound to the FR, folic acid enters the cell through receptor-mediated endocytosis. Notably, folic acid conjugates retain the ability to bind to and be internalized by this receptor, making the FR an attractive molecular target for cancer research (28). This receptor-targeting strategy has been used to de-

*To whom correspondence should be addressed. Tel: +1 905 721 8668 (Ext. 3621); Fax: +1 905 721 3304; Email: jean-paul.desaulniers@ontariotechu.ca

© The Author(s) 2019. Published by Oxford University Press on behalf of Nucleic Acids Research.
This is an Open Access article distributed under the terms of the Creative Commons Attribution Non-Commercial License (http://creativecommons.org/licenses/by-nc/4.0/), which permits non-commercial re-use, distribution, and reproduction in any medium, provided the original work is properly cited. For commercial re-use, please contact journals.permissions@oup.com

Downloaded from https://academic.oup.com/nar/article/48/1/75/5644999 by guest on 28 April 2021

liver siRNAs by functionalizing liposomes and nanoparticles with folic acid (29–33) although selective delivery can also be achieved by direct conjugation of folic acid to siRNAs.

Previous studies have successfully incorporated folic acid modifications at either the 3′ or 5′ end of siRNA and achieved selective, carrier-free delivery to target cells (34,35). In these studies, moderate gene-silencing activity against exogenous gene targets (40–60% knockdown after 1 μM treatment) was reported. These results show promise in the use of folic acid as a delivery system for siRNAs. However, there is a need to improve the gene-silencing potency of folic acid–siRNA constructs. Recently, our lab group reported a method to destabilize the central region of siRNAs, which spans the Ago2 cleavage site. We showed that chemical modifications within this region can lead to potent gene-silencing (36,37). To the best of our knowledge, folic acid has not been incorporated into the central region of siRNAs. Based on this, we report the copper-catalyzed azide-alkyne cycloaddition (CuAAC) synthesis of siRNAs bearing folic acid modifications at different positions within the sense strand, with a particular emphasis on the central region. In the absence of a transfection carrier, these siRNAs were selectively taken up by FR-expressing cell lines. We show that internal modified folic acid–siRNAs display enhanced gene-silencing activity, with minimal toxicity, against exogenous firefly luciferase mRNA (∼80% knockdown after 0.75 μM treatment). In addition, these siRNAs achieved potent dose-dependent knockdown of the oncogene Bcl-2 (∼72% knockdown after 1 μM treatment).

MATERIALS AND METHODS

General methodology and materials as well as NMR spectra are provided in the Supplementary Data.

Synthesis of propargyl phosphoramidite

Compound 1. To a solution of diethanolamine (10 g, 95.1 mmol) in 150 ml of anhydrous CH_2Cl_2, cooled in an ice bath, was added anhydrous potassium carbonate (65.7 g, 0.476 mol) under an argon atmosphere. Propargyl bromide (80 wt% in toluene, 8.5 ml, 95.1 mmol) was added drop-wise over a 5-minute period and the solution was left to stir vigorously for 60 h at room temperature. The crude product was filtered to remove the potassium carbonate and the collected filtrate was concentrated *in vacuo* to produce a dark amber oil, which was purified by flash chromatography (elution with 2 to 10% $MeOH/CH_2Cl_2$). The final product was isolated as a clear amber oil (9.53 g, 70%). ^{1}H NMR (400 MHz, $CDCl_3$) δ 2.19 (t, 1H), 2.68 (t, 4H), 3.40 (s, 2H), 3.60 (t, 4H). ^{13}C NMR (101 MHz, $CDCl_3$) δ 42.05, 55.21, 59.05, 73.15, 78.31. (Scheme 1)

Compound 2. To a solution of **1** (2 g, 14 mmol) in 25 ml anhydrous CH_2Cl_2 was added freshly-distilled triethylamine (1.7 ml, 12.6 mmol) under an argon atmosphere. This was followed by the drop-wise addition of 4,4′-dimethoxytriphenylmethyl chloride (3.79 g, 11.2 mmol) in 5 ml anhydrous CH_2Cl_2. The reaction mixture was stirred overnight at room temperature after which the crude product was extracted three times with a saturated $NaHCO_3$ solution. The combined organic layers were dried over Na_2SO_4 and concentrated *in vacuo* to produce a cloudy yellow oil which was purified by flash chromatography (elution with 2 to 10% $MeOH/CH_2Cl_2$). The final product was isolated as a clear yellow oil (2.8 g, 45%). ^{1}H NMR (400 MHz, $CDCl_3$) δ 2.23 (t, 1H), 2.75 (t, 2H), 2.83 (t, 2H), 3.23 (t, 2H), 3.44(d, 2H), 3.60 (t, 2H), 3.80 (s, 6H), 6.87 (dt, 4H), 7.29 (m, 1H), 7.31 (td, 2H), 7.38 (dt, 4H), 7.47 (d, 2H); ^{13}C NMR (101 MHz, $CDCl_3$) δ 42.76, 52.58, 55.19, 55.65, 58.57, 61.94, 72.83, 78.82, 86.21, 113.07, 126.71, 127.77, 128.13, 129.96, 136.28, 144.95, 158.41.

Compound 3. To a flame-dried round-bottomed flask containing a solution of **2** (180 mg, 0.404 mmol) in 5 ml anhydrous CH_2Cl_2 was added freshly-distilled triethylamine (0.28 ml, 2.02 mmol) under an argon atmosphere. This was followed by the dropwise addition of 2-cyanoethyl-*N*,*N*-diisopropylchlorophosphoramidite (0.27 ml, 1.21 mmol). The reaction mixture was stirred for 3 h and then concentrated *in vacuo* to produce a cloudy oil which was purified by flash chromatography (elution 20–60% EtOAc/hexanes, maintaining 5% triethylamine). The product was isolated as a clear oil (0.22 g, 84%). ^{1}H NMR (400 MHz, $CDCl_3$) δ 1.17 (dd, 12H), 2.19 (t, 1H), 2.55 (m, 2H), 2.82 (dt, 4H), 3.15 (t, 2H), 3.45 (d, 2H), 3.57 (m, 2H), 3.66 (m, 2H), 3.76 (m, 2H), 3.78 (s, 6H), 6.83 (dt, 4H), 7.20 (tt, 1H), 7.27 (t, 2H), 7.32 (dt, 4H), 7.44 (d, 2H). ^{13}C NMR (101 MHz, $CDCl_3$) δ 20.33, 21.02, 24.63, 42.98, 43.10, 46.30, 54.20, 55.15, 58.41, 62.03, 62.65, 72.79, 79.27, 86.05, 113.04, 117.71, 126.58, 127.75, 128.18, 130.02, 136.46, 145.22, 158.36. ^{31}P (162 MHz, $CDCl_3$) δ 147.28.

Oligonucleotide synthesis, deprotection and purification

Wild-type and propargyl oligonucleotides were synthesized using an Applied Biosystems 394 DNA/RNA synthesizer using a 1.0 μM dT controlled-pore glass (CPG) support and a 1.0 μM cycle with a 999-second coupling time. Immediately prior to synthesis, phosphoramidites were resuspended in anhydrous acetonitrile to a final concentration of 0.1 M. Oligonucleotide sense strands were chemically phosphorylated at the 5′ end using 2-[2-(4,4-dimethoxytrityloxy)ethylsulfonyl]ethyl-(2-cyanoethyl)-(*N*,*N*-diisopropyl)-phosphoramidite. Cleavage of oligonucleotides from the solid support was achieved by flushing the CPG columns with 1 ml EMAM solution (1:1 methylamine 33 wt% in ethanol and methylamine 40% wt. in H_2O) for 1 h at room temperature, followed by overnight incubation in EMAM to deprotect the bases. Oligonucleotides were concentrated in a miVac Quattro concentrator and desilylated in DMSO (100 μl) and 3HF-Et_3N (125 μl) for 3 h at 65°C. Crude oligonucleotides were precipitated in ethanol and desalted using Millipore Amicon Ultra 3000 MW cellulose centrifugal filters. Strands were purified using reverse-phase HPLC eluting from 5% to 95% ACN in 0.1 M TEAA buffer (pH 7.0).

Synthesis and purification of folic acid–conjugated siRNAs

Compound 4. Folic acid (0.5 g, 1.13 mmol) was dissolved in anhydrous DMSO (30 ml) under an argon atmosphere. *N*-Hydroxysuccinimide (0.26 g, 2.27 mmol) and

Downloaded from https://academic.oup.com/nar/article/48/1/75/5644999 by guest on 28 April 2021

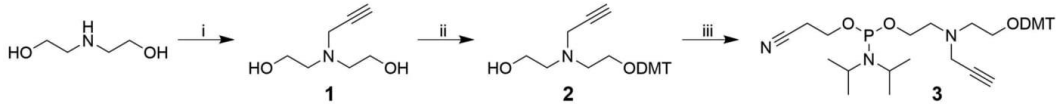

Scheme 1. Reagents and conditions: (i) propargyl bromide, K_2CO_3, CH_2Cl_2, 60 h, 69%; (ii) DMTCl, Et_3N, CH_2Cl_2, rt, overnight, 45%; (iii) 2-cyanoethyl *N,N*-diisopropylchlorophosphoramidite, Et_3N, CH_2Cl_2, rt, 3 h, 84%.

N,N′-dicyclohexylcarbodiimide (0.26 g, 1.25 mmol) were simultaneously added and the reaction mixture was left to stir overnight in the dark. The dicyclohexylurea by-product was removed by filtration and the filtrate was collected in a round-bottomed flask to which a solution 2-azidoethanamine (0.12 g, 1.37 mmol) in 10 ml anhydrous DMSO was added. The reaction mixture was left to stir in the dark for an additional 24 h. After removing most of the DMSO *in vacuo*, the crude product was precipitated in cold diethyl ether and the collected yellow crystals were washed with THF and CH_2Cl_2. The product was further purified by automated flash chromatography, eluting with a slow gradient (0–100%) of solution A (2:1:1 NH_4OH/MeOH/ACN) to solution B (ACN). The product was isolated as bright yellow crystals (0.48 g, 84%). ^{1}H NMR (400 MHz, DMSO-d_6) δ 1.84–2.00 (m, 2H), 2.05–2.20 (m, 2H), 3.19 (t, 2H), 3.32 (t, 2H), 4.30 (m, 1H), 4.45 (d, 2H), 6.61 (d, 2H), 6.90 (m, 1H), 7.66 (d, 2H), 8.04 (m, 1H), 8.59 (s, 1H), 11.86 (br, 1H). ESI-HRMS (ES+) *m/z* calculated for $C_{21}H_{23}N_{11}O_5$: 510.1956, found 510.1953 $[M+H]^+$ (Scheme 2).

Copper-catalyzed azide-alkyne cycloaddition (CuAAC) procedure. To a solution of propargyl-modified RNA (100 μM, 5 μl) in DMSO/H_2O/t-BuOH (1:2:1) was added **4** (2.5 mM, 5 μl) under an argon atmosphere. This was followed by the addition of a pre-chelated mixture of $CuSO_4$ (2.5 mM) and tris(benzyltriazolylmethyl)amine (TBTA) (12.5 mM, 5 μl). A fresh solution of sodium ascorbate (2.5 mM, 10 μl) was added, and the reaction mixture was stirred at 40°C in the dark for 3.5 h. At this point, sodium acetate (0.3 M solution in H_2O, 50 μl) was added and the mixture was stirred for an additional 20 min at room temperature. Crude RNA was precipitated in cold EtOH, centrifuged at 13 400 rpm for 15 min and washed twice with cold EtOH. Strands were purified using reverse-phase HPLC eluting from 5% to 95% ACN in 0.1 M TEAA buffer (pH 7.0). (Scheme 3)

Thermal denaturation and CD studies

Thermal denaturation and CD studies were performed using a Jasco J-815 Circular Dichroism (CD) Spectropolarimeter equipped with a temperature controller. For duplex formation, equimolar amounts of complementary sequences were combined, dried down and resuspended in 300 μl pH 7 sodium phosphate buffer (90.0 mM NaCl, 10.0 mM Na_2HPO_4, 1.00 mM EDTA). Samples were heated at 90°C for 2 min and then allowed to slowly cool to room temperature. To determine melting temperature (T_m), UV absorbance was measured at 260 nm and temperature was increased from 10 to 95°C at a rate of 0.5°C per minute. T_m data was analysed using Meltwin v3.5 software and represents the average of three independent runs. Circular dichroism spectra were recorded at 25°C, scanning from 200 to 350 nm with a screening rate of 20.0 nm/min and a 0.20 nm data pitch. All scans were performed in triplicate and averaged using Jasco's Spectra Manager v2 software.

Cell culture

HeLa and HT-29 cells were maintained in Dulbecco's modified Eagle's medium (DMEM) and Roswell Park Memorial Institute (RPMI) 1640 Medium respectively, both supplemented with 10% fetal bovine serum (FBS) and 1% penicillin–streptomycin (Sigma). Cells were maintained at 37°C in a humidified atmosphere with 5% CO_2 and passaged at 80% confluency.

Carrier-free transfections for luciferase assay

Transfection in HeLa. The day before transfection, HeLa cells were seeded into 96-well plates, containing 50 μl folate-free RPMI 1640, at a density of 1.0×10^4 cells per well and incubated for 24 h. Two plasmids, pGL3 (firefly luciferase, 200 ng) and pRLSV40 (*Renilla* luciferase, 50 ng), were co-transfected using 1 μl Lipofectamine 2000™ (Invitrogen) following the manufacturer's protocol. Plates were incubated for 4 hours at 37°C in a humidified atmosphere with 5% CO_2 after which the medium was removed from each well. Cells were washed twice with 1× phosphate-buffered saline (PBS) after which 50 μl folate-free RPMI 1640 medium (without antibiotics) was added to each well. Each siRNA was diluted in 50 μl 1× Gibco's Opti-MEM Reduced Serum Medium (Invitrogen) on ice and the diluted samples were immediately transferred to the respective wells of the 96-well plate. Plates were gently rocked back and forth for a few minutes and then incubated for an additional 16 h prior to cell lysis.

Transfection in HT-29. The day before transfection, HT-29 cells were seeded into 96-well plates, containing 50 μl folate-free RPMI 1640, at a density of 5.0×10^4 cells per well and incubated for 24 h. For plasmid transfection, pGL3 (firefly luciferase, 600 ng) and pRLSV40 (*Renilla* luciferase, 150 ng) were combined and diluted in 1× Gibco's Opti-MEM Reduced Serum Medium (Invitrogen) to a final volume of 50 μl. This was followed by the addition of 4 μl Lipofectamine® LTX (Thermo Fisher). After a 30-minute incubation period at room temperature, complexes were transferred to each well and plates were incubated for 6 h at 37°C in a humidified atmosphere with 5% CO_2 after which the medium was removed from each well. Cells were washed twice with 1× phosphate-buffered saline (PBS) after which 50 μl folate-free RPMI 1640 medium (without antibiotics) was added to each well. Each siRNA was diluted in 50 μl

Downloaded from https://academic.oup.com/nar/article/48/1/75/5644999 by guest on 28 April 2021

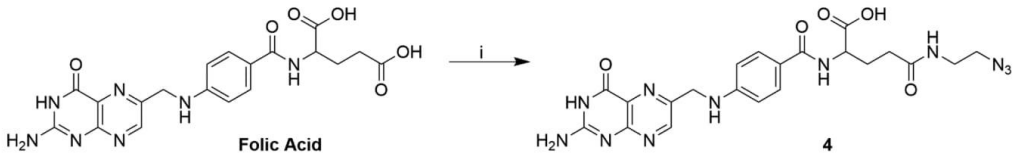

Scheme 2. Reagents and conditions: (i) **3**, *N*-Hydroxysuccinimide, *N,N'*-Dicyclohexylcarbodiimide, DMSO, rt, overnight, 2-azidoethanamine, 24 h., 83%.

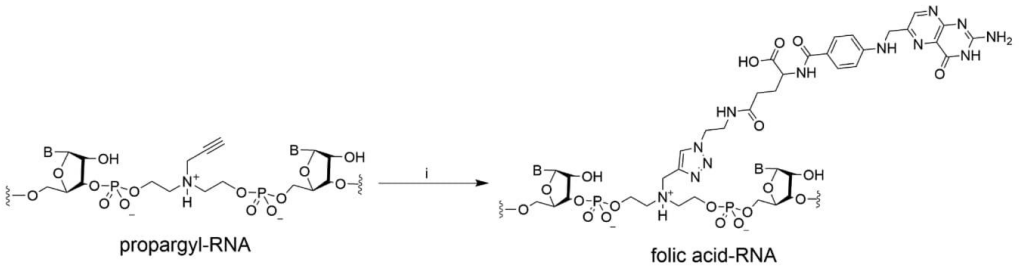

Scheme 3. Reagents and conditions: **4**, $CuSO_4$, TBTA, sodium ascorbate, DMSO/H_2O/t-BuOH (1:2:1), 40°C, 4 h, 69–80%

1× Gibco's Opti-MEM Reduced Serum Medium (Invitrogen) on ice and the diluted samples were immediately transferred to the respective wells of the 96-well plate. Plates were gently rocked back and forth for a few minutes and then incubated for an additional 20 h prior to cell lysis.

Dual-luciferase® reporter assay

Cells were lysed with 1× passive lysis buffer for 20 min at room temperature. Cell lysates were transferred to microcentrifuge tubes and were immediately used to assess the gene-silencing activity of siRNAs using a Dual-Luciferase® Reporter Assay (Promega). Luciferase Assay Reagent II (LAR II) and Stop & Glo® Reagent were prepared following the manufacturer's protocol. Cell lysates (10 μl) were transferred to Costar 96-well plates in triplicate. LAR II reagent (50 μl) was added to each well and the first luminescence measurement was taken on a Synergy HT (Bio-Tek) plate luminometer. Stop & Glo® Reagent (50 μl) was then added to each well and the second luminescence measurement was taken. Results are expressed as the ratio of firefly/*Renilla* luminescence taken as a percentage of an untreated control. Each value is the average of at least three biological replicates and error bars indicate standard deviation.

Statistical analysis

Prism 8.0 (GraphPad Software, San Diego, CA, USA) was used to generate dose-response curves after carrier-free siRNA transfection in HeLa cells. Dose-response curves for folic acid-conjugated anti-luciferase siRNAs can be found in the Supplement (Supplementary Figure S2). The half-maximal inhibitory concentration (IC_{50}) of each siRNA was determined using Prism's variable slope (four-parameter) model. Anti-luciferase siRNAs were tested at seven concentrations in carrier-free conditions. Anti-Bcl-2 siRNAs were tested at three concentrations in carrier-free conditions. Standard errors (S.E.) were determined for a minimum of two biological replicates.

Cell viability assay

HeLa and HT-29 cells were seeded into 96-well plates at a density 5.0×10^3 cells per well and incubated for 24 h. Cells were transfected following the described carrier-free protocol and were incubated for an additional 24 h. Cell viability was assessed using the XTT Cell Proliferation Assay Kit (ATCC™) following the manufacturer's protocol. Absorbance readings were taken using a Synergy HT (Bio-Tek) plate luminometer.

Flow cytometry

PE anti-FOLR1 (Folate Binding Protein) Antibody and PE Mouse IgG2a, κ Isotype Control (FC) Antibody were purchased from Biolegend. Cells were dislodged from the culture flask using trypsin and transferred into tubes. Cells were then centrifuged at 300 g for 10 min (4°C). After aspirating the supernatant, cells were resuspended in 150 μl cell staining buffer (2.5 ml FBS, 47.5 ml PBS). Cells were stained with trypan blue and counted using a Haemocytometer. For each study, cells were resuspended in staining buffer to achieve a final concentration of 1×10^6 cells/100 μl. Antibodies were added to each cell suspension and cells were incubated in the dark for 30 min (on ice). Samples were centrifuged at 300 g for 5 min (4°C) after which the supernatant was aspirated and cells were washed with 1 ml staining buffer. The last two steps, centrifugation and washing, were repeated once more. Samples were then centrifuged one last time. After removing the supernatant, cells were resuspended in 500 μl ice-cold

Downloaded from https://academic.oup.com/nar/article/48/1/75/5644999 by guest on 28 April 2021

PBS and incubated at room temperature for 5 min. Flow cytometry studies were performed immediately on a BD Accuri C6 Plus flow cytometer following the manufacturer's protocol.

RT-qPCR

Detailed methods for total RNA extraction and cDNA synthesis can be found in the Supplementary Data. Real-time PCR was performed in a total reaction volume of 20 μl including 10 ul SsoFast EvaGreen Supermix (Bio-Rad, Hercules, CA, USA) containing Sso 7-d Fusion Polymerase, 0.5 μM forward primer and reverse primer and 2 μl cDNA template. In the final reaction, cDNA was diluted 40× to produce the best results. Pre-designed primers BCL-2F 5′-CTG GTG GGA GCT TGC ATC AC-3′ and BCL-2R 5′-ACA GCC TGC AGC TTT GTT TC-3′ were purchased to target the Bcl-2 gene and yielding a 150-bp amplicon and 18S-F 5′-CGG CTA CCA CAT CCA AGG AAG-3′ and 18S-R 5′-CGC TCC CAA GAT CCA ACT ACT-3′ (Integrated DNA Technologies Inc, San Diego, California) were used to target the 18s gene in Hela cells and yielding a 247-bp amplicon. Reactions were incubated in the Bio-Rad CFX 96 Real-Time Detection System using the following cycle conditions: 50°C for 10 min, 95°C for 10 min, followed by 40 cycles at 95°C for 15 s and 60°C for 1 min. Reaction specificity was assessed by melting curve analysis immediately after the qPCR experiment. The efficiency of each primer set for RT-qPCR was determined to be between 95 and 100% using the standard curve method. NRT controls were performed during standard curve analysis to confirm that amplification of the PCR product was cDNA and not genomic DNA. NTC controls were also performed to ensure that amplification of the PCR product was not a result of primer–dimers. Results were analyzed using the Bio-Rad CFX manager 3.1 software where the Bcl-2 expression data was normalized against 18s gene as the reference and expression profiles were generated using the comparative Delta-CT method of analysis. The final data was represented by averages and standard deviations compiled from two biological replicates for each treatment for which three technical replicates were included for the qPCR experiments.

RESULTS

Preparation of propargyl and folic acid-modified oligonucleotides

Propargyl phosphoramidite **3** was synthesized as described above. Propargyl and wild-type oligonucleotides were synthesized following standard solid-phase phosphoramidite chemistry. Propargyl-modified oligonucleotides were conjugated with azido-folate derivative **4** as described above. Oligonucleotides were purified using reverse-phase HPLC (Supplementary Figure S5) and characterized by mass spectrometry (Supplementary Table S1).

Thermal stability and CD studies

Synthesized sense strands were annealed to their complementary antisense sequences as described above. CD studies were performed to confirm that siRNAs adopted an A-form helical conformation (Supplementary Figure S1). Melting temperatures (T_m) were measured for anti-firefly luciferase and anti-Bcl-2 siRNAs (Table 1). Modifications placed at the 3′ end of the sense strand were well-tolerated and did not cause significant destabilizing effects. In these siRNAs, the propargyl and folic acid modifications replaced the 3′ dTdT overhang, leading to a 3.5 and 4.7°C decrease in melting temperature for aL-P4 and aL-F4, respectively. This is likely due to the loss of stacking interactions which have been reported with 3′ dTdT overhangs (38). We observed a similar destabilizing effect when the modifications were placed at position 5 from the sense strand 3′ end ($\Delta T_m = -6.00$ and -5.5°C for propargyl and folic acid–siRNAs, respectively). On the other hand, internally-modified anti-luciferase siRNAs exhibited significant thermal destabilization. The greatest decrease in T_m was observed when the propargyl spacer replaced a single nucleotide at position 9 from the sense strand 5′ end (aL-P1, $\Delta T_m = -22.2$°C). Placing the folic acid modification at this position produced a similar effect (aL-F1, $\Delta T_m = -17.2$°C). This thermal destabilization is consistent with previous studies examining the effect of central region modifications on siRNA stability (39). Next, we tested whether our propargyl and folic acid modifications would be better accommodated within the helix if they replaced two nucleotides instead of one (positions 9 and 10 from the sense strand 5′ end). However, there was no significant increase in melting temperature ($\Delta T_m = -20.5$ and -19.9 for aL-P2 and aL-F2 siRNAs respectively). Similar destabilizing effects were observed with internal modified anti-Bcl-2 siRNAs (aB-P and aB-F) and scramble siRNAs (aL-scr-P, aL-scr-F, aB-scr-P and aB-scr-F).

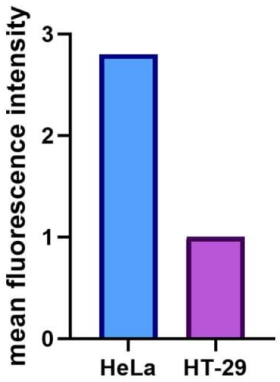

Figure 1. Relative expression of folate receptor α (FRα) levels in HeLa and HT-29 cells determined by flow cytometry.

Relative expression of folate receptor α in HeLa and HT-29 cells

The relative expression of cell-surface folate receptor α (FRα) was assessed in HeLa and HT-29 cells using flow cytometry. The procedure was performed as described above and results are summarized in Figure 1. HeLa cells dis-

Downloaded from https://academic.oup.com/nar/article/48/1/75/5644999 by guest on 28 April 2021

Table 1. siRNA sequences, melting temperatures and *IC_{50} values

siRNA	Duplex	T_m (°C)	ΔT_m (°C)	IC_{50} ± S.E. (nM)
aL-wt	5′ CUUACGCU<u>GA</u>GUACUUCGAtt 3′ 3′ ttGAAUGCGACUCAUGAAGCU 5′	76.1	–	Inactive
aL-P1	5′ CUUACGCU**P**AGUACUUCGAtt 3′ 3′ ttGAAUGCGACUCAUGAAGCU 5′	53.9	−22.2	Inactive
aL-F1	5′ CUUACGCU**F**AGUACUUCGAtt 3′ 3′ ttGAAUGCGACUCAUGAAGCU 5′	58.9	−17.2	171.0 ± 48.8
aL-P2	5′ CUUACGCU**P**GUACUUCGAtt 3′ 3′ ttGAAUGCGACUCAUGAAGCU 5′	55.6	−20.5	Inactive
aL-F2	5′ CUUACGCU**F**GUACUUCGAtt 3′ 3′ ttGAAUGCGACUCAUGAAGCU 5′	56.2	−19.9	128.95 ± 9.7
aL-P3	5′ CUUACGCU<u>GA</u>GUACU**P**GAtt 3′ 3′ ttGAAUGCGACUCAUGAAGCU 5′	70.1	−6.0	Inactive
aL-F3	5′ CUUACGCU<u>GA</u>GUACU**F**GAtt 3′ 3′ ttGAAUGCGACUCAUGAAGCU 5′	70.6	−5.5	283.9 ± 62.9
aL-P4	5′ CUUACGCU<u>GA</u>GUACUUCGA**P** 3′ 3′ ttGAAUGCGACUCAUGAAGCU 5′	72.6	−3.5	Inactive
aL-F4	5′ CUUACGCU<u>GA</u>GUACUUCGA**F** 3′ 3′ ttGAAUGCGACUCAUGAAGCU 5′	71.4	−4.7	1044 ± 23.0
aL-scr	5′ GGUAUCCC<u>UC</u>GUGAAUCAUtt 3′ 3′ ttCCAUAGGGAGCACUUAGUA 5′	74.5	–	Inactive
aL-scr-P	5′ GGUAUCCC**P**GUGAAUCAUtt 3′ 3′ ttCCAUAGGGAGCACUUAGUA 5′	59.1	−15.4	Inactive
aL-scr-F	5′ GGUAUCCC**F**GUGAAUCAUtt 3′ 3′ ttCCAUAGGGAGCACUUAGUA 5′	54.6	−19.9	Inactive
aB-wt	5′ GCCUUCUU<u>UG</u>AGUUCGGUGtt 3′ 3′ ttCGGAAGAAACUCAAGCCAC 5′	72.8	–	Inactive
aB-P	5′ GCCUUCUU**P**AGUUCGGUGtt 3′ 3′ ttCGGAAGAAACUCAAGCCAC 5′	56.6	−16.2	Inactive
aB-F	5′ GCCUUCUU**F**AGUUCGGUGtt 3′ 3′ ttCGGAAGAAACUCAAGCCAC 5′	47.6	−25.2	419.3
aB-scr	5′ GGUGUACG<u>UC</u>GUCUGUUCUtt 3′ 3′ ttCCACAUGCAGCAGACAAGA 5′	73.1	–	Inactive
aB-scr-P	5′ GGUGUACG**P**GUCUGUUCUtt 3′ 3′ ttCCACAUGCAGCAGACAAGA 5′	67.1	−6.0	Inactive
aB-scr-F	5′ GGUGUACG**F**GUCUGUUCUtt 3′ 3′ ttCCACAUGCAGCAGACAAGA 5′	55.0	−18.1	Inactive

The top strand corresponds to the sense strand; the bottom strand corresponds to the antisense strand. **P** corresponds to the propargyl spacer. **F** represents the folic acid spacer. The Argonaute2 cleavage site is underlined. **aL** represents anti-luciferase siRNAs. **aB** represents anti-Bcl-2 siRNAs.
*IC_{50} values were calculated after siRNA transfection in a carrier-free environment. Inhibitory dose-response curves can be found in the Supplementary Data (Supplementary Figure S2).

played a 3-fold increase in FRα expression compared to HT-29 cells.

Carrier-free gene silencing of exogenous firefly luciferase mRNA

Prior to carrier-free studies, we confirmed the biological activity of all siRNAs in HeLa and HT-29 cells after transfection with Lipofectamine reagent (Lipofectamine 2000™ in HeLa and Lipofectamine® LTX in HT-29). In both cell lines, anti-luciferase siRNAs achieved excellent dose-dependent knockdown of firefly luciferase after 8, 80 and 800 pM treatments (Figure 2). Consistently, siRNAs bearing internal modifications (propargyl or folic acid) showed much higher gene-silencing potency than the 3′-end modified siRNAs. As expected, scramble controls displayed no gene-silencing activity.

To assess the cellular uptake and delivery of siRNAs, HeLa and HT-29 cells were transfected following the respective carrier-free protocols described earlier with siRNA concentrations ranging from 1 to 3000 nM. In HeLa cells, gene-silencing activity was only observed in anti-luciferase siRNAs bearing folic acid modifications and not in the wild-type (aL-wt) or propargyl siRNAs (aL-P1 to aL-P4) (Figure 3). As expected, scramble controls showed no gene-silencing activity, even with the folic acid modification present. The two siRNAs bearing centrally-placed folic acid modifications displayed the highest gene-silencing potency with IC_{50} values of 171.0±48.8 and 128.95±9.7 nM for aL-F1 and aL-F2 respectively. Notably, at the lowest concentration tested, 1 nM, the centrally-modified folic acid siRNAs still showed ∼20% gene-silencing activity. When the folic acid modification was placed at position 5 from sense strand 3′ end (aL-F3), the gene-silencing potency was decreased by more than half (IC_{50}: 283.9±62.9 nM) whereas placing the folic acid modification at the 3′ greatly reduced siRNA activity (IC_{50}: 1044±23.0 nM). To validate that the folic-acid siRNAs are being internalized via FR, we subjected the same type of experiment to HeLa cells that were maintained in DMEM supplemented with folic acid. As seen in Figure 4, there is a significant decrease in the gene-silencing activity of centrally modified folic acid–siRNAs (aL-F1 and aL-F2) when free folic acid is present in the media. When the carrier-free siRNA transfection was performed in HT-29 cells, we observed no silencing activity for any of the tested siRNAs (Figure 5).

Downloaded from https://academic.oup.com/nar/article/48/1/75/5644999 by guest on 28 April 2021

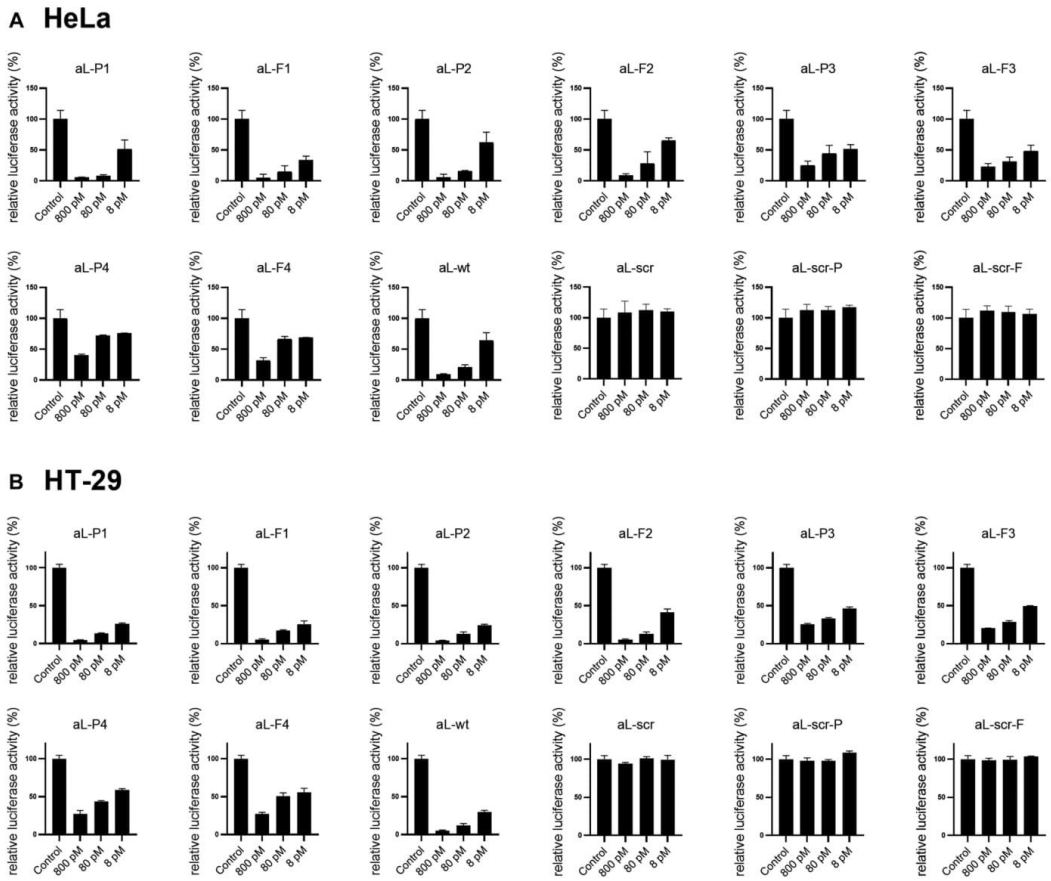

Figure 2. Relative expression of firefly luciferase in HeLa (**A**) and HT-29 cells (**B**) 24 h after anti-luciferase siRNA transfections at 8, 80 and 800 pM using Lipofectamine. Firefly luciferase expression was assessed with a dual-luciferase reporter assay and was normalized to *Renilla* luciferase. Error bars indicate SD of at least two independent biological replicates.

Viability of HeLa and HT-29 cells after siRNA treatment

The XTT Cell Proliferation Assay was employed to assess HeLa and HT-29 cell viability after treatment with increasing siRNA concentrations (1, 25, 75, 150, 375, 750, 1500 and 3000 nM). At the highest concentration tested (3000 nM), cells treated with propargyl and folic acid–siRNAs displayed 80–90% viability, whereas cells treated with wild-type anti-firefly luciferase siRNA displayed reduced viability in HeLa cells (67%) (Supplementary Figure S4). At lower concentrations, cell viability remained high even after siRNA treatment.

Carrier-free gene silencing of endogenous Bcl-2 mRNA

The gene-silencing activity of internally-modified anti-Bcl-2 siRNAs was first tested in HeLa cells after transfection with Lipofectamine 2000^{TM}. Both the propargyl and folic acid-modified siRNAs (aB-P and aB-F, respectively) displayed ~70% knockdown after 20 nM treatment, comparable to wild-type siRNA (aB-wt), whereas scramble controls displayed no activity (Supplementary Figure S3). The carrier-free transfection protocol for this assay is described in the Supplementary Data file. In a carrier-free environment, the internally-modified folic acid–siRNA, aB-F, displayed potent gene-silencing activity of endogenous Bcl-2. At the highest concentration tested, 1 μM, 70% knockdown was achieved (Figure 6).

DISCUSSION

Direct conjugation of folic acid to siRNAs has shown great success as a selective, self-delivering system to target cancer cells. Nevertheless, only 40–60% gene silencing has been achieved even after 1 μM siRNA treatment (34). Therefore, given the promise of using folic acid as a delivery vehicle

Downloaded from https://academic.oup.com/nar/article/48/1/75/5644999 by guest on 28 April 2021

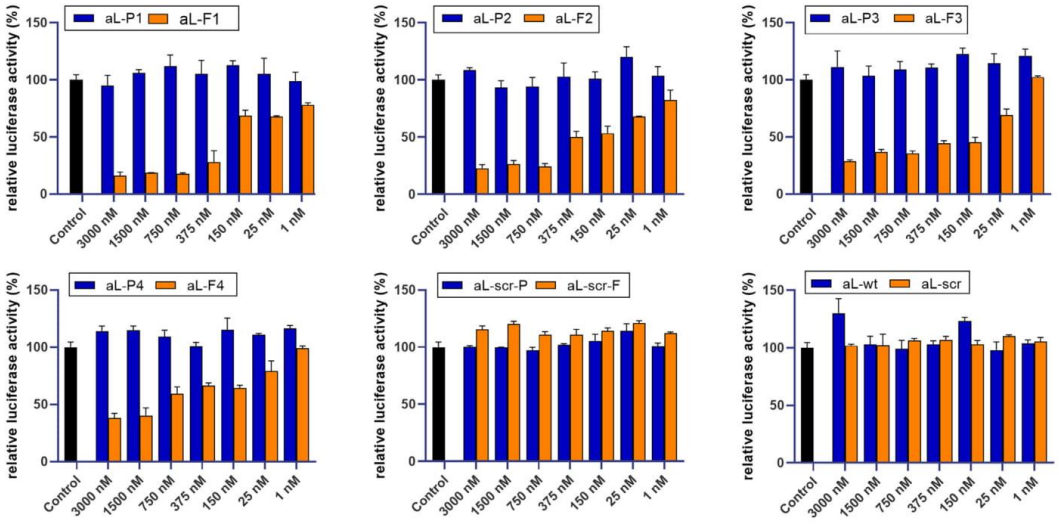

Figure 3. Relative expression of firefly luciferase in HeLa cells 16 h after anti-luciferase siRNA transfections at 1, 25, 150, 375, 750, 1500 and 3000 nM without the use of a transfection reagent. Firefly luciferase expression was assessed with a dual-luciferase reporter assay and was normalized to *Renilla* luciferase. Error bars indicate SD of at least two independent biological replicates.

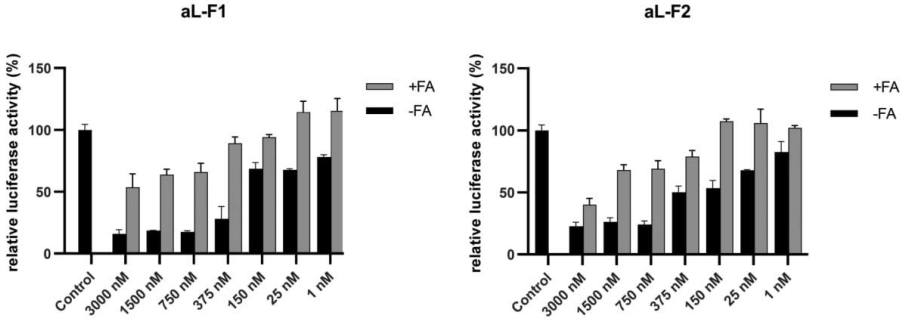

Figure 4. Relative expression of firefly luciferase in HeLa cells 16 h after carrier-free transfection of centrally-modified folic acid–siRNAs (aL-F1 and aL-F2). Cells were maintained in either folate-free RPMI 1640 (–FA) or folate-containing DMEM (+FA). Firefly luciferase expression was assessed with a dual-luciferase reporter assay and was normalized to Renilla luciferase. Error bars indicate SD of at least two independent biological replicates.

for siRNAs, there is room for improving its efficacy. Here we have investigated the gene-silencing activity of siRNAs bearing a triazole-linked folic acid modification at different positions within the sense strand, as previous work has only focused on the 3′ and 5′ ends. We have shown that placing the folic acid modification within the central region, spanning the Ago2 cleavage site of the sense strand, increased the gene-silencing activity of anti-luciferase and anti-Bcl-2 siRNAs.

We first assessed the biophysical properties of our synthesized siRNAs. Using CD spectroscopy, we confirmed that our siRNA duplexes adopted an A-form alpha helix conformation (Supplementary Figure S1). RISC recognizes the A-form major groove of the siRNA helix, so the ability of modified siRNAs to adopt an A-form helical structure is desirable for proper RNAi activity (40). We then assessed the thermal stability of each siRNA duplex, as the thermodynamic properties of siRNA have been shown to play a role in their silencing activity (41). Modifications placed at or close to the 3′ end did not cause significant thermal destabilization. This was expected, as this area has been shown to be fairly tolerant to chemical modifications (14). On the other hand, modifications spanning the central region of the sense strand caused significant thermal destabilization. Some studies suggest that destabilization in this region can lead to increase silencing activity (39,42) and previous work from our group has reported success using internally-modified siRNAs bearing a variety of chemically-modified spacer linkages (36,43). A crucial step for RNAi function is the dissociation of the sense strand, facilitated by Ago2

Downloaded from https://academic.oup.com/nar/article/48/1/75/5644999 by guest on 28 April 2021

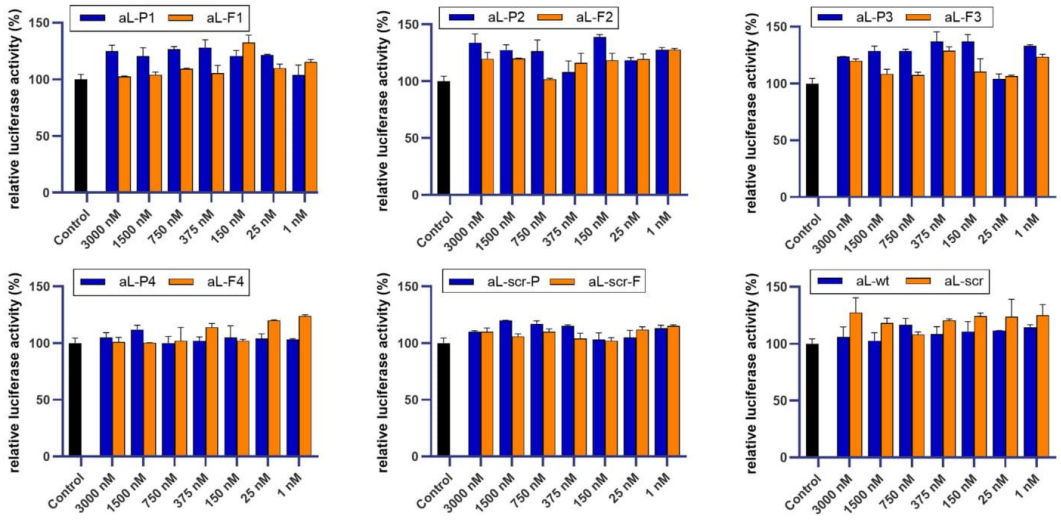

Figure 5. Relative expression of firefly luciferase in HT-29 cells 16 h after anti-luciferase siRNA transfections at 1, 25, 150, 375, 750, 1500 and 3000 nM without the use of a transfection reagent. Firefly luciferase expression was assessed with a dual-luciferase reporter assay and was normalized to *Renilla* luciferase. Error bars indicate SD of at least two independent biological replicates.

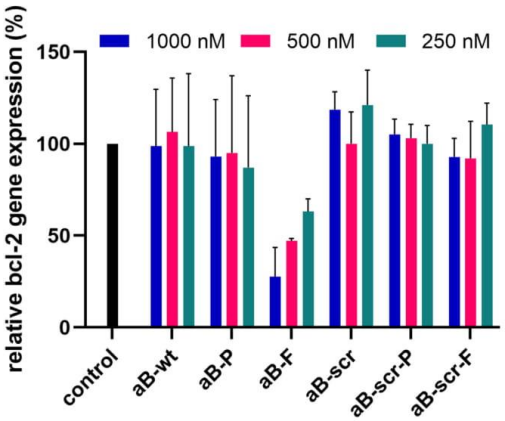

Figure 6. Normalized Bcl-2 gene expression in HeLa cells 24 h after carrier-free transfection with internally-modified anti-Bcl-2 and scramble siRNAs at 250, 500, 1000 nM concentrations. Data was normalized using the 18S gene as a reference gene. Error bars indicate SD of two independent biological replicates.

cleavage at the central region. It has been proposed that low thermal stability in this region could improve RNAi activity by facilitating passenger strand release (44). To investigate the gene-silencing potency of centrally-modified folic acid–siRNAs, we first targeted the exogenous gene firefly luciferase in two cell lines, HeLa and HT-29. HeLa cells are derived from human cervical cancer and HT-29 cells are derived from human colon cancer. We assessed the relative expression of FRs in HeLa and HT-29 cells using flow cytometry and found that HeLa cells displayed a 3-fold increase in FR expression compared to HT-29 (Figure 1). Although this is not a quantitative measure, a 3-fold increase in receptor expression can be biologically significant. Multiple examples are provided in Leamon's study (26), which quantitatively measured the expression of FR in various human cancer and normal tissues. High FR-positive tissues and cells, such as HeLa, express at least 6 pmol FR/mg protein whereas tissues or cells expressing no more than 2.5 pmol FR/mg protein are considered to have low FR expression, suggesting that a small difference in expression can lead to significantly different biological activity. Several literature reports indicate that HeLa cells express high levels of FR (45) whereas HT-29 cells express low levels of FR (46). Based on this, HeLa was chosen as the FR-positive cell line and HT-29 as the FR-negative cell line.

In HeLa cells, we show that internally-modified propargyl and folic acid–siRNAs displayed more potent gene-silencing activity than their 3′-modified counterparts after transfection with Lipofectamine 2000™ (Figure 2A). Even in the absence of a transfection reagent, internally-modified folic acid–siRNAs aL-F1 and aL-F2 still displayed enhanced gene-silencing potency and much lower IC_{50} values than aL-F3 (modified at position 5 from sense strand 3′ end) and aL-F4 (modified at the 3′ end). We only observed 40–65% knockdown after 0.75 μM treatment of aL-F3 and aL-F4. However, treatment with the centrally-modified folic acid siRNAs aL-F1 and aL-F2 at the same 0.75 μM concentration led to 80% knockdown (Figure 3), a significant improvement from literature reports. Although Low's study reported selective *in vivo* delivery of 5′-modified folic acid–siRNAs to tumours in mice bearing KB tumour xenografts,

Downloaded from https://academic.oup.com/nar/article/48/1/75/5644999 by guest on 28 April 2021

these siRNAs were trapped in intracellular endosomes after internalization and did not display efficient gene-silencing activity (35). Carell's study, on the other hand, achieved moderate gene-silencing activity with a 3′-modified folic-acid siRNA (34). This study targeted exogenous luciferase mRNA in HeLa cells and reported ∼50% gene-silencing activity after 1 μM siRNA treatment. One potential reason for this saturation could be due to off-target effects, namely, the strand selection process. If the 3′ folic acid-modified passenger strand is selected as the guide strand for the RISC complex, it is possible that reduced overall gene silencing may occur. The central region of the antisense strand has been shown to be less tolerant to chemical modifications (47). Therefore, by using the central region in the passenger strand for a folic acid modification, it is possible that enhanced efficacy could be attributed to loss of passenger strand uptake by the RISC complex.

To validate that the folic-acid siRNAs are being internalized via FRs, we performed a folic acid competition study. Following the same carrier-free protocol described earlier, we transfected the two centrally-modified folic acid–siRNAs (aL-F1 and aL-F2) into HeLa cells that were maintained in DMEM supplemented with folic acid (9 μM). FRs are found on the cell surface and are able to internalize folic acid and folic acid-conjugates via receptor-mediated endocytosis. When excess folic acid was present in the media, there was a significant decrease in siRNA gene-silencing activity compared to previously-described studies in folate-free media (Figure 4). After confirming the self-delivering properties of our anti-luciferase folic acid–siRNAs in HeLa cells, we investigated their selectivity for FR-expressing cell lines by testing them in FR-negative HT-29 cells. We first performed the transfection using Lipofectamine® LTX to ensure that the siRNAs were biologically active once inside the cell. We observed a similar pattern of gene-silencing activity as we did in HeLa cells, with internally-modified siRNAs displaying much higher potency than 3′-modified siRNAs (Figure 2B). In the absence of a transfection carrier, however, none of the tested siRNAs displayed activity, confirming their selectivity for FR-expressing cells (Figure 5). In both cell lines, siRNA treatment caused low to no cytotoxic effects (Supplementary Figure S4), even at the highest concentrations tested (3000 nM). Given the selectivity and potent gene-silencing activity of our internally-modified folic acid–siRNAs against the exogenous target firefly luciferase, we designed siRNAs targeting the endogenous gene Bcl-2. This oncogene is overexpressed in 50–70% of all human cancers and is a desirable target for siRNA therapeutics (48–50). The triazole-linked folic acid modification was incorporated at position 10 from the sense strand 5′ end of our anti-Bcl-2 siRNA (aB-F) and gene-silencing activity was assessed using real-time polymerase chain reaction (RT-PCR) in HeLa cells, which endogenously express *bcl-2*. This internally-modified folic acid–siRNA displayed potent gene-silencing activity even in the absence of a transfection reagent (Figure 6). Notably, we observed ∼72% knockdown of endogenous Bcl-2 after 1 μM siRNA treatment.

In summary, we report a straightforward and efficient post-column CuAAC synthetic strategy to prepare self-delivering folic acid–siRNAs that selectively target FR-expressing cells. Furthermore, we have developed an approach to enhance the gene-silencing potency of folic acid–siRNA constructs by modifying the central region of the siRNA sense strand and achieved improvement in siRNA activity compared to literature reports. Overall, our data show that siRNAs with internal folic acid modifications are able to effectively downregulate the expression of both exogenous and endogenous gene targets with minimal toxicity. Given that folate receptors are vastly overexpressed in a variety of cancers, our synthetic approach could be employed to achieve selective delivery of siRNAs to cancer cells without the use of transfection reagents or sophisticated carriers while maintaining potent RNAi activity. Next steps could involve examining our folic acid–siRNA conjugates in higher-level organisms that have folic receptor alpha positive tumors. Therefore, our work can open new avenues for the design and development of novel RNAi-based cancer therapeutics.

DATA AVAILABILITY

Data available in the supplementary material.

SUPPLEMENTARY DATA

Supplementary Data are available at NAR Online.

ACKNOWLEDGEMENTS

The authors thank Dr. Julia Green-Johnson for providing HT-29 cells and Michael Jeffrey for assistance in HT-29 cell culture as well as flow cytometry training.

FUNDING

Natural Sciences and Engineering Research Council of Canada (NSERC). Funding for open access charge: Natural Sciences and Engineering Research Council.
Conflict of interest statement. None declared.

REFERENCES

1. Hannon,G.J. (2002) RNA interference. *Nature*, **418**, 244–251.
2. Sharp,P.A. and Zamore,P.D. (2000) RNA interference. *Science*, **287**, 2431–2433.
3. Kobayashi,H. and Tomari,Y. (2016) RISC assembly: coordination between small RNAs and Argonaute proteins. *Biochim. Biophys. Acta*, **1859**, 71–82.
4. Wang,Y., Juranek,S., Li,H., Sheng,G., Wardle,G.S., Tuschl,T. and Patel1,D.J. (2010) Nucleation, propagation and cleavage of target RNAs in Ago silencing complexes. *Nature*, **461**, 754–761.
5. Leuschner,P.J.F., Ameres,S.L., Kueng,S. and Martinez,J. (2006) Cleavage of the siRNA passenger strand during RISC assembly in human cells. *EMBO Rep.*, **7**, 314–320.
6. Pratt,A.J. and MacRae,I.J. (2009) The RNA-induced silencing complex: a versatile gene-silencing machine. *J. Biol. Chem.*, **284**, 17897–17901.
7. Tang,G. (2005) siRNA and miRNA: an insight into RISCs. *Trends Biochem. Sci.*, **30**, 106–114.
8. Elbashir,S.M., Harborth,J., Lendeckel,W., Yalciz,A., Weber,K. and Tuschl,T. (2001) Duplexes of 21-nucleotide RNAs mediate RNA interference in cultured mammalian cells. *Nature*, **411**, 494–498.
9. Curtis,C.D. and Nardulli,A.M. (2014) Using RNA interference to study protein function. *Methods Mol. Biol.*, **505**, 187–204.

Downloaded from https://academic.oup.com/nar/article/48/1/75/5644999 by guest on 28 April 2021

10. Dana,H., Chalbatani,G.M., Mahmoodzadeh,H., Karimloo,R., Rezaiean,O., Moradzadeh,A., Mehmandoost,N., Moazzen,F., Mazraeh,A., Marmari,V. *et al.* (2017) Molecular mechanisms and biological functions of siRNA. *Int. J. Biomed. Sci.*, **13**, 48–57.
11. Aagaard,L. and Rossi,J.J. (2007) RNAi therapeutics: principles, prospects and challenges. *Adv. Drug. Deliv. Rev.*, **59**, 75–86.
12. Ryther,R., Flynt,A.S., Phillips,J.A. III and Patton,J. (2005) siRNA therapeutics: big potential from small RNAs. *Gene Ther.*, **12**, 5–11.
13. Wittrup,A. and Lieberman,J. (2015) Knocking down disease: a progress report on siRNA therapeutics. *Nat. Rev. Genet.*, **16**, 543–552.
14. Bramsen,J. and Kjems,J. (2012) Development of therapeutic-grade small interfering RNAs by chemical engineering. *Front. Genet.*, **3**, 1–22.
15. Haussecker,D. (2014) Current issues of RNAi therapeutics delivery and development. *J. Control. Release*, **195**, 49–54.
16. Haupenthal,J., Baehr,C., Kiermayer,S., Zeuzem,S. and Piiper,A. (2006) Inhibition of RNAse A family enzymes prevents degradation and loss of silencing activity of siRNAs in serum. *Biochem. Pharmacol.*, **71**, 702–710.
17. Shukla,S., Sumaria,C. and Pradeepkumar,P. (2010) Exploring chemical modifications for siRNA therapeutics: a structural and functional outlook. *ChemMedChem*, **5**, 328–349.
18. Braasch,D., Jensen,S., Liu,Y., Kaur,K., Arar,K., White,M. and Corey,D. (2003) RNA interference in mammalian cells by chemically-modified RNA. *Biochemistry*, **42**, 7967–7975.
19. Adams,D., Gonzalez-Duarte,A., O'Riordan,W.D., Yang,C.-C., Ueda,M., Kristen,A.V., Tournev,I., Schmidt,H.H., Coelho,T., Berk,J.L. *et al.* (2018) Patisiran, an RNAi therapeutic, for hereditary transthyretin amyloidosis. *N. Engl. J. Med.*, **379**, 11–21.
20. Wang,J., Lu,Z., Wientjes,M.G. and Au,J.L.-S. (2010) Delivery of siRNA therapeutics: barriers and carriers. *AAPS J.*, **12**, 492–503.
21. Meade,B.R. and Dowdy,S.F. (2009) The road to therapeutic RNA interference (RNAi): tackling the 800 pound siRNA delivery gorilla. *Discov. Med.* **8**, 253–256.
22. Nair,J.K., Willoughby,J.L.S., Chan,A., Charisse,K., Alam,R., Wang,Q., Hoekstra,M., Kandasamy,P., Kel'in,A.V., Milstein,S. *et al.* (2014) Multivalent N-acetylgalactosamine-conjugated sirna localizes in hepatocytes and elicits robust RNAi-mediated gene silencing. *J. Am. Chem. Soc.*, **136**, 16958–16961.
23. Liang,X., Fan,J., Zhao,Y., Cheng,M., Wang,X., Jin,R. and Sun,T. (2017) A targeted drug delivery system based on folic acid-functionalized upconversion luminescent nanoparticles. *J. Biomater. Appl.*, **31**, 1247–1256.
24. Moghimipoura,E., Rezaeic,M., Ramezania,Z., Kouchaka,M., Aminid,M., Angalie,K.A., Dorkooshf,F.A. and Handali,S. (2018) Folic acid-modified liposomal drug delivery strategy for tumor targeting of 5-fluorouracil. *Eur. J. Pharm. Sci.* **114**, 166–174.
25. Chen,C., Ke,J., Zhou,X.E., Yi,W., Brunzelle,J.S., Li,J., Yong,E.-L., Xu,H.E. and Melcher,K. (2013) Structural basis for molecular recognition of folic acid by folate receptors. *Nature*, **500**, 486–489.
26. Parker,N., Turk,M.J., Westrick,E., Lewis,J.D., Low,P.S. and Leamon,C.P. (2005) Folate receptor expression in carcinomas and normal tissues determined by a quantitative radioligand binding assay. *Anal. Biochem.*, **338**, 284–293.
27. Toffoli,G., Cernigoi,C., Russo,A., Gallo,A., Bagnoli,M. and Boiocchi,M. (1997) Overexpression of folate binding protein in ovarian cancers. *Int. J. Cancer*, **74**, 193–198.
28. Zwicke,G.L., Mansoori,G.A. and Jeffery,C.J. (2012) Utilizing the folate receptor for active targeting of cancer nanotherapeutics. *Nano Rev.*, **3**, 18496.
29. Babu,A., Muralidharan,R., Amreddy,N., Mehta,M., Munshi,A. and Ramesh,R. (2016) Nanoparticles for siRNA-based gene silencing in tumor therapy. *IEEE Trans. Nanobioscience*, **15**, 849–863.
30. Li,J.-M., Wang,Y.-Y., Zhang,W., Su,H., Ji,L.-N. and Mao,Z.-W. (2013) Low-weight polyethylenimine cross-linked 2-hydroxypopyl-β-cyclodextrin and folic acid as an efficient and nontoxic siRNA carrier for gene silencing and tumor inhibition by VEGF siRNA. *Int. J. Nanomed.*, **8**, 2101–2117.
31. Leng,Q., Woodle,M.C. and Mixson,A.J. (2017) Targeted delivery of siRNA therapeutics to malignant tumors. *J. Drug Deliv.*, **2017**, 1–22.
32. Yoshizawa,T., Hattori,Y., Hakoshima,M., Koga,K. and Maitani,Y. (2008) Folate-linked lipid-based nanoparticles for synthetic siRNA delivery in KB tumor xenografts. *Eur. J. Pharm. Biopharm.*, **70**, 718–725.
33. Zheng,B., Yang,S., Wang,M., Yang,X., Teng,L., Xie,J., Teng,L. and Lee,R.J. (2015) Non-covalent nanocomplexes of folic acid and reducible polyethylenimine for survivin siRNA delivery. *Anticancer Res.*, **35**, 5433–5441.
34. Willibald,J., Harder,J., Sparrer,K., Conzelmann,K.-K. and Carell,T. (2012) Click-modified anandamide siRNA enables delivery and gene silencing in neuronal and immune cells. *J. Am. Chem. Soc.*, **134**, 12330–12333.
35. Thomas,M., Kularatne,S.A., Qi,L., Kleindl,P., Leamon,C.P., Hansen,M.J. and Low,P.S. (2009) Ligand-targeted delivery of small interfering RNAs to malignant cells and tissues. *Ann. N. Y. Acad. Sci.*, **1175**, 32–39.
36. Desaulniers,J.-P., Hagen,G., Anderson,J., McKim,Chris and Roberts,B. (2017) Effective gene-silencing of siRNAs that contain functionalized spacer linkages within the central region. *RSC Adv.*, **7**, 3450–3454.
37. Salim,L., McKim,C. and Desaulniers,J.-P. (2018) Effective carrier-free gene-silencing activity of cholesterol-modified siRNAs. *RSC Adv.*, **8**, 22963–22966.
38. O'Toole,A.S., Miller,S. and Serra,M.J. (2005) Stability of 3′ double nucleotide overhangs that model the 3′ ends of siRNA. *RNA*, **11**, 512–516.
39. Addepalli,H., Meena, Peng,C.G., Wang,G., Fan,Y., Charisse,K., Rajeev,K.G., Pandey,R.K., Lavine,G. *et al.* (2010) Modulation of thermal stability can enhance the potency of siRNA. *Nucleic Acids Res.*, **38**, 7320–7331.
40. Hernández,A.R., Peterson,L.W. and Kool,E.T. (2013) Steric restrictions of RISC in RNA interference identified with size-expanded RNA nucleobases. *ACS Chem. Biol.* **7**, 1454–1461.
41. Kurreck,J. (2006) siRNA efficiency: structure or sequence—that is the question. *J. Biomed. Biotechnol.*, **2006**, 83757.
42. Petrova,N.S., Meschaninova,M.I., Venyaminova,A.G., Zenkova,M.A., Vlassov,V.V. and Chernolovskaya,E.L. (2011) Silencing activity of 2′-O-methyl modified anti-MDR1 siRNAs with mismatches in the central part of the duplexes. *FEBS Lett.*, **585**, 2352–2356.
43. Efthymiou,T.C., Peel,B., Huynh,V. and Desaulniers,J.-P. (2012) Evaluation of siRNAs that contain internal variable-length spacer linkages. *Bioorg. Med. Chem. Lett.*, **22**, 5590–5594.
44. Khvorova,A., Reynolds,A. and Jayasena,S.D. (2003) Functional siRNAs and miRNAs exhibit strand bias. *Cell*, **115**, 209–216.
45. Siwowska,K., Schmid,R.M., Cohrs,S., Schibli,R. and Müller,C. (2017) Folate receptor-positive gynecological cancer cells: in vitro and in vivo characterization. *Pharmaceuticals*, **10**, E72.
46. Yin,J.-J., Sharma,S., Shumyak,S.P., Wang,Z.-X., Zhou,Z.-W., Zhang,Y., Guo,P., Li,C.-Z., Kanwar,J.R., Yang,T. *et al.* (2013) Synthesis and biological evaluation of novel folic acid receptor-targeted, β-Cyclodextrin-based drug complexes for cancer treatment. *PLoS One*, **8**, e62289.
47. Chernikov,I.V., Vlassov,V.V. and Chernolovskaya,E.L. (2019) Current development of siRNA bioconjugates: from research to the clinic. *Front. Pharmacol.*, **10**, 444.
48. Akar,U., Chaves-Reyez,A., Barria,M., Tari,A., Sanguino,A., Kondo,Y., Kondo,S., Arun,B., Lopez-Berestein,G. and Ozpolat,B. (2008) Silencing of Bcl-2 expression by small interfering RNA induces autophagic cell death in MCF-7 breast cancer cells. *Autophagy*, **4**, 669–679.
49. Feng,L.-F., Zhong,M., Lei,X.-Y., Zhu,B.-Y., Tang,S. and Liao,D.-F. (2006) Bcl-2 siRNA induced apoptosis and increased sensitivity to 5-fluorouracil and HCPT in HepG2 cells. *J. Drug Target.*, **14**, 21–26.
50. Tekedereli,I., Alpay,S.N., Akar,U., Yuca,E., Ayugo-Rodriguez,C., Han,H.-D., Sood,A.K., Lopez-Berestein,G. and Ozpolat,B. (2013) Therapeutic silencing of Bcl-2 by systemically administered siRNA nanotherapeutics inhibits tumor growth by autophagy and apoptosis and enhances the efficacy of chemotherapy in orthotopic xenograft models of ER (−) and ER (+) breast cancer. *Mol. Ther. Nucleic Acids*, **2**, e121.

Downloaded from https://academic.oup.com/nar/article/48/1/75/5644999 by guest on 28 April 2021

Supplementary Data

Targeted delivery and enhanced gene-silencing activity of centrally modified folic acid-siRNA conjugates

Lidya Salim, Golam Islam and Jean-Paul Desaulniers

Faculty of Science, University of Ontario Institute of Technology, Oshawa, ON L1G 0C5

Table of Contents

General methodology and materials

Unless otherwise indicated, all starting reagents and solvents were obtained from commercial sources and used without further purification. Anhydrous CH_2Cl_2 and Et_3N were purchased from Sigma-Aldrich and kept dry using a PureSolv 400 Solvent Purification System. Standard flash chromatography was performed using Silicycle Siliaflash 60 (230-400 mesh) while automated flash chromatography was performed on a Biotage® Isolera flash chromatography system using a 100 g Biotage® SNAP KP-Sil cartridge. ^1H, ^{13}C and ^{31}P NMRs were recorded in $CDCl_3$ or DMSO-d_6 using a Bruker Ascend (600 MHz) NMR spectrometer. NMR spectra were processed with ACD/NMR Processor. High-performance liquid chromatography (HPLC) was performed on a Waters 1525 binary HPLC pump with a Waters 2489 UV/Vis detector, using a C18 4.6 mm x 150 mm reverse-phase column and eluting from 5 to 100% acetonitrile in a triethylamine-acetic acid (TEAA) buffer (pH 7.00) over 30 minutes. ESI-HRSM were recorded on an Agilent Q-TOF and analysed through positive electrospray ionization using a mobile phase of acetonitrile/MeOH (95:5) with 0.1% formic acid.

Procedure for anti-luciferase siRNA transfection with Lipofectamine

HeLa cells were seeded into 24-well plates, containing 400 µL DMEM (10% FBS), at a density of 5.0×10^4 cells per well. Plates were incubated for 24 hours at 37°C in a humidified atmosphere with 5% CO_2. For each transfection sample, a mixture of 1 µL of Lipofectamine 2000™ (Invitrogen) and 49 µL of Gibco's 1X Opti-Mem Reduced Serum Medium was prepared and incubated at room temperature for 5 minutes. Each siRNA was diluted in 1X Gibco's Opti-MEM Reduced Serum Medium (Invitrogen) on ice and mixed with 200 ng pGL3 and 50 ng pRLSV40 plasmids to a total volume of 50 µL. The diluted siRNA/plasmid mixture was combined with the diluted Lipofectamine 2000™ mixture and incubated at room temperature. After 20 minutes, the complexes were transferred to the respective wells and the plates were gently rocked back and forth for a few minutes. Plates were incubated for an additional 24 hours at 37°C in a humidified atmosphere with 5% CO_2.

HT-29 cells were seeded into 24-well plates, containing 350 µL RPMI 1640 (10% FBS), at a density of 1.5×10^5 cells per well (for a total volume of 500 µL). Plates were incubated for 24 hours at 37°C in a humidified atmosphere with 5% CO_2 after which the medium was removed from each well and replaced with 400 µL fresh medium. Each siRNA was diluted in 1X Gibco's Opti-MEM Reduced Serum Medium (Invitrogen) and mixed with 600 ng pGL3 and 150 ng pRLSV40 plasmids to a total volume of 100 µL. To each tube containing the siRNA/plasmid mixture, 4 µL Lipofectamine® LTX (ThermoFisher) was added. After a 30-minute incubation at room temperature, complexes were transferred to the respective wells and the plates were gently rocked back and forth for a few minutes. Plates were incubated for an additional 24 hours at 37°C in a humidified atmosphere with 5% CO_2.

Procedure for anti-Bcl-2 siRNA transfection with Lipofectamine

HeLa cells were seeded into 24-well plates, containing 400 µL DMEM (10% FBS), at a density of 4.0×10^4 cells per well. Plates were incubated for 24 hours at 37°C in a humidified atmosphere with 5% CO_2. For

each transfection sample, a mixture of 1 µL of Lipofectamine 2000™ (Invitrogen) and 49 µL of Gibco's 1X Opti-Mem Reduced Serum Medium was prepared and incubated at room temperature for 5 minutes. Each siRNA was diluted in 1X Gibco's Opti-MEM Reduced Serum Medium (Invitrogen) on ice. Diluted siRNAs were combined with the diluted Lipofectamine 2000™ mixture and incubated at room temperature for 20 minutes. Complexes were then transferred to the respective wells and the plates were gently rocked back and forth for a few minutes. Plates were incubated for an additional 24 hours at 37°C in a humidified atmosphere with 5% CO_2.

Procedure for carrier-free anti-Bcl-2 siRNA transfection

HeLa cells were seeded into 96-well plates, containing 50 µL folate-free RPMI 1640 (10% FBS), at a density of $2.0x10^4$ cells per well. Plates were incubated for 24 hours at 37°C in a humidified atmosphere with 5% CO_2. Each siRNA was diluted in 50 µL 1X Gibco's Opti-MEM Reduced Serum Medium (Invitrogen) on ice and the diluted samples were immediately transferred to the respective wells of the 96-well plate. Plates were incubated for an additional 24 hours at 37°C in a humidified atmosphere with 5% CO_2.

Procedure for RNA extraction and cDNA synthesis

HeLa cells were transfected with anti-Bcl-2 siRNAs as described. RNA extraction, cDNA production and RT-qPCR. Prior to the RNA extraction, each well of the 24-well plate washed twice with 1X PBS. Total RNA was extracted from the Hela cells using the manufacturer's instructions of the Total RNA Purification Plus Kit (Cat#: 48400. Norgen BioTek Corp, Thorold, ON, Canada). In addition, an on-column DNA digestion was performed using RNase Free DNase I Kit (Cat#:25710. Norgen BioTek Corp, Thorold, ON, Canada). Two microliter of each extracted RNA sample was used to measure the concentration and RNA integrity (A260/280) on the BioDrop Duo Plus (UK), and the presence of the RNA was confirmed by gel electrophoresis on a 1% (w vol-1) agarose.

The RT reaction was performed using the IScript cDNA synthesis kit (Cat #: 1708891. Bio-Rad, Hercules, California) in a total reaction volume of 20µL. The reaction mixture contained 400 ng of total RNA, M-MLV reverse transcriptase, oligo (DT) and random primers. Two negative controls were performed with all reactions. The first control contained the RNA template and all DNAse/RT reagents, except for the final addition of the RT enzyme. A second control contained no template (water only) to ensure that all reagents were free from possible contaminants. RT reactions were placed in 200 µL PCR tubes and incubated within a BIORAD T100 Thermal Cycler for 5 min at 25°C followed by 20 min at 46°C, 1 min at 95°C and then held at 4°C. Once cDNA was produced, the products could be amplified (RT-qPCR).

Real-time PCR was performed in a total reaction volume of 20 µL containing 10 uL SsoFast EverGreen Supermix (Bio-Rad, Hercules, California) containing Sso 7-d Fusion Polymerase, 0.5 µM forward primer and reverse primer and 2 µL cDNA template. In the final reaction, cDNA was diluted 40x to produce the best results. Pre-designed primers BCL-2F 5'-CTG GTG GGA GCT TGC ATC AC-3' and BCL-2R-5'-ACA

GCC TGC AGC TTT GTT TC-3' were purchased to target the Bcl-2 gene and yielding a 247-bp amplicon and 18S-F 5'-CGG CTA CCA CAT CCA AGG AAG-3' and 18S-R 5'-CGC TCC CAA GAT CCA ACT ACT-3' (Integrated DNA Technologies Inc, San Diego, California) were used to target the 18s gene in Hela cells and yielding a 247-bp amplicon. Reactions were incubated in the Bio-Rad CFX 96 Real-Time Detection System using the following cycle conditions: 50°C for 10 minutes, 95°C for 10 minutes, followed by 40 cycles at 95°C for 15 seconds and 60°C for 1 minute. Reaction specificity was assessed by melting curve analysis immediately after the qPCR experiment. The efficiency of each primer set for RT-qPCR was determined to be between 95 and 100% using the standard curve method. NRT controls were performed during standard curve analysis to confirm that amplification of the PCR product was cDNA and not genomic DNA. NTC controls were also performed to ensure that amplification of the PCR product was not a result of primer- dimers. Results were analyzed using the Bio-Rad CFX manager 3.1 software where the Bcl-2 expression data was normalized against 18s gene as the reference and expression profiles were generated using the comparative Delta-CT method of analysis. The repeatability of the RT-qPCR was assessed by measuring the imprecision of the standard deviations of Cq values compiled from two biological replicates for each treatment and three technical replicates having the same input RNA.

Figures and Tables

Table S1. Oligonucleotide sequences and mass spectrometry data

RNA	Duplex	Mass (predicted)	Mass (recorded)
aL-P1 (S)	5' CUUACGCUPAGUACUUCGAtt 3'	6562.9	6562.9
aL-F1 (S)	5' CUUACGCUFAGUACUUCGAtt 3'	7072.4	7072.2
aL-P2 (S)	5' CUUACGCUPGUACUUCGAtt 3'	6217.7	6216.9
aL-F2 (S)	5' CUUACGCUFGUACUUCGAtt 3'	6727.2	6729.1
aL-P3 (S)	5' CUUACGCUGAGUACUPGAtt 3'	6280.8	6280.1
aL-F3 (S)	5' CUUACGCUGAGUACUFGAtt 3'	6790.3	6789.1
aL-P4 (S)	5' CUUACGCUGAGUACUUCGAP 3'	6283.8	6283.0
aL-F4 (S)	5' CUUACGCUGAGUACUUCGAF 3'	6793.2	6793.1
aL-scr (S)	5' GGUAUCCCUCGUGAAUCAUtt 3'	6687.0	6686.8
aL-scr (AS)	5' AUGAUUCACGAGGGAUACCtt 3'	6693.1	6692.9
aL-scr-P (S)	5' GGUAUCCCPGUGAAUCAUtt 3'	6586.0	6584.9
aL-scr-F (S)	5' GGUAUCCCFGUGAAUCAUtt 3'	7095.5	7095.6
aB-P (S)	5' GCCUUCUUUPAGUUCGGUGtt 3'	6556.9	6556.8
aB-F (S)	5' GCCUUCUUUFAGUUCGGUGtt 3'	7096.4	7096.6
aB-scr (S)	5' GGUGUACGUCGUCUGUUCUtt 3'	6696.9	6697.1
aB-scr-P (S)	5' GGUGUACGPGUCUGUUCUtt 3'	6290.7	6290.9
aB-scr-F (S)	5' GGUGUACGFGUCUGUUCUtt 3'	6800.2	6801.3

(S) corresponds to the sense strand; (AS) corresponds to the antisense strand. **P** corresponds to the propargyl spacer. **F** represents the folic acid spacer. The Ago2 cleavage site is underlined.

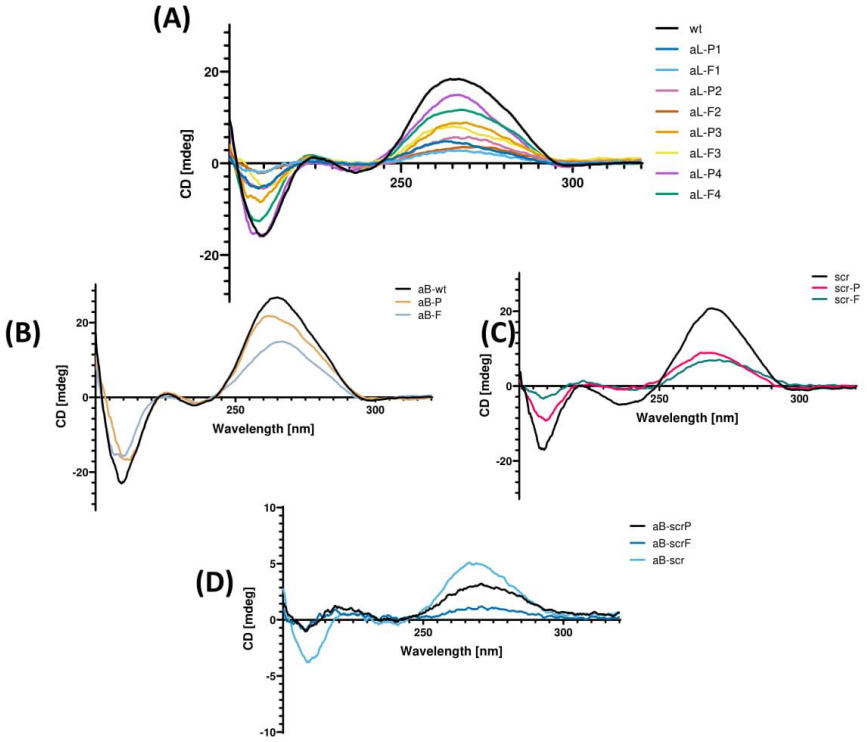

Figure S1. CD spectra of (A) anti-firefly luciferase siRNAs, (B) anti-luciferase scramble controls, (C) anti-Bcl-2 siRNAs and (D) anti-Bcl-2 scramble controls.

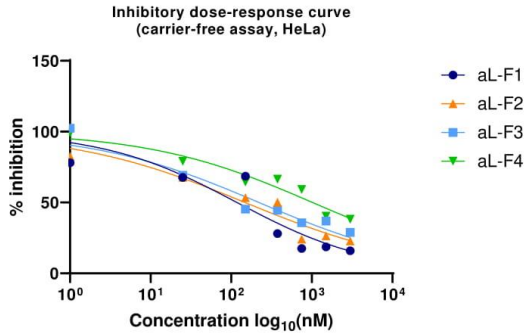

Figure S2. Inhibitory dose-response curves for folic acid-conjugated siRNAs targeting exogenous firefly luciferase in HeLa cells following a carrier-free transfection protocol.

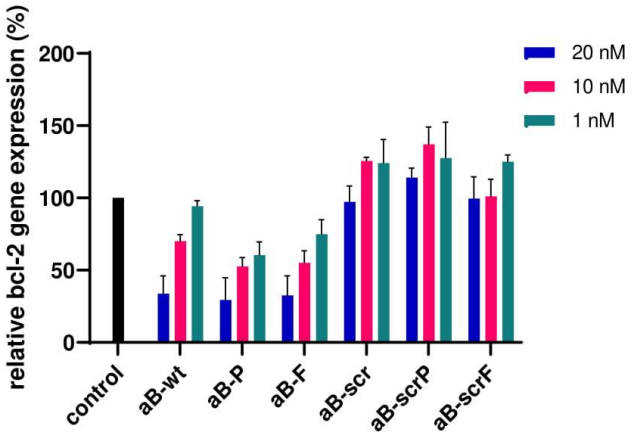

Figure S3. Normalized Bcl-2 gene expression in HeLa cells 24 hours after transfection with internally-modified propargyl-siRNA (aB-P), folic acid-siRNA (aB-F), wild-type siRNA (aB-wt) or scramble controls (aB-scr-P and aB-scr-F). siRNAs were tested at 1, 10, and 20 nM concentrations and were transfected using Lipofectamine 2000™. Data was normalized using the 18s gene as a reference gene. Error bars indicate SD of two independent biological replicates.

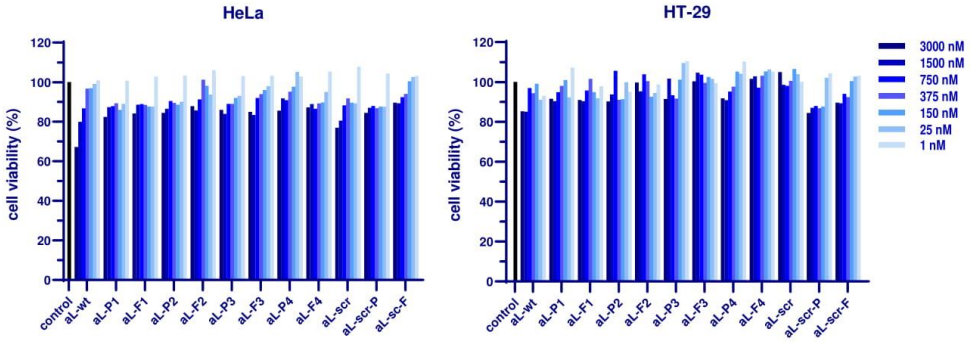

Figure S4. Relative viability of HeLa and HT-29 cells after treatment with anti-luciferase siRNAs (1, 25, 75, 150, 375, 750, 1500 and 3000 nM).

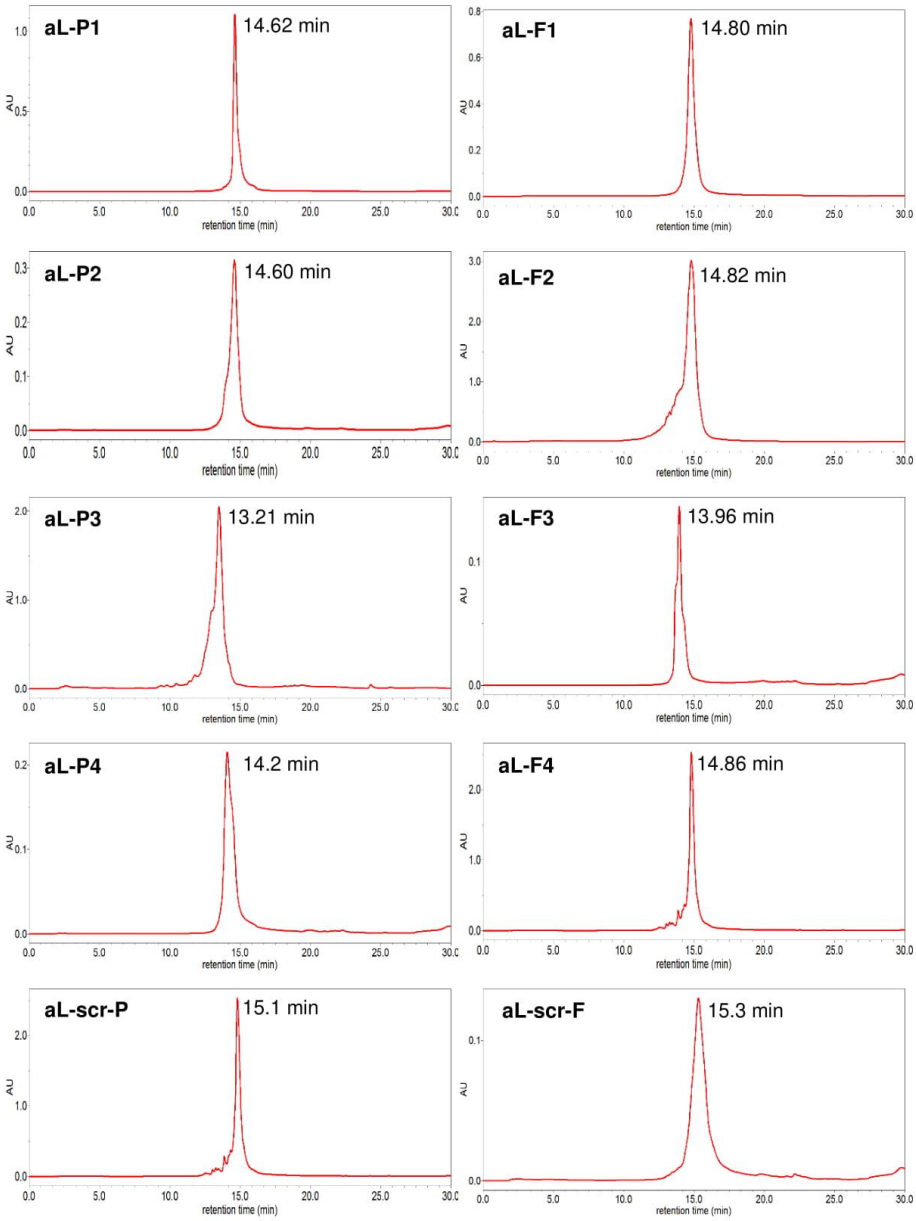
aL-P1
14.62 min
aL-F1
14.80 min
aL-P2
14.60 min
aL-F2
14.82 min
aL-P3
13.21 min
aL-F3
13.96 min
aL-P4
14.2 min
aL-F4
14.86 min
aL-scr-P
15.1 min
aL-scr-F
15.3 min
AU
retention time (min)

8

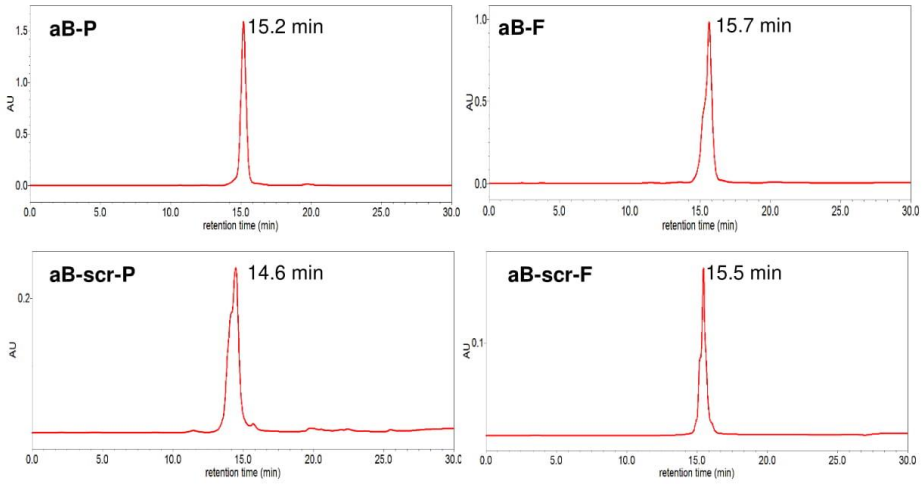

Figure S5. Analytical HPLC spectra of propargyl and folic acid siRNAs. Corresponding sequences can be found in table S1.

NMR spectra

^{1}H NMR spectrum of compound **1**

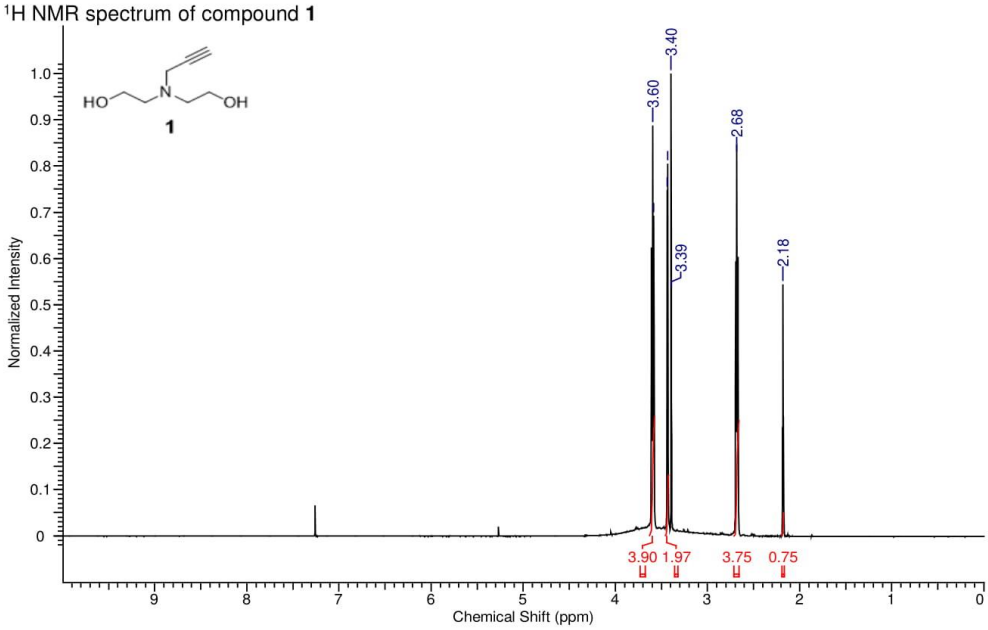

^{13}C NMR spectrum of compound **1**

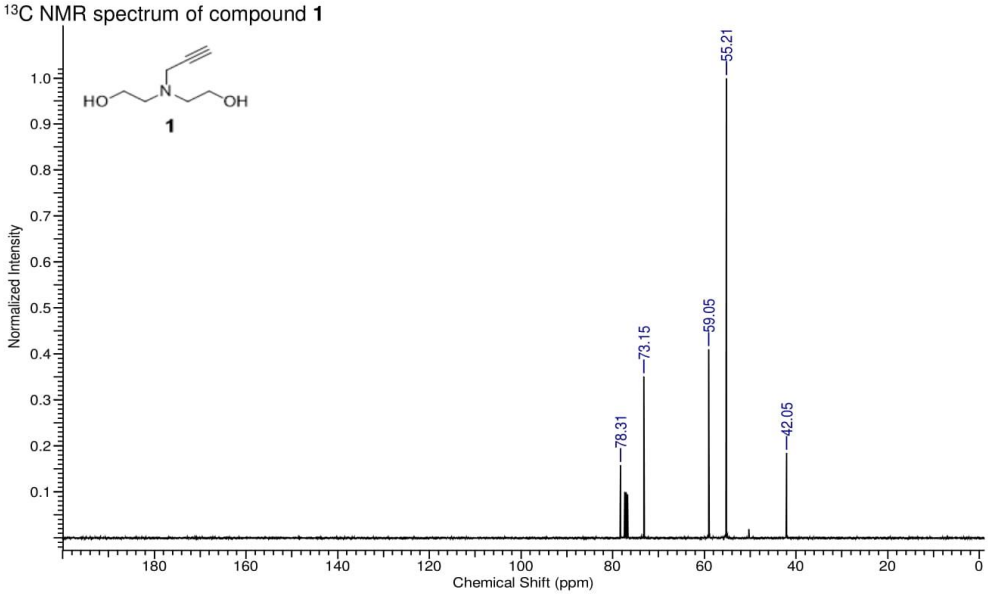

^{1}H NMR spectrum of compound **2**

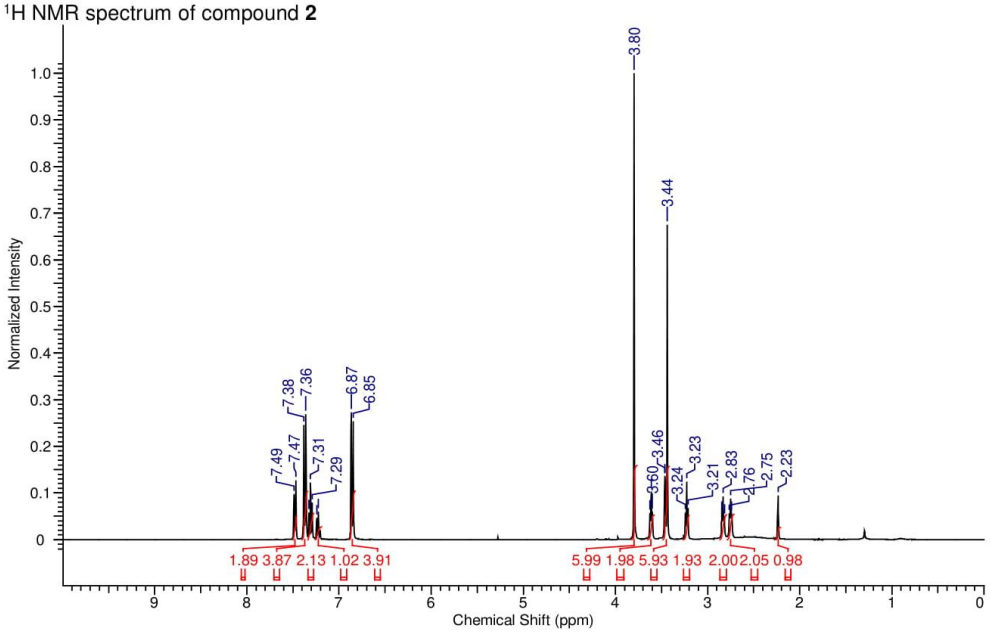

^{13}C NMR spectrum of compound **2**

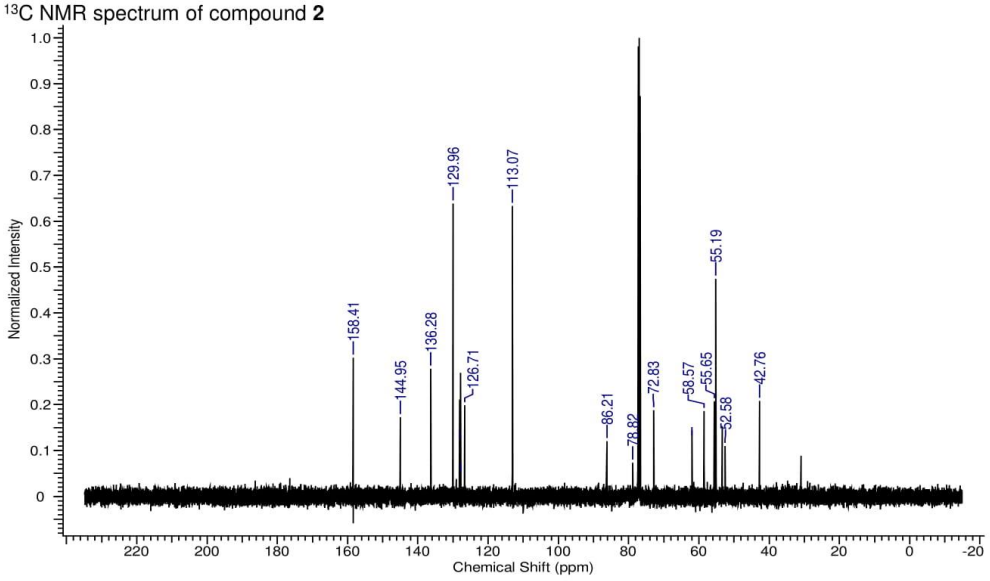

11

^{1}H NMR spectrum of compound **3**

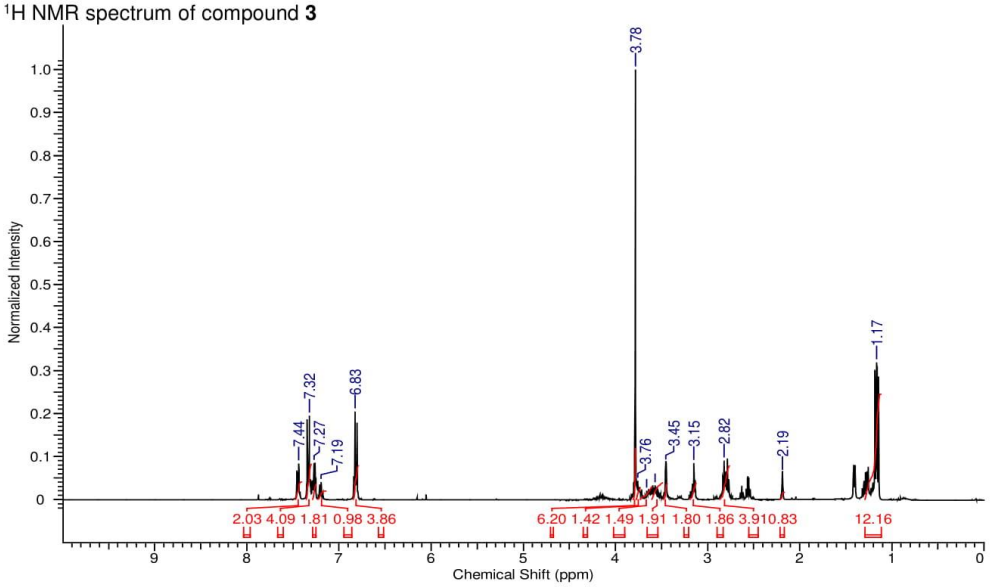

^{13}C NMR spectrum of compound **3**

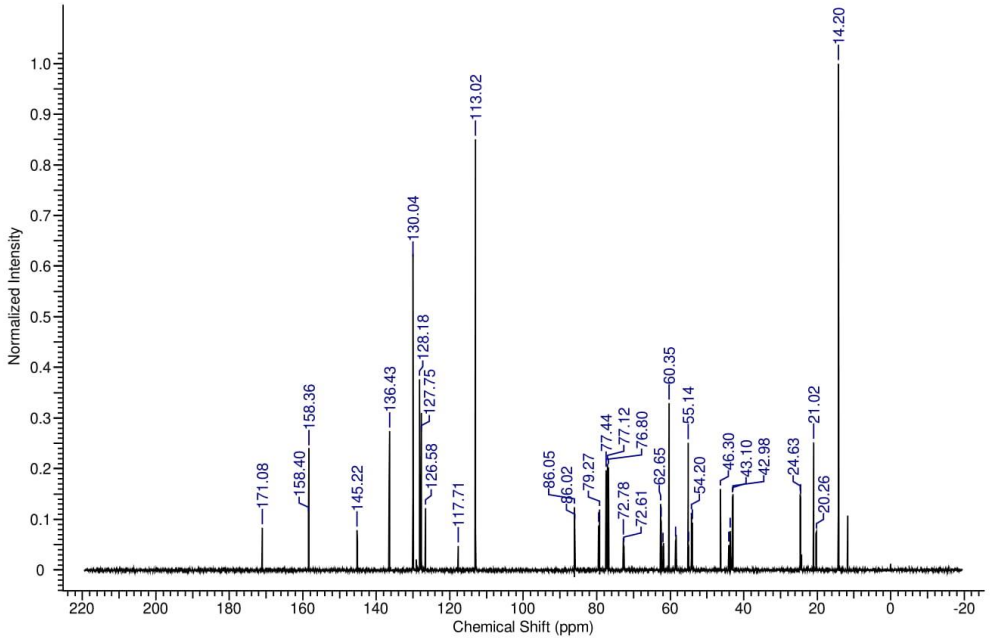

12

^{31}P NMR spectrum of compound **3**

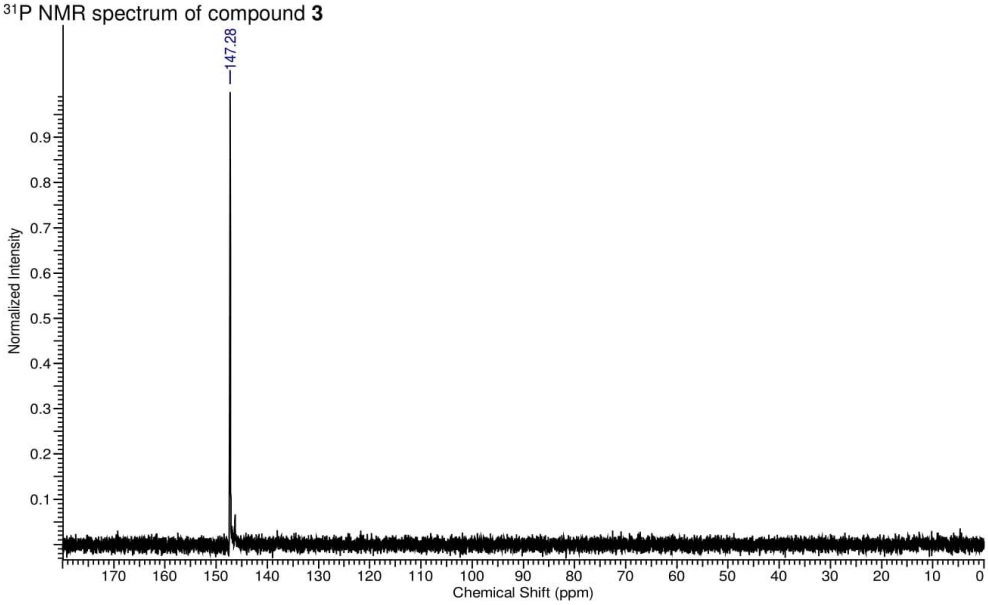

^{1}H NMR spectrum of compound **4**

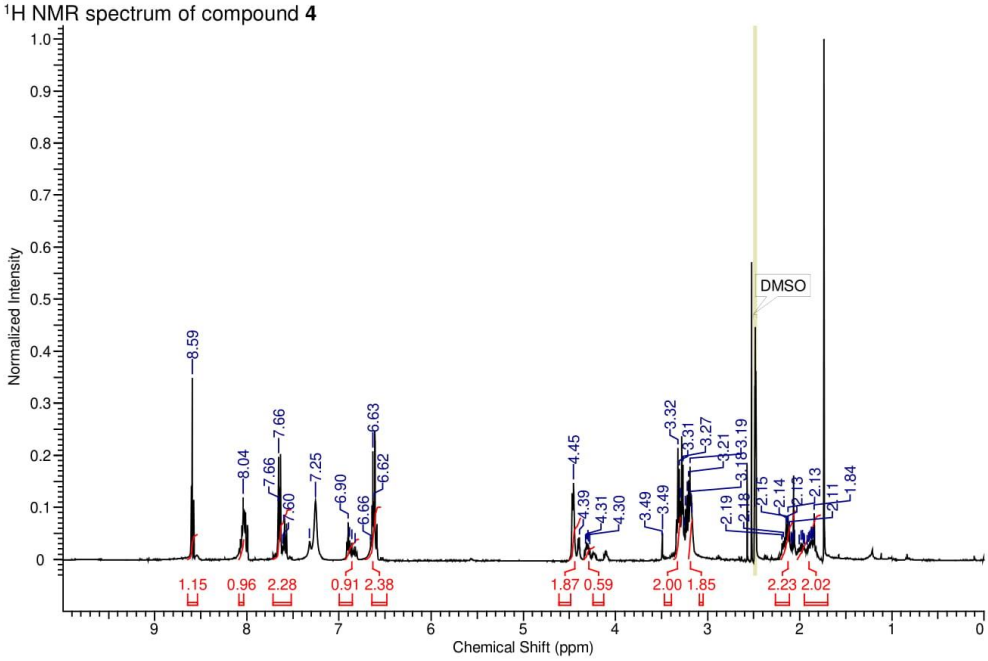

13

Appendix C. Supplementary Data for Chapter 4

Chapter 4: NMR data

^{1}H NMR of Compound **C**

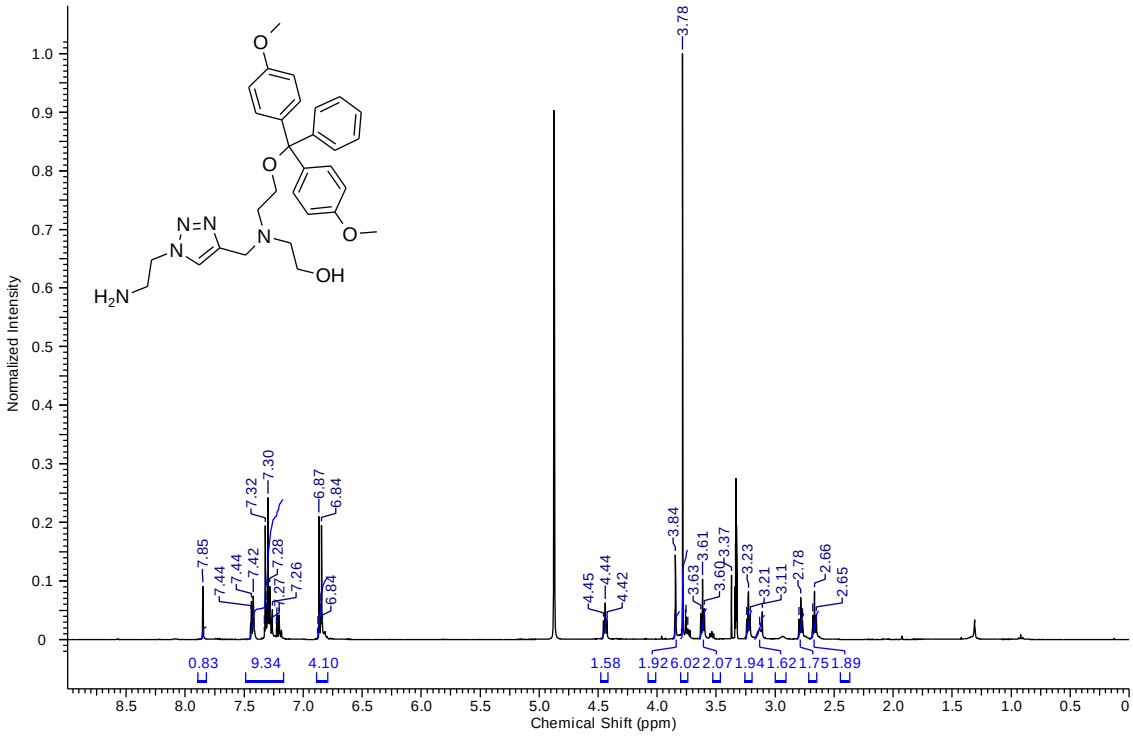

^{13}C NMR of Compound **C**

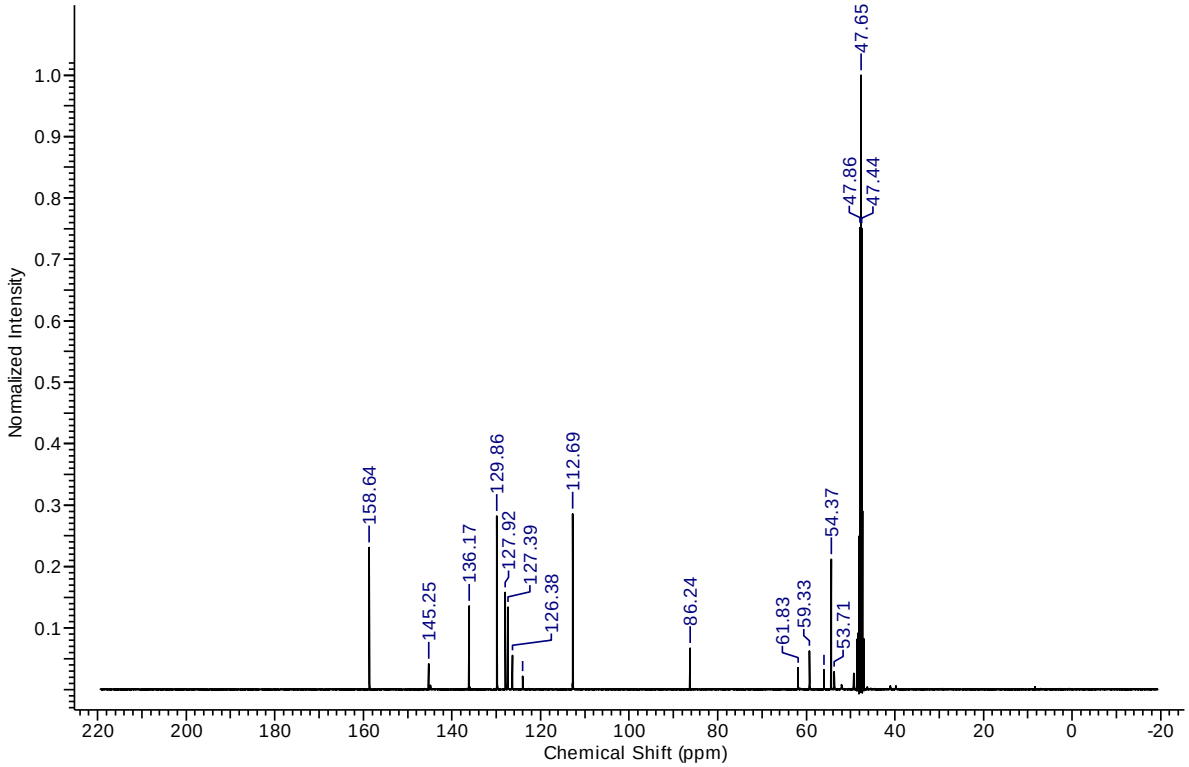

^{1}H NMR of Compound **1**

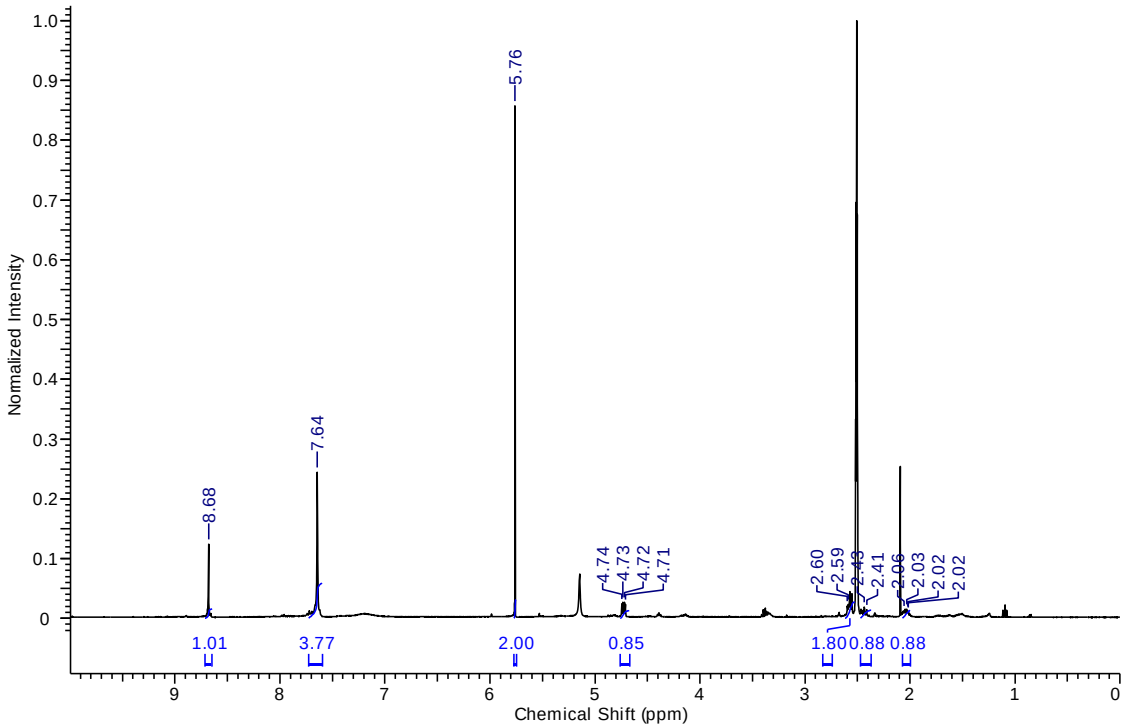

^{19}F NMR of Compound **1**

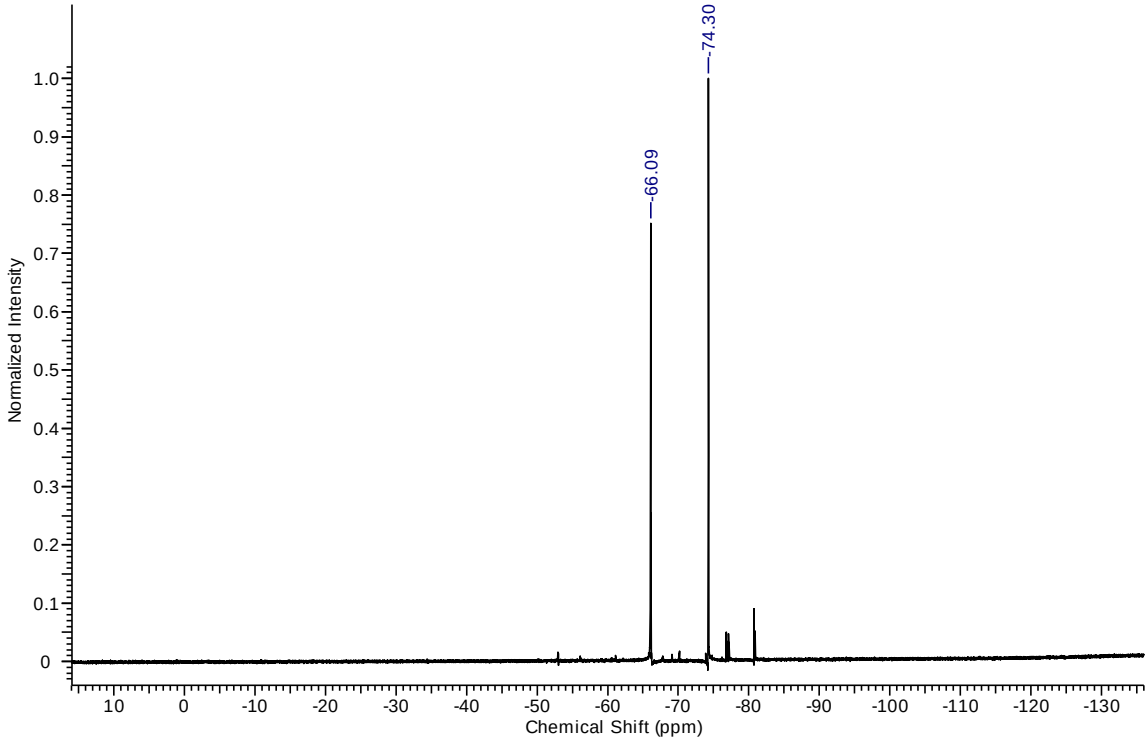

^{19}F NMR of Compound **2**

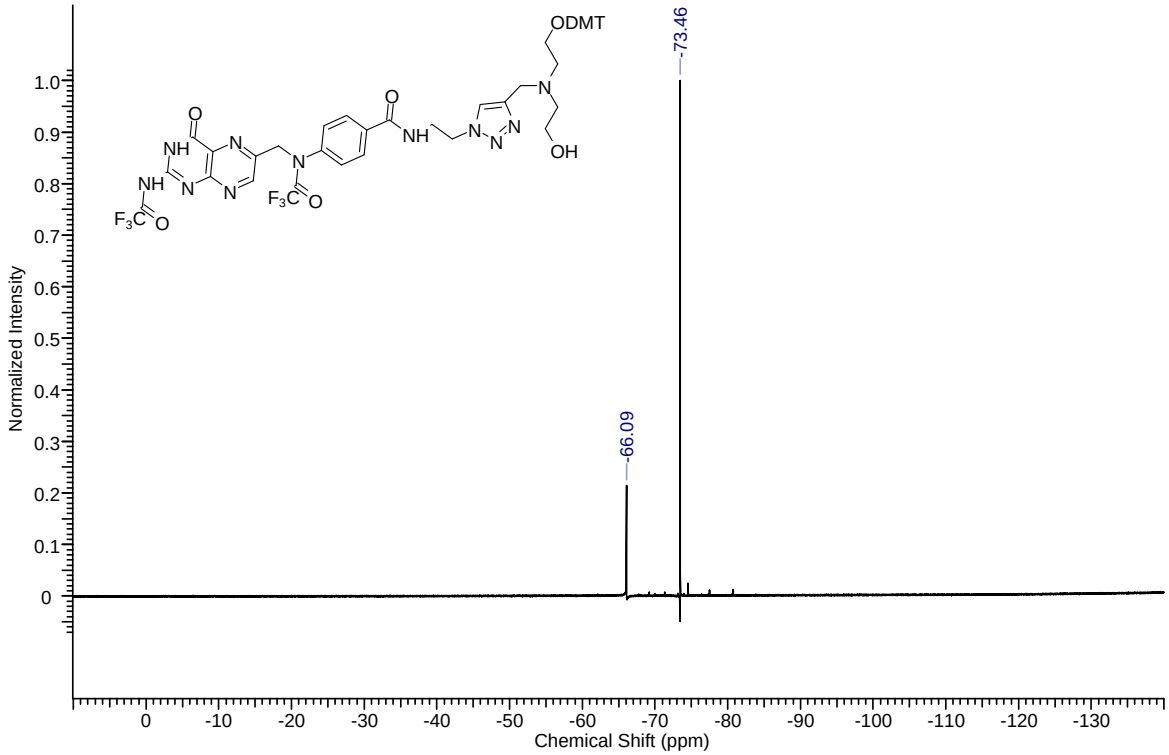

^{19}F NMR of Compound **3**

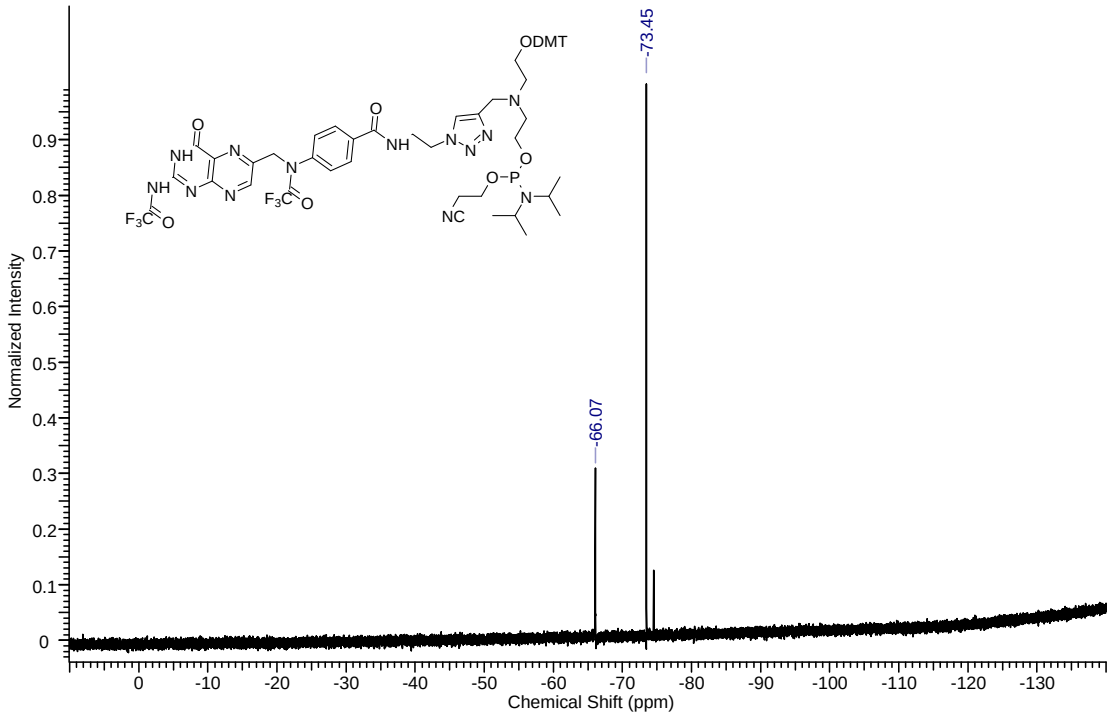

^{31}P NMR of Compound **3**

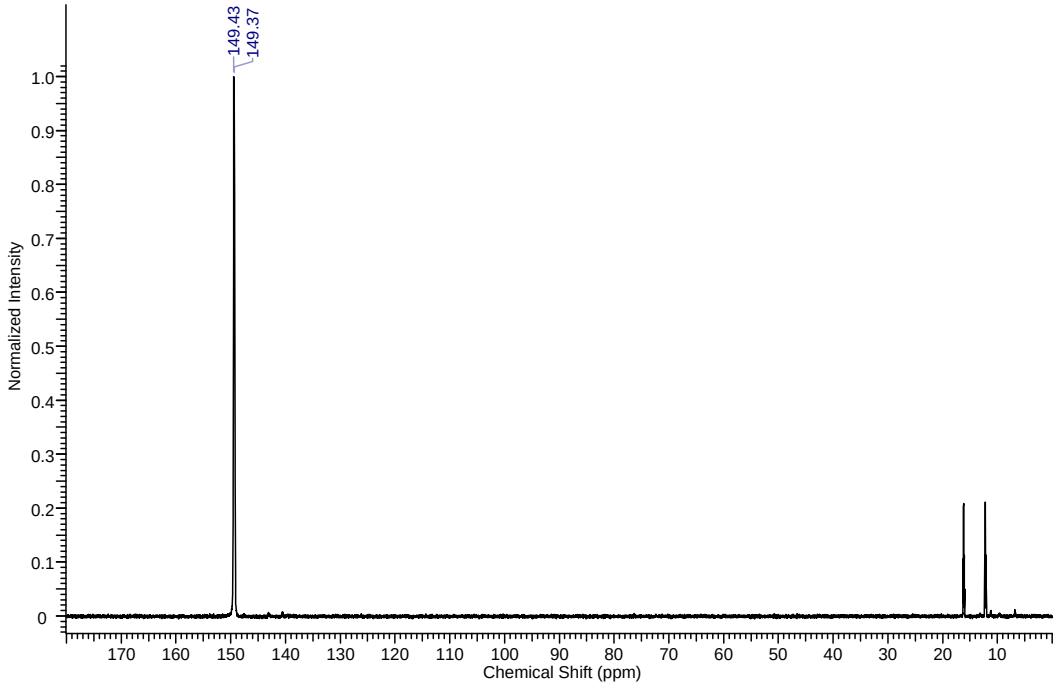

Appendix D. Manuscript III and Supplementary Data

RSC Advances

ROYAL SOCIETY OF CHEMISTRY

PAPER

View Article Online
View Journal | View Issue

Open Access Article. Published on 01 March 2021. Downloaded on 4/28/2021 9:03:51 AM.
This article is licensed under a Creative Commons Attribution 3.0 Unported Licence.

Check for updates

Cite this: *RSC Adv.*, 2021, **11**, 9285

Synthesis and evaluation of modified siRNA molecules containing a novel glucose derivative†

Lidya Salim,[a] Eva Goss[b] and Jean-Paul Desaulniers *[a]

Received 3rd February 2021
Accepted 24th February 2021

DOI: 10.1039/d1ra00922b

rsc.li/rsc-advances

Chemical modifications are critical for the development of safe and effective siRNAs for downstream applications. In this study, we report the synthesis of a novel glucose phosphoramidite, a triazole-linked to uracil at position one, for incorporation into oligonucleotides. Biological testing revealed that the glucose derivative at key positions within the sense or antisense strand can lead to potent gene-silencing activity, thus highlighting its tolerance in both sense and antisense positions. Furthermore, the A-form helical formation was maintained with this modification. Overall, placing the modification at the 3′ end and at key internal positions led to effective RNAi gene-silencing activity.

Introduction

RNA interference (RNAi) is a natural mechanism that mediates sequence-specific gene silencing by targeting messenger RNA and suppressing translation.[1] This pathway involves the assembly of an RNA-induced silencing complex (RISC) which incorporates double-stranded RNA sequences called short interfering RNAs (siRNAs).[2] Each siRNA duplex is ~21 nucleotides in length and is made up of a guide (antisense) strand and a passenger (sense) strand. After the siRNA duplex is unwound by RISC, the passenger strand is removed by the endonuclease Argonaute2 (Ago2), while the guide strand is retained and used as a guide sequence to locate and cleave the mRNA target.[3] Synthetic siRNAs are compatible with the endogenous RNAi pathway and are able to reduce the expression of target proteins, serving not only as experimental tools but also as gene-silencing therapeutics. Despite recent advances in the field, such as the U.S. FDA approval of three RNAi-based therapies,[4,5] the development of safe and effective siRNA therapeutics has been limited by the inherent structure of RNA which poses challenges like low stability, poor cellular uptake, and off-target effects.[6,7]

Chemical modifications can be used to optimize the pharmacokinetic properties of siRNAs for *in vivo* applications. Several modifications have been developed to date, including backbone, nucleobase, and sugar modifications, which can be incorporated individually or in combination.[8–10] Nevertheless, there is still no universal modification that mitigates all the aforementioned challenges, so there is great interest in designing and investigating novel modifications that could be incorporated in for future siRNA design.

Modifications of the ribose sugar have been extensively studied to improve stability and siRNA potency. The presence of the 2′ hydroxyl group makes RNA more susceptible to hydrolysis and is often modified, as it is not required for RNAi activity.[11] Common 2′ modifications include 2′-fluoro and 2′-methoxy, which increase siRNA stability.[12] Other modifications include bicyclic derivatives like locked nucleic acids (LNA), which lock the ribose sugar in the C'_3-*endo* conformation,[13] and acyclic derivatives like unlocked nucleic acids (UNA), which lack the $C'_2 - C'_3$-bond of the ribose sugar.[14]

A more recent approach involves replacing the ribose sugar with six-carbon moieties. Altritol nucleic acids have displayed stronger activity than unmodified siRNAs, particularly when placed at the 3′ end of the sense or antisense strand.[15] Cyclohexenyl and hexitol nucleic acids have also shown increased activity as well as nuclease stability.[16,17] Herein, we explore the synthesis of a novel glucose phosphoramidite derivative, which is a triazole-linked to a uracil nucleobase at position one. This modification was introduced at either terminal or internal positions of the sense or antisense strand, resulting in siRNA duplexes containing a single 3′-6′/2′-5′ phosphodiester linkage.

Experimental

Chemicals and general methods

β-D-Glucopyranosyl azide was obtained from Synthose, Inc. Canada. Other starting reagents and solvents were obtained from other commercial sources such as Sigma Aldrich and used without further purification, unless otherwise stated. Standard flash chromatography was performed using Silicycle Siliaflash 60 (230–400 mesh). ^{1}H, ^{13}C and ^{31}P NMRs were recorded in $CDCl_3$ or CD_3OD using a Bruker Avance III NMR spectrometer. NMR spectra are provided in the ESI Data.†

[a]*University of Ontario Institute of Technology, Faculty of Science, 2000 Simcoe Street North, Oshawa, ON L1G 0C5, Canada. E-mail: jean-paul.desaulniers@ontariotechu.ca*

[b]*Synthose Inc., 50 Viceroy Road Unit 7, Concord, ON L4K 3A7, Canada*

† Electronic supplementary information (ESI) available. See DOI: 10.1039/d1ra00922b

© 2021 The Author(s). Published by the Royal Society of Chemistry

Open Access Article. Published on 01 March 2021. Downloaded on 4/28/2021 9:03:51 AM.
This article is licensed under a Creative Commons Attribution 3.0 Unported Licence.

Compound 1

To a solution of β-D-glucopyranosyl azide (0.5 g, 2.44 mmol) in anhydrous pyridine (7 mL) at 0 °C was added 1,3-dichloro-1,1,3,3-tetraisopropyldisiloxane (1.1 eq., 2.68 mmol, 0.86 mL). The mixture was allowed to equilibrate to room temperature and was stirred under argon for 6 hours. The reaction was quenched with methanol and concentrated *in vacuo*. The crude product was taken up in ethyl acetate and washed with water and sodium bicarbonate. The organic layer was dried over sodium sulphate, concentrated *in vacuo* and purified using flash chromatography (3 : 7 ethyl acetate/*n*-hexanes) to yield compound **1** as a white solid (0.677 g, 62%). ^{1}H NMR (400 MHz, $CDCl_3$). δ 4.59 (d, 1H), 4.10 (dd, 1H), 4.00 (dd, 1H), 3.82 (t, 1H), 3.6 (t, 1H), 3.33–3.28 (m, 2H), 1.11–1.02 (m, 28H). ^{13}C NMR (101 MHz, $CDCl_3$). δ 90.8, 78.7, 76.5, 73.4, 68.8, 60.6, 17.4, 17.3, 17.2, 17.1, 13.6, 13.2, 12.5.

Compound 2

To a solution of compound **1** (0.45 g, 1 mmol) in DMF (5.5 mL) was added *p*-toluenesulfonic acid monohydrate (0.2 eq., 0.2 mmol, 0.038 g). The mixture was stirred at room temperature under argon. After 6.5 hours, the reaction mixture was diluted with ethyl acetate and washed with water and sodium bicarbonate. The organic layer was dried over sodium sulphate, concentrated *in vacuo* and purified using flash chromatography (3 : 7 ethyl acetate/*n*-hexanes) to yield compound **2** as a white solid (0.248 g, 55%).^{1}H NMR (400 MHz, $CDCl_3$). δ 4.62 (d, 1H), 3.95 (dd, 1H), 3.78 (dd, 1H), 3.73–3.66 (m, 2H), 3.48–3.44 (m, 1H), 3.39 (t, 1H), 2.62 (d, 1H), 1.12–1.02 (m, 28H). ^{13}C NMR (101 MHz, $CDCl_3$). δ 89.6, 79.8, 78.4, 73.8, 72.1, 61.9, 17.2, 12.9, 12.8, 12.1.

Compound 3

To a solution of compound **2** (0.6 g, 1.34 mmol) in anhydrous pyridine (3 mL) was added anhydrous trimethylamine (0.56 mL, 4 mmol) under argon. While stirring the reaction at 0 °C, 4,4′-dimethoxytrityl chloride (1.5 eq., 2 mmol, 0.681 g) was added in 5 equal portions over a 5 hour period. The reaction mixture was allowed to equilibrate to room temperature and was stirred for an additional 7 hours. The solvent was removed *in vacuo* and the crude product was taken up in dichloromethane and washed with sodium bicarbonate. The organic layer was dried over sodium sulphate, concentrated *in vacuo* and purified using flash chromatography (3 : 7 ethyl acetate/*n*-hexane) to yield compound **3** as a yellow oil (0.75 g, 75%). ^{1}H NMR (400 MHz, $CDCl_3$). δ 7.22–7.08 (m, 9H), 6.75–6.73 (m, 4H), 4.5 (d, 1H), 3.85 (ddd, 1H), 3.7 (s, 6H), 3.7–3.64 (m, 1H), 3.61–3.58 (m, 1H), 3.38–3.34 (m, 1H), 3.31–3.27 (td, 1H), 2.6 (d, 1H), 1.03–0.93 (m, 28H). ^{13}C NMR (101 MHz, $CDCl_3$). δ 158.6, 147.3, 139.5, 129.1, 127.8, 127.1, 113.6, 113.2, 112.6, 89.6, 79.8, 73.9, 72.1, 61.9, 60.4, 17.2, 12.8, 12.1.

Compound 4

To a mixture of compound **3** (0.25 g, 0.33 mmol) and propargyl uracil (0.055 g, 0.37 mmol) in anhydrous acetonitrile (5 mL) was added copper(I) iodide (0.007 g, 0.036 mmol) under argon. The solution was stirred at room temperature for 6 hours. The solvent was removed *in vacuo* and the crude product was purified using flash chromatography (gradient: 0% to 5% methanol/dichloromethane) to yield compound **4** as an off-yellow foam (0.23 g, 77%). ^{1}H NMR (400 MHz, CD_3OD). δ 9.10 (s, 1H), 7.52 (d, 1H), 7.46 (d, 1H), 7.36–7.31 (m, 5H), 7.25–7.19 (m, 4H), 7.10 (d, 1H), 6.87–6.84 (m, 4H), 5.73–5.64 (m, 1H), 5.0 (s, 1H), 4.10 (t, 1H), 3.97–3.87 (m, 2H), 3.72–3.63 (m, 2H), 3.57 (d, 1H), 2.8 (brs, 1H), 1.33–1.03 (m, 28H). ^{13}C NMR (101 MHz, $CDCl_3$). δ 158.6, 158.4, 147.3, 144.9, 139.5, 130.1, 129.1, 127.9, 127.8, 127.1, 113.6, 113.2, 102.8, 87.26, 86.44, 81.4, 79.9, 72.9, 71.9, 61.6, 51.9, 29.7, 17.3, 12.8, 12.1. ESI-HRMS (ES+) *m*/*z* calculated for $C_{46}H_{61}N_5O_{10}Si_2 + H^+$: 900.3957, found 900.4038 [M + H$^+$].

Compound 5

To a flame-dried round-bottomed flask was added a solution of compound **4** (0.25 g, 0.29 mmol) in anhydrous dichloromethane (4 mL), followed by the addition of anhydrous triethylamine (0.14 mL, 1.4 mmol) under an argon atmosphere. 2-Cyanoethyl-*N*,*N*-diisopropylchlorophosphoramidite (0.19 mL, 0.833 mmol) was then added drop-wise and the reaction was stirred at room temperature for 1.5 hours. Due to stability concerns, the crude product was purified using a short flash chromatography column (gradient: 20% to 70% ethyl acetate/*n*-hexane, maintaining 5% triethylamine) to yield compound **5** as a yellow oil (0.26 g, 84%), which was immediately used for solid-phase oligonucleotide synthesis. ^{31}P NMR (162 MHz, $CDCl_3$). δ ppm 147.83, 147.79.

Oligonucleotide synthesis

Oligonucleotides were synthesized on an Applied Biosystems 394 DNA/RNA synthesizer using 1.0 μM controlled-pore glass (CPG) support columns and a 1.0 μM cycle with a 999 second coupling time. Phosphoramidites were resuspended in anhydrous acetonitrile, immediately before use, to a final concentration of 0.1 M. Oligonucleotide cleavage from the solid support columns was achieved by flushing the CPG columns with 1 mL EMAM solution (1 : 1 methylamine 33 wt% in ethanol/methylamine 40 wt% in water) for 1 hour at room temperature, followed by overnight incubation in EMAM to deprotect the bases. Oligonucleotides were concentrated in a MiVac Quattro Concentrator and later resuspended in DMSO (100 μM). The silyl protecting groups were removed by incubating the oligonucleotides with 3HF–Et_3N (125 μL) for 3 hours at 65 °C. Crude oligonucleotides were precipitated in ethanol and desalted using Millipore Ampicon Ultra 3000 MW cellulose centrifugal filters. Strands were purified using reverse-phase HPLC eluting from 5% to 95% ACN in 0.1 M TEAA buffer (pH 7.0).

Thermal denaturation and circular dichroism (CD) studies

For duplex formation, equimolar amounts of the respective sense and antisense strands were combined, dried down and resuspended in 400 μL sodium phosphate buffer (90 mM NaCl, 10 mM Na_2HPO_4, 1 mM EDTA; pH 7.0). Samples were heated for 2 minutes at 90 °C and allowed to slowly equilibrate to room temperature. Thermal denaturation and CD studies were

 © 2021 The Author(s). Published by the Royal Society of Chemistry

Open Access Article. Published on 01 March 2021. Downloaded on 4/28/2021 9:03:51 AM.
This article is licensed under a Creative Commons Attribution 3.0 Unported Licence.

performed using a Jasco J-815 CD Spectropolarimeter equipped with a temperature controller. To determine the melting temperature (T_m) of each duplex, the change in absorbance at 260 nm was measured against a temperature gradient from 15 to 95 °C, at 0.5 °C min^{-1}. Data were analysed using Meltwin v3.5 software. CD spectra were recorded at 25 °C, scanning from 200 to 40 nm with a screening rate of 20.0 nm min^{-1} and a 0.20 nm data pitch. Scans were performed in triplicate and averaged using Jasco's Spectra Manager v2 software.

Biological assays

Cell culture and transfection. HeLa cells were maintained in Dulbecco's Modified Eagle's Medium (DMEM) supplemented with 10% fetal bovine serum (FBS) and 1% penicillin-streptomycin (Sigma). Cells were maintained at 37 °C in a humidified atmosphere with 5% CO_2 and were passaged at 80% confluency. HeLa cells were seeded into 24-well plates, containing 400 μL DMEM (10% FBS), at a density of 5.0×10^4 cells per well. Cells were incubated for 24 hours at 37 °C in a humidified atmosphere with 5% CO_2 after which the culture medium was removed. For each transfection sample, a mixture of 1 μL Lipofectamine 2000™ (Invitrogen) and 49 μL 1X Gibco's Opti-MEM Reduced Serum Medium (Invitrogen) was incubated at room temperature for 5 min. Each siRNA was diluted in 1X Gibco's Opti-MEM Reduced Serum Medium on ice and mixed with 200 ng pGL3 and 50 ng pRLSV40 plasmids to achieve a final volume of 50 μL. The siRNA-plasmid mix was added to the Lipofectamine 2000™ Opti-MEM mix and incubated for 40 minutes at room temperature. These samples were then transferred to the respective wells of the 24-well plate and incubated for 24 hours at 37 °C prior to cell lysis.

Dual-Luciferase® Reporter Assay. Cells were lysed with 1× passive lysis buffer for 30 min at room temperature. Cell lysates (10 μL) were transferred to opaque Costar 96-well plates in triplicate for the Dual-Luciferase® Reporter Assay (Promega). Luciferase Assay Reagent II (LAR II) and Stop & Glo® Reagent were prepared following the manufacturer's protocol. LAR II (50 μL) was added to each well and luminescence was immediately measured using a Synergy HT (Bio-Tek) plate luminometer. Stop & Glo® (50 μL) was then added to each well and a second luminescence measurement was taken. Results are expressed as the ratio of firefly/*Renilla* luminescence taken as a percentage of an untreated control.

Results and discussion

Preparation of oligonucleotides

To synthesize the glucose phosphoramidite **5**, we first treated β-D-glucopyranosyl azide with $TIPDSCl_2$. This was followed by the acid-catalyzed migration of the 4,6-TIPDS protecting group to yield the 3,4-protected derivative **2**, as previously reported in the literature.[18] This compound was protected with 4,4′-dimethoxytrityl (DMT) and then reacted with *N*1-propargyl uracil *via* copper(I)-catalyzed azide–alkyne cycloaddition (CuAAC). The resulting compound **4** was phosphitylated with 2-cyanoethyl-*N*,*N*-diisopropylchlorophosphoramidite to yield the phosphoramidite derivative **5** (Scheme 1), which was used for solid-phase oligonucleotide synthesis as described above. The modification was incorporated at key positions within the sense or antisense strand, replacing either the 3′ dTdT overhang or an internal uridine nucleotide. Oligonucleotides strands were purified using reverse-phase HPLC (ESI Fig. S1†) and characterized by mass spectrometry (ESI Table S1†).

CD studies

Modified sense and antisense strands were annealed to their complementary wild-type sequences. The resulting duplexes were characterized using circular dichroism spectroscopy as described above to confirm that siRNAs adopted an A-form helical conformation. Recognition of the A-form major groove by RISC is required for proper RNAi activity, so this is an important criterion in siRNA design.[19] An A-form helical structure is characterized by a broad positive band at 260 nm in addition to a negative band at ~210 nm.[20] As seen in Fig. 1, our

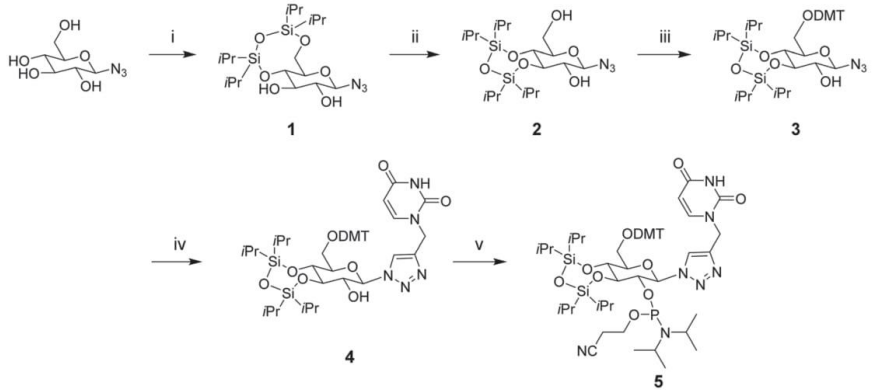

Scheme 1 Synthesis of a glucose nucleoside containing a triazole-linked uracil base, and its phosphoramidite derivative. Reagents and conditions: (i) $TIPDSCl_2$, pyridine, 0 °C → rt, 6 h (62%), (ii) *p*-TsOH·H_2O, DMF, RT, 6.5 h (55%), (iii) DMT–Cl, Et_3N/pyridine, 0 °C, 5 h, 0 °C → rt, 7 h (75%), (iv) *N*1-propargyl uracil, CuI, ACN, rt, 6 h (77%), (v) 2-cyanoethyl-*N*,*N*-diisopropylchlorophosphoramidite, Et_3N/DCM, rt, 1.5 h (84%).

Open Access Article. Published on 01 March 2021. Downloaded on 4/28/2021 9:03:51 AM.
This article is licensed under a Creative Commons Attribution 3.0 Unported Licence.

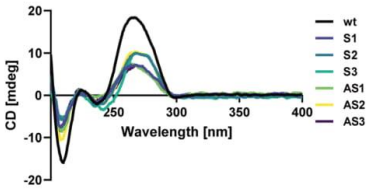

Fig. 1 Circular dichroism (CD) spectra of anti-luciferase siRNAs.

modification did not distort the A-form helical structure of the siRNA duplex, regardless of its placement in the sequence.

Thermal denaturation

Since the thermodynamic properties of siRNAs have been shown to impact siRNA potency, we assessed the thermal stability of each duplex. The resulting melting temperatures (T_m) are indicated in Table 1. Placing our modification at the 3′ end of the sense or antisense strand, replacing the dTdT overhang, had a small impact on thermal stability with ΔT_m values of −5 °C. This could be due to the loss of stacking interactions which have been reported with 3′ dTdT overhangs.[21] Internal modifications resulted in strong thermal destabilization.

Placing the modification at positions 12 or 16 from the sense strand 5′ end resulted in ΔT_m values of −22 °C and −26 °C, respectively. Similar effects were observed when placing the modification at positions 10 and 16 from the antisense strand 5′ end, with ΔT_m values of −22.5 °C and −17 °C, respectively. These results were expected as the internal region of siRNA is far less tolerant to bulky chemical modifications than the 3′ end.[22]

Gene-silencing activity

To assess the gene-silencing activity of siRNAs, HeLa cells were co-transfected with plasmids coding for firefly and *Renilla* luciferases as well as siRNAs, using Lipofectamine 2000™ (Invitrogen). We then used the Dual-Luciferase® Reporter Assay to evaluate the relative expression of target firefly luciferase after

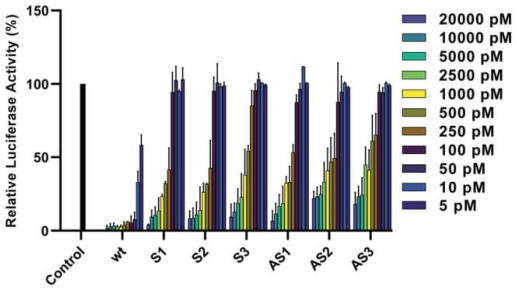

Fig. 2 Relative expression of normalized firefly luciferase in HeLa cells 24 hours after siRNA treatment. Error bars indicate standard deviation of at least two independent biological replicates.

siRNA treatments ranging from 5 to 20 000 pM. As seen in Fig. 2, all tested siRNAs showed dose-dependent knockdown of firefly luciferase after 24 hours. IC_{50} values are summarized in Table 1. Duplexes bearing terminal modifications, placed at the 3′ end of the sense or antisense strand, showed high gene-silencing activity with IC_{50} values of 218 pM and 226 pM, respectively. This is consistent with literature reports showing that six-carbon sugar derivatives are well-tolerated and can lead to strong gene-silencing activity when placed at the 3′ end of the siRNA sense or antisense strand. Although internal modifications were tolerated in both the sense and the antisense strand, their effect on siRNA activity was position dependent. Placing our modification at position 16 from the sense or antisense strand 5′ end led to efficient gene-silencing activity (IC_{50} of 219 pM), comparable to our terminal-modified siRNAs. On the other hand, placing our modification at position 10 from the antisense strand 5′ end led to a decrease in gene-silencing activity (IC_{50} of 483 pM). It has been reported that the seed region, which directs the initial target recognition by RISC, is more sensitive to chemical modifications, particularly if they disrupt the thermal stability of the duplex.[22] The lowest activity,

Table 1 Sequences, melting temperatures and IC_{50} values of anti-firefly luciferase siRNAs[a]

Code	Duplex	T_m (°C)	ΔT_m (°C)	IC_{50} (pM)
wt	5′ CUU ACG CUG AGU ACU UCG ATT 3′ 3′ TTG AAU GCG ACU CAU GAA GCU 5′	76.1	—	1.90
S1	5′ CUU ACG CUG AGU ACU UCG AX 3′ 3′ TTG AAU GCG ACU CAU GAA GCU 5′	71.1	−5.0	218
S2	5′ CUU ACG CUG AGU ACU XCG ATT 3′ 3′ TTG AAU GCG ACU CAU GAA GCU 5′	50.1	−26.0	219
S3	5′ CUU ACG CUG AGX ACU UCG ATT 3′ 3′ TTG AAU GCG ACU CAU GAA GCU 5′	54.1	−22.0	524
AS1	5′ CUU ACG CUG AGU ACU UCG ATT 3′ 3′ XG AAU GCG ACU CAU GAA GCU 5′	71.1	−5.0	226
AS2	5′ CUU ACG CUG AGU ACU UCG ATT 3′ 3′ TTG AAX GCG ACU CAU GAA GCU 5′	59.1	−17.0	219
AS3	5′ CUU ACG CUG AGU ACU UCG ATT 3′ 3′ TTG AAU GCG ACX CAU GAA GCU 5′	53.6	−22.5	483

[a] The top strand corresponds to the sense strand. The bottom strand corresponds to the antisense strand. X corresponds to the triazole-linked uracil modification. Inhibitory dose–response curves can be found in the ESI Data (ESI Fig. S2).

 © 2021 The Author(s). Published by the Royal Society of Chemistry

Open Access Article. Published on 01 March 2021. Downloaded on 4/28/2021 9:03:51 AM.
This article is licensed under a Creative Commons Attribution 3.0 Unported Licence.

however, was observed with siRNA S3, bearing the modification at position 12 from the sense strand 5′ end (IC_{50} of 524 pM).

Some reports suggest that this position can be less tolerant to chemical modifications, including altritol nucleic acids.[23] Given the proximity to the Ago2 cleavage site, it has been proposed that some chemical modifications at this position can interfere with the enzymatic activity of Ago2 thus compromising siRNA potency.[24] Based on these data, this modification may be better suited for incorporation at the 3′ end of the sense or antisense strand as well as at some internal in order to maximize gene-silencing activity.

Conclusion

In summary, we report the synthesis of a novel glucose phosphoramidite with a triazole-linked uracil moiety at position 1 for incorporation into oligonucleotides using standard solid-phase synthetic conditions. This modification was placed at terminal and internal positions of the siRNA sense or antisense strand to investigate its biophysical and biological effects. Overall, this modification was well-tolerated within the sense and the antisense strand and did not distort the A-form helical conformation of the siRNAs, making it suitable for RNAi applications. Notably, our modified siRNAs show position-dependent gene-silencing activity. Replacing the dT overhang at the 3′ end or modifying position 16 from the 5′ end of either stand resulted in high siRNA activity. This position-dependent effect could be further investigated to optimize siRNA potency. Although there are some general guidelines for siRNA design, these criteria are not universally applicable, highlighting the importance of assessing the effect of each chemical modification individually. To the best of our knowledge, this is the first report of an siRNA bearing a single 3′-6′/2′-5′ phosphodiester linkage.

Author contributions

Lidya Salim: data curation; investigation; methodology; visualization; writing – original draft. Eva Goss: funding acquisition; project administration; resources. Jean-Paul Desaulniers: conceptualization; funding acquisition; project administration; resources; supervision; writing – review & editing.

Conflicts of interest

There are no conflicts to declare.

Acknowledgements

We acknowledge the Natural Sciences and Engineering Research Council (NSERC) for funding. We also acknowledge Ifrodet Giorgees for assistance with mass spectrometry analysis.

Notes and references

1 N. Agrawal, P. V. Dasaradhi, A. Mohmmed, P. Malhotra, R. K. Bhatnagar and S. K. Mukherjee, *Microbiol. Mol. Biol. Rev.*, 2003, **67**, 657–685.
2 G. J. Hannon, *Nature*, 2002, **418**, 244–251.
3 S. M. Elbashir, J. Harborth, W. Lendeckel, A. Yalcin, K. Weber and T. Tuschl, *Nature*, 2001, **411**, 494–498.
4 D. Adams, A. Gonzalez-Duarte, W. D. O'Riordan, C. C. Yang, M. Ueda, A. V. Kristen, I. Tournev, H. H. Schmidt, T. Coelho, J. L. Berk, K. P. Lin, G. Vita, S. Attarian, V. Planté-Bordeneuve, M. M. Mezei, J. M. Campistol, J. Buades, T. H. Brannagan III, B. J. Kim, J. Oh, Y. Parman, Y. Sekijima, P. N. Hawkins, S. D. Solomon, M. Polydefkis, P. J. Dyck, P. J. Gandhi, S. Goyal, J. Chen, A. L. Strahs, S. V. Nochur, M. T. Sweetser, P. P. Garg, A. K. Vaishnaw, J. A. Gollob and O. B. Suhr, *N. Engl. J. Med.*, 2018, **379**, 11–21.
5 L. J. Scott, *Drugs*, 2020, **80**, 335–339.
6 L. Aagaard and J. J. Rossi, *Adv. Drug Delivery Rev.*, 2007, **59**, 75–86.
7 D. Haussecker, *J. Controlled Release*, 2014, **195**, 49–54.
8 C. Selvam, D. Mutisya, S. Prakash, K. Ranganna and R. Thilagavathi, *Chem. Biol. Drug Des.*, 2017, **90**, 665–678.
9 J. K. Watts, G. F. Deleavey and M. J. Damha, *Drug Discovery Today*, 2008, **13**, 842–855.
10 D. A. Braasch, S. Jensen, Y. Liu, K. Kaur, K. Arar, M. A. White and D. R. Corey, *Biochemistry*, 2003, **42**, 7967–7975.
11 Y.-L. Chiu and T. M. Rana, *RNA*, 2003, **9**, 1034–1048.
12 D. M. Kenski, G. Butora, A. T. Willingham, A. J. Cooper, W. Fu, N. Qi, F. Soriano, I. W. Davies and W. M. Flanagan, *Mol. Ther.–Nucleic Acids*, 2012, **1**, e5.
13 J. Elmén, H. Thonberg, K. Ljungberg, M. Frieden, M. Westergaard, Y. Xu, B. Wahren, Z. Liang, H. Ørum, T. Koch and C. Wahlestedt, *Nucleic Acids Res.*, 2005, **33**, 439–447.
14 P. Nielsen, L. H. Dreiøe and J. Wengel, *Bioorg. Med. Chem.*, 1995, **3**, 19–28.
15 M. Fisher, M. Abramov, A. Van Aerschot, D. Xu, R. L. Juliano and P. Herdewijn, *Nucleic Acids Res.*, 2007, **35**, 1064–1074.
16 K. Nauwelaerts, M. Fisher, M. Froeyen, E. Lescrinier, A. Van Aerschot, D. Xu, R. DeLong, H. Kang, R. L. Juliano and P. Herdewijn, *J. Am. Chem. Soc.*, 2007, **129**, 9340–9348.
17 M. Fisher, M. Abramov, A. Van Aerschot, J. Rozenski, V. Dixit, R. L. Juliano and P. Herdewijn, *Eur. J. Pharmacol.*, 2009, **606**, 38–44.
18 M. Farrell, J. Zhou and P. V. Murphy, *Chem. –Eur. J.*, 2013, **19**, 14836–14851.
19 A. R. Hernández, L. W. Peterson and E. T. Kool, *ACS Chem. Biol.*, 2012, **7**, 1454–1461.
20 J. Kypr, I. Kejnovská, D. Renciuk and M. Vorlícková, *Nucleic Acids Res.*, 2009, **37**, 1713–1725.
21 A. S. O'Toole, S. Miller and M. J. Serra, *RNA*, 2005, **11**, 512–516.
22 J. Bramsen and J. Kjems, *Front. Genet.*, 2012, **3**, 1–22.
23 P. Kumar, R. Degaonkar, D. C. Guenther, M. Abramov, G. Schepers, M. Capobianco, Y. Jiang, J. Harp, C. Kaittanis, M. M. Janas, A. Castoreno, I. Zlatev, M. K. Schlegel, P. Herdewijn, M. Egli and M. Manoharan, *Nucleic Acids Res.*, 2020, **48**, 4028–4040.
24 J. Zheng, L. Zhang, J. Zhang, X. Wang, K. Ye, Z. Xi, Q. Du and Z. Liang, *FASEB J.*, 2013, **27**, 4017–4026.

Electronic Supplementary Material (ESI) for RSC Advances.
This journal is © The Royal Society of Chemistry 2021

Supplementary Data

Synthesis and Evaluation of Modified siRNA Molecules Containing a Novel Glucose Derivative

Lidya Salim,[1] Eva Goss[2] and Jean-Paul Desaulniers[1]

[1]Faculty of Science, University of Ontario Institute of Technology, Faculty of Science, 2000 Simcoe Street North, Oshawa, ON L1G 0C5 Canada

[2]Synthose, Inc. 50 Viceroy Road, Unit 7, Concord, ON L4K 3A7 Canada

Procedures

Tables

Figures

NMR spectra

Procedures

Procedure for LC/MS: LC/MS chromatograms were acquired on an Agilent 6545 QTOF-MS with Agilent 1260 Infinity Binary Pump HPLC using a ZORBAX Eclipse Plus C18 2.1x100mm 1.8-Micron Agilent column and a mobile phase of 5 mM ammonium acetate buffer (pH 7)/acetonitrile (95:5). Oligonucleotide samples were prepared at a concentration of 0.01 O.D/µL with an injection volume of 20 µL. Data were analysed using Agilent Technologies MassHunter Workstation Qualitative Analysis Software (Qual. 10.0).

Tables

Table S1. Sequences and mass spectrometry data of modified oligonucleotide strands

Code	*Sequence*	*Mass (predicted)*	*Mass (found)*
S1	5′ CUU ACG CUG AGU ACU UCG AX 3′ (S)	6796.88	6796.52
S2	5′ CUU ACG CUG AGU ACU XCG ATT 3′ (S)	6794.90	6795.56
S3	5′ CUU ACG CUG AGX ACU UCG ATT 3′ (S)	6794.90	6794.62
AS1	3′ XG AAU GCG ACU CAU GAA GCU 5′ (AS)	6882.94	6882.87
AS2	3′ TTG AAX GCG ACU CAU GAA GCU 5′ (AS)	6880.96	6880.80
AS3	3′ TTG AAU GCG ACX CAU GAA GCU 5′ (AS)	6880.96	6880.61

(S) corresponds to the sense strand; (AS) corresponds to the antisense strand. X corresponds to the position of the glucose nucleoside with a triazole-linked uracil.

Figures

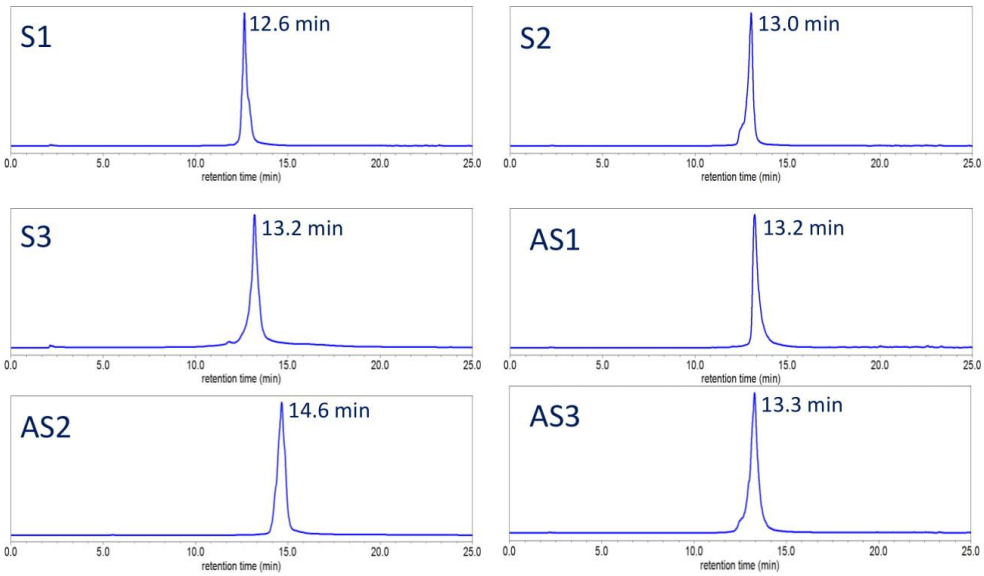

Figure S1. Analytical HPLC traces of modified oligonucleotides. Corresponding sequences can be found in Table S1. HPLC was performed on a Waters 1525 binary HPLC pump with a Waters 2489 UV/Vis detector, using a C18 4.6 x 150 mm reverse-phase column, eluting from 5 to 95% ACN in 0.1 M TEAA buffer (pH 7.0).

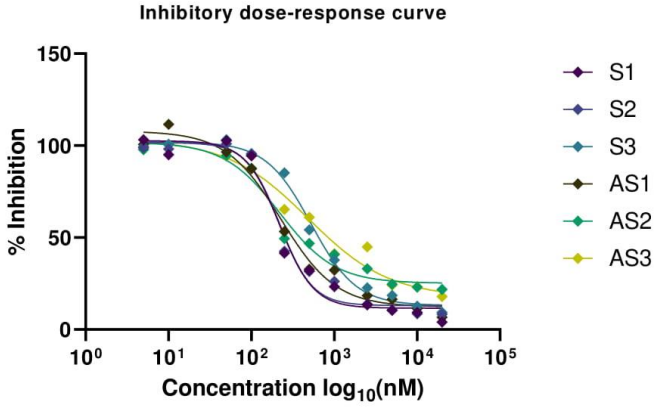

Figure S2. Inhibitory dose-response curves for modified anti-luciferase siRNAs, tested in HeLa at concentrations from 5 to 20,000 pM.

NMR Spectra

^{1}H NMR Spectrum of Compound **1**

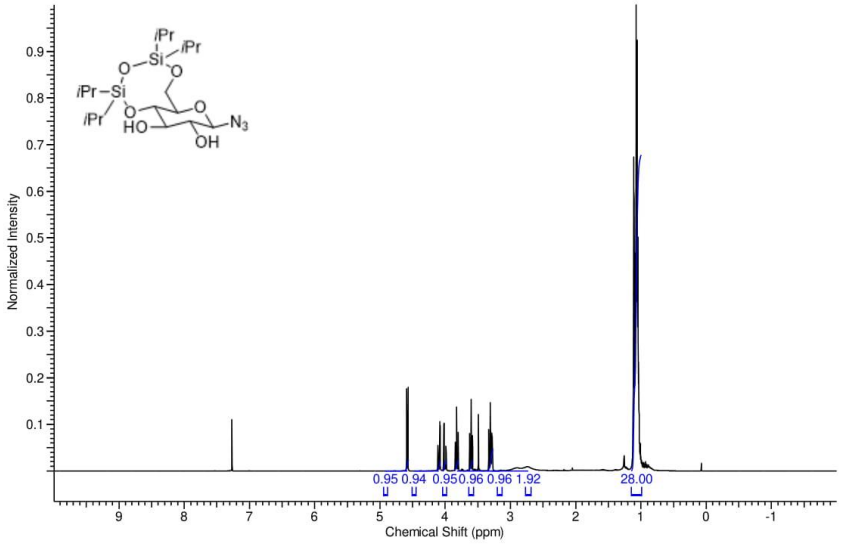

^{13}C NMR Spectrum of Compound **1**

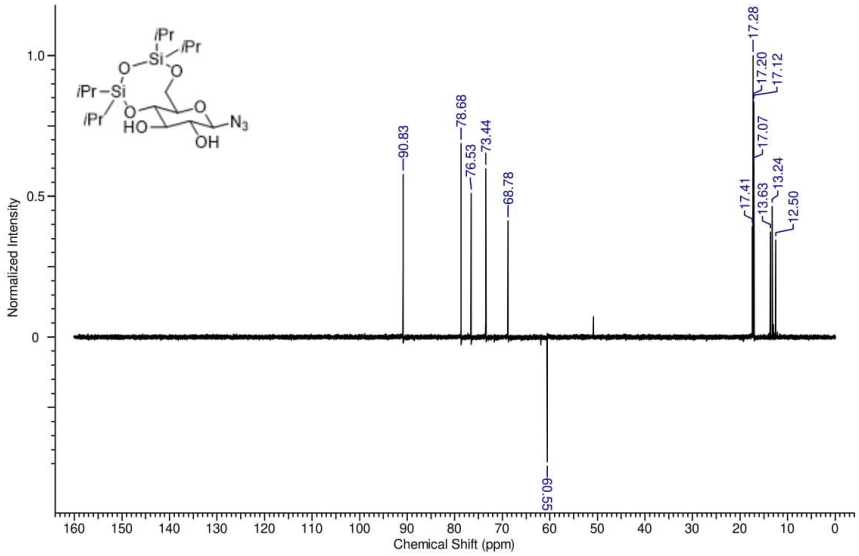

^{1}H NMR Spectrum of Compound **2**

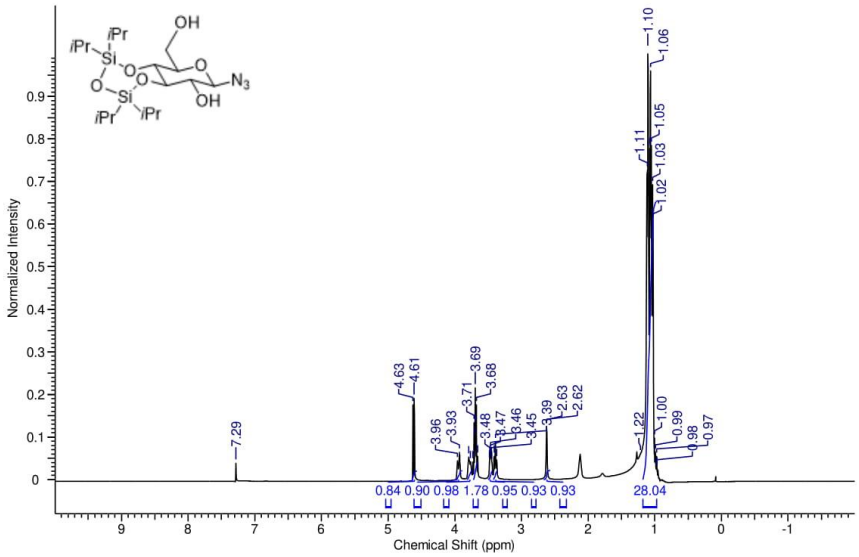

^{13}C NMR Spectrum of Compound **2**

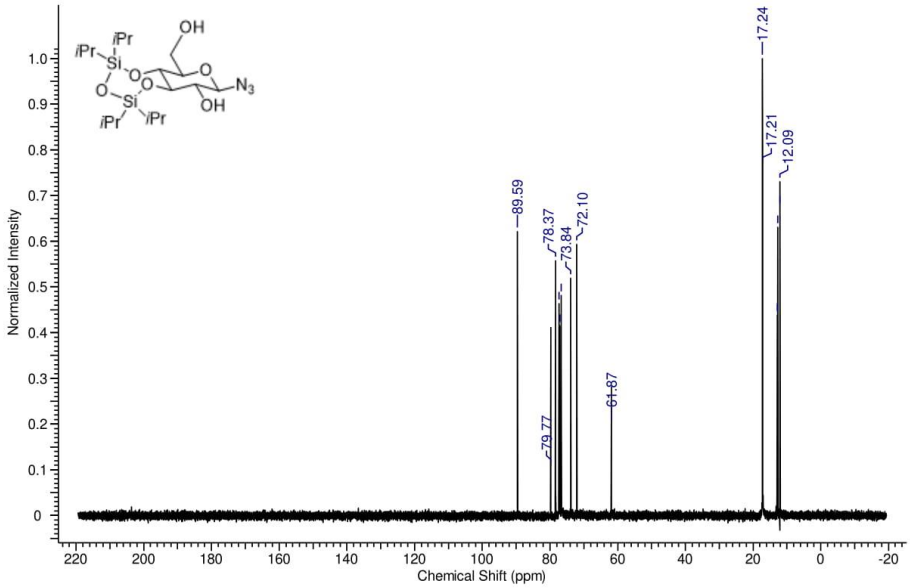

^{1}H NMR Spectrum of Compound **3**

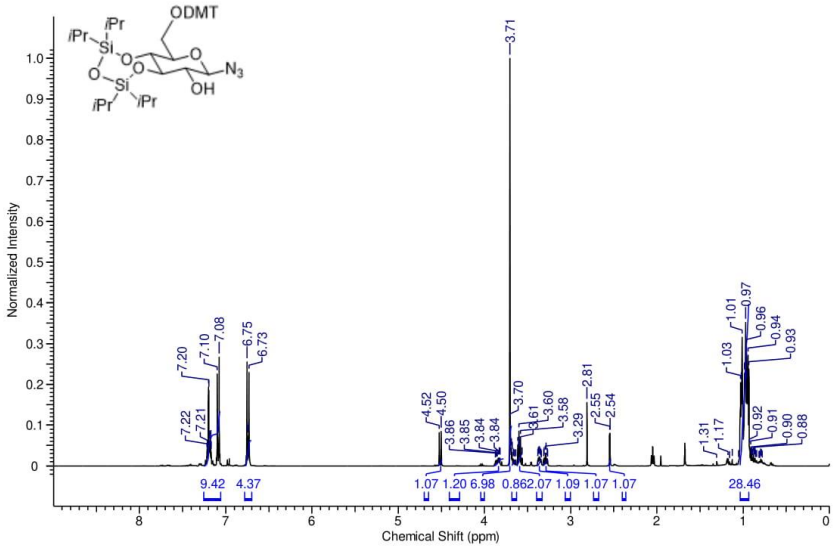

^{13}C NMR Spectrum of Compound **3**

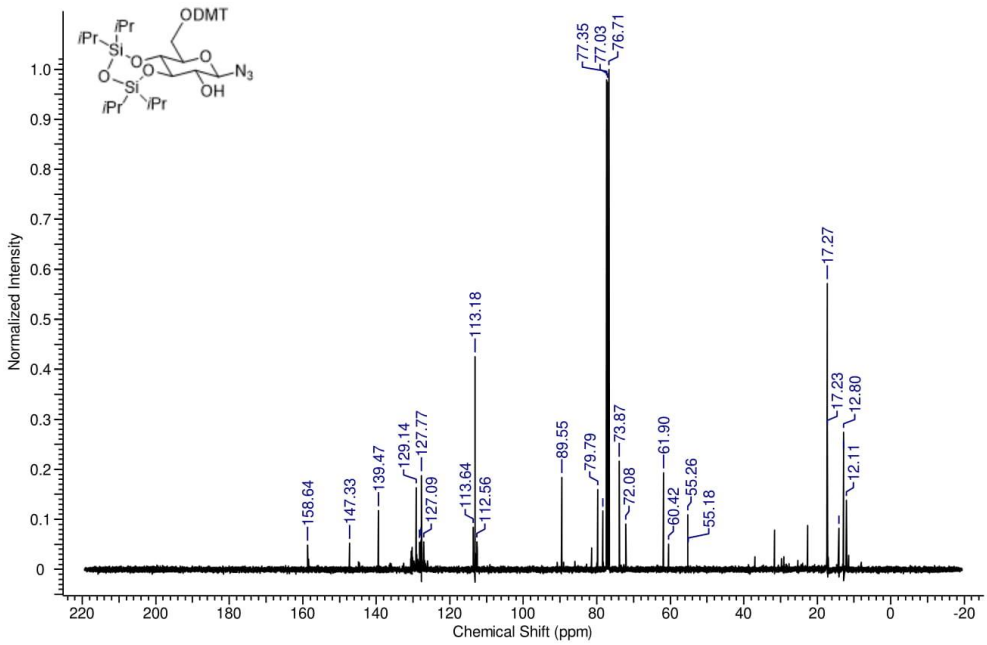

^{1}H NMR Spectrum of Compound **4**

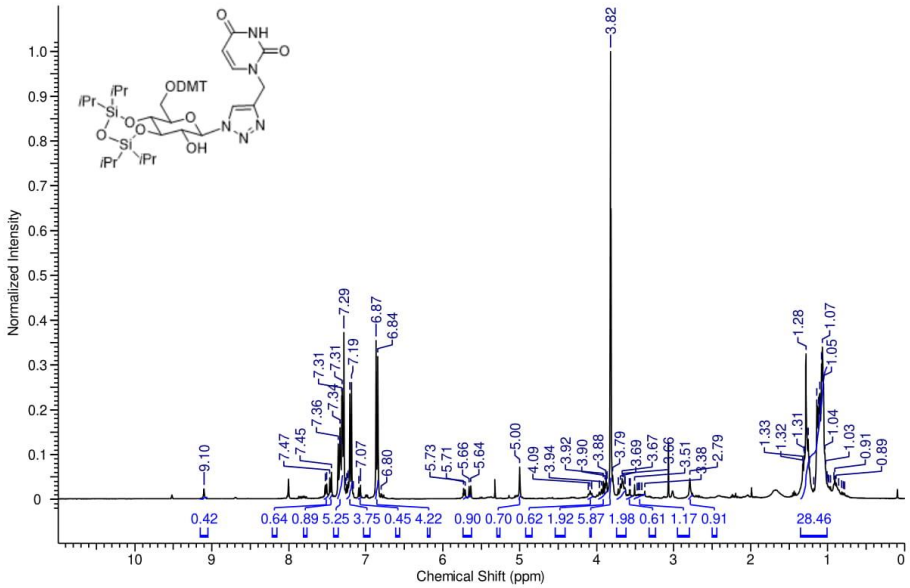

^{13}C NMR Spectrum of Compound **4**

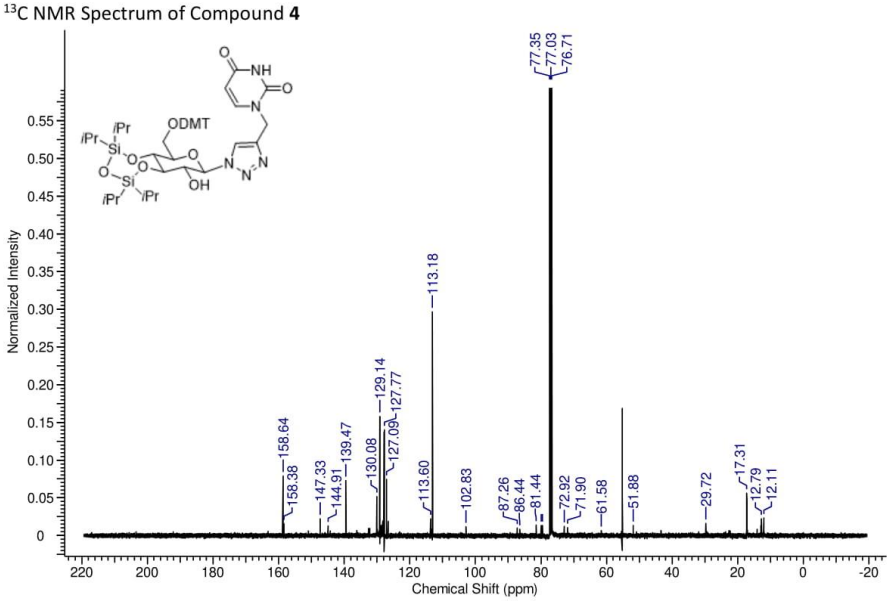

^{31}P NMR Spectrum of Compound **5**

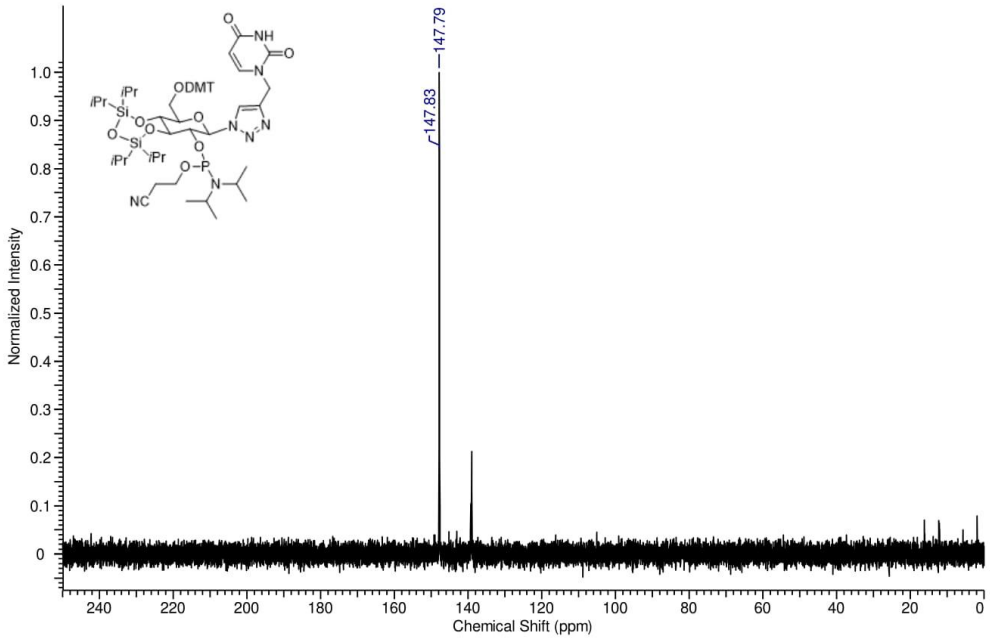

Appendix E. Review Article

NUCLEIC ACID THERAPEUTICS
Volume 00, Number 00, 2020
© Mary Ann Liebert, Inc.
DOI: 10.1089/nat.2020.0893

To Conjugate or to Package? A Look at Targeted siRNA Delivery Through Folate Receptors

Lidya Salim and Jean-Paul Desaulniers

Downloaded by GLASGOW UNIVERSITY LIBRARY/Swetsblackwell Inc/ 93868820 from www.liebertpub.com at 10/31/20. For personal use only.

RNA interference (RNAi) applications have evolved from experimental tools to study gene function to the development of a novel class of gene-silencing therapeutics. Despite decades of research, it was not until August 2018 that the US FDA approved the first-ever RNAi drug, marking a new era for RNAi therapeutics. Although there are many limitations associated with the inherent structure of RNA, delivery to target cells and tissues remains the most challenging. RNAs are unable to diffuse across cellular membranes due to their large size and polyanionic backbone and, therefore, require a delivery vector. RNAi molecules can be conjugated to a targeting ligand or packaged into a delivery vehicle. Alnylam has used both strategies in their FDA-approved formulations to achieve efficient delivery to the liver. To harness the full potential of RNAi therapeutics, however, we must be able to target additional cells and tissues. One promising target is the folate receptor α, which is overexpressed in a variety of tumors despite having limited expression and distribution in normal tissues. Folate can be conjugated directly to the RNAi molecule or used to functionalize delivery vehicles. In this review, we compare both delivery strategies and discuss the current state of research in the area of folate-mediated delivery of RNAi molecules.

Keywords: folic acid, siRNA, conjugate

Introduction

RNA interference (RNAi) is a natural regulatory mechanism that uses small noncoding RNA molecules to inhibit translation [1]. The endogenous triggers of RNAi include short interfering RNAs (siRNAs) and microRNAs (miRNAs). Although these molecules share many similarities, they have distinct modes of action. Long, double-stranded RNA is cleaved by Dicer into ~21–23 nucleotide siRNAs, with 3′ overhangs, which are then incorporated into the RNA-induced silencing complex (RISC) [2,3]. In the latent complex, the siRNA duplex is unwound by Argonaute 2 (Ago2), and the sense strand is cleaved between base pairs 9 and 10 relative to the sense strand 5′ end [4]. The antisense strand remains bound to the now active RISC and is used as a guide sequence to locate and cleave the target mRNA with which it is fully complementary [2].

The gene-silencing mechanism of miRNAs differs from that of siRNAs. Before Dicer processing, the primary miRNA (pri-miRNA) is cleaved by Drosha to form a pre-miRNA, which is then transported to the cytoplasm by Exportin 5 [5]. Dicer processes the pre-miRNA into ~19–25 nucleotide miRNAs, with 3′ overhangs, which are then loaded into RISC forming a new complex called miRISC [6]. The miRNA duplex is unwound, releasing the sense strand and leaving the antisense strand as the guide sequence. Unlike siRNAs, miRNAs are only partially complementary to the target mRNA and mediate gene silencing through mRNA cleavage and translational repression [7,8]. Synthetic siRNA and miRNA molecules are compatible with the endogenous RNAi machinery and have been investigated as both experimental tools and gene-silencing therapeutics [9–13].

Many diseases are characterized by aberrant gene expression, making RNAi molecules ideal therapeutics. Despite this potential, the development of RNAi therapeutics has been limited by the inherent nature of RNA, which poses challenges like poor cellular uptake, immune activation, and off-target effects [14]. Several chemical modifications have been investigated to mitigate these effects and improve the pharmacokinetic profiles of RNAi molecules. This includes backbone modifications, such as phosphorothioate (PS) and boranophosphate, to increase nuclease stability [15,16] and sugar modifications, like 2′-*O*-methyl (2′-OMe) and 2′-deoxy-2′-fluoro (2′-F), to increase thermal stability, reduce immune activation, and improve nuclease resistance [17]. Nevertheless, the delivery of RNAi molecules remains a major challenge in the development of RNAi-based therapeutics. Current delivery strategies involve either

Faculty of Science, University of Ontario Institute of Technology, Oshawa, Canada.

encapsulation within a delivery vehicle or conjugation to a targeting ligand. This review will discuss both strategies and highlight the use of folate as a tumor-targeting ligand in various clinical applications, with an emphasis on RNAi molecules.

RNAi Delivery Issues

RNAs are unable to cross the hydrophobic cell membrane due to their large size, hydrophilic nature, and polyanionic backbone. The challenges associated with RNAi delivery strategies have been reviewed extensively [18–21]. Non-targeted oligonucleotides tend to accumulate in the liver and kidneys [22], so it is not surprising that the most successful RNAi-based therapeutics have targeted this organ [23]. To exploit the full potential of RNAi therapeutics, however, efficient extrahepatic delivery must be achieved. Other notable limitations include nuclease stability, immunogenicity, and off-target effects, but the rate-limiting step for oligonucleotide delivery is certainly endosomal escape. Regardless of the delivery method used, oligonucleotides are generally internalized by endocytosis. Multiple endocytic pathways have been identified and have been found to result in successful oligonucleotide uptake [24]. Early endosomal vesicles fuse into a late endosome, which is rapidly acidified by the membrane-bound ATPase proton pump [25–27]. Oligonucleotides must be translocated from the late endosome into the cytoplasm. If this does not occur, the late endosome will eventually fuse with lysosomes and be further acidified. Digestive enzymes in the lysosome will promote nucleic acid degradation, preventing RNAi activity. With these limitations in mind, many research efforts are now focused on the development of safe and efficient delivery systems for RNAi molecules.

FDA-Approved RNAi Formulations

In August 2018, Alnylam's ONPATTRO® (Patisiran) became the first RNAi-based drug to receive US FDA approval, marking a new era for RNAi therapeutics. Patisiran treats

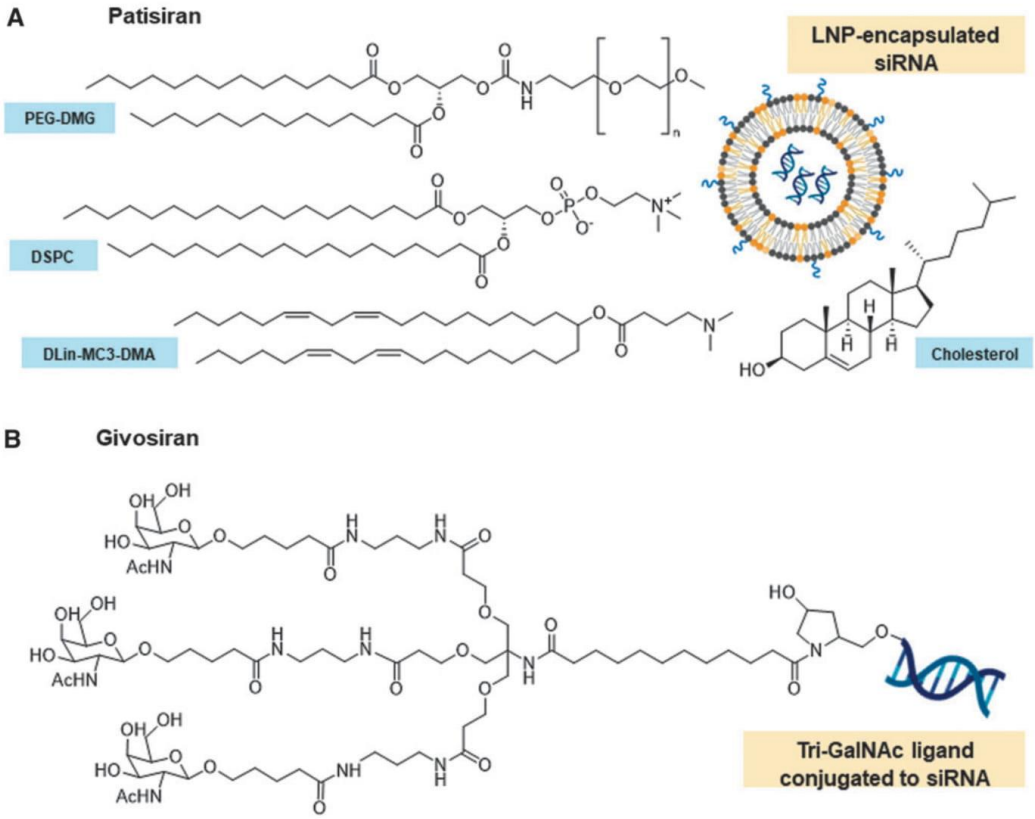

FIG. 1. Composition of Patisiran and Givosiran's delivery vehicles/ligands. **(A)** Patisiran is a LNP-encapsulated siRNA. The LNP is a multicomponent formulation made up of α-(3′-{[1,2-di(myristyloxy)proponoxy]carbonylamino}propyl)-ω-methoxy, polyoxyethylene (PEG-DMG), 1,2-distearoyl-sn-glycero-3-phosphocholine (DSPC), (6Z, 9Z, 28Z, 31Z)-heptatriaconta-6, 9, 28, 31-tetraen-19-yl-4-(dimethylamino) butanoate (DLin-MC3-DMA), and cholesterol. **(B)** Givosiran is an siRNA conjugated to a tri-GalNAc ligand to target the ASGPR. ASGPR, asialoglycoprotein receptor; LNP, lipid nanoparticle. Color images are available online.

Downloaded by GLASGOW UNIVERSITY LIBRARY/Swetsblackwell Inc/ 93868820 from www.liebertpub.com at 10/31/20. For personal use only.

Downloaded by GLASGOW UNIVERSITY LIBRARY/Swetsblackwell Inc/ 93868820 from www.liebertpub.com at 10/31/20. For personal use only.

hereditary transthyretin amyloidosis (hATTR) with polyneuropathy by targeting transthyretin (TTR) [28]. This was followed by the US FDA approval of GIVLAARI® (Givosiran), in November 2019, which treats acute hepatic porphyria by targeting aminolevulinic acid synthase 1 (ALAS1). [29]. Although both siRNA drugs target the liver, they use different delivery strategies (Fig. 1).

Patisiran uses a multicomponent lipid nanoparticle (LNP) formulation and is administered intravenously [28]. LNPs encapsulate the siRNAs, protecting them from enzymatic degradation and shielding their negative charge [30,31]. It has been proposed that LNP uptake in the liver is mediated by apolipoprotein E (ApoE) (Fig. 2) [31,32]. After ApoE associates with the LNP, it facilitates endocytosis through ApoE-binding cell surface receptors, such as the low-density lipoprotein receptor. As the pH of the endosome decreases, the ionizable lipids of the LNP are protonated. These positively charged lipids interact with the negatively charged endosomal lipids, destabilizing the endosomal membrane and causing the disintegration of the LNP [31,32]. This results in the release of the siRNAs into the cytoplasm.

Givosiran, on the other hand, is made up of a modified siRNA conjugated to a tri-GalNAc (N-acetylgalactosamine) ligand and is administered subcutaneously. GalNAc binds to the asialoglycoprotein receptor (ASGPR), a cell surface receptor highly expressed in hepatocytes [30,33]. GalNAc-siRNA conjugates are internalized through receptor-mediated endocytosis (Fig. 2). After endosomal acidification, siRNAs are released into the cytoplasm and the GalNAc ligand is rapidly cleaved and degraded, whereas the ASGPR is recycled onto the cell surface [30]. Unlike the LNP formulation, GalNAc-siRNAs are smaller and can be synthesized under solid-phase conditions but also require extensive siRNA modification to provide protection from nucleases [30,34]. Alnylam's GalNAc-siRNAs use Enhanced Stability Chemistry (ESC). They are fully modified using 2′-F and 2′-OMe groups, as well as PS linkages at key positions [35,36].

Alnylam's next generation GalNAc-siRNA conjugates use an ESC+ design, which introduces thermal destabilizing modifications, like glycol nucleic acid (GNA), in the siRNA antisense seed region. The ESC+ design reduces off-target effects and provides enhanced specificity [37]. Despite the success of Patisiran's LNP formulation, Alnylam's current clinical pipeline is focused on exploiting the ESC-GalNAc delivery platform (Table 1). Late-stage development RNAi

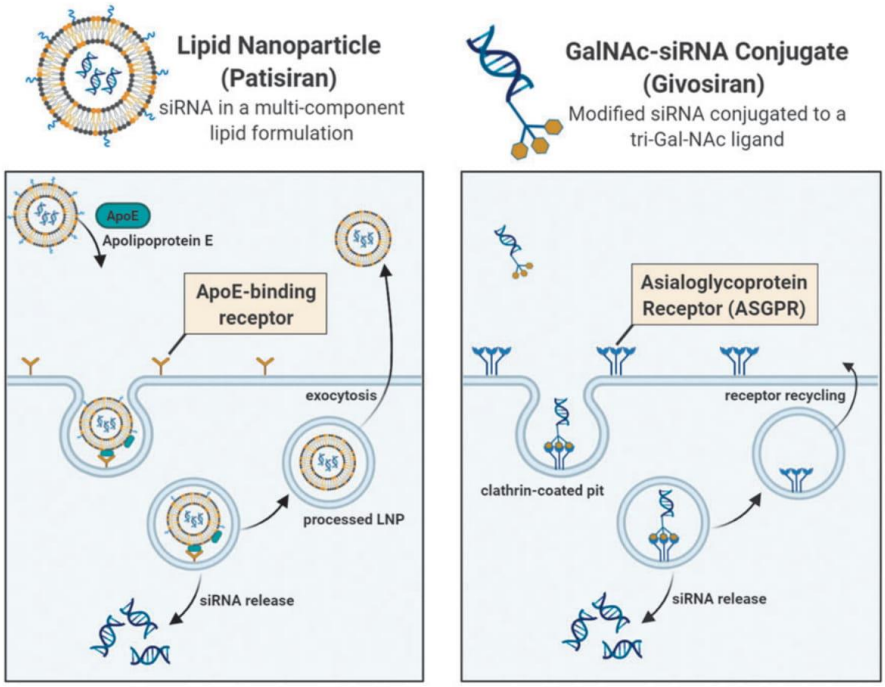

FIG. 2. Proposed internalization mechanisms of Patisiran and Givosiran in the liver. *Left panel:* Uptake of Patisiran's LNP is mediated by ApoE after intravenous administration. ApoE binds to ApoE-binding cell-surface receptors in the liver and aids in internalization of the LNP. Following endosomal acidification, the siRNA is released into the cytoplasm although the majority of the LNPs are recycled back into circulation using exocytosis [31,32]. *Right panel:* Uptake of Givosiran's GalNAc-siRNA is mediated by the ASGPR after subcutaneous administration. The tri-GalNAc ligand, conjugated to the siRNA, binds the ASGPR leading to receptor-mediated endocytosis. Endosomal acidification results in siRNA release into the cytoplasm and allows the ASGPR to be recycled back to the cell surface [30]. Color images are available online.

Downloaded by GLASGOW UNIVERSITY LIBRARY/Swetsblackwell Inc/ 93868820 from www.liebertpub.com at 10/31/20. For personal use only.

Table 1. Alnylam's RNA Interference Therapeutics Clinical Pipeline

Therapeutic	*Condition*	*Target*	*Delivery platform*	*Status**	*Ref*
ONPATTRO® (Patisiran)	Hereditary ATTR amyloidosis	Transthyretin (TTR)	Lipid nanoparticle (LNP)	Approved[a]	[28]
GIVLAARI® (Givosiran)	Acute hepatic porphyria (AHP)	Aminolevulinic acid synthase 1 (ALAS1)	GalNAc Conjugate	Approved[b]	[29]
Lumasiran (ALN-GO1)	Primary hyperoxaluria type 1 (PH1)	Glycolate oxidase (GO)	ESC-GalNAc Conjugate	NDA and MAA accepted	[38]
Inclisiran (ALN-PCSsc)[c]	Hypercholesterolemia	Proprotein convertase subtilisin kexin type 9 (PCSK9)	ESC-GalNAc Conjugate	NDA and MAA accepted	[39]
Vutrisiran (ALN-TTRsc02)	ATTR amyloidosis	Transthyretin (TTR)	ESC-GalNAc Conjugate	Phase 3 (NCT04153149)	[40]
Fitusiran (ALN-AT3)[d]	Hemophilia and rare bleeding disorders	Antithrombin (AT)	ESC-GalNAc Conjugate	Phase 3 (NCT03549871)	[41]
Cemdisiran (ALN-CC5)	Complement-mediated diseases	Complement component 5 (C5)	ESC-GalNAc Conjugate	Phase 2 (NCT03841448)	
ALN-AAT02/ DCR-A1AT[e]	Alpha-1 liver disease	Alpha-1 antitrypsin (AAT)	ESC+-GalNAc Conjugate	Phase 1/2 (NCT03767829)	
ALN-HBV02 (VIR-2218)[f]	Hepatitis B infection	Hepatitis B virus (HBV) genome	ESC+-GalNAc Conjugate	Phase 1/2 (NCT03672188)	[42]
ALN-AGT	Hypertension	Angiotensinogen (AGT)	ESC+-GalNAc Conjugate	Phase 1 (NCT03934307)	
ALN-HSD[g]	Nonalcoholic steatohepatitis (NASH)	Hydroxysteroid 17-Beta Dehydrogenase 13 (HSD17B13)	ESC+-GalNAc Conjugate	CTA submitted	[43]
ALN-COV (VIR-2703)[h]	COVID-19	SARS-CoV-2 viral genome	ESC combined with a novel conjugate for lung delivery	2020 IND candidate	[44]

*Status as of August 2020.

[a]Approved in the United States and Canada for the treatment of polyneuropathy of hATTR amyloidosis in adults. Approved in the European Union, Switzerland, and Brazil for the treatment of hATTR amyloidosis in adults with stage 1 or 2 polyneuropathy. Approved in Japan for the treatment of TTR-type familial amyloidosis with polyneuropathy.

[b]Approved in the United States and Brazil for the treatment of adults with AHP. Approved in the European Union for the treatment of AHP in adults and adolescents aged 12 and older.

[c]Novartis is leading the development of Inclisiran.

[d]Sanofi Genzyme is leading the development of Fitusiran.

[e]Dicerna is leading and funding the development of ALN-AAT02 and DCR-A1AT and will select which candidate to advance in development.

[f]Developed in collaboration with Vir Biotechnology.

[g]Developed in collaboration with Regeneron.

[h]Developed in collaboration with Vir Biotechnology.

ESC, enhanced stability chemistry; ESC+, enhanced stability chemistry for improved specificity and reduced off-target effects; NDA, new drug application; MAA, marketing authorization application; CTA, clinical trial authorization; IND, investigational new drug.

Downloaded by GLASGOW UNIVERSITY LIBRARY/Swetsblackwell Inc/ 93868820 from www.liebertpub.com at 10/31/20. For personal use only.

drugs (Lumasiran, Inclisiran, Vutrisiran, and Fitusiran) use the ESC-GalNAc design, whereas early-stage development RNAi drugs use the ESC+-GalNAc formulation.

Bioconjugates for RNAi Molecules

Bioconjugation has been widely used as a delivery strategy for RNAi molecules. Some bioconjugates, like lipids and sterols, can increase cellular uptake through natural transport mechanisms. Cholesterol was the first reported conjugate used for systemic siRNA delivery [45] and has been widely used as a direct carrier for RNAi molecules [46–49] and for LNP functionalization [50]. Although many lipids will accumulate in the liver, extrahepatic delivery can be also achieved with some lipid conjugates [51].

Other bioconjugates target cell surface receptors and can be utilized for selective delivery to target cells and tissues. GalNAc has been the most successful conjugate for this purpose, as its target, the ASGPR, is not only highly expressed in hepatocytes but also has a short recycling time (10–15 min) [52,53]. In addition, GalNAc-conjugate activity is retained even after a 50% reduction in ASGPR expression [54]. Because of this, GalNAc conjugation has become the delivery system of choice for hepatocyte targeting and has paved the way for targeting other tissue types using similar strategies. Herein, we focus on folic acid, the synthetic form of folate, which has been investigated as a targeting ligand for delivery to tumor cells using folate receptors (FRs).

Folate and folate transport

Folates are a group of essential B_9 vitamins that play a key role in mammalian one-carbon metabolism. They serve as cofactors in a variety of metabolic reactions and are required for the synthesis of purines, the pyrimidine thymidine, and the amino acids glycine, serine, and methionine [55,56]. Folates are hydrophilic molecules that are polyanionic at physiological pH and therefore cannot readily diffuse through cellular membranes.

Mammals have evolved several systems to transport and uptake folates [57]. The reduced folate carrier (RFC), which is expressed ubiquitously, is the major transport system for folates in mammals and plays a vital role in *in vivo* folate homeostasis [58]. The RFC relies on a bidirectional anion-exchange mechanism to pump folates into the cytoplasm. It has high affinity for reduced folates but poor affinity for oxidized folic acid [59]. The proton-coupled folate transporter (PCFT) functions at low pH and transports folates using a transmembrane proton gradient. The PCFT is the major transport system in the small intestine and is highly expressed at the apical brush-border membrane of the duodenum and the proximal jejunum where folates are absorbed [60]. In addition to this, the PCFT is involved in folate transport into the central nervous system [61].

Finally, the FR is expressed on the cell surface and transports folates and folate conjugates with high affinity [59]. FRs cluster in invaginations of the cell membrane. Once the folate ligand binds, the receptors are internalized as the membrane transiently closes. Inside the cell, the endosome's acidic environment promotes the release of folate from the receptor and into the cytoplasm, allowing the FR to be recycled onto the cell surface [62–64].

There are four known FR isoforms in humans: FRα, FRβ, FRγ, and FRδ encoded by *FOLR1*, *FOLR2, FOLR3,* and *FOLR4,* respectively. Out of these, the α, β, and δ isoforms are glycosylphosphatidylinositol (GPI)-anchored receptors, whereas the γ isoform is a soluble protein found only in hematopoietic cells [64–66]. FR-δ has been found on ova and regulatory T cells [67]. Notably, FRα and FRβ share ~70% homology and similar affinities for folic acid, but they have different tissue distribution [68]. FRα is the most widely expressed and studied isoform in humans. This isoform has minimal physiological roles after embryogenesis and thus is expressed at low levels in most nonmalignant tissues. The expression of FRα is restricted to tissues involved in folate resorption or embryonic development, including placenta, kidney, lung, breast, fallopian tubes, and choroid plexus tissues [69–72], whereas FRβ is expressed on activated myeloid cells involved in inflammatory and autoimmune diseases [73,74].

FRα Targeting in Oncology

FRα is highly expressed on numerous cancerous tumors, including 90% of ovarian carcinomas, as well as breast, endometrial, lung, brain, and kidney cancers [71,72]. Due to its low expression in nonmalignant tissues and high affinity for folic acid (K_d < 1 nM), FRα has become an important biomarker in oncology and has been exploited for cancer diagnostics and therapeutics. Folate is a small nonimmunogenic molecule. It is inexpensive and stable over a wide range of pH values and temperatures [75].

Structural and mutational analyses have shown that the pteridine moiety of folate is required for receptor binding, whereas the glutamate moiety is available for conjugation (Fig. 3) [72]. Folate conjugates are recognized and internalized by FRα, making folate a promising ligand for tumor targeting. In 1991, Leamon and Low described the use of folate conjugation to deliver macromolecules through FRs [76], and numerous clinical applications of FRα targeting have been described since (Fig. 4). Table 2 summarizes key FRα-targeted conjugates that have been investigated in clinical trials.

Immunotherapy

Immunotherapy approaches that target FRα include chimeric antigen receptor (CAR) T cells [77–81] and vaccines [82–84]. Several monoclonal antibodies (mAbs) have also been studied. A notable example is farletuzumab (MORab-003), a fully humanized immunoglobulin G1 (IgG1) antibody that targets FRα. Farletuzumab is thought to induce cell death through various modes of action, including antibody-dependent

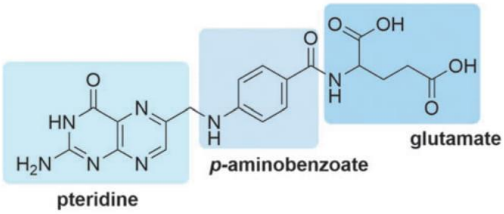

FIG. 3. Chemical structure of folate. Folate is composed of a pteridine ring, *p*-aminobenzoate, and a glutamic acid tail. The pteridine ring is docked deep inside of the folate receptor binding pocket, whereas the glutamate moiety is solvent exposed and is thus available for conjugation. Color images are available online.

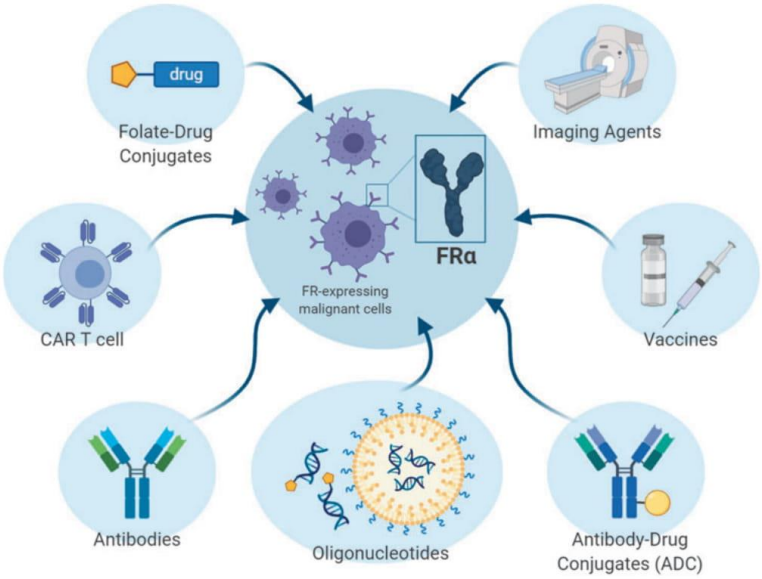

FIG. 4. Overview of the clinical applications of FRα-targeting in oncology. The FRα is an important cancer biomarker and has been targeted for cancer diagnostics and therapies. Delivery of cytotoxic drugs to cancer cells through FRα can be achieved by conjugation of the drug to a folate ligand to form a folate–drug conjugate. Imaging agents can detect FRα-expressing tumors and serve as companion diagnostics for FRα-targeting therapeutics. Immunotherapy approaches include CAR T cells, vaccines, antibodies, and ADC. Oligonucleotides have been conjugated to folate or encapsulated in folate-functionalized delivery vehicles to target cancer cells. ADC, antibody–drug conjugate; CAR, chimeric antigen receptor; FRα, folate receptor α. Color images are available online.

Downloaded by GLASGOW UNIVERSITY LIBRARY/Swetsblackwell Inc/ 93868820 from www.liebertpub.com at 10/31/20. For personal use only.

cellular cytotoxicity, complement-dependent cytotoxicity, sustained tumor cell autophagy, and inhibition of FOLR1 and Lyn kinase association [85–89]. Farletuzumab has been evaluated in several phase I and II trials [90–94], as well as in a double-blind, randomized phase III study in patients with platinum-sensitive recurrent ovarian cancer [95]. In this phase III trial, the efficacy of farletuzumab in combination with the anticancer drug carboplatin and a taxane was compared to carboplatin/taxane alone but the study's primary progression-free survival (PFS) end point was not met [95]. However, PFS improvements were reported in some patient subgroups after treatment with higher doses of farletuzumab [96].

Another example is MOv18 IgG1, a murine monoclonal antibody, which was generated by vaccinating mice with human ovarian carcinoma cells [97]. A chimeric version of MOv18 IgG1 was later engineered [98], and its safety in patients with ovarian cancer was evaluated in a phase I study [99]. A chimeric IgE antibody (Mov18 IgE) targeting the FRα [100,101], as well as several radiolabeled forms of the MOv18 IgG1 [102–106], has also been investigated.

Anti-FRα antibodies can also be conjugated to cytotoxic drugs to yield antibody–drug conjugates (ADCs) [107,108]. One example is mirvetuximab soravtansine (IMGN853), a conjugate of the maytansinoid DM4, a potent cytotoxic agent, and a FRα-binding monoclonal antibody. The safety and efficacy of this ADC were evaluated in phase I trials either alone [109] or in combination with carboplatin [110]. A randomized, multicenter phase III trial (FORWARD I) compared mirvetuximab soravtansine treatment to other chemotherapeutic drugs (topotecan, paclitaxel, pegylated liposomal doxorubicin) in patients with FRα-positive platinum-resistant epithelial ovarian cancer, primary peritoneal cancer, or fallopian tube cancer [111]. However, this trial did not meet the PFS primary end point in the intention-to-treat and high-FRα populations [112]. A repeat phase III trial is currently recruiting patients with ovarian, primary peritoneal, or fallopian tube cancer whose tumors express a high level of FRα (ClinicalTrials.gov Identifier: NCT04209855).

Imaging agents

FRα-targeted imaging agents have been used as a diagnostic tool to assess the severity of FRα-positive cancers. This includes magnetic resonance contrast agents [113–117], optical imaging agents [118–120], and radioimaging agents [121]. In a phase I/II clinical study, ^{111}In-diethylenetriaminepentaacetic acid (DTPA) folate was evaluated for diagnosis of ovarian malignancy in 35 women [122]. Most patients either had a pathologically proven malignancy or suspected case of new ovarian cancer. ^{111}In-DTPA-folate exhibited rapid target-tissue uptake and nontarget-tissue clearance. However, its use in human imaging was eventually suspended due to high costs in addition to the long half-life of ^{111}In ($\sim$68 h) [121].

Another notable imaging agent is ^{99m}Tc-etarfolatide, a peptide derivative of folic acid designed to coordinate ^{99m}Tc. This radioisotope is more cost-effective and has a much shorter half-life ($\sim$6 h) than ^{111}In [123]. In preclinical studies, ^{99m}Tc-etarfolatide predominantly accumulated in FRα-positive tumor and kidney tissues. It was also found to be removed rapidly from circulation and excreted into the urine [124,125]. Given these findings, ^{99m}Tc-etarfolatide has been evaluated in several clinical trials as a companion diagnostic imaging agent to identify tumors that express FRα and that may respond to FRα-targeted therapies [126,127].

More recently, folate has been conjugated to fluorescent dyes for use in image-guided surgery. Van Dam *et al.* reported real-time intraoperative imaging of ovarian cancer cells using a folate-fluorescein isothiocyanate (FITC) conjugate [128]. Cancer surgery highly relies on visual inspection and palpation to discriminate between malignant and

Downloaded by GLASGOW UNIVERSITY LIBRARY/Swetsblackwell Inc/ 93868820 from www.liebertpub.com at 10/31/20. For personal use only.

Table 2. Key Clinical Folate Receptor α-Targeted Conjugates

Immunotherapy				
Name	*Description*	*Mode of action*	*Condition*	*Key clinical trials*
Farletuzumab (MORab-003)	Fully humanized monoclonal antibody targeting FRα	Various. All induce cell death.	NSCLC, ovarian cancer	Phase I & II [90–94] Phase III [95]
MOv18 IgG	Murine monoclonal antibody targeting FRα	Immune-mediated tumor cell death	Ovarian cancer	Phase I [99]
MOv18 IgE	Chimeric IgE antibody targeting FRα	Immune-mediated tumor cell death	FRα+ advanced tumors	Phase I: Recruiting (NCT02546921)
Mirvetuximab soravtansine (IMGN853)	Maytansinoid DM4 with FRα-binding monoclonal antibody	Induces cell-cycle arrest and cell death	Ovarian cancer	Phase I [109,110] Phase III [111] Phase III: Recruiting (NCT04209855)
Imaging agents				
Name	*Description*	*Application*	*Condition*	*Key clinical trials*
^{111}In-DTPA-folate	Radiolabeled imaging agent	Diagnostic agent	Ovarian cancer	Phase I/II [122]
^{99m}Tc-etarfolatide	Radiolabeled imaging agent	Companion agent (preselection of patients with FRα+ tumors)	Epithelial cancers (ovarian, breast, endometrial, NSCL)	Phase II [127]
EC17 (Folate-FITC)	Fluorescent imaging agent	Intraoperative cancer imaging	Ovarian cancer	Phase I (NCT02000778)
Pafolacianine sodium (OTL38)	Near infrared dye	Intraoperative cancer imaging	Various cancer (endometrial, ovarian, pituitary, NSCL)	Phase II [133] Phase III: First Patient Recruited
Folate–drug conjugates				
Name	*Description*	*Mode of action*	*Condition*	*Key clinical trials*
Vintafolide (EC145)	Folate-DAVLBH conjugate	DAVLBH prevents microtubule formation and leads to cell death	FRα+ tumors	Phase I & II [136–138]
EC0489	Folate-DAVLBH conjugate with a modified linker	DAVLBH prevents microtubule formation and leads to cell death	Solid Tumors	Phase I (NCT00852189)
EC0225	Folate conjugated to DAVLBH and mitomycin C	Inhibits DNA synthesis, mitosis, and microtubule formation	Solid Tumors	Phase I (NCT00441870)
EC1456	Folate-tubulysin conjugate	Inhibits mitosis and tubulin formation	NSCLC, TNBC, ovarian cancer	Phase I (NCT01999738)

NSCLC, nonsmall cell lung cancer; DAVLBH, desacetylvinblastine monohydrazide; TNBC, triple-negative breast cancer.

healthy tissues. Folate-FITC (EC17) was able to detect ovarian cancer lesions that were otherwise not detectable by inspection or palpation. However, autofluorescence led to false-positive lesions in ovarian cancer [129]. Infrared dyes, on the contrary, display less autofluorescence and have deeper tissue penetration compared to fluorescein. Pafolacianine sodium (formerly OTL38), another prominent folate-conjugated imaging agent, contains a near-infrared cyanine dye and has been investigated for intraoperative detection of several cancer types, including endometrial [130], nonsmall cell lung cancer [131], and pituitary adenomas [132]. On Target Laboratories, Inc., completed two Phase II clinical trials of pafolacianine sodium for intraoperative imaging of ovarian (ClinicalTrials.gov Identifier: NCT02317705) [133] and lung cancer lesions (ClinicalTrials.gov Identifier: NCT02872701), respectively. In July 2020, On Target

Downloaded by GLASGOW UNIVERSITY LIBRARY/Swetsblackwell Inc/ 93868820 from www.liebertpub.com at 10/31/20. For personal use only.

Laboratories, Inc., enrolled the first patient in a Phase III clinical trial (ELUCIDATE) to further evaluate the safety and efficacy, as well as the tolerability of pafolacianine sodium, in patients with lung cancer [134].

Folate–drug conjugates

One of the most notable folate–drug conjugates is vintafolide (EC145), a derivative of desacetylvinblastine monohydrazide (DAVLBH) conjugated to folate through a peptide spacer and a disulfide linker. DAVLBH is a vinca alkaloid that inhibits cell division and induces cell death by disrupting the formation of the mitotic spindle [135]. Vintafolide has been tested in various phase I and II trials with promising results [136–138]. However, a phase III randomized controlled trial (PROCEED) was suspended in 2014 due to failure to meet the prespecified outcome of PFS [139]. This trial evaluated the safety and efficacy of the combination of vintafolide and pegylated liposomal doxorubicin. Several other folate–drug conjugates have been studied as well, including EC0489 (a vintafolide analog) [140,141], EC0225 (a vinca alkaloid and mitomycin conjugate linked to folate) [142], and EC1456 (a folate-tubulysin conjugate) [143].

Gene and antisense therapy

Several FR-targeting viral and nonviral vectors for gene therapy have been reported [144–148]. Nonviral vectors include cationic polymers and liposomes [149]. Folate is either linked indirectly through a polyethylene glycol (PEG) spacer or directly to a component of the polymer or lipid [149]. Formulations of FR-targeting polyplexes have used chitosan [150], polyethylenimine (PEI) [151], poly-L-lysine (PLL) [152–154], and combinations of PEG with PEI [151,155] and PLL [153]. In addition, several FR-targeting liposomes have been used in gene therapy [156–160].

This FR-mediated delivery strategy has also been used with antisense oligonucleotides [161–163]. In one study, Lee and Low (1997) reported the use of folate-functionalized liposomes as a delivery vehicle for fluorescently-tagged antisense oligonucleotides, targeting the epidermal growth factor receptor (EGFR), in KB cells (a contaminant of the human cervical cancer cell line HeLa) [164]. The uptake of antisense oligonucleotides encapsulated in the folate liposome was 16-times higher than the control and could be inhibited by addition of 1 mM free folic acid. After 48 h, these antisense oligonucleotides reduced KB cell proliferation by more than 90%.

More recently, Leamon *et al.* reported the folate liposome-mediated delivery of antisense oligodeoxynucleotides (ODNs) [165]. This formulation was tested in KB xenograft nude mice models after intravenous injection and compared to a non-targeted PEG-containing control. Results show a $\sim$1.8-fold increase in liver uptake of the folate liposomes compared to the control. However, there was no significant uptake in tumors despite previous reports of *in vitro* uptake in FR-expressing cells.

Folate-Mediated Delivery of RNAi Molecules

With the success of the receptor-targeting ligand GalNAc and the need for selective extrahepatic RNAi delivery systems, folate has gained a lot of attention as a targeting ligand due to its relevance in oncology. Folate has been mostly used to functionalize delivery vehicles although recent applications have attempted to directly conjugate folate to siRNA and miRNA molecules. This section will highlight key studies in this field and discuss some of the limitations of these delivery approaches.

Packaging siRNAs into folate-functionalized vehicles

Nanoparticle and liposome-based vehicles have been widely used to deliver RNAi molecules into cells. Functionalization of these vehicles with folate for targeted delivery to cancer cells has been reported in several studies with varying results [166–171].

In 2008, Hattori's group reported the synthesis of folate-functionalized LNPs to deliver siRNAs, targeting human EGFR (*Her-2*), to KB cells [172]. *Her-2* is overexpressed in several cancers and is usually associated with poor prognosis [173,174]. Treatment with folate nanocomplexes of anti-Her-2 siRNA decreased cell growth and inhibited the expression of Her-2 *in vitro*. This delivery system was also investigated *in vivo* in male BALB/c *nu/nu* mice bearing KB tumor xenografts. Intratumoral injection of Her-2 siRNA nanoplexes led to reduced tumor growth. This study proposed conditions for the formation of folate-linked nanoplexes, but further *in vivo* studies are required to assess their safety and efficacy. A comparison between systemic and local delivery would be beneficial, as intratumoral delivery can be impractical for the treatment of certain tumors [175].

As discussed earlier, a major barrier for efficient siRNA delivery is the successful release of siRNA from endosomes. Many strategies have been investigated over the years to promote endosomal escape, such as the use of cationic lipids in lipoplex formulations [176]. Hattori's group recently reported the preparation of cationic liposomes for siRNA delivery [177,178] in addition to three types of folate-PEG liposomes [179]. This last study revealed that the type of cationic lipid used may impact the optimal formulation ratio of folate-poly(ethylene glycol)-distearoylphosphatidylethanolamine (PEG_{2000}-DSPE). Notably, formulations with longer PEG chains inhibited cellular uptake of lipoplexes. This is consistent with previous reports that PEG lipids can hinder membrane destabilization, thus decreasing cellular internalization [180].

Once the formulations were optimized, they were tested in KB cells and were able to suppress target enhanced green fluorescent protein (EGFP) and PLK1. Interestingly, intratumoral injections of these folate-PEG lipoplexes in female BALB/c *nu/nu* mice did not lead to a significant inhibition of tumor growth compared to the control siRNA. This lack of correlation between *in vitro* and *in vivo* outcomes suggests that the formulation of these nanoparticle-based delivery systems needs to be optimized and validated for *in vivo* use, posing a major challenge for the development of folate-functionalized vehicles.

Wagner's group reported similar limitations with their defined folate-PEG siRNA conjugates and polyplexes in 2017 [181]. In this study, a folate-PEG-azide ligand was prepared by solid phase peptide chemistry and was later conjugated to an siRNA bearing an alkyne (hexynyl-ss-C_6) at the sense strand 5′-end. KB/eGFP-Luc cells were able to internalize the folate-PEG-siRNAs, and the uptake could be inhibited by the addition of free folic acid. Nevertheless, these siRNAs did not result in gene-silencing activity due to a lack of endosomal escape functionality. To overcome this, the folate-PEG-siRNA was combined with a monodisperse polycationic carrier to build polyplexes. The carrier was composed of three arms, each

Downloaded by GLASGOW UNIVERSITY LIBRARY/Swetsblackwell Inc/ 93868820 from www.liebertpub.com at 10/31/20. For personal use only.

made up of three succinoyl-tetraethylenepentamine (Stp) units linked by a branching lysine, as well as a cysteine group at each terminus. In this formulation, the proton sponge effect of the carrier's PEI-like 1,2-diaminoethane units can help mediate endosomal escape. The efficacy of these siRNA polyplexes was tested in KB/eGFP-Luc cells. These newly-formulated targeted polyplexes were able to induce significant reporter gene silencing compared to nontargeted and unconjugated controls. This study reports that maximal knockdown was achieved with formulations of 5% folate-PEG-siRNA, highlighting the importance of optimizing formulations for uptake, endosomal escape, and intracellular activity.

Endosomal escape functionality has proven to be an important factor for the formulation of delivery vehicles. However, recent studies suggest that siRNA stability may be equally important. Kataoka and Wagner's groups recently reported the synthesis of targeted siRNA lipopolyplexes, made by co-formulations of a PEGylated folate-equipped oligomer, one of three lipo-oligomers, and siRNA [182]. Three formulations were investigated *in vitro*: TLP1 (a tyrosine-modified oleic acid-based oligomer), TLP2 (a tyrosine-free analog of TLP1), and TLP3 (a linoleic acid-based oligomer).

Translocation profiles of siRNAs from late endosomes to cytosol showed that TLP2 and TLP3, the tyrosine-free formulations, displayed earlier endosomal escape compared to TLP1. All TLPs also displayed similar physiochemical properties. Nevertheless, the intracellular stability of siRNAs in each formulation differed significantly. Despite early endosomal escape functionality, siRNAs in TLP2 and TLP3 were less stable than in TLP1. TLP1 also mediated the best gene-silencing effect and was chosen for further *in vivo* studies in NMRI *nu/nu* mice bearing subcutaneous leukemic (L1210) tumors. After intravenous administration, TLP1 downregulated distant FR-directed tumoral EG5 expression by 65% without adverse side effects. The ability of oligonucleotides to escape intracellular endosomes has been a major challenge in the development of effective delivery vehicles. Nevertheless, this study suggests that, for this system, siRNA stability was more significant for gene silencing efficacy than the ability to escape the endosome early.

Altogether, these findings enhance our knowledge and provide a foundation for effective vehicle design. An ideal delivery vehicle should display efficient tissue penetration and cell uptake, provide endosomal escape functionality, be nontoxic and nonimmunogenic, and increase the stability and efficacy of the siRNA and miRNA molecules. Although some progress has been made, there are still some significant limitations associated with some of these delivery vehicles.

Nanoparticle-based delivery is usually limited to clearance organs and requires intravenous administration. The large size of these delivery vehicles can also impede penetration into solid tumors [183], further limiting the tissues that could be targeted. In addition, about 70% of the siRNA internalized by these vehicles will undergo exocytosis [184] and only a small percentage (1–2%) of the total administered siRNA is released into the cytosol [185]. Many cationic polymers and liposomes also display high toxicity *in vivo*, hindering their clinical applications [186].

Conjugating siRNAs to folate

Direct conjugation of folate or folate derivatives to siRNA and miRNA can help overcome some of the limitations associated with delivery vehicles by improving targeted delivery without the added cytotoxic effects. Unfortunately, the use of folate conjugates in RNAi research has been limited by sophisticated, and often expensive, chemistry. Folate has poor solubility in most organic solvents, apart from DMSO, making it difficult to separate and purify folate conjugates. In addition, direct conjugation to folate usually leads to a mixture of α- and γ-isomers due to the presence of two carboxylic acid groups in the glutamate moiety [187].

Folate phosphoramidites are not commercially available, and there is a lack of reliable protocols for their synthesis. It should be noted that Berry & Associates offered a 5′-folate-triethylene glycol (TEG) cyanoethyl phosphoramidite (BA 0349) in the past (around 2011) at a cost of $843 USD for 100 μmol, but the product has been discontinued and there are no reports using this molecule. Despite this, there have been successful syntheses preparing folate-conjugated RNAi molecules without the use of a folate phosphoramidite (Fig. 5).

One of the most well-known attempts to directly conjugate folate to siRNAs was reported by Low's group in 2009 [188]. Folate-conjugated siRNAs were tagged with the fluorophore DY647, and cellular uptake studies were performed in FR-positive RAW264.7 cells. Although these cells were able to internalize folate-siRNA conjugates, further *in vitro* studies indicated that these siRNAs accumulated in intracellular endosomes.

To test the biodistribution of folate-siRNAs *in vivo*, *nu/nu* mice bearing KB tumor xenografts were injected retro-orbitally with DY647-labeled folate-siRNAs. Results showed significantly higher tumor accumulation with folate-conjugated siRNAs compared to the control. This was followed by *ex vivo* organ imaging, which showed little accumulation of folate siRNAs in healthy tissues (liver, spleen, intestine, muscle, lung, heart, and blood) but high accumulation in the tumor site. This study demonstrated the selective delivery of folate-siRNAs to FR-positive tumors both *in vitro* and *in vivo*, showcasing the potential of FR-targeted RNAi molecules as cancer therapeutics. However, it also revealed a lack of endosomal escape functionality, which must be addressed before this system can be fully exploited for targeted delivery to cancer cells.

In 2008, Zhang *et al.* reported a new strategy to synthesize folate-conjugate siRNAs [189]. In this system, a 17-nucleotide ODN, with a 5′ folate molecule, was used to tether the siRNA through noncovalent interactions. The ODN sequence was randomly chosen and does not code for any known human mRNA. The folate-ODN siRNAs (F-ODN:siRNAs) targeted either αV integrin, which plays an important role in angiogenesis, or survivin, an apoptosis inhibitor.

The gene-silencing activity of these F-ODN:siRNAs was assessed *in vitro* in the FR-expressing cell lines human umbilical vein endothelial cells (HUVECs) and KB. F-ODN:αV siRNA treatment resulted in $\sim$80% inhibition of αV mRNA expression but no inhibition of the nontargeted control. In addition, gene-silencing activity of the survivin siRNA (F-ODN:Sur siRNA) was observed in both cell lines, but to a much lower extent in HUVECs. Since siRNA treatment can lead to immune activation, the expression of interferon-β (IFN-β) in HUVECs was measured, resulting in no significant increase in IFN-β mRNA expression after treatment. Overall, these F-ODN:siRNA complexes led to specific cellular uptake and silencing activity *in vitro*. There are many advantages to this synthetic approach. The preparation of these molecules is simple and cost-effective preparation,

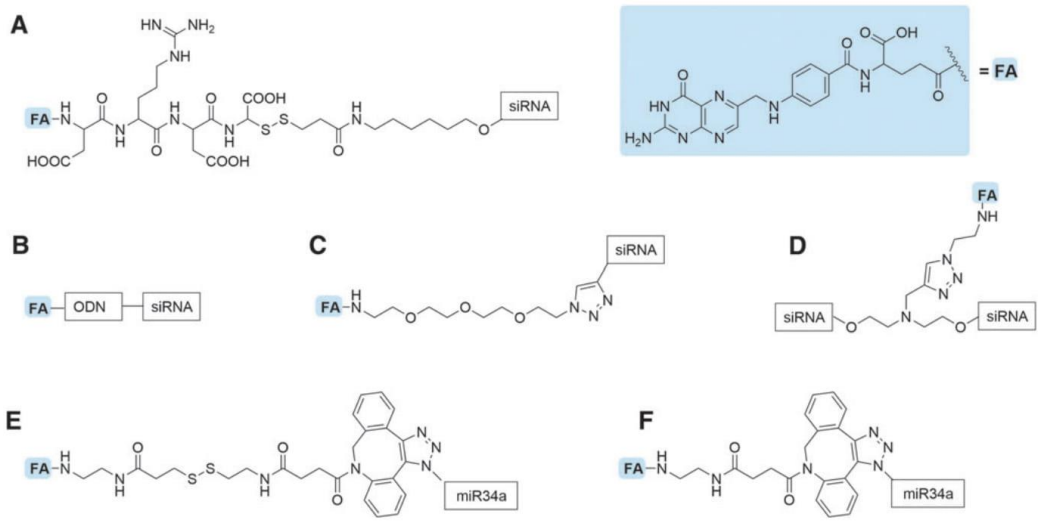

FIG. 5. Chemical structures of key folate linkers conjugated to siRNA and miRNA molecules. **(A)** *Low group:* 5′ folate-conjugated siRNA synthesized [188]. **(B)** *Huang group:* siRNA tethered to an oligodeoxynucleotide (ODN) tagged with folate at the 5′ [189]. **(C)** *Carell group:* 3′ folate-conjugated siRNA prepared by Cu(I)-catalyzed azide-alkyne cycloaddition (CuAAC) [190]. **(D)** *Desaulniers group:* folate spacer incorporated in the central region of the siRNA sense strand through CuAAC [191]. **(E)** *Kasinski group:* 5′ folate conjugated miR34a through a releasable (S-S) linker using Cu-free azide-alkyne cycloaddition. **(F)** *Kasinski group:* 5′ folate conjugated miR34a through an unreleasable linker using Cu-free azide-alkyne cycloaddition. Color images are available online.

Downloaded by GLASGOW UNIVERSITY LIBRARY/Swetsblackwell Inc/ 93868820 from www.liebertpub.com at 10/31/20. For personal use only.

allowing for large-scale production. In addition, a single conjugated ODN can simultaneously deliver multiple siRNAs to the target tissue, and ODNs and siRNAs can also be modified to enhance their pharmacokinetic profiles. Despite the potential of ODN:siRNAs, *in vivo* studies are required to assess their safety and efficacy for future clinical application.

A more popular approach to prepare folate-siRNA conjugates relies on a Cu(I)-catalyzed azide-alkyne cycloaddition (CuAAC) reaction. In 2012, Carell's group described the synthesis of siRNA conjugated to various derivatives, including folate, using CuAAC click chemistry [190]. This study reported the elaborate synthesis of an azidofolate derivative, from a protected glutamic acid derivative, and an amino-azide tetraethyleneglycol derivative, which was then reacted with a 3′ alkyne-modified oligonucleotide in solution.

Cellular uptake of the resulting folate-siRNAs, bearing a fluorescein label on the antisense strand, was assessed in FR-expressing HeLa cells using confocal microscopy. As expected, folate-modified siRNAs were readily taken up by HeLa cells, whereas the unmodified siRNA controls were not. Folate-siRNAs induced dose-dependent knockdown of target *Renilla* luciferase in HeLa cells although only 50% knockdown was reported after 1 μM siRNA treatment, the highest concentration tested. Nevertheless, this click chemistry synthetic approach could be further used and optimized for the preparation of folate-siRNA conjugates, which are notoriously challenging to access.

In 2020, the Desaulniers group reported a simpler CuAAC approach to prepare folate-siRNA conjugates [191]. The azidofolate derivative used in this study was synthesized and purified in a single step by conjugating folic acid to 2-azidoethanamine. A propargyl phosphoramidite was synthesized over three steps and was used for solid phase oligonucleotide synthesis. The propargyl modification was then incorporated at a different position within the sense strand, including the central region. Some reports show that thermal destabilization of the siRNA central region can lead to increase in silencing activity [192], yet this region had not been modified with folic acid before this study. Propargyl-modified oligonucleotides were conjugated to the azidofolate derivative through a CuAAC reaction in solution, and the resulting folate siRNAs were tested *in vitro* in FR-positive HeLa cells and FR-negative HT-29 cells.

Notably, centrally-modified siRNAs displayed enhanced gene-silencing potency in HeLa cells (~80% knockdown after 0.75 μM treatment) compared to their 3′-modified counterparts (~40–65% knockdown after 0.75 μM treatment). Further studies targeted the endogenous gene *Bcl-2*, an antiapoptotic gene overexpressed in ~70% of cancers. HeLa cells, which express *Bcl-2*, were treated with a centrally modified folate siRNA, resulting in ~70% Bcl-2 knockdown after 1 μM treatment. Overall, this study showed that potent siRNA activity can be achieved *in vitro* with centrally modified folate-siRNAs, providing a novel way to boost gene silencing activity for further RNAi applications although the results need to be validated in *in vivo* studies.

In addition to siRNAs, the synthesis of folate-miRNA conjugates (called FolamiRs) was recently reported by the Kasinski group [193]. Folate-ethylenediamine (folate-EDA) was prepared in a peptide synthesis vessel and was used for

Downloaded by GLASGOW UNIVERSITY LIBRARY/Swetsblackwell Inc/ 93868820 from www.liebertpub.com at 10/31/20. For personal use only.

the synthesis of folate-dibenzocyclooctyne (folate-DBCO) conjugates, either bearing or lacking a reducible disulfide linkage (SS), which were then conjugated to the sense strand 5′ end. In FR-positive MDA-MB-231 (breast cancer) cells, both FolamiR-34a and FolamiR-SS-34a were able to reduce *Renilla* activity. FolamiR-34a was more stable than its unconjugated counterpart, miR-34a, suggesting that the folate conjugate could provide some protection against serum nucleases.

This study also investigated the activity of FolamiR, tagged with a near infrared dye (NIR), *in vivo* using animals with MB-231 sensor cell xenografts. A single dose of each NIR-FolamiR (with a releasable or unreleasable linker) was delivered through tail vein injection. NIR-FolamiRs were mostly retained in tumors and cleared from other tissues. However, only the unreleasable NIR-FolamiR was able to induce gene silencing. One explanation for this is that the releasable formulation was found to be highly unstable in serum, whereas the unreleasable formulation was stable for over 6 h.

Another *in vivo* study tested the specificity of FolamiR-34a in nude mice with FR-expressing cells engrafted on the right shoulder and FR-deficient cells engrafted on the left shoulder. After intravenous administration, FolamiRs accumulated in the FR-positive tumor. Further studies revealed that FolamiR-34a treatment could reduce tumor growth in MB-231 xenograft animals without evidence of whole-organ toxicity or immune activation. FolamiR treatment was effective in an immunocompetent aggressive mouse model. In addition to this, a folate-conjugated siRNA (siLuc2) was able to reduce target firefly luciferase activity in MDA-MB-231 cells, demonstrating that this system is applicable to other small RNAs.

Recently, Kasinski and Low reported a novel strategy to promote endosomal release of folate-RNA conjugates, including FolamiRs, using nigericin [194]. This strategy exploits the difference in solute concentration between the cytoplasm, which is rich in potassium ions, and the early endosome, which is rich in sodium ions. Upon internalization, nigericin gets cleaved from the folate carrier. It then localizes to the endosomal membrane where it can exchange potassium and water for an osmotically inactive proton without compensatory sodium release. This causes an osmotic differential that then leads to endosomal swelling and bursting, facilitating the escape of miRNA and siRNA molecules into the cytoplasm.

The evidence presented in this study shows that this nigericin-folate delivery system facilitates endosomal escape, increases RNA availability in the cytoplasm, and improves RNAi activity. Nigericin is nontoxic at the tested doses and is simple to conjugate to small RNAs, making it a good candidate for clinical applications. Although this system needs to be validated *in vivo,* it offers a promising solution to the endosomal entrapment challenge that could finally enable the shift of FR-targeted RNAi therapeutics from bench to clinic.

Summary and Conclusions

The lack of safe and effective delivery systems for RNAi molecules has been a major challenge in the development of RNAi therapeutics. After decades of research, GalNAc-conjugated siRNAs have emerged as a simple solution to this delivery issue. GalNAc targets the ASGPR, which is expressed at high levels in hepatocytes, allowing for selective delivery to the liver. While the rapid turnover and recycling time of ASGPRs have contributed to the success of GalNAc siRNAs, the lessons learned with this receptor-targeting approach could be applicable for the development of extrahepatic delivery systems.

Folate has gained a lot of interest due to its high affinity for the FRα, an important biomarker in oncology, and has been investigated for the delivery of RNAi molecules to FRα-expressing tumors. There are two main FR-targeting approaches. The most common approach involves packaging siRNAs into folate-functionalized vehicles such as liposomes and polyplexes. Although there have been some promising results from *in vitro* and *in vivo* studies, delivery vehicles can impede uptake into solid tumors due to their large size. In addition, delivery vehicles often display high toxicity *in vivo*, which can limit their clinical applications.

Another approach involves the direct conjugation of folate to RNAi molecules to avoid the negative side effects associated with delivery vehicles. Surprisingly, despite the great potential of folate-conjugated RNAi molecules, only a few studies have been reported. Part of the limitation is attributed to the sophisticated and often expensive chemistry required for their synthesis and the lack of reliable methods to prepare folate phosphoramidites.

More recently, synthetic approaches based on click chemistry have been used to prepare folate-conjugated siRNA and miRNA molecules with great success in various *in vitro* and *in vivo* studies. However, several *in vivo* studies have reported siRNA and miRNA entrapment in intracellular endosomes. As discussed earlier, endosomal entrapment is the rate-limiting step when it comes to the delivery of RNAi molecules yet there are few research efforts focused on the development of folate delivery vehicles with endosomal escape functionality. More resources need to be put into the development of simple and cost-effective folate conjugates for RNAi research to allow for further investigation of these *in vivo* effects, as well as the delivery mechanism. If the synthesis of folate conjugates can be streamlined and the endosomal entrapment challenge can be addressed, these types of molecules have the potential of contributing to the next generation of RNAi therapeutics.

Acknowledgment

Illustrations were created with Biorender.

Author Disclosure Statement

No competing financial interests exist.

Funding Information

No funding was received for this article.

References

1. Hannon GJ. (2002). RNA interference. Nature 418:244–251.
2. Ameres SL and RS Javier Martinez. (2007). Molecular basis for target RNA recognition and cleavage by human RISC. Cell 130:101–112.
3. Gredell JA, MJ Dittmer, M Wu, C Chan and SP Walton. (2010). Recognition of siRNA asymmetry by TAR RNA binding protein (TRBP). Biochemistry 49:3148–3155.

Downloaded by GLASGOW UNIVERSITY LIBRARY/Swetsblackwell Inc/ 93868820 from www.liebertpub.com at 10/31/20. For personal use only.

4. Matranga C, Y Tomari, C Shin, DP Bartel and PD Zamore. (2005). Passenger-strand cleavage facilitates assembly of siRNA Into Ago2-containing RNAi enzyme complexes. Cell 123:607–620.
5. Yi R, Y Qin, IG Macara and BR Cullen. (2003). Exportin-5 mediates the nuclear export of pre-microRNAs and short hairpin RNAs. Genes Dev 17:3011–3016.
6. Fabian MR and N Sonenberg. (2012). The mechanics of miRNA-mediated gene silencing: a look under the hood of miRISC. Nat Struct Mol Biol 19:586–593.
7. Ha M and VN Kim. (2014). Regulation of microRNA biogenesis. Nat Rev Mol Cell Biol 15:509–524.
8. van den Berg A, J Mols and J Han. (2009). RISC-Target Interaction: cleavage and translational suppression. Biochim Biophys Act 1779:668–677.
9. Curtis CD and AM Nardulli. (2014). Using RNA interference to study protein function. Methods Mol Biol 505: 187–204.
10. Dana H, GM Chalbatani, H Mahmoodzadeh, R Karimloo, O Rezaiean, A Moradzadeh, N Mehmandoost, F Moazzen, A Mazraeh, *et al.* (2007). Molecular mechanisms and biological functions of siRNA. Int J Biomed Sci 13:48–57.
11. Rythe RCC, AS Flynt, JAP III and JG Patton. (2004). siRNA therapeutics: big potential from small RNAs. Gene Ther 12:5–11.
12. Alvarez JP, I Pekker, A Goldshmidt, E Blum, Z Amsellem and Y Esheda. (2006). Endogenous and synthetic MicroRNAs stimulate simultaneous, efficient, and localized regulation of multiple targets in diverse species. Plant Cell 18:1134–1151.
13. Elbashir SM, J Harborth, W Lendeckel, A Yalcin, K Weber and T Tuschl. (2001). Duplexes of 21-nucleotide RNAs mediate RNA interference in cultured mammalian cells. Nature 411:494–498.
14. Haussecker D. (2014). Current issues of RNAi therapeutics delivery and development. J Controll Release 195: 49–54.
15. Hall AHS, J Wan, A Spesock, Z Sergueeva, BR Shaw and KA Alexander. (2006). High potency silencing by single-stranded boranophosphate siRNA. Nucleic Acids Res 34: 2773–2781.
16. Kanasty R, JR Dorkin, A Vegas and D Anderson. (2013). Delivery materials for siRNA therapeutics. Nat Mater 12: 967–977.
17. Chiu Y-L and TM Rana. (2003). siRNA function in RNAi: a chemical modification analysis. RNA 9:1034–1048.
18. Tatiparti K, S Sau, SK Kashaw and AK Iyer. (2017). siRNA Delivery Strategies: a comprehensive review of recent developments. Nanomaterials (Basel) 7:77.
19. Whitehead KA, R Langer and DG Anderson. (2009). Knocking down barriers: advances in siRNA delivery. Nat Rev Drug Discov 8:129–138.
20. Xie FY, MC Woodle and PY Lu. (2006). Harnessing in vivo siRNA delivery for drug discovery and therapeutic development. Drug Discov Today 11:67–73.
21. Johannes L and M Lucchino. (2018). Current challenges in delivery and cytosolic translocation of therapeutic RNAs. Nucleic Acid Ther 28:178–193.
22. Juliano R, J Bauman, H Kang and X Ming. (2009). Biological barriers to therapy with antisense and siRNA oligonucleotides. Mol Pharm 6:686–695.
23. Sehgal A, A Vaishnaw and K Fitzgerald. (2013). Liver as a target for oligonucleotide therapeutics. J Hepatol 59: 1354–1359.
24. Vocelle D, C Chan and SP Walton. (2019). Endocytosis Controls siRNA Efficiency: implications for siRNA delivery vehicle design and cell-specific targeting. Nucleic Acid Ther 30:22–32.
25. Hu Y-B, EB Dammer, R-J Ren and G Wang. (2015). The endosomal-lysosomal system: from acidification and cargo sorting to neurodegeneration. Transl Neurodegener 4: 18.
26. Subhan MA and VP Torchilin. (2020). siRNA based drug design, quality, delivery and clinical translation. Nanomed Nanotechnol Biol Med 29:102239.
27. Varkouhi AK, M Scholte, G Storm and HJ Haisma. (2011). Endosomal escape pathways for delivery of biologicals. J Controll Release 151:220–228.
28. Adams D, A Gonzalez-Duarte, WD O'Riordan, CC Yang, M Ueda, AV Kristen, I Tournev, HH Schmidt, T Coelho, *et al.* (2018). Patisiran, an RNAi therapeutic, for hereditary transthyretin amyloidosis. N Engl J Med 379:11–21.
29. Scott LJ. (2020). Givosiran: first approval. Drugs 80:335–339.
30. Springer AD and SF Dowdy. (2018). GalNAc-siRNA Conjugates: leading the way for delivery of RNAi therapeutics. Nucleic Acid Ther 23:109–118.
31. Zhang X, V Goel and GJ Robbie. (2019). Pharmacokinetics of patisiran, the first approved RNA interference therapy in patients with hereditary transthyretin-mediated amyloidosis. J Clin Pharmacol 60:573–585.
32. Cullis PR and MJ Hope. (2017). Lipid nanoparticle systems for enabling gene therapies. Mol Ther 25:1467–1475.
33. Ashwell G and AG Morell. (1974). The role of surface carbohydrates in the hepatic recognition and transport of circulating glycoproteins. Adv Enzymol Relat Areas Mol Biol 41:99–128.
34. Rajeev KG, JK Nair, M Jayaraman, K Charisse, N Taneja, J O'Shea, JL Willoughby, K Yucius, T Nguyen, *et al.* (2015). Hepatocyte-specific delivery of siRNAs conjugated to novel non-nucleosidic trivalent N-acetylgalactosamine elicits robust gene silencing in vivo. Chembiochem 16: 903–908.
35. Setten RL, JJ Rossi and S-p Han. (2019). The current state and future directions of RNAi-based therapeutics. Nat Rev Drug Discov 18:421–446.
36. Foster DJ, CR Brown, S Shaikh, C Trapp, MK Schlegel, K Qian, A Sehgal, KG Rajeev, V Jadhav, *et al.* (2018). Advanced siRNA designs further improve in vivo performance of GalNAc-siRNA conjugates. Mol Ther 26: 708–717.
37. *New Pre-Clinical Data on "Enhanced Stabilization Chemistry Plus" (ESC+) GalNAc-siRNA Conjugate Platform.* Cambridge, MA: Alnylam Pharmaceuticals, Inc., 2020
38. *Alnylam Announces U.S. Food and Drug Administration Has Granted Priority Review of the Lumasiran New Drug Application for the Treatment of Primary Hyperoxaluria Type 1.* Cambridge, MA: Alnylam Pharmaceuticals, Inc., 2020
39. *Novartis Successfully Completes Acquisition of The Medicines Company, Adding a Potentially First-in-Class, Investigational Cholesterol-Lowering Therapy Inclisiran.* Basel, Switzerland: Novartis, 2020.
40. Shilling R, V Karsten, N Silliman, J Chen, W Li and J Vest. (2020). Study Design and Rationale of HELIOS-B: a phase 3 study to evaluate the clinical efficacy and safety of vutrisiran in patients with ATTR amyloidosis with cardiomyopathy. J Am Coll Cardiol 75:3579.

Downloaded by GLASGOW UNIVERSITY LIBRARY/Swetsblackwell Inc/ 93868820 from www.liebertpub.com at 10/31/20. For personal use only.

41. Pipe S, MV Ragni, C Négrier, Q Yu, N Bajwa, J Caminis, B Mei and SR Andersson. (2019). Fitusiran, an RNAi Therapeutic Targeting Antithrombin to Restore Hemostatic Balance in Patients with Hemophilia a or B with or without Inhibitors: management of acute bleeding events. Blood 134:1138.
42. *VIR-2218 Demonstrates Dose-Dependent and Durable Reductions of Hepatitis B Surface Antigen in Phase 1/2 Trial*. San Francisco, CA: Vir Biotechnology, Inc., 2020.
43. *Alnylam Submits CTA Application for ALN-HSD, an Investigational RNAi Therapeutic for the Treatment of Nonalcoholic Steatohepatitis (NASH)*. Cambridge, MA: Alnylam Pharmaceuticals, Inc., 2020.
44. *Vir and Alnylam Identify RNAi Therapeutic Development Candidate, VIR-2703 (ALN-COV), Targeting SARS-CoV-2 for the Treatment of COVID-19*. San Francisco, CA & Cambridge, MA: Alnylam Pharmaceuticals, Inc., 2020.
45. Soutschek J, A Akinc, B Bramlage, K Charisse, R Constien, M Donoghue, S Elbashir, A Geick, P Hadwiger, *et al.* (2004). Therapeutic silencing of an endogenous gene by systemic administration of modified siRNAs. Nature 432:173–178.
46. Lorenz C, P Hadwiger, M John, HP Vornlocher and C Unverzagt. (2004). Steroid and lipid conjugates of siRNAs to enhance cellular uptake and gene silencing in liver cells. Bioorg Med Chem Lett 14:4975–4977.
47. Osborn MF and A Khvorova. (2018). Cholesteryl-conjugated oligonucleotides: synthesis, properties, and activity as inhibitors of replication of human immunodeficiency. Nucleic Acid Ther 28:128–136.
48. Tai W. (2019). Chemical modulation of siRNA lipophilicity for efficient delivery. J Controll Release 307:98–107.
49. Salim L, C McKim and J-P Desaulniers. (2018). Effective carrier-free gene-silencing activity of cholesterol-modified siRNAs. RSC Adv 8:22963–22966.
50. Kulkarni JA, D Witzigmann, J Leung, R van der Meel, J Zaifman, MM Darjuan, HM Grisch-Chan, B Thöny, YYC Tam and PR Cullis. (2019). Fusion-dependent formation of lipid nanoparticles containing macromolecular payloads. Nanoscale 11:9023–9031.
51. Biscans A, A Coles, R Haraszti, D Echeverria, M Hassler, M Osborn and A Khvorova. (2018). Diverse lipid conjugates for functional extra-hepatic siRNA delivery in vivo. Nucleic Acids Res 47:1082–1096.
52. Schwartz AL, SE Fridovich and HF Lodish. (1982). Kinetics of internalization and recycling of the asialoglycoprotein receptor in a hepatoma cell line. J Biol Chem 257:4230–4237.
53. Spiess M. (1990). The asialoglycoprotein receptor: a model for endocytic transport receptors. Biochemistry 29: 10009–10018.
54. Willoughby JLS, A Chan, A Sehgal, JS Butler, JK Nair, T Racie, S Shulga-Morskaya, T Nguyen, K Qian, *et al.* (2018). Evaluation of GalNAc-siRNA conjugate activity in pre-clinical animal models with reduced asialoglycoprotein receptor expression. Mol Ther 26:105–114.
55. Ducker GS and JD Rabinowitz. (2017). One-carbon metabolism in health and disease. Cell Metab 25:27–42.
56. Choi S-W and JB Mason. (2000). Folate and Carcinogenesis: an integrated scheme. J Nutr 130:129–132.
57. Matherly LH and DI Goldman. (2003). Membrane transport of folates. Vitam Horm 66:403–456.
58. Matherly LH and Z Hou. (2008). Structure and Function of the Reduced Folate Carrier: a paradigm of a major facilitator superfamily mammalian nutrient transporter. Vitam Horm 79:145–184.
59. Kelemen LE. (2006). The role of folate receptor α in cancer development, progression and treatment: cause, consequence or innocent bystander? Int J Cancer 119: 243–250.
60. Zhao R, SH Min, Y Wang, E Campanell, PS Low and ID Goldman. (2009). A Role for the Proton-coupled Folate Transporter (PCFT-SLC46A1) in Folate Receptor-mediated Endocytosis. J Biol Chem 284:4267–4274.
61. Torres A, SA Newton, B Crompton, A Borzutzky, EJ Neufeld, L Notarangelo and GT Berry. (2015). CSF 5-methyltetrahydrofolate serial monitoring to guide treatment of congenital folate malabsorption due to proton-coupled folate transporter (PCFT) Deficiency. JIMD Rep 24:91–96.
62. Rothberg KG, YS Ying, JF Kolhouse, BA Kamen and R Anderson. (1990). The glycophospholipid-linked folate receptor internalizes folate without entering the clathrin-coated pit endocytic pathway. J Cell Biol 110:637–649.
63. Ritter TE, O Fajardo, H Matsue, RG Anderson and SW Lacey. (1995). Folate receptors targeted to clathrin-coated pits cannot regulate vitamin uptake. Proc Natl Acad Sci U S A 92:3824–3828.
64. Sabharanjak S and S Mayor. (2004). Folate receptor endocytosis and trafficking. Adv Drug Del Rev 56:1099–1109.
65. Ledermann JA, S Canevari and T Thigpen. (2015). Targeting the folate receptor: diagnostic and therapeutic approaches to personalize cancer treatments. Ann Oncol 26: 2034–2043.
66. Mironava T, M Simon, MH Rafailovich and B Rigas. (2013). Platinum folate nanoparticles toxicity: cancer vs. normal cells. Toxicol In Vitro 27:882–889.
67. Tian Y, G Wu, J-C Xing, J Tang, Y Zhang, Z-M Huang, Z-C Jia, R Zhao, Z-Q Tian, *et al.* (2009). A novel splice variant of folate receptor 4 predominantly expressed in regulatory T cells. BMC Immunol 13:20.
68. Lynn RC, M Poussin, A Kalota, Y Feng, PS Low, DS Dimitrov and DJP Jr. (2015). Targeting of folate receptor β on acute myeloid leukemia blasts with chimeric antigen receptor–expressing T cells. Blood 125:3466–3476.
69. O'Shannessy DJ, EB Somers, L-C Wang, H Wang and R Hsu. (2015). Expression of folate receptors alpha and beta in normal and cancerous gynecologic tissues: correlation of expression of the beta isoform with macrophage markers. J Ovarian Res 8:29.
70. Weitman SD, RH Lark, LR Coney, DW Fort, V Frasca, VR Zurawski Jr and BA Kamen. (1992). Distribution of the folate receptor GP38 in normal and malignant cell lines and tissues. Cancer Res 52:3396–3401.
71. Parker N, MJ Turk, E Westrick, JD Lewis, P Low and CP Leamon. (2005). Folate receptor expression in carcinomas and normal tissues determined by a quantitative radioligand binding assay. Anal Biochem 338:284–293.
72. Chen C, J Ke, XE Zhou, W Yi, JS Brunzelle, J Li, E-L Yong, HE Xu and K Melcher. (2013). Structural basis for molecular recognition of folic acid by folate receptors. Nature 500:486–489.
73. Fernández M, F Javaid and V Chudasama. (2018). Advances in targeting the folate receptor in the treatment/imaging of cancers. Chem Sci 9:790–810.
74. Shen J, Y Hu, KS Putt, S Singhal, H Han, DW Visscher, LM Murphy and PS Low. (2018). Assessment of folate

Downloaded by GLASGOW UNIVERSITY LIBRARY/Swetsblackwell Inc/ 93868820 from www.liebertpub.com at 10/31/20. For personal use only.

receptor alpha and beta expression in selection of lung and pancreatic cancer patients for receptor targeted therapies. Oncotarget 9:4485–4495.

75. Müller C and R Schibli. (2011). Folic acid conjugates for nuclear imaging of folate receptor-positive cancer. J Nuclear Med 52:1–4.
76. Leamon CP and PS Low. (1991). Delivery of macromolecules into living cells: a method that exploits folate receptor endocytosis. Proc Natl Acad Sci U S A 88:5572–5576.
77. Kershaw MH, JA Westwood, LL Parker, G Wang, Z Eshhar, SA Mavroukakis, DE White, JR Wunderlich, S Canevari, *et al.* (2006). A phase I study on adoptive immunotherapy using gene-modified T cells for ovarian cancer. Clin Cancer Res 12:6106–6115.
78. Lu YJ, H Chu, LW Wheeler, M Nelson, E Westrick, JF Matthaei, Cardle, II, A Johnson, J Gustafson, *et al.* (2019). Preclinical evaluation of bispecific adaptor molecule controlled folate receptor CAR-T cell therapy with special focus on pediatric malignancies. Front Oncol 9:151.
79. Song DG, Q Ye, C Carpenito, M Poussin, LP Wang, C Ji, M Figini, CH June, G Coukos and DJ Powell, Jr. (2011). In vivo persistence, tumor localization, and antitumor activity of CAR-engineered T cells is enhanced by costimulatory signaling through CD137 (4–1BB). Cancer Res 71:4617–4627.
80. Kandalaft LE, DJ Powell, Jr. and G Coukos. (2012). A phase I clinical trial of adoptive transfer of folate receptor-alpha redirected autologous T cells for recurrent ovarian cancer. J Transl Med 10:157.
81. Kim M, S Pyo, CH Kang, CO Lee, HK Lee, SU Choi and CH Park. (2018). Folate receptor 1 (FOLR1) targeted chimeric antigen receptor (CAR) T cells for the treatment of gastric cancer. PLoS One 13:e0198347.
82. Amato RJ, A Shetty, Y Lu, R Ellis and PS Low. (2013). A phase I study of folate immune therapy (EC90 vaccine administered with GPI-0100 adjuvant followed by EC17) in patients with renal cell carcinoma. J Immunother 36: 268–275.
83. Hernando JJ, TW Park, HP Fischer, O Zivanovic, M Braun, M Pölcher, U Grünn, C Leutner, B Pötzsch and W Kuhn. (2007). Vaccination with dendritic cells transfected with mRNA-encoded folate-receptor-alpha for relapsed metastatic ovarian cancer. Lancet Oncol 8:451–454.
84. Kalli KR, MS Block, PM Kasi, CL Erskine, TJ Hobday, A Dietz, D Padley, MP Gustafson, B Shreeder, *et al.* (2018). Folate receptor alpha peptide vaccine generates immunity in breast and ovarian cancer patients. Clin Cancer Res 24: 3014–3025.
85. Ebel W, EL Routhier, B Foley, S Jacob, JM McDonough, RK Patel, HA Turchin, Q Chao, JB Kline, *et al.* (2007). Preclinical evaluation of MORAb-003, a humanized monoclonal antibody antagonizing folate receptor-alpha. Cancer Immunity 7:6.
86. Kamen BA and AK Smith. (2012). Farletuzumab, an anti-folate receptor α antibody, does not block binding of folate or anti-folates to receptor nor does it alter the potency of anti-folates in vitro. Cancer Chemother Pharmacol 70: 113–120.
87. Lin J, JL Spidel, CJ Maddage, KA Rybinski, RP Kennedy, CLM Krauthauser, YC Park, EF Albone, S Jacob, *et al.* (2013). The antitumor activity of the human FOLR1-specific monoclonal antibody, farletuzumab, in an ovarian cancer mouse model is mediated by antibody-dependent cellular cytotoxicity. Cancer Biol Ther 14:1032–1038.
88. Kline JB, S Fernando, S Harley, L Grasso and NC Nicolaides. (2017). Effect of CA125/MUC16 on complement-dependent cytotoxicity (CDC) of farletuzumab and other CDC-mediating antibodies via inhibition of antibody-C1q binding. J Clin Oncol 35:e23082.
89. Wen Y, WS Graybill, RA Previs, W Hu, C Ivan, LS Mangala, B Zand, AM Nick, NB Jennings, *et al.* (2015). Immunotherapy targeting folate receptor induces cell death associated with autophagy in ovarian cancer. Clin Cancer Res 21:448–459.
90. Konner JA, KM Bell-McGuinn, P Sabbatini, ML Hensley, WP Tew, N Pandit-Taskar, N Vander Els, MD Phillips, C Schweizer, *et al.* (2010). Farletuzumab, a humanized monoclonal antibody against folate receptor alpha, in epithelial ovarian cancer: a phase I study. Clin Cancer Res 16:5288–5295.
91. Sasaki Y, K Miwa, K Yamashita, Y Sunakawa, K Shimada, H Ishida, K Hasegawa, K Fujiwara, M Kodaira, *et al.* (2015). A phase I study of farletuzumab, a humanized anti-folate receptor α monoclonal antibody, in patients with solid tumors. Invest. New Drugs 33:332–340.
92. Kim KH, D Jelovac, DK Armstrong, B Schwartz, SC Weil, C Schweizer and RD Alvarez. (2016). Phase 1b safety study of farletuzumab, carboplatin and pegylated liposomal doxorubicin in patients with platinum-sensitive epithelial ovarian cancer. Gynecol Oncol 140:210–214.
93. Armstrong DK, AJ White, SC Weil, M Phillips and RL Coleman. (2013). Farletuzumab (a monoclonal antibody against folate receptor alpha) in relapsed platinum-sensitive ovarian cancer. Gynecol Oncol 129:452–458.
94. Sasaki Y, K Miwa, K Yamashita, K Fujiwara, N Katsumata, Y Fujiwara, M Namiki and N Koyanagi. (2012). Phase I and pharmacokinetic study of farletuzumab in solid tumors. J Clin Oncol 30:3084.
95. Vergote I, D Armstrong, G Scambia, M Teneriello, J Sehouli, C Schweizer, SC Weil, A Bamias, K Fujiwara, *et al.* (2016). A Randomized, Double-Blind, Placebo-Controlled, Phase III study to assess efficacy and safety of weekly farletuzumab in combination with carboplatin and taxane in patients with ovarian cancer in first platinum-sensitive relapse. J Clin Oncol 34:2271–2278.
96. Vergote IB, C Marth and RL Coleman. (2015). Role of the folate receptor in ovarian cancer treatment: evidence, mechanism, and clinical implications. Cancer Metastasis Rev 34:41–52.
97. Miotti S, S Canevari, S Ménard, D Mezzanzanica, G Porro, SM Pupa, M Regazzoni, E Tagliabue and MI Colnaghi. (1987). Characterization of human ovarian carcinoma-associated antigens defined by novel monoclonal antibodies with tumor-restricted specificity. Int J Cancer 39:297–303.
98. Coney LR, D Mezzanzanica, D Sanborn, P Casalini, MI Colnaghi and VR Zurawski, Jr. (1994). Chimeric murine-human antibodies directed against folate binding receptor are efficient mediators of ovarian carcinoma cell killing. Cancer Res 54:2448–2455.
99. Molthoff CF, HM Prinssen, P Kenemans, AC van Hof, W den Hollander and RH Verheijen. (1997). Escalating protein doses of chimeric monoclonal antibody MOv18 immunoglobulin G in ovarian carcinoma patients: a phase I study. Cancer 80:2712–2720.
100. Gould HJ, GA Mackay, SN Karagiannis, CM O'Toole, PJ Marsh, BE Daniel, LR Coney, VR Zurawski, Jr., M Joseph, *et al.* (1999). Comparison of IgE and IgG antibody-

Downloaded by GLASGOW UNIVERSITY LIBRARY/Swetsblackwell Inc/ 93868820 from www.liebertpub.com at 10/31/20. For personal use only.

dependent cytotoxicity in vitro and in a SCID mouse xenograft model of ovarian carcinoma. Eur J Immunol 29: 3527–3537.

101. Karagiannis SN, DH Josephs, P Karagiannis, AE Gilbert, L Saul, SM Rudman, T Dodev, A Koers, PJ Blower, *et al.* (2012). Recombinant IgE antibodies for passive immunotherapy of solid tumours: from concept towards clinical application. Cancer Immunol Immunother 61:1547–1564.
102. van Zanten-Przybysz I, C Molthoff, JK Gebbinck, S von Mensdorff-Pouilly, R Verstraeten, P Kenemans and R Verheijen. (2002). Cellular and humoral responses after multiple injections of unconjugated chimeric monoclonal antibody MOv18 in ovarian cancer patients: a pilot study. J Cancer Res Clin Oncol 128:484–492.
103. Buijs WC, JG Tibben, OC Boerman, CF Molthoff, LF Massuger, EB Koenders, CP Schijf, JA Siegel and FH Corstens. (1998). Dosimetric analysis of chimeric monoclonal antibody cMOv18 IgG in ovarian carcinoma patients after intraperitoneal and intravenous administration. Eur J Nucl Med 25:1552–1561.
104. Crippa F, G Bolis, E Seregni, N Gavoni, G Scarfone, C Ferraris, GL Buraggi and E Bombardieri. (1995). Single-dose intraperitoneal radioimmunotherapy with the murine monoclonal antibody I-131 MOv18: clinical results in patients with minimal residual disease of ovarian cancer. Eur J Cancer 31:686–690.
105. Andersson H, S Lindegren, T Back, L Jacobsson, G Leser and G Horvath. (2000). Radioimmunotherapy of nude mice with intraperitoneally growing ovarian cancer xenograft utilizing 211At-labelled monoclonal antibody MOv18. Anticancer Res 20:459–462.
106. Zacchetti A, A Coliva, E Luison, E Seregni, E Bombardieri, A Giussani, M Figini and S Canevari. (2009). (177)Lu-labeled MOv18 as compared to (131)I- or (90)Y-labeled MOv18 has the better therapeutic effect in eradication of alpha folate receptor-expressing tumor xenografts. Nucl Med Biol 36:759–770.
107. Cheng X, J Li, K Tanaka, U Majumder, AZ Milinichik, AC Verdi, CJ Maddage, KA Rybinski, S Fernando, *et al.* (2018). MORAb-202, an antibody-drug conjugate utilizing humanized anti-human FRα farletuzumab and the microtubule-targeting agent eribulin, has potent antitumor activity. Mol Cancer Ther 17:2665–2675.
108. De Almeida V, C Abrahams, W Solis, X Li, T Kline, J Hanson, MR Masikat, J Zawada, G Sarma and M Lupher, Jr. (2018). Preclinical activity and safety of STRO-002, a novel ADC targeting folate receptor alpha for ovarian cancer. Gynecol Oncol 149:50.
109. Moore KN, H Borghaei, DM O'Malley, W Jeong, SM Seward, TM Bauer, RP Perez, UA Matulonis, KL Running, *et al.* (2017). Phase 1 dose-escalation study of mirvetuximab soravtansine (IMGN853), a folate receptor α-targeting antibody-drug conjugate, in patients with solid tumors. Cancer 123:3080–3087.
110. Moore KN, DM O'Malley, I Vergote, LP Martin, A Gonzalez-Martin, K Malek and MJ Birrer. (2018). Safety and activity findings from a phase 1b escalation study of mirvetuximab soravtansine, a folate receptor alpha (FRα)-targeting antibody-drug conjugate (ADC), in combination with carboplatin in patients with platinum-sensitive ovarian cancer. Gynecol Oncol 151:46–52.
111. Moore KN, I Vergote, A Oaknin, N Colombo, S Banerjee, A Oza, P Pautier, K Malek and MJ Birrer. (2018). FORWARD I: a Phase III study of mirvetuximab soravtansine versus chemotherapy in platinum-resistant ovarian cancer. Future Oncol 14:1669–1678.
112. Moore KN, AM Oza, N Colombo, A Oaknin, G Scambia, D Lorusso, R Farias-Eisner, S Banerjee, C Murphy, *et al.* (2019). FORWARD I (GOG 3011): A Phase III study of mirvetuximab soravtansine, a folate receptor alpha (FRa)-targeting antibody-drug conjugate, versus chemotherapy in patients with platinum-resistant ovarian cancer. ESMO, Barcelona.
113. Meier R, TD Henning, S Boddington, S Tavri, S Arora, G Piontek, M Rudelius, C Corot and HE Daldrup-Link. (2010). Breast cancers: MR imaging of folate-receptor expression with the folate-specific nanoparticle P1133. Radiology 255:527–535.
114. Konda SD, M Aref, M Brechbiel and EC Wiener. (2000). Development of a Tumor-Targeting MR contrast agent using the high-affinity folate receptor: work in progress. Invest Radiol 35:50.
115. Choi H, SR Choi, R Zhou, HF Kung and IW Chen. (2004). Iron oxide nanoparticles as magnetic resonance contrast agent for tumor imaging via folate receptor-targeted delivery. Acad Radiol 11:996–1004.
116. Saborowski O, GH Simon, HJ Raatschen, MF Wendland, Y Fu, T Henning, R Baehner, C Corot, MH Chen and HE Daldrup-Link. (2007). MR imaging of antigen-induced arthritis with a new, folate receptor-targeted contrast agent. Contrast Media Mol Imaging 2:72–81.
117. Yuan Z, WT Li, XD Ye, SY Liu and XS Xiao. (2012). Folate receptor-mediated targeted polymeric gadolinium complexes for magnetic resonance imaging in pulmonary tumor xenografts. Exp Ther Med 3:903–907.
118. Tung CH, Y Lin, WK Moon and R Weissleder. (2002). A receptor-targeted near-infrared fluorescence probe for in vivo tumor imaging. Chembiochem 3:784–786.
119. Bharali DJ, DW Lucey, H Jayakumar, HE Pudavar and PN Prasad. (2005). Folate-receptor-mediated delivery of InP quantum dots for bioimaging using confocal and two-photon microscopy. J Am Chem Soc 127:11364–11371.
120. Cho SS, R Zeh, JT Pierce, J Jeon, M Nasrallah, ND Adappa, JN Palmer, JG Newman, C White, *et al.* (2019). Folate Receptor Near-Infrared Optical Imaging Provides Sensitive and Specific Intraoperative Visualization of Nonfunctional Pituitary Adenomas. Oper Neurosurg (Hagerstown) 16:59–70.
121. Sega EI and PS Low. (2008). Tumor detection using folate receptor-targeted imaging agents. Cancer Metastasis Rev 27:655–664.
122. Siegel BA, F Dehdashti, DG Mutch, DA Podoloff, R Wendt, GP Sutton, RW Burt, PR Ellis, CJ Mathias, *et al.* (2003). Evaluation of 111In-DTPA-folate as a receptor-targeted diagnostic agent for ovarian cancer: initial clinical results. J Nucl Med 44:700–707.
123. Serpe L, M Gallicchio, R Canaparo and F Dosio. (2014). Targeted treatment of folate receptor-positive platinum-resistant ovarian cancer and companion diagnostics, with specific focus on vintafolide and etarfolatide. Pharmgenomics Pers Med 7:31–42.
124. Reddy JA, LC Xu, N Parker, M Vetzel and CP Leamon. (2004). Preclinical evaluation of (99m)Tc-EC20 for imaging folate receptor-positive tumors. J Nucl Med 45:857–866.
125. Leamon CP, MA Parker, IR Vlahov, LC Xu, JA Reddy, M Vetzel and N Douglas. (2002). Synthesis and biological evaluation of EC20: a new folate-derived, (99m)Tc-based radiopharmaceutical. Bioconjug Chem 13:1200–1210.

Downloaded by GLASGOW UNIVERSITY LIBRARY/Swetsblackwell Inc/ 93868820 from www.liebertpub.com at 10/31/20. For personal use only.

126. Fisher RE, BA Siegel, SL Edell, NM Oyesiku, DE Morgenstern, RA Messmann and RJ Amato. (2008). Exploratory study of 99mTc-EC20 imaging for identifying patients with folate receptor-positive solid tumors. J Nucl Med 49:899–906.
127. Morris RT, RN Joyrich, RW Naumann, NP Shah, AH Maurer, HW Strauss, JM Uszler, JT Symanowski, PR Ellis and WA Harb. (2014). Phase II study of treatment of advanced ovarian cancer with folate-receptor-targeted therapeutic (vintafolide) and companion SPECT-based imaging agent (99mTc-etarfolatide). Ann Oncol 25:852–858.
128. van Dam GM, G Themelis, LMA Crane, NJ Harlaar, RG Pleijhuis, W Kelder, A Sarantopoulos, JS de Jong, HJG Arts, *et al.* (2011). Intraoperative tumor-specific fluorescence imaging in ovarian cancer by folate receptor-α targeting: first in-human results. Nat Med 17:1315–1319.
129. Tummers QRJG, CES Hoogstins, KN Gaarenstroom, CD de Kroon, MIE van Poelgeest, J Vuyk, T Bosse, VTHBM Smit, CJH van de Velde, *et al.* (2016). Intraoperative imaging of folate receptor alpha positive ovarian and breast cancer using the tumor specific agent EC17. Oncotarget 7:32144–32155.
130. Boogerd LSF, CES Hoogstins, KN Gaarenstroom, CD de Kroon, JJ Beltman, T Bosse, E Stelloo, J Vuyk, PS Low, *et al.* (2017). Folate receptor-α targeted near-infrared fluorescence imaging in high-risk endometrial cancer patients: a tissue microarray and clinical feasibility study. Oncotarget 9:791–801.
131. Predina JD, AD Newton, C Connolly, A Dunbar, M Baldassari, C Deshpande, E Cantu, 3rd, J Stadanlick, SA Kularatne, *et al.* (2018). Identification of a folate receptor-targeted near-infrared molecular contrast agent to localize pulmonary adenocarcinomas. Mol Ther 26:390–403.
132. Lee JYK, SS Cho, R Zeh, JT Pierce, M Martinez-Lage, ND Adappa, JN Palmer, JG Newman, KO Learned, *et al.* (2018). Folate receptor overexpression can be visualized in real time during pituitary adenoma endoscopic transsphenoidal surgery with near-infrared imaging. J Neurosurg 129:390–403.
133. Randall LM, RM Wenham, PS Low, SC Dowdy and JL Tanyi. (2019). A phase II, multicenter, open-label trial of OTL38 injection for the intra-operative imaging of folate receptor-alpha positive ovarian cancer. Gynecol Oncol 155:63–68.
134. *First Patient Enrolled in the Phase 3 ELUCIDATE Trial of Pafolacianine Sodium (formerly OTL38) in the Intraoperative Identification of Lung Cancer Lesions*. West Lafayette, IN: On Target Laboratories, Inc., 2020.
135. Dosio F, P Milla and L Cattel. (2010). EC-145, a folate-targeted Vinca alkaloid conjugate for the potential treatment of folate receptor-expressing cancers. Curr Opin Invest Drugs 11:1424–1433.
136. Naumann RW, RL Coleman, RA Burger, EA Sausville, E Kutarska, SA Ghamande, NY Gabrail, SE Depasquale, E Nowara, *et al.* (2013). PRECEDENT: a randomized phase II trial comparing vintafolide (EC145) and pegylated liposomal doxorubicin (PLD) in combination versus PLD alone in patients with platinum-resistant ovarian cancer. J Clin Oncol 31:4400–4406.
137. Edelman MJ, WA Harb, SE Pal, RV Boccia, MJ Kraut, P Bonomi, BA Conley, JS Rogers, RA Messmann and EB Garon. (2012). Multicenter trial of EC145 in advanced, folate-receptor positive adenocarcinoma of the lung. J Thorac Oncol 7:1618–1621.
138. Hanna N, E Juhász, C Cainap, O Gladkov, R Ramlau, O Juan-Vidal, R Lal, J Symanowski, W Perez, *et al.* (2014). Target: a randomized, phase Ii trial comparing vintafolide versus vintafolide plus docetaxel, versus docetaxel alone in second-line treatment of folate-receptor-positive non-small cell lung cancer (Nsclc) patients. Ann Oncol 25:v1.
139. Naumann RW, L Gilbert, AM Miller, H Ma, SA Ghamande and I Vergote. (2013). A randomized double-blind phase III trial comparing vintafolide plus pegylated liposomal doxorubicin (PLD) versus PLD plus placebo in patients with platinum-resistant ovarian cancer (PROCEED). J Clin Oncol 31:TPS5613.
140. Leamon CP, JA Reddy, PJ Klein, IR Vlahov, R Dorton, A Bloomfield, M Nelson, E Westrick, N Parker, *et al.* (2011). Reducing undesirable hepatic clearance of a tumor-targeted vinca alkaloid via novel saccharopeptidic modifications. J Pharmacol Exp Ther 336:336–343.
141. Harb WA, BA Conley, P LoRusso, EA Sausville, EI Heath, SR Chandana, M Hamm, J Carter, WJ Perez and RA Messmann. (2010). A phase I study of the folate-targeted conjugate EC0489 in patients with refractory or advanced metastatic cancer. J Clin Oncol 28:3088.
142. Sharma S, EA Sausville, P LoRusso, NJ Vogelzang, WE Samlowski, J Carter, K Forman, S Bever and RA Messmann. (2010). A phase I study of EC0225 administered weeks 1 and 2 of a 4-week cycle. J Clin Oncol 28:3082.
143. Reddy JA, R Dorton, A Bloomfield, M Nelson, C Dircksen, M Vetzel, P Kleindl, H Santhapuram, IR Vlahov and CP Leamon. (2018). Pre-clinical evaluation of EC1456, a folate-tubulysin anti-cancer therapeutic. Sci Rep 8:8943.
144. Douglas JT, BE Rogers, ME Rosenfeld, SI Michael, M Feng and DT Curiel. (1996). Targeted gene delivery by tropism-modified adenoviral vectors. Nat Biotechnol 14:1574–1578.
145. Kim YK, JY Choi, MK Yoo, HL Jiang, R Arote, YH Je, MH Cho and CS Cho. (2007). Receptor-mediated gene delivery by folate-PEG-baculovirus in vitro. J Biotechnol 131:353–361.
146. Hattori Y. (2010). Development of non-viral vector for cancer gene therapy. Yakugaku Zasshi 130:917–923.
147. Jreyssaty C, Q Shi, H Wang, X Qiu, FM Winnik, X Zhang, K Dai, M Benderdour and JC Fernandes. (2012). Efficient Nonviral Gene Therapy Using Folate-Targeted Chitosan-DNA Nanoparticles In Vitro. ISRN Pharm 2012: 369270.
148. Ward CM. (2000). Folate-targeted non-viral DNA vectors for cancer gene therapy. Curr Opin Mol Ther 2:182–187.
149. Zhao X, H Li and RJ Lee. (2008). Targeted drug delivery via folate receptors. Expert Opin Drug Deliv 5:309–319.
150. Chan P, M Kurisawa, JE Chung and YY Yang. (2007). Synthesis and characterization of chitosan-g-poly(ethylene glycol)-folate as a non-viral carrier for tumor-targeted gene delivery. Biomaterials 28:540–549.
151. Guo W and RL Lee. (1999). Receptor-targeted gene delivery via folate-conjugated polyethylenimine. AAPS PharmSci 1:E19.
152. Mislick KA, JD Baldeschwieler, JF Kayyem and TJ Meade. (1995). Transfection of Folate-Polylysine DNA Complexes: evidence for lysosomal delivery. Bioconjugate Chem 6:512–515.
153. Ward CM, M Pechar, D Oupicky, K Ulbrich and LW Seymour. (2002). Modification of pLL/DNA complexes with a multivalent hydrophilic polymer permits folate-mediated targeting in vitro and prolonged plasma circulation in vivo. J Gene Med 4:536–547.

Downloaded by GLASGOW UNIVERSITY LIBRARY/Swetsblackwell Inc/ 93868820 from www.liebertpub.com at 10/31/20. For personal use only.

154. Gottschalk S, RJ Cristiano, LC Smith and SL Woo. (1994). Folate receptor mediated DNA delivery into tumor cells: potosomal disruption results in enhanced gene expression. Gene Ther 1:185–191.
155. Benns JM, A Maheshwari, DY Furgeson, RI Mahato and SW Kim. (2001). Folate-PEG-folate-graft-polyethylenimine-based gene delivery. J Drug Target 9:123–139.
156. Lee RJ and L Huang. (1996). Folate-targeted, anionic liposome-entrapped polylysine-condensed DNA for tumor cell-specific gene transfer. J Biol Chem 271:8481–8487.
157. Reddy JA, D Dean, MD Kennedy and PS Low. (1999). Optimization of folate-conjugated liposomal vectors for folate receptor-mediated gene therapy. J Pharm Sci 88: 1112–1118.
158. Reddy JA and PS Low. (2000). Enhanced folate receptor mediated gene therapy using a novel pH-sensitive lipid formulation. J Control Release 64:27–37.
159. Xu L, K Pirollo, A Rait, AL Murray and EH Chang. (1999). Systemic p53 gene therapy in combination with radiation results in human tumor regression. Tumor Target 4:92–104.
160. Shi G, W Guo, SM Stephenson and RJ Lee. (2002). Efficient intracellular drug and gene delivery using folate receptor-targeted pH-sensitive liposomes composed of cationic/anionic lipid combinations. J Control Release 80: 309–319.
161. Citro G, C Szczylik, P Ginobbi, G Zupi and B Calabretta. (1994). Inhibition of leukaemia cell proliferation by folic acid-polylysine-mediated introduction of c-myb antisense oligodeoxynucleotides into HL-60 cells. Br J Cancer 69:463–467.
162. Li S and L Huang. (2008). Targeted delivery of antisense oligodeoxynucleotides by LPDII. J Liposome Res 7: 63–75.
163. Li S, HM Deshmukh and L Huang. (1998). Folate-mediated targeting of antisense oligodeoxynucleotides to ovarian cancer cells. Pharm Res 15:1540–1545.
164. Lee RJ and PS Low. (1997). Folate-targeted liposomes for drug delivery. J Liposome Res 7:455–466.
165. Leamon CP, SR Cooper and GE Hardee. (2003). Folate-Liposome-Mediated Antisense Oligodeoxynucleotide Targeting to Cancer Cells: evaluation in vitro and in vivo. Bioconjugate Chem 14:738–747.
166. Lopes I, ACN Oliveira, MP Sárria, JP Neves Silva, O Gonçalves, AC Gomes and MECD Real Oliveira. (2016). Monoolein-based nanocarriers for enhanced folate receptor-mediated RNA delivery to cancer cells. J Liposome Res 26: 199–210.
167. Shi Q, EP Rondon-Cavanzo, IP Dalla Picola, MJ Tiera, X Zhang, K Dai, HA Benabdoune, M Benderdour and JC Fernandes. (2018). In vivo therapeutic efficacy of TNFα silencing by folate-PEG-chitosan-DEAE/siRNA nanoparticles in arthritic mice. Int J Nanomed 13:387–402.
168. Yang T, B Li, S Qi, Y Liu, Y Gai, P Ye, G Yang, W Zhang, P Zhang, *et al.* (2014). Co-delivery of doxorubicin and Bmi1 siRNA by folate receptor targeted liposomes exhibits enhanced anti-tumor effects in vitro and in vivo. Theranostics 4:1096–1111.
169. Muralidharan R, A Babu, N Amreddy, K Basalingappa, M Mehta, A Chen, YD Zhao, UB Kompella, A Munshi and R Ramesh. (2016). Folate receptor-targeted nanoparticle delivery of HuR-RNAi suppresses lung cancer cell proliferation and migration. J Nanobiotechnol 14:47.
170. Li JM, YY Wang, W Zhang, H Su, LN Ji and ZW Mao. (2013). Low-weight polyethylenimine cross-linked 2-hydroxypopyl-β-cyclodextrin and folic acid as an efficient and nontoxic siRNA carrier for gene silencing and tumor inhibition by VEGF siRNA. Int J Nanomed 8:2101–2117.
171. Lin S-Y, W-Y Zhao, H-C Tsai, W-H Hsu, C-L Lo and G-H Hsiue. (2012). Sterically Polymer-Based Liposomal Complexes with Dual-Shell Structure for Enhancing the siRNA Delivery. Biomacromolecules 13:664–675.
172. Yoshizawa T, Y Hattori, M Hakoshima, K Koga and Y Maitani. (2008). Folate-linked lipid-based nanoparticles for synthetic siRNA delivery in KB tumor xenografts. Eur J Pharm Biopharm 70:718–725.
173. Zheng H, A Zhong, S Xie, Y Wang, J Sun, J Zhang, Y Tong, M Chen, G Zhang, *et al.* (2019). Elevated serum HER-2 predicts poor prognosis in breast cancer and is correlated to ADAM10 expression. Cancer Med 8:679–685.
174. Iqbal N and N Iqbal. (2014). Human Epidermal Growth Factor Receptor 2 (HER2) in Cancers: overexpression and therapeutic implications. Mol Biol Int 2014:852748.
175. Kim YI, B-C Ahn, JA Ronald, R Katzenberg, A Singh, R Paulmurugan, S Ray, SS Gambhir and LV Hofmann. (2012). Intratumoral versus intravenous gene therapy using a transcriptionally targeted viral vector in an orthotopic hepatocellular carcinoma rat model. J Vasc Intervent Radiol 23:704–711.
176. Degors IMS, C Wang, ZU Rehman and IS Zuhorn. (2019). Carriers break barriers in drug delivery: endocytosis and endosomal escape of gene delivery vectors. Acc Chem Res 52:1750–1760.
177. Hattori Y, M Nakamura, N Takeuchi, K Tamaki, S Shimizu, Y Yoshiike, M Taguchi, H Ohno, K-I Ozaki and H Onishi. (2019). Effect of cationic lipid in cationic liposomes on siRNA delivery into the lung by intravenous injection of cationic lipoplex. J Drug Target 27:217–227.
178. Hattori Y, N Takeuchi, M Nakamura, Y Yoshiike, M Taguchi, H Ohno, K-I Ozaki and H Onishi. (2018). Effect of cationic lipid type in cationic liposomes for siRNA delivery into the liver by sequential injection of chondroitin sulfate and cationic lipoplex. J Drug Deliv Sci Technol 48:235–244.
179. Hattori Y, S Shimizu, KI Ozaki and H Onishi. (2019). Effect of cationic lipid type in folate-PEG-modified cationic liposomes on folate receptor-mediated sirna transfection in tumor cells. Pharmaceutics 11:181.
180. Zatsepin TS, YV Kotelevtsev and V Koteliansky. (2016). Lipid nanoparticles for targeted siRNA delivery - going from bench to bedside. Int J Nanomed 11:3077–3086.
181. Dohmen C, T Fröhlich, U Lächelt, I Röhl, H-P Vornlocher, P Hadwiger and E Wagner. (2012). Defined Folate-PEG-siRNA conjugates for receptor-specific gene silencing. Mol Ther Nucleic Acids 1:e7.
182. Lee DJ, E Kessel, T Lehto, X Liu, N Yoshinaga, K Padari, YC Chen, S Kempter, S Uchida, *et al.* (2017). Systemic Delivery of Folate-PEG siRNA lipopolyplexes with enhanced intracellular stability for in vivo gene silencing in leukemia. Bioconjug Chem 28:2393–2409.
183. Vlashi E, LE Kelderhouse, JE Sturgis and PS Low. (2013). Effect of folate-targeted nanoparticle size on their rates of penetration into solid tumors. ACS Nano 7:8573–8582.
184. Sahay G, W Querbes, C Alabi, A Eltoukhy, S Sarkar, C Zurenko, E Karagiannis, K Love, D Chen, *et al.* (2013). Efficiency of siRNA delivery by lipid nanoparticles is limited by endocytic recycling. Nat Biotechnol 31:653–658.

185. Gilleron J, W Querbes, A Zeigerer, A Borodovsky, G Marsico, U Schubert, K Manygoats, S Seifert, C Andree, *et al.* (2013). Image-based analysis of lipid nanoparticle–mediated siRNA delivery, intracellular trafficking and endosomal escape. Nat Biotechnol 31:638–646.
186. Lv H, S Zhang, B Wang, S Cui and J Yan. (2006). Toxicity of cationic lipids and cationic polymers in gene delivery. J Control Release 114:100–109.
187. Boss SD, T Betzel, C Müller, CR Fischer, S Haller, J Reber, V Groehn, R Schibli and SM Ametamey. (2016). Comparative studies of three pairs of α- and γ-conjugated folic acid derivatives labeled with fluorine-18. Bioconjugate Chem 27:74–86.
188. Thomas M, SA Kularatne, L Qi, P Kleindl, CP Leamon, MJ Hansen and PS Low. (2009). Ligand-targeted delivery of small interfering RNAs to malignant cells and tissues. Ann N Y Acad Sci 1175:32–39.
189. Zhang K, Q Wang, Y Xie, G Mor, E Sega, PS Low and Y Huang. (2008). Receptor-mediated delivery of siRNAs by tethered nucleic acid base-paired interactions. RNA 14: 577–583.
190. Willibald J, J Harder, K Sparrer, KK Conzelmann and T Carell. (2012). Click-modified anandamide siRNA enables delivery and gene silencing in neuronal and immune cells. J Am Chem Soc 134:12330–12333.
191. Salim L, G Islam and J-P Desaulniers. (2020). Targeted delivery and enhanced gene-silencing activity of centrally modified folic acid–siRNA conjugates. Nucleic Acids Res 48:75–85.
192. Addepalli H, Meena, CG Peng, G Wang, Y Fan, K Charisse, KN Jayaprakash, KG Rajeev, RK Pandey, *et al.* (2010). Modulation of thermal stability can enhance the potency of siRNA. Nucleic Acids Res 38:7320–7331.
193. Orellana EA, S Tenneti, L Rangasamy, LT Lyle, PS Low and AL Kasinski. (2017). FolamiRs: ligand-targeted, vehicle-free delivery of microRNAs for the treatment of cancer. Sci Transl Med 9:eaam9327.
194. Orellana EA, AM Abdelaal, L Rangasamy, S Tenneti, S Myoung, PS Low and AL Kasinski. (2019). Enhancing MicroRNA activity through increased endosomal release mediated by nigericin. Mol Ther Nucleic Acids 16:505–518.

Address correspondence to:
Jean-Paul Desaulniers, PhD
Faculty of Science
University of Ontario Institute of Technology
Oshawa L1G 0C5
Canada

E-mail: jean-paul.desaulniers@ontariotechu.ca

Received for publication July 7, 2020; accepted after revision September 18, 2020.

Downloaded by GLASGOW UNIVERSITY LIBRARY/Swetsblackwell Inc/ 93868820 from www.liebertpub.com at 10/31/20. For personal use only.

Appendix F. Copyright Permission Forms

OntarioTech UNIVERSITY

Copyright Permission Letter

March 16, 2021

I am preparing my Doctor of Philosophy thesis for submission to the School of Graduate and Postdoctoral Studies at the University of Ontario Institute of Technology (Ontario Tech University) in Oshawa, Ontario, Canada. I am seeking your permission to include a manuscript version of the following papers as a chapter in the thesis:

L. Salim, E. Goss and J.-P. Desaulniers. "Synthesis and Evaluation of Modified siRNA Molecules Containing a Novel Glucose Derivatives" *RSC Advances* **2021**, 11, 9285–9289.

L. Salim, G. Islam, and J.-P. Desaulniers. "Targeted Delivery and Enhanced Gene-Silencing Activity of Centrally-Modified Folic Acid-siRNA Conjugates" *Nucleic Acids Res*. **2020**, 48, 75-85.

L. Salim, C. McKim, and J.-P. Desaulniers. "Effective Carrier-Free Gene-Silencing Activity of Cholesterol-Modified siRNAs" *RSC Advances* **2018**, 8, 22963-22966.

Canadian graduate theses are reproduced by the Library and Archives of Canada (formerly National Library of Canada) through a non-exclusive, world-wide license to reproduce, loan, distribute, or sell theses. I am also seeking your permission for the material described above to be reproduced and distributed by the LAC (NLC). Further details about the LAC (NLC) thesis program are available on the LAC (NLC) website (www.nlc-bnc.ca).

Full publication details and a copy of this permission letter will be included in the thesis.

Yours sincerely,
Lidya Salim

Permission is granted for:
a) The inclusion of the material described above in your thesis.
b) For the material described above to be included in the copy of your thesis that is sent to the Library and Archives of Canada (formerly National Library of Canada) for reproduction and distribution.

Name: Jean-Paul Desaulniers Title: Professor

Signature: Date (dd/mmm/yyyy) 16/03/2021

OntarioTech UNIVERSITY

Copyright Permission Letter

March 16, 2021

Publication Title: Effective Carrier-Free Gene-Silencing Activity of Cholesterol-Modified siRNAs

I am preparing my Doctor of Philosophy thesis for submission to the School of Graduate and Postdoctoral Studies at the University of Ontario Institute of Technology (Ontario Tech University) in Oshawa, Ontario, Canada. I am seeking your permission to include a manuscript version of the following paper as a chapter in the thesis:

L. Salim, C. McKim, and J.-P. Desaulniers. "Effective Carrier-Free Gene-Silencing Activity of Cholesterol-Modified siRNAs" *RSC Advances* **2018**, 8, 22963-22966.

Canadian graduate theses are reproduced by the Library and Archives of Canada (formerly National Library of Canada) through a non-exclusive, world-wide license to reproduce, loan, distribute, or sell theses. I am also seeking your permission for the material described above to be reproduced and distributed by the LAC (NLC). Further details about the LAC (NLC) thesis program are available on the LAC (NLC) website (www.nlc-bnc.ca).

Full publication details and a copy of this permission letter will be included in the thesis.

Yours sincerely,
Lidya Salim

Permission is granted for:
a) The inclusion of the material described above in your thesis.
b) For the material described above to be included in the copy of your thesis that is sent to the Library and Archives of Canada (formerly National Library of Canada) for reproduction and distribution.

Name: Christopher McKim Title: Mr.

Signature: Date (dd/mmm/yyyy) 06/04/2021

Ontario Tech University | 2000 Simcoe Street North, Oshawa, Ontario L1G 0C5 Canada | ontariotechu.ca

OntarioTech UNIVERSITY

Copyright Permission Letter

March 16, 2021

Publication Title: Targeted Delivery and Enhanced Gene-Silencing Activity of Centrally-Modified Folic Acid-siRNA Conjugates

I am preparing my Doctor of Philosophy thesis for submission to the School of Graduate and Postdoctoral Studies at the University of Ontario Institute of Technology (Ontario Tech University) in Oshawa, Ontario, Canada. I am seeking your permission to include a manuscript version of the following paper as a chapter in the thesis:

L. Salim, G. Islam, and J.-P. Desaulniers. "Targeted Delivery and Enhanced Gene-Silencing Activity of Centrally-Modified Folic Acid-siRNA Conjugates" *Nucleic Acids Res*. **2020**, 48, 75-85.

Canadian graduate theses are reproduced by the Library and Archives of Canada (formerly National Library of Canada) through a non-exclusive, world-wide license to reproduce, loan, distribute, or sell theses. I am also seeking your permission for the material described above to be reproduced and distributed by the LAC (NLC). Further details about the LAC (NLC) thesis program are available on the LAC (NLC) website (www.nlc-bnc.ca).

Full publication details and a copy of this permission letter will be included in the thesis.

Yours sincerely,
Lidya Salim

Permission is granted for:
a) The inclusion of the material described above in your thesis.
b) For the material described above to be included in the copy of your thesis that is sent to the Library and Archives of Canada (formerly National Library of Canada) for reproduction and distribution.

Name: Golam Islam Title: Dr.

Signature: G.M.Itheshamul Islam Date (dd/mmm/yyyy) 16/03/2021

OntarioTech UNIVERSITY

Copyright Permission Letter

March 16, 2021

Publication Title: Synthesis and Evaluation of Modified siRNA Molecules Containing a Novel Glucose Derivatives

I am preparing my Doctor of Philosophy thesis for submission to the School of Graduate and Postdoctoral Studies at the University of Ontario Institute of Technology (Ontario Tech University) in Oshawa, Ontario, Canada. I am seeking your permission to include a manuscript version of the following paper as a chapter in the thesis:

L. Salim, E. Goss and J.-P. Desaulniers. "Synthesis and Evaluation of Modified siRNA Molecules Containing a Novel Glucose Derivatives" *RSC Advances* **2021**, 11, 9285–9289.

Canadian graduate theses are reproduced by the Library and Archives of Canada (formerly National Library of Canada) through a non-exclusive, world-wide license to reproduce, loan, distribute, or sell theses. I am also seeking your permission for the material described above to be reproduced and distributed by the LAC (NLC). Further details about the LAC (NLC) thesis program are available on the LAC (NLC) website (www.nlc-bnc.ca).

Full publication details and a copy of this permission letter will be included in the thesis.

Yours sincerely,
Lidya Salim

Permission is granted for:
a) The inclusion of the material described above in your thesis.
b) For the material described above to be included in the copy of your thesis that is sent to the Library and Archives of Canada (formerly National Library of Canada) for reproduction and distribution.

Name: Eva Goss Title: President, Synthose Inc

Signature: Date (dd/mmm/yyyy) 16/03/2021

Ontario Tech University | 2000 Simcoe Street North, Oshawa, Ontario L1G 0C5 Canada | ontariotechu.ca